Hot and Ultrafast Carrier Extraction from Colloidal Semiconductor Nanocrystals with Different Quantum Confinement Dimensionality

Thesis for the Degree of

Doctor of Science

Submitted to

School of Science and Technology

Kwansei Gakuin University

Tomoki OKUHATA

December, 2016

Chapter 1
Introduction

1.1   Preface

1.2   Semiconductor nanocrystals

    1.2.1   General properties of semiconductor quantum dots

    1.2.2   Shape control of semiconductor nanocrystals

    1.2.3   Electronic structures of semiconductor nanocrystals

    1.2.4   Exiton dynamics of semiconductor nanocrystals

1.3   Carrier transfer from semiconductor nanocrystals

    1.3.1   Electron transfer in molecular chromophores

    1.3.2   Electron transfer in semiconductor nanocrystals

1.4   Outline of this thesis

Chapter 2

Synthesis of Colloidal Semiconductor Nanocrystals and Semiconductor-metal HNs

2.1   CdSe/CdS core/shell QD and core/shell QD-MV^{2+} complexes

    a) Synthesis of CdSe/CdS core/shell QDs

    b) Preparation of CdSe/CdS core/shell QD-MV^{2+} complexes

2.2   4-monolayer CdSe NPLs and CdSe NPL-MV^{2+} complexes

    a) Synthesis of CdSe NPLs with different lateral size

    b) Preparation of CdSe NPL-MV^{2+} complexes

2.3   Oleylamine capped PbS QDs and PbS QD-Au HNs

    a) Synthesis of PbS QDs

    b) Synthesis of PbS QD-Au HNs

Chapter 3

Hot Electron Transfer from CdSe/CdS Core/shell QD to Methyl Viologen

Chapter 4

Elementary Electron Transfer Processes from CdSe NPL to Methyl Viologen

Chapter 5

Ultrafast and Hot Carrier Dynamics in PbS QD-Au HNs

Chapter 6

Ultrafast and Hot Electron Transfer Processes from CdSe QD to Au NPs

Chapter 7

Electron Transfer Processes from CdSe NPL to Au NPs

Summary

Acknowledgement

Publication list

Chapter 1
Introduction

1.1 Preface

In the semiconductor nanocrystals, electron and hole are confined in the region smaller than the exciton Bohr radius. The strong confinement of electron and hole leads to the various unique properties in semiconductor nanocrystals, for example, size-tunable optical absorption and emission spectra, discrete energy states, strong electron-hole interaction etc. In 1982, the first synthesis of colloidal CdS nanocrystals in the reversed micelle was reported by Henglein group[1] and Brus group.[2] Then, the size dependent electronic spectra where the band-edge absorption shifted to the longer wavelength region as the size of nanocrystals increase were clearly observed, and this phenomenon is well known as the quantum size effect.[3] The further progress in the colloidal synthesis of semiconductor nanocrystals was achieved by Murray et al. in 1993.[4] They reported the synthetic method of high quality CdSe, CdS, and CdTe quantum dots (QDs) using organometallic compounds (dimethylcadmium and Se-trioctylphosphine) at high temperature. Furthermore, the synthesis of several kinds of core/shell QDs in which the surface of core QDs was coated with the different semiconductor shell were reported.[5,6] These core/shell nanocrystals can be classify into type I, quasi-type II, and type II by the difference of the energy of conduction and valence band-edge states. In the type I core/shell nanocrystals, the energy levels of conduction and valence band-edge states of shell were higher than those of core nanocrystals, indicating electron and hole wavefunctions were confined core region. Moreover, by passivating surface defects with the shell, the remarkable increase of luminescence quantum yield was observed in type I core/shell nanocrystals.[5,6] In the quasi-type II core/shell nanocrystals, only the electron (hole) wavefunction spread over the whole core/shell nanocrystals, and hole (electron) wavefuncton was confined in the core region.[7,8] In the type II core/shell nanocrystals, electron and hole wavefunctions were separated in the core and shell region. Consequently, the overlap of electron and hole wavefunctions reduces in the type II core/shell nanocrystals, leading that the

radiative lifetime becomes longer.[9,10] In 2000, Peng et al. reported the one-dimensional growth of wurtzite CdSe nanocrystals where electron and hole were confined in the short axis direction.[11] The important factors in the shape control of nanocrystals are the crystal structure, precursor concentration, and capping reagents.[11-15] In addition to QDs (three dimensional confinement) and NRs (two dimensional confinement), S. Ithurria and B. Dubertret synthesized colloidal semiconductor nanoplatelets (NPLs, one dimensional confinement) with atomic-layer precision in 2008.[16] The two dimensional growth of NPLs was achieved by the selective passivation of the (100) face of zinc-blend CdSe nanocrystals with carboxylic acid.[17-19] Colloidal semiconductor NPLs exhibit thickness-tunable, bright luminescence with narrow line width, and large absorption cross section.[20-22] Then, synthetic methods of core/shell and core/crown heterostructure-NPLs were reported.[19,23,24] The control of quantum confinement dimensionality leads to the variation of electronic structures and carrier relaxation processes. Furthermore, Mokari et al. have reported the synthesis and characterization of semiconductor-metal hybrid nanostructures (HNs) where metal nanoparticles (NPs) attached semiconductor NRs, tetrapods, and QDs.[25,26] Much attention has been paid for these HNs in terms of photovoltaics and photocatalysis because of the efficient charge separation between semiconductor and metal.

Since the semiconductor nanocrystals have discrete energy states, photoexcited hot carriers relax to the band-edge state through different processes from bulk semiconductor. For bulk semiconductor, hot carrier relax to the band-edge state immediately via phonon emission. However, in the semiconductor QDs where the energy separation between 1S and 1P states is much larger than the phonon energy,[27] the hot carrier relax via energy transfer between electron and hole,[28-32] energy transfer to the vibrational state of capping reagents,[33] and multiphonon emission.[34] The rate constant of these mechanisms can be controlled by capping reagents,[33] spatial separation between electron and hole,[33,35] and changing temperature.[34]

Actually, Pandey and Gyot-Sionnest reported the extremely slow hot electron relaxation with the lifetime over 1 ns in CdSe/ZnSe/ZnS/CdSe multishell QDs.[35] Consequently, the slow intraband reraxation in semiconductor nanocrystals can potentially allow for efficient hot carrier extraction. Furthermore, the enhancement of electron-hole interaction in semiconductor nanocrystals leads to the highly efficient multiple exciton generation (MEG) in which multiexcitons generate from the absorption of only one photon, and the MEG process was observed in several kinds of semiconductor nanocrystals.[36-41] However, the multiexcitons generated in semiconductor nanocrystals disappear nonradiatively by the Auger recombination process with the lifetime of tens of ps.[42-45] From the hot carrier relaxation and MEG processes, the semiconductor nanocrystals are the promising materials for the highly efficient solar cells which are beyond the Shockley−Queisser limit (32.7%).[46] In the theoretical work by Ross and Nozik, the maximum conversion efficiency in QDs solar cells was reported to reach ~67% when the excess energy of hot carriers was utilized.[47] As a result, efficient carrier transfer from semiconductor nanocrystals before the hot carrier relaxation or multiexciton annihilation is the key process for the development of the new generation solar cells using the semiconductor nanocrystals.

The electron transfer process is one of the most basic and important chemical reaction. In 1956, R. A. Marcus reported the theoretical equation of the electron transfer between donor and acceptor molecules in polar solvent.[48,49] The Marcus theory predicted the unique parabolic energy gap law of electron transfer rate and the existence of the Marcus inverted region, where the electron transfer rate decrease with increasing the driving force of electron transfer reaction. In 1984, the experimental work by Miller et al. revealed the existence of Marcus inverted region for the electron transfer from biphenyl anion radical to several kinds of acceptor molecules.[50] In addition, the electron transfer from semiconductor nanocrystals to the outside have been reported by various groups.[51-62] Recently, Zhu et al.

have reported the efficient electron transfer from II-VI semiconductor QDs to acceptor molecules different from systems of molecular chromophores.[53] According to this report, electron transfer rate from QDs to acceptor molecule increases monotonically with increasing the Gibbs energy change, indicating that the Marcus inverted region does not exist. Therefore, excited carriers in colloidal semiconductor nanocrystals can be extracted to the outside efficiently, which strongly suggests that the semiconductor nanocrystals is the promising material for the highly efficient solar cells.

In the present thesis, carrier transfer from band-edge state and higher excited states of semiconductor nanocrystals with different quantum confinement dimensionality and composition to the metal NPs and acceptor molecules are discussed. An understanding of the nature of hot electron transfer as well as the electron transfer from the band-edge state is very important for the development of highly efficient solar cells and scientific interest. We hope that the present study will provide the insight into the elementary carrier extraction mechanism from semiconductor nanocrystals.

1.2   Semiconductor nanocrystals

1.2.1   General properties of semiconductor quantum dots

Semiconductor QDs are nm-scale spherical particles whose diameter is smaller than the exciton Bohr radius. In this size range, the electron and hole were confined along the three-dimensional direction, and the absorption and emission properties were strongly depends on the size of QDs (Figure 1.1).[3,27,63] The latter is well known as "quantum size effect", and can be described approximately by a "particle in a box" model. In addition to size-dependent optical properties, the electronic structure in QDs becomes discrete while the bulk semiconductor have the continuous band structure (Figure 1.1). Notations of discrete electronic states in QDs in order of increasing the energy are 1S, 1P, and 1D, and the energy

spacing between 1S and 1P states is especially large as compared with the phonon energy.[27,64,65] These discrete energy states lead to the drastic change of hot carrier relaxation processes in semiconductor QDs.[29,33,66] Furthermore, the strong spacial confinement of electron and hole in QDs induced the enhancement of carrier-carrier Coulomb interaction. This effect leads to the efficient MEG process and annihilation of multiexciton such as Auger recombination (Figure 1.2).[36-44] In addition, the strong Coulomb interaction leads to the unique and highly efficient electron transfer process from semiconductor QDs to acceptor molecules, where the Marcus inverted region does not exist.[53]

Previously, a great deal of researcher have prepared the semiconductor QDs by using "physical" or "chemical" methods. In physical methods, semiconductor QDs grow on the substrate using the molecular beam epitaxy and metalorganic chemical vapor deposition methods. Semiconductor QDs prepared by the physical processes have an advantage in terms of carrier extraction from QDs. However, manufacturing equipments for these QDs are very expensive and large. On the other hand, semiconductor QDs were also prepared using colloidal synthetic method. By using the chemical synthetic method, semiconductor QDs which are covered with the organic ligand layer are dispersed in the polar or nonpolar solvents. In contrast to semiconductor QDs prepared by physical methods, colloidal semiconductor QDs are easy to prepare and cheaper. In addition, colloidal semiconductor QDs are freestanding which is different from epitaxial QDs grown on the substrate, and have the good size dispersion.[67,68]

1.2.2   Shape control of semiconductor nanocrystals

As described in 1.2.1, spherical colloidal semiconductor QDs confines electron and hole along three dimensional directions. In addition to QDs, the elongated (NRs) and planer (NPLs) nanocrystals corresponding to the two and one dimensional quantum confinement

system have been synthesized by colloidal synthetic method.[11,16] The general growth mechanism of colloidal semiconductor QDs was explained based on the previous study by La Mer and Dinegar.[69] The high quality and monodisperse QDs can be synthesized by injecting organometallic precursor solution, such as Se-trioctylphosphine, to the coordinating solvent at high temperature (~300 °C).[70] As shown in Figure 1.3, immediately after the precursor injection, the precursor concentration in the reaction mixture increases quickly over the nucleation threshold, and the concentration decreases rapidly by the formation of small nuclei which is the assembly of several precursors. When the precursor concentration became lower than the threshold of nucleation, the precursor reacts with the formed nuclei without the formation of new nuclei. After the further decrease of the precursor concentration by growing nuclei, the colloidal semiconductor QDs grow through the Ostwald ripening process, where smaller nanoparticle with the higher surface energy dissolved into the solution and larger nanoparticles further grow, and the concentration of nanoparticles decreases during the growth process.[67,68,71]

In addition to QDs, colloidal semiconductor nanocrystals elongated along one direction, which is called "nanorods (NRs)", have been synthesized.[11,14] Key factors for the shape control of nanocrystals are the crystal structure, precursor concentration, and capping reagents.[12,13,72] We describe the mechanism of shape control of CdSe nanocrystals as the model system in the following sentences. In the CdSe nanocrystals, there are two possible crystal structures, zinc-blende and wurtzite structures. It is known that the crystals structures of nanocrystals can be controlled by the reaction temperature, where the wurtzite is the preferential structure at high temperature (thermodynamic phase) and the zinc-blende is the preferential structure at low temperature (kinetic phase).[67,68] The wurtzite structure has the intrinsic anisotropy with the c/a ratio of ~1.6, although the zinc-blende is the cubic structure. In 2000, Peng et al. and Manna et al. have reported the one dimensional growth of wurtzite

CdSe nanocrystals along the *c*-axis, which is capped with trioctylphosphine oxide and hexylphosphonic acid.[11,12] In 2001, Z. A. Peng and X. Peng have revealed the anisotropic growth mechanism of CdSe NRs.[13] Wrutzite CdSe NRs have two facets which are perpendicular to the *c*-axis, (001) and $(00\bar{1})$ facets, and these facets have different chemical compositions shown in Figure 1.4a. All atoms on both facet have a dangling bond, where (001) and $(00\bar{1})$ facets are terminated by positively charged Cd atoms and negatively charged Se atoms, respectively. Since the electron-donating ligand are used for the synthesis of CdSe NRs, the negatively charged $(00\bar{1})$ facet was not passivated by ligands, leading that $(00\bar{1})$ facet easily react with the Cd precursor in the solution. In addition, even if the Cd precursor react with the $(00\bar{1})$ facet, surface Cd atoms on the $(00\bar{1})$ facet have three dangling bonds different from Cd atoms on the (001) facet. Moreover, electron-donating ligands such as alkylphosphonic acid passivate the $\{110\}$ facets on the side of NRs as well as (001) facet. As a results, the highly reactivity of $(00\bar{1})$ facet compared with the $(00\bar{1})$ facet and side facets induces the efficient one-dimensional growth of CdSe nanocrystals. Wang et al. reported that the aspect ratio of CdSe NRs could be controlled by the selection of ligands, where the phosphonic acid with longer alkyl chain lead to the lower aspect ratio of CdSe NRs.[15] Furthermore, the precursor concentration during the growth process is the important factor for the anisotropic growth of colloidal semiconductor nanocrystals. Peng et al. observed that the growth kinetics of CdSe nanocrystals was strongly depend on the Cd precursor concentration during the growth process.[13] Immediately after the nucleation, in the high Cd precursor concentration region, the aspect ratio of CdSe nanocrystals increased as the Cd precursor in the solution decreased (the reaction time increased). In the middle Cd precursor concentration region, the aspect ratio did not change although the volume of CdSe nanocrystals increased, suggesting the three dimensional growth. Finally, in the low Cd precursor concentration region, the aspect ratio of CdSe nanocrystals decreased with increasing the reaction time

8

without the decrease of volume and concentration, indicating that the monomer likely moved on the surface of a crystals from c-axis to the other two dimensions. The precursor concentration dependence of the growth of CdSe nanocrystals suggests that effective one dimensional growth is induced by maintaining the high precursor concentration during the growth process as shown in Figure 1.4b. Actually, Shieh et al. synthesized the colloidal CdSe, CdS, and CdTe NRs by the multiple injection of precursor solution.[14] This precursor concentration dependence of the growth kinetics was interpreted by the diffusion-controlled process. In the higher precursor concentration, the chemical potential in the bulk solution is much higher than that in the vicinity of each facets of wurtzite CdSe nanocrystals, leading the diffusion of precursors from bulk solution to the surrounding region of CdSe nanocrystals. As mentioned above, the $(00\bar{1})$ facet of wurtzite CdSe nanocrystals have the unique structural features. In addition, Blanton et al. observed the permanent dipole moment of CdSe nanocrystals along c-axis.[73] The unique $(00\bar{1})$ facet and dipole moment along c-axis increases the chemical potential of the $(00\bar{1})$ facet compared with the other facets. Therefore, the growth rate along c-axis is much faster than that along the others, and CdSe nanocrystals preferentially grows along the c-axis. In the lower precursor concentration, the gradient of chemical potential between the bulk solution and each facets of CdSe nanocrystals decreases. The impact of this decrease significantly affects to the growth at the $(00\bar{1})$ facet compared with the other facets because of the high chemical potential of the $(00\bar{1})$ facet. The smaller gradient of chemical potential between bulk solution and the vicinity of $(00\bar{1})$ facet leads to the difficulty of precursor diffusion into the $(00\bar{1})$ facet. As a result, the higher growth rate and small diffusion of precursors at the facets along c-axis cancel each other, and CdSe nanocrystals grows along three dimensional directions.

Furthermore, in 2008, S. Ithurria and B. Dubertret reported the colloidal synthetic method of CdSe NPLs which corresponds to the quantum wells.[16] After this report, the

colloidal synthesis of cadmium chalcogenide NPLs with various thicknesses and hetero-structure NPLs (core/shell and core/crown NPLs) are reported.[19,23,24,74-76] Key factors for the two-dimensional growth of semiconductor nanocrystals are crystal structure and passivation by carboxylic acids ligands. In the synthesis of CdSe NPLs as a model system, the nucleation of CdSe seed crystals occurs at the relatively low temperature (<240 °C), leading the formation of the zinc-blende crystal structure of CdSe nanocrystals.[74] In the zinc-blende CdSe NPLs, the thickness direction is confirmed to be [100] direction using the high resolution transmission electron microscopy, and perpendicular facets to the thickness direction (top and bottom facets) are {100} facets.[74,77] The {100} facets of zinc-blende CdSe are terminated by cadmium atoms.[19,78,79] Therefore, these facets of CdSe seed crystals are well passivated by carboxylic acid ligands, which induces the prevention of the growth of CdSe seeds along the only thickness direction. Consequently, CdSe nanocrystals grow along two dimensional directions.

1.2.3   Electronic structures of semiconductor nanocrystals

As mentioned above, the semiconductor QDs (three dimensional quantum confinement system) have discrete electronic states while bulk semiconductors have the continuous band structures. In early studies, electron and hole which are strongly confined in QDs can be treated in the simple model, *particle-in-a-sphere* model, where wavefunctions of electron and hole are represented as the product of a spherical harmonic and a spherical Bessel function.[80,81] In this model, the wavefunction can be described in the simple atomic-like orbital labeled by the angular momentum number (L) and radial quantum number (n), and energy levels in order of increasing energy is described as 1S, 1P, 1D, 2S, etc. Moreover, the first exciton band in the absorption spectrum of QDs is assigned to $1S_h$-$1S_e$ transition.

In the simple *particle-in-a-sphere* model, the conduction and valence band were approximated by simple parabolic bands. However, the actual band structure of II-VI semiconductors is more complicated. In the theoretical work which takes into account the valence band degeneracy and mixing of valence band, the total angular momentum F is appropriate quantum number for the label of the hole wavefunction. The total angular momentum F is sum of the Bloch-function angular momentum J and the orbital momentum of hole wavefunction L_h, $F = J + L_h$. Therefore, the hole states in the QDs are labeled as $n_h L_F$, although the electron states are not affected by the complexities of valence band and labeled as $n_e L_e$. According to this theory, the lowest three absorption band observed in CdSe QDs can be assigned to $1S_{3/2}$-$1S_e$, $2S_{3/2}$-$1S_e$, and $1P_{3/2}$-$1P_e$ (Figure 1.5).[64,65,82]

The quantum confinement dimensionality of semiconductor nanocrystals significantly affects the electronic structures. Hu et al. examined the aspect ratio dependent electronic structures of CdSe NRs (two dimensional quantum confinement system) by the semiempirical psuedopotential calculation.[83] In this report, the additional electronic states arising from the weak quantum confinement along the long axis generated between the discrete electronic states for QDs with the aspect ratio of 1, and the density of states increases with increasing the aspect ratio of CdSe NRs. According to this calculation, lowest three absorption band of CdSe NRs in Figure 1.6 can be assigned to transition of $1\sigma_v$-$1\sigma_c$ (1Σ band), $2\sigma_v$-$2\sigma_c$ (2Σ band), and $1\pi_v$-$1\pi_c$ (1Π band).[62]

Furthermore, the recent progress in the colloidal synthesis of semiconductor nanocrystals allows us to synthesize the colloidal CdSe NPLs (one dimensional quantum confinement system) with the atomic-layer precision. These NPLs have very narrow absorption and emission bands arising from the small contribution of inhomogeneous broadening (size distribution) and coherent motion of the exciton.[74,78,79] As shown in Figure 1.7, the lowest two absorption band observed in colloidal NPLs can be assigned to heavy-hole

band (from heavy-hole band edge to conduction band-edge state) and light-hole band (from light-hole band edge to conduction band-edge state) similar to absorption bands of epitaxial quantum wells.[16,74] In the theoretical work by Bose et al., first 10 electron levels exist in the range of few hundreds of meV, although the energy spacing between $1S_e$ and $1P_e$ states in QDs is a few hundreds of meV.[84]

1.2.4 Carrier dynamics of semiconductor nanocrystals

As mentioned above, colloidal semiconductor QDs exhibit the discrete energy state and enhancement of Coulomb interaction, which significantly affect to the hot carrier relaxation and single- and multi-exciton dynamics. The strong electron-hole Coulomb interaction in semiconductor nanocrystals enhance the probability of radiative recombination compared with the bulk semiconductors. However, in the semiconductor nanocrystals, the surface condition strongly affect to the nonradiative recombination process such as the carrier trapping at the surface defects.[27] The carrier trapping to surface defect states can be suppressed by the coating of the surface with different semiconductor shell.[5,6] In addition to the single exciton dynamics, the multiexciton dynamics in semiconductor nanocrystals is different from bulk semiconductors. In the semiconductor QDs, multiple exciton annihilation process is dominated by the nonradiative Auger recombination with the lifetime of several tens of ps, which is a process that electron and hole recombine nonradiatively by the energy transfer to another carrier (electron or hole).[27,63] The Auger recombination process in QDs is significantly enhanced as compared to that in bulk because of the strong exciton-exciton interaction and relaxation of momentum conservation.[85] In our group, Kobayashi et al reported that the lifetime of Auger recombination in CdS QDs depends only on the size of QDs, which is irrespective of surface defects and ligands, and was proportional to $\sim D^6$ (D: diameter of QDs).[44] Moreover, the temperature dependence of Auger recombination lifetime

for CdTe QDs (D = ~4.0 nm) capped with oleic acids were examined using a streak camera.[86] In this report, the biexciton Auger rate in CdTe QDs exhibited the moderate temperature dependence and is proportional to the natural logarithm of temperature, where the contribution of phonon probably have important role for the satisfaction of energy conservation. The theoretical study by Kim et al revealed that the logarithm temperature dependence of Auger recombination, which agree well with the experimental work by Kobayashi et al., can be interpreted in terms of electron-phonon coupling accompanied by Auger recombination.[87] The multiple exciton annihilation dynamics can be modified by controlling the quantum confinement dimensionality. A.V. Barzykin and M. Tachiya analyzed the multiexciton Auger process in semiconductor nanocrystals using stochastic models.[88] The multiexciton Auger recombination process in QDs was analyzed by the three-particle model or two-particle model. In the three-particle model, electron and hole does not form an exciton because of the strong confinement energy and Auger recombination occurs between two electrons and one hole (or one electron and two holes). In this case, the multiexciton Auger recombination rate in the n exciton state (k_n^A) is represented as $k_n^A = \frac{1}{2} n^2 (n - 1) k_2^A$. On the other hand, in the two-particle model, electron and hole are bound and form an exciton and Auger recombination occurs between two excitons. In this case, the k_n^A is represented as $k_n^A = \frac{1}{2} n(n - 1) k_2^A$. In the theoretical work by A.V. Barzykin and M. Tachiya, multiexciton Auger recombination processes can be expressed by the two-particle (bimolecular) model rather than the three-particle model, since the average number of excitons per one QD is only a few. In the previous experimental studies, the higher order multiexciton Auger recombination process occurs with the three-particle process.[89-91] Moreover, V. I. Klimov and coworkers analyzed the multiexciton Auger recombination dynamics in CdSe QDs and NRs, and found the transition of the multiexciton Auger recombination process from three-particle process to bimolecular process with increasing the aspect ratio of CdSe NRs.[89] This transition

13

of Auger recombination process was attributed to the formation of 1D exciton arising from the decrease of confinement energy and enhancement of Coulomb interaction.[39,89,92] Considering the number of exciton (n) dependence of k_n^A, high order ($n > 2$) multiexciton Auger recombination in a bimolecular process is slower than that in a three-particle process. Actually, CdSe NRs exhibited the decrease of τ_2^A / τ_3^A and longer τ_3^A as compared to the CdSe QDs, suggesting the bimolecular Auger recombination process in CdSe NRs. Moreover, Aerts et al. reported the similar transition of multiexciton annihilation process in PbSe QDs and NRs.[90] In addition to the semiconductor NRs, Kunnemann et al. revealed that colloidal CdSe NPLs and CdSe/CdS/ZnS NPLs (one dimensional quantum confinement system) exhibited the significantly slow biexciton Auger recombination with the lifetime of ~10 ns and the bimolecular multiexciton annihilation process, suggesting the electron and hole form an exciton in semiconductor NPLs.[93]

The hot electron and hole relaxation processes in colloidal semiconductor QDs is much different from that in bulk semiconductor because of discrete energy states in QDs as mentioned in 1.2.3. In the II-VI semiconductor nanocrystals such as CdSe QDs, since the energy spacing between $1S_e$ and $1P_e$ states are especially large, which is 10 times larger than the LO phonon energy of CdSe QDs (~ 30 meV), a hot electron cannot relaxed to the $1S_e$ state by the phonon emission in contrast with bulk semiconductors.[27] In the previous studies, three possible processes are proposed for the hot electron relaxation mechanism, which are Auger cooling, energy transfer to ligands and multiple phonon emission (Figure 1.8).[29-34] First, the Auger cooling process was proposed as the hot electron relaxation mechanism in CdSe QDs by Efros et al., where a hot electron relaxes from the $1P_e$ state to $1S_e$ state through the transfer of excess electron energy to a hole.[28] The Auger cooling process can be very efficient in semiconductor QDs because of the large wavefunction overlap, enhanced electron-hole Coulomb interaction, and relaxation of momentum conservation.[29] In the experimental works

by Klimov and coworkers, the Auger cooling process in CdSe QDs was examined using the femtosecond pump-prove spectroscopy.[27,66,94] In their report, hot electron relaxation rates from $1P_e$ to $1S_e$ state decreased as the size of CdSe QDs increased. Moreover, they compared the hot electron relaxation dynamics of CdSe/ZnS QDs with that of CdSe QDs capped with pyridine (hole acceptor) and found that the hot electron transfer time became longer in pyridine-capped CdSe QDs (from ~320 fs to 3 ps), resulting from the reduction of electron-hole interaction by the spacial charge separation between CdSe QDs and pyridine molecules.[27] This experimental result indicates the contribution of Auger cooling process to the hot electron relaxation. However, even in the charge separated CdSe QDs-pyridine system, the ps-scale hot electron relaxation time was much faster compared with the relaxation via phonon emission, suggesting the existence of other hot electron relaxation mechanism. Second, the role of surface ligands to the hot electron relaxation process was revealed by Gyot-Sionnest group. They examined the hot electron relaxation dynamics from $1P_e$ to $1S_e$ state in CdSe QDs with different surface ligands.[33] According to their report, the hot electron relaxation rate can be modified by changing surface ligands, and the $1P_e$ electron relaxes to $1S_e$ state via energy transfer to high-frequency vibration of surface ligands. Furthermore, Kambhampati group analyzed the hot electron and hole relaxation mechanism in CdSe QDs in more detail with the state-selective excitation experiments.[29,31,32] They revealed that the Auger cooling process and energy transfer to surface ligands contributed dominantly to the hot electron relaxation from $1P_e$ to $1S_e$ and hot hole relaxation from $2S_h$ to $1S_h$, respectively. In II-VI semiconductor QDs, the Auger cooling process occurs effectively because of the higher density of states in valence band as compared to that in conduction band. On the other hand, IV-VI semiconductor QDs have a mirrorlike symmetry between conduction and valence band, leading the suppression of an Auger cooling process. Schaller et al. reported the clear temperature dependence of hot carrier relaxation from 1P-to-1S states in PbSe QDs, although

the hot electron relaxation time in CdSe QDs is independent of the temperature, suggesting the contribution of phonon.[34] Therefore, they concluded that the hot carrier relaxation in PbSe QDs was due to the multiphonon emission process. These experimental results of intraband transition processes in semiconductor QDs indicates that the hot carrier relaxation time can be controlled by the charge separation, surface ligands, and temperature. Since the electronic structure of semiconductor nanocrystals are modified by the change of quantum confinement dimensionality, hot carrier relaxation dynamics in NRs and NPLs can be different from that in QDs. Nevertheless, in contrast to semiconductor QDs, the hot electron and hole relaxation mechanism in semiconductor NRs and NPLs are still not established. Yu et al. examined the hot electron relaxation in CdSe NRs with thin (2.2 nm) and thick (7.2 nm) short axes.[95] They reported that hot electron relaxation rates of CdSe NRs were similar or slower than those of CdSe QDs, and the hot electron relaxation rate of thinner CdSe NRs (~3.2 eV/ps) is faster than that of thicker CdSe NRs (~0.39 eV/ps). The latter suggested that the dominant hot electron relaxation mechanism in CdSe NRs was probably not the LO phonon emission. Moreover, Sipple et al. reported that the hot electron relaxation in colloidal CdSe NPLs occurred by the phonon emission via continuous conduction band arising from the weak confinement along lateral directions.[96]

1.3   Carrier transfer from semiconductor nanocrystals

1.3.1   Electron transfer in molecular chromophores

The electron transfer process is one of the most basic and important chemical reaction. In 1956, R. A. Marcus reported the theoretical equation of the electron transfer between donor and acceptor molecules in polar solvent.[48,49] In the Marcus theory, the electron transfer rate (k_{ET}) was derived based on the transition state theory as following equation,

$$k_{ET} = Z exp(-\frac{\Delta G^*}{k_B T}) \qquad (1)$$

where Z is the frequency factor, k_B is the boltzmann constant. ΔG^* is the activation energy of electron transfer reaction (shown in Figure 1.9) which is represented as following equation,

$$\Delta G^* = \frac{(\Delta G + \lambda)^2}{4\lambda} \qquad (2)$$

where ΔG is the change in Gibbs energy corresponding the energy difference between the initial state and final state. λ is the reorganization energy which corresponds to the energy required to change the orientation of solvent molecules for the stabilization of the products, and represented as below,

$$\lambda = \frac{e^2}{4\pi\varepsilon_0} \left(\frac{1}{2a_D} + \frac{1}{2a_A} - \frac{1}{r_{DA}}\right) \left(\frac{1}{\varepsilon_{op}} - \frac{1}{\varepsilon_s}\right) \qquad (3)$$

where a_D and a_A are radius of donor and acceptor molecules, r_{DA} is the distance between donor and acceptor molecules, ε_{op} and ε_s are optical and static dielectric constant of the solvent. The remarkable point of the equation in Marcus theory is the energy gap law of electron transfer rate, where the electron transfer rate reaches the maximum value at $-\Delta G = \lambda$ and decreases with increasing the $-\Delta G$ (> λ) which is well known as the "Marcus inverted region" (Figure 1.10). After this report, the validity of Marcus theory was proven experimentally by Miller et al in 1984.[50,97] They examined the correlation between $-\Delta G$ and electron transfer rate from the biphenyl anion radical to the several kinds of acceptor molecule, where the donor and acceptor molecules were connected with a rigid saturated hydrocarbon spacer. In that experiment, the decrease of electron transfer rate as the $-\Delta G$ increased were

clearly observed, revealing the existence of the Marcus inverted region.

1.3.2   Electron transfer in semiconductor nanocrystals

The electron transfer from semiconductor nanocrystals to the outside (metal oxides, acceptor molecules, metal NPs, etc.) have been reported by various groups.[51-62] Yang et al. examined electron transfer dynamics from PbS QDs to TiO_2 NPs.[58] In this system, the existence of the ultrafast adiabatic electron transfer from the $1S_e$ state of PbS QDs with the lifetime of ~6 fs were suggested, resulting from strong mixing of electronic states of PbS QDs and TiO_2 NPs. In addition, Sambur et al. reported the multiple exciton collection from PbS QDs to single crystalline TiO_2 using the photon-to-current efficiency measurements, where the multiexciton were generated by a MEG process.[59] The multiple electrons extraction was also observed in the semiconductor nanocrystal-acceptor molecules complexes. Matylitsky et al. reported ~4 electrons can be extracted from CdSe QDs to methyl viologen (electron acceptor, MV^{2+}) adsorbed on the surface of QDs.[51] In addition, the more efficient multiple electron transfer was achieved in CdSe NR-MV^{2+} and CdSe/CdS core/shell QD-MV^{2+} complexes by controlling quantum confinement dimensionality and the electron and hole wavefunction, respectively.[52,54] Moreover, the ultrafast electron transfer from the band-edge state in semiconductor-metal HNs were detected in CdS NR-Au HNs and PbS QD-Au HNs, suggesting the possibility of multi carrier collection in semiconductor-metal HNs.[60,98]

In addition to ultrafast electron transfer, as mentioned above, the hot electron transfer can potentially allow the increase of the photon-to-current conversion efficiency. Tisdale et al. reported the hot electron transfer from thiol-capped PbSe QDs to single crystalline TiO_2 at low temperature (~80 K).[99] Zhu et al. and Wang et al. reported the hot electron transfer from CdSe NRs and CdSe QDs, respectively.[54,100] In addition, in the our previous study on CdSe NR-Au HNs, hot electron transfer rate and yield were analyzed using femtosecond

pump-prove spectroscopy with the state-selective excitation technique.[62,101] CdSe NR-Au HNs with the largest diameter of Au NPs (~2.2 nm) exhibited the hot electron transfer with the lifetime of ~0.5-1.0 ps and the highest hot electron transfer yield of ~23%.

Furthermore, a recent work by T. Lian and co-workers examined the energy gap law of electron transfer rate from band-edge state of cadmium chalcogenide (CdX) QDs to several kinds of acceptor molecules.[53] They reported the unique and efficient electron transfer processes where the electron transfer rate monotonically increased with increasing the $-\Delta G$, meaning the Marcus inverted region does not exist. As mentioned above, colloidal semiconductor QDs strongly confines electron and hole in itself, leading the enhancement of electron-hole Coulomb interaction. This enhancement affects the electron transfer process as well as the hot carrier relaxation and multiexciton dynamics in semiconductor nanocrystals. In the conventional electron transfer theory, the contribution of hole dynamics associated with electron transfer from QDs to acceptor molecules is neglected, where the product state is represented as $QD^+(1S_h)$-A^-. In contrast, Lian et al. consider that the excess electron energy is conserved by the excitation of 1S hole to the deeper conduction band states ($E_{h,i}$) associated with the electron transfer, which is like an Auger cooling process, and there is a manifold of product state represented as $QD^+(E_{h,i})$-A^-. In addition, authors further assumed that the electronic coupling constant depends not only on the overlap of $1S_e$ state and acceptor orbital but also on the electron-hole Coulomb interaction, and the density of hole states in the quasi-continuum valence band was represented by $\rho_h(E_h, R)dE_h \propto E_h R^3$. In the nonadiabatic limit, the total electron transfer rate (k'_{ET}) from $1S_e$ state of CdX QDs with the radius of R to acceptor molecules accompanied with the 1S hole excitation can be represented by the following equation,

$$k'_{ET}(R) = C|\Psi_{1S_e}(R)_0|^2 R^2 \int_{E_h=0}^{\infty} dE_h E_h \frac{2\pi}{\hbar} \frac{1}{\sqrt{4\pi\lambda k_B T}} exp\left[-\frac{(\lambda+\Delta G(R)+E_h)^2}{4\lambda k_B T}\right] \qquad (4)$$

where $C|\Psi_{1S_e}(R)_0|^2$ represents the electronic coupling constant between QDs and acceptor molecules, which is represented as $|\bar{H}(E)|$ in the conventional electron transfer theory. The electronic coupling constant between QDs and acceptor molecules strongly depends on the 1S electron density at the surface of QDs ($|\Psi_{1S_e}(R)_0|^2$). The C is the size independent factor that depends on the material of QDs and molecules. To more clearly illustrate the $-\Delta G$ dependence of electron transfer rate, the electron transfer rate ($k'_{ET}(R)$) is divided by the size and material dependent factor. The scaled electron transfer rate ($k'_{ET}(-\Delta G)$) is given in the following equation,

$$k'_{ET}(-\Delta G) = \int_{E_h=0}^{\infty} dE_h E_h \frac{2\pi}{\hbar} \frac{1}{\sqrt{4\pi\lambda k_B T}} exp\left[-\frac{(\lambda+\Delta G(R)+E_h)^2}{4\lambda k_B T}\right] \qquad (5)$$

By using equation 4 and 5, the obtained size and $-\Delta G$ dependence of the electron transfer rate from CdX QDs to acceptor molecules can be well fitted. Therefore, the unique electron transfer processes in the semiconductor QDs are originated from the strong electron-hole Coulomb interaction in QDs and the excitation of 1S hole to the deeper valence band states. This novel efficient electron transfer process in semiconductor nanocrystals is named "Auger-assisted electron transfer".

1.4 Outline of this thesis

In this thesis, basic photophysical properties of colloidal semiconductor nanocrystals, and the quantum confinement dimensionality effect on their properties are given in Chapter 1. Chapter 2 introduces synthetic methods of several kinds of colloidal semiconductor nanocrystals and semiconductor-metal hybrid nanostructures. In Chapter 3, electron transfer

dynamics from $1S_e$ and higher excited states of CdSe/CdS core/shell QDs to MV^{2+} are examined. From the analyses of transient absorption dynamics at 1S bleach band and MV^+ radical band, hot electron transfer time in CdSe/CdS QDs with thicker shell is similar or slightly faster as compared to that in CdSe/CdS QDs with thinner shell in contrast with the shell thickness dependence of electron transfer from the $1S_e$ state. Elementary electron transfer processes from CdSe NPLs to MV^{2+} are discussed in Chapter 4. The lateral size dependence of electron transfer rate from band-edge state of CdSe NPLs to MV^{2+} reveals that the electron transfer rate depends on the CdSe NPLs face where MV^{2+} adsorbs on. In Chapter 5, carrier transfer dynamics in PbS QD-Au HNs were analyzed from initial bleach amplitude and relaxation dynamics at 1S bleach band. The ultrafast electron transfer whose lifetime is much faster than the instrumental response function (~60 fs) was observed in the 1S excitation experiments. In Chapter 6, we synthesized CdSe QD-Au HNs and examined electron transfer dynamics from $1S_e$ state and higher excited states using the femtosecond pump-probe spectroscopy. State-selective excitation experiments revealed that hot electron transfer occurred from $1P_e$ state whose lifetime and yields are estimated to be ~300 fs and 50%, respectively. Moreover, in 1S excitation experiments, the initial 1S bleach amplitude became lower with increasing the size of Au NPs, indicating the existence of ultrafast electron transfer from $1S_e$ state. We compared the obtained results for CdSe QD-Au HNs to those for CdSe NR-Au HNs. In addition, the electron transfer dynamics in CdSe NPL-Au HNs was discussed in Chapter 7. In contrast with CdSe QD-Au HNs, hot electron transfer and ultrafast electron transfer from band-edge state are not observed in CdSe NPL-Au HNs.

References

(1) Alfassi, Z.; Bahnemann, D.; Henglein, A. Photochemistry of colloidal metal sulfides. 3. Photoelectron emission from cadmium sulfide and cadmium sulfide-zinc sulfide cocolloids *J. Phys. Chem.*, **1982**, *86*, 4656–4657.

(2) Rossetti, R.; Brus, L. Electron-hole recombination emission as a probe of surface chemistry in aqueous cadmium sulfide colloids *J. Phys. Chem.* **1982**, *86*, 4470–4472.

(3) Rossetti, R.; Nakahara, S.; Brus, L. Quantum size effects in the redox potentials, resonance Raman spectra, and electronic spectra of CdS crystallites in aqueous solution *J. Chem. Phys.* **1983**, *79*, 1086–1088.

(4) Murray, C. B.; Norris, D. J.; Bawendi, M. G. Synthesis and characterization of nearly monodisperse CdE (E = sulfur, selenium, tellurium) semiconductor nanocrystallites. *J. Am. Chem. Soc.* **1993**, *115*, 8706–8715.

(5) Peng, X.; Schlamp, M. C.; Kadavanich, A. V.; Alivisatos, A. P. Epitaxial Growth of Highly Luminescent CdSe/CdS Core/Shell Nanocrystals with Photostability and Electronic Accessibility *J. Am. Chem. Soc.* **1997**, *119*, 7019–7029.

(6) Dabbousi , B. O.; Rodriguez-Viejo, J.; Mikulec, F. V.; Heine, J. R.; Mattoussi, H.; Ober, R.; Jensen, K. F.; Bawendi, M. G. (CdSe)ZnS Core−Shell Quantum Dots: Synthesis and Characterization of a Size Series of Highly Luminescent Nanocrystallites. *J. Phys. Chem. B* **1997**, *101*, 9463–9475.

(7) Talapn, D. V.; Koeppe, R.; Götzinger, S.; Kornowski, A.; Lupton, J. M.; Rogach, A. L.; Benson, O.; Feldmann, J.; Weller, H. Highly Emissive Colloidal CdSe/CdS Heterostructures of Mixed Dimensionality. *Nano Lett.* **2003**, *3*, 1677–1681.

(8) Müller, J.; Lupton, J. M.; Lagoudakis, P. G.; Koeppe, R.; Rogach, A. L.; Feldmann, J.; Talapn, D. V.; Weller, H. Wave Function Engineering in Elongated Semiconductor Nanocrystals with Heterogeneous Carrier Confinement. *Nano Lett.* **2005**, *5*, pp 2044–2049.

(9) Chuang, C.-H.; Lo, S. S.; Scholes, G. D.; Burda, C. Charge Separation and Recombination in CdTe/CdSe Core/Shell Nanocrystals as a Function of Shell Coverage: Probing the Onset of the Quasi Type-II Regime. *J. Phys. Chem. Lett.* **2010**, *1*, 2530–2535.

(10) Kim, S.; Brent, F.; Eisler, H.-J. Bawendi, M. Type-II Quantum Dots: CdTe/CdSe(Core/Shell) and CdSe/ZnTe(Core/Shell) Heterostructures. *J. Am. Chem. Soc.* **2003**, *125*, 11466–11467.

(11) Peng, X.; Manna, L.; Yang, W.; Wickham, J.; Scher, E.; Kadavanich, A.; Alivisatos, A. P. Shape control of CdSe nanocrystals. *Science*, **2000**, *404*, 59–61.

(12) Manna, L.; Scher, E. C.; Alivisatos, P. A. Synthesis of Soluble and Processable Rod-, Arrow-, Teardrop-, and Tetrapod-Shaped CdSe Nanocrystals. *J. Am. Chem. Soc.* **2000**, *122*, 12700–12706.

(13) Peng, Z. A.; Peng, X. Mechanisms of the Shape Evolution of CdSe Nanocrystals. *J.*

Am. Chem. Soc. **2001**, *123*, 1389–1395.

(14)   Shieh, F.; Saunders, A. E.; Korgel, B. A. General Shape Control of Colloidal CdS,

CdSe, CdTe Quantum Rods and Quantum Rod Heterostructures. J. Phys. Chem. B, 2005,

109, 8538–8542.

(15)   Wang, W.; Banerjee, S.; Jia, S.; Steigerwald, M. L.; Herman, I. P. Ligand Control of

Growth, Morphology, and Capping Structure of Colloidal CdSe Nanorods. *Chem. Mater.*

2007, *19*, 2573–2580.

(16)   Ithurria, S.; Dubertret, B. Quasi 2D Colloidal CdSe Platelets with Thicknesses

Controlled at the Atomic Level. *J. Am. Chem. Soc.* **2008**, *130*, 16504−16505.

(17)   Lhuillier, E.; Pedetti, S.; Ithurria, S.; Nadal, B.; Heuclin, H.; Dubertret, B.

Two-Dimensional Colloidal Metal Chalcogenides Semiconductors: Synthesis,

Spectroscopy, and Applications. *Acc. Chem. Res.* **2015**, *48*, 22−30.

(18)   Tessier, M. D.; Javaux, C.; Maksimovic, I.; Loriette, V.; Dubertret, B. Spectroscopy

of Single CdSe Nanoplatelets. *ACS Nano* **2012**, *6*, 6751–6758.

(19)   Mahler, B.; Nadal, B.; Bouet, C.; Patriarche, G.; Dubertret, B. Core/Shell Colloidal

Semiconductor Nanoplatelets. *J. Am. Chem. Soc.* **2012**, *134*, 18591–18598.

(20)   She, C.; Fedin, I.; Dolzhnikov, D. S.; Dahlberg, P. D.; Engel, G. S.; Schaller, R. D.;

Talapin, D. V. Red, Yellow, Green, and Blue Amplified Spontaneous Emission and

Lasing Using Colloidal CdSe Nanoplatelets. *ACS Nano* **2015**, *9*, 9475−9485.

(21)   Ithurria, S.; Tessier, M. D.; Mahler, B.; Lobo, R. P. S. M.; Dubertret, B.; Efros, Al. L. Colloidal Nanoplatelets with Two−dimensional Electronic Structure. *Nat. Mater.* **2011**, *10*, 936−941.

(22)   Pelton, M.; Ithurria, S.; Schaller, R. D.; Dolzhnikov, D. S.; Talapin, D. V. Carrier Cooling in Colloidal Quantum Wells. *Nano Lett.* **2012**, *12*, 6158−6163.

(23)   Tessier, M. D.; Spinicelli, P.; dupont, D.; Patriarche, G.; Ithurria, S.; Dubertret B. Efficient Exciton Concentrators Built from Colloidal Core/Crown CdSe/CdS Semiconductor Nanoplatelets. *Nano Lett.*, **2014**, *14*, 207−213.

(24)   Pedetti, S.; Ithurria, S.; Heuclin, H.; Patriarche, G.; Dubertret, B. Type−II CdSe/CdTe Core/Crown Semiconductor Nanoplatelets. *J. Am. Chem. Soc.* **2014**, *136*, 16430−16438.

(25)   Mokari, T.; Rothenberg, E.; Popov, I.; Costi, R.; Banin, U. Selective Growth of Metal Tips onto Semiconductor Quantum Rods and Tetrapods. *Science* **2004**, *304*, 1787−1790.

(26)   Mokari, T.; Sztrum, C. G.; Salant, A. Rabani, E.; Banin, U. Formation of Asymmetric One-sided Metal-tipped Semiconductor Nanocrystal Dots and Rods. *Nat. Mater.* **2005**, *4*, 855−863.

(27)   Klimov, V. I. Optical Nonlinearities and Ultrafast Carrier Dynamics in Semiconductor Nanocrystals. *J. Phys. Chem. B* **2000**, *104*, 6112−6123.

(28)   Efros, A. L.; Kharchenko, V. A.; Rosen, M. Breaking the Phonon Bottleneck in

Nanometer Quantum Dots: Role of Auger-like Process. *Solid State Communication* **1995**,

93, 281−284.

(29)   Kambhampati, P. Hot Exciton Relaxation Dynamics in Semiconductor Quantum

Dots: Radiationless Transitions on the Nanoscale. *J. Phys. Chem. C* **2011**, *115*,

22089−22109.

(30)   Kambhampati, P. Unraveling the Structure and Dynamics of Excitons in

Semiconductor Quantum Dots. *Acc. Chem. Res.* **2011**, *44*, 1−13.

(31)   Sewall, S. L.; Cooney, R. R.; Anderson, K. E. H.; Dias, E. A.; Kambhampati, P.

State-to-State Exciton Dynamics in Semiconductor Quantum Dots. *Phys. Rev. B* **2006**, *74*,

235328.

(32)   Cooney, R. R.; Sewall, S. L.; Dias, E. A.; Sagar, D. M.; Anderson, K. E. H.;

Kambhampati, P. Unified Picture of Electron and Hole Relaxation Pathways in

Semiconductor Quantum Dots. *Phys. Rev. B* **2007**, *75*, 245311.

(33)   Guyot−Sionnest, P.; Wehrenberg, B.; Yu, D. Intraband Relaxation in CdSe

Nanocrystals and the Strong Influence of the Surface Ligands. *J. Chem. Phys.* **2005**, *123*,

074709.

(34)   Schaller, R. D.; Pietryga, J. M.; Goupalov, S. V.; Petruska, M. A.; Ivanov, S. A.;

Klimov, V. I. Breaking the Phonon Bottleneck in Semiconductor Nanocrystals via

Multiphonon Emission Induced by Intrinsic Nonadiabatic Interactions. *Phys. Rev. Lett.* **2005**, *95*, 196401.

(35)   Pandey, A.; Guyot-Sionnest, P. Slow Electron Cooling in Colloidal Quantum Dots. *Science* **2008**, *322*, 929−932.

(36)   Schaller, R. D.; Klimov, V. I. High Efficiency Carrier Multiplication in PbSe Nanocrystals: Implications for Solar Energy Conversion. *Phys. Rev. Lett.* **2004**, *92*, 186601.

(37)   Scheller, R. D.; Petruska, M. A.; Klimov, V. I. Effect of Electronic Structure on Carrier Multiplication Efficiency: Comparative Study of PbSe and CdSe Nanocrystals. *Appl. Phys. Lett.* **2005**, *87*, 253102.

(38)   Scheller, R. D.; Pietryga, J. M.; Klimov, V. I. Carrier Multiplication in InAs Nanocrystal Quantum Dots with an Onset Defined by the Energy Conservation Limit. *Nano Lett.* **2007**, *7*, 3469−3476.

(39)   Padilha, L. A.; Stewart, J. T.; Sandberg, R. L.; Bae, W. K.; Koh, W.-K.; Pietryga, J. M.; Klimov, V. I. Aspect Ratio Dependence of Auger Recombination and CarrierMultiplication in PbSe Nanorods. *Nano Lett.*, **2013**, *13*, 1092–1099.

(40)   Stewart, J. T.; Padilha, L. A.; Bae, W. K.; Koh, W.-K.; Pietryga, J. M.; Klimov, V. I. Carrier Multiplication in Quantum Dots within the Framework of Two Competing Energy Relaxation Mechanisms. *J. Phys. Chem. Lett.* **2013**, *4*, 2061–2068.

(41)   Kobayashi, Y.; Udagawa, T.; Tamai, N. Carrier Multiplication in CdTe Quantum

Dots by Single−Photon Timing Spectroscopy. *Chem. Lett.* **2009**, *38*, 830−831.

(42)   Klimov, V. I.; Mikhailovsky, A. A.; McBranch, D. W.; Leatherdale, C. A.; Bawendi,

M. G. Quantization of Multiparticle Auger Rates in Semiconductor Quantum Dots.

Science **2000**, *287*, 1011−1013.

(43)   Kobayashi, Y.; Pan, L.; Tamai, N. Effects of Size and Capping Reagents on

Biexciton Auger Recombination Dynamics of CdTe Quantum Dots. *J. Phys. Chem. C*,

2009, *113*, 11783−11789.

(44)   Kobayashi, Y.; Nishimura, T.; Yamagushi, H.; Tamai, N. Effect of Surface Defects

on Auger Recombination in Colloidal CdS Quantum Dots. *J. Phys. Chem. Lett.*, **2011**, *2*,

1051−1055.

(45)   Stewart, J. T.; Padilha, L. A.; Qazilbash, M. M.; Pietryga, J. M.; Midgett, A. G.;

Luther, J. M.; Beard, M. C.; Nozik, A. J.; Klimov, V. I. Comparison of Carrier

Multiplication Yields in PbS and PbSe Nanocrystals: The Role of Competing

Energy-Loss Processes. *Nano Lett*. **2012**, *12*, 622−628.

(46)   Shockley, W.; Queisser, H. J. Detailed Balance Limit of Efficiency of p−n Junction

Solar Cells. *J. Appl. Phys.* **1961**, *32*, 510−519.

(47)   Ross, R. T.; Nozik, A. J. Efficiency of hot−carrier solar energy converters. *J. Appl.

Phys.* **1982**, *53*, 3813−3818.

(48)   Marcus, R. A. On the Theory of Oxidation−Reduction Reactions Involving Electron

Transfer. I. *J. Chem. Phys.* **1956**, *24*, 966−978.

(49)   Marcus, R. A. Electrostatic Free Energy and Other Properties of States Having

Nonequilibrium Polarization. I. *J. Chem. Phys.* **1956**, *24*, 979−989.

(50)   Miller, J. R.; Calcaterra, L. T.; Closs, G. L. Intramolecular Long-Distance Electron

Transfer in Radical Anions. The Effects of Free Energy and Solvent on the Reaction Rates.

J. Am. Chem. Soc. **1984**, *106*, 3047–3049.

(51)   Matylitsky, V. V.; Dworak, L.; Breus, V. V.; Basché, T.; Wachtveitl, J. Ultrafast

Charge Separation in Multiexcited CdSe Quantum Dots Mediated by Adsorbed Electron

Acceptors. *J. Am. Chem. Soc.* **2009**, *131*, 2424–2425.

(52)   Zhu, H.; Song, N.; Rodríguez–Córdoba, W.; Lian, T. Wave Function Engineering for

Efficient Extraction of up to Nineteen Electrons from One CdSe/CdS Quasi–Type II

Quantum Dot. *J. Am. Chem. Soc.* **2012**, *134*, 4250–4257.

(53)   Zhu, H.; Yang, Y.; Hyeon−Deuk, K.; Califano, M.; Song, N.; Wang, Y.; Zhang, W.;

Prezhdo, O. V.; Lian, T. Auger−Assisted Electron Transfer from Photoexcited

Semiconductor Quantum Dots. *Nano Lett.* **2014**, *14*, 1263−1269.

(54)   Zhu, H.; Lian, T. Enhanced Multiple Exciton Dissociation from CdSe Quantum

Rods: The Effect of Nanocrystal Shape. *J. Am. Chem. Soc.* **2012**, *134*, 11289−11297.

(55)   Zhu, H.; Song, N.; Lian, T. Controlling Charge Separation and Recombination Rates

in CdSe/ZnS Type I Core−Shell Quantum Dots by Shell Thicknesses. *J. Am. Chem. Soc.* **2010**, *132*, 15038−15045.

(56)   Yang, Y.; Rodríguez–Córdoba, W.; Lian, T. Multiple Exciton Generation and Dissociation in PbS Quantum Dot–Electron Acceptor Complexes. *Nano Lett.*, **2012**, *12*, 4235–4241.

(57)   Tisdale, W. A.; Zhu, X. Y. Artificial Atoms on Semiconductor Surfaces. *Proc. Natl. Acad. Sci. U. S. A.* **2011**, *108*, 965−970.

(58)   Yang, Y.; Rodríguez−Córdoba, W.; Xiang, X.; Lian, T. Strong Electronic Coupling and Ultrafast Electron Transfer between PbS Quantum Dots and TiO_2 Nanocrystalline Films. *Nano Lett.* **2012**, *12*, 303−309.

(59)   Sambur, J. B.; Novet, T.; Parkinson, B. A. Multiple Exciton Collection in a Sensitized Photovoltaic System. *Science* **2010**, *330*, 63−66.

(60)   Mongin, D.; Shaviv, E.; Maioli, P.; Crut, A. Banin, U.; Fatti, N. D.; Vallée, F. Ultrafast Photoinduced Charge Separation in Metal–Semiconductor Nanohybrids. *ACS Nano* **2012**, *6*, 7034–7043.

(61)   Wu, K.; Li, Q.; Du, Y.; Chen, Z.; Lian, T. Ultrafast Exciton Quenching by Energy and Electron Transfer in Colloidal CdSe Nanosheet−Pt Heterostructures. *Chem. Sci.* **2015**, *6*, 1049−1054.

(62)   Sagarzazu, G.; Inoue, K.; Saruyama, M.; Sakamoto, M.; Teranishi, T.; Masuo, S.;

Tamai, N. Ultrafast Dynamics and Single Particle Spectroscopy of Au–CdSe Nanorods. *Phys. Chem. Chem. Phys.* **2013**, *15*, 2141–2152.

(63)   Klimov, V. I. Spectral and Dynamical Properties of Multiexcitons in Semiconductor Nanocrystals. *Annu Rev Phys Chem.* **2007**, *58*, 635–673.

(64)   Efros, A. L.; Rosen, M. The Electronic Structure of Semiconductor Nanocrystals. *Annu Rev Phys Chem.* **2000**, *30*, 475–521.

(65)   Norris, D. J.; Bawendi, M. G. Measurement and Assignment of the Size-dependent Optical Spectrum in CdSe Quantum Dots. *Phys. Rev. B* **1996**, *53*, 16338–16346.

(66)   Klimov, V. I.; McBranch, D. W. Femtosecond 1P-to-1S Electron Relaxation in Strongly Confined Semiconductor Nanocrystals. *Phys. Rev. Lett.* **1998**, *80*, 4028–4031.

(67)   Klimov, V. I. Nanocrystal Quantum Dots Second Edition. *CRC Press* **2010**.

(68)   Klimov, V. I. Semiconductor and Metal Nanocrystals: Synthesis and Electronic and Optical Properties *CRC Press* **2003**.

(69)   La Mer, V. K.; Dinegar, R. H. Theory, Production and Mechanism of Formation of Monodispersed Hydrosols. *J. Am. Chem. Soc.* **1950**, *72*, 4847.

(70)   Qu, L.; Peng, Z. A.; Peng, X. Alternative Routes toward High Quality CdSe Nanocrystals. *Nano Lett.*, **2001**, *1*, 333–337.

(71)   Murray, C. B.; Kagan, C. R. Bawendi, M. G. Synthesis and Characterization of Monodisperse Nanocrystals and Close-Packed Nanocrystal Assemblies. *Annu Rev Phys*

Chem. **2000**, *30*, 545–610.

(72)   Nasilowski, M.; Mahler, B.; Lhuillier, E.; Ithurria, S.; Dubertret, B. Two-Dimensional Colloidal Nanocrystals. *Chem. Rev.* **2016**, *116*, 10934–10982.

(73)   Blanton, S. A.; Leheny, R. L.; Hines, M. A.; Guyot-Sionnest, P Dielectric Dispersion Measurements of CdSe Nanocrystal Colloids: Observation of a Permanent Dipole Moment. *Phys. Rev. Lett.* **1997**, *79*, 865–868.

(74)   Ithurria, S.; Tessier, M. D.; Mahler, B.; Lobo, R. P. S. M.; Dubertret, B.; Efros, Al. L. Colloidal Nanoplatelets with Two−dimensional Electronic Structure. *Nat. Mater.* **2011**, *10*, 936−941.

(75)   Prudnikau, A.; Chuvilin, A.; Artemyev, M. CdSe−CdS Nanoheteroplatelets with Efficient Photoexcitation of Central CdSe Region through Epitaxially Grown CdS Wings. *J. Am. Chem. Soc.* **2013**, *135*, 14476−14479.

(76)   Delikanli, S.; Guzelturk, B.; Hernández-Martínez, P. L.; Erdem, T.; Kelestemur, Y.; Olutas, M.; Akgul, M. Z.; Demir, H. V. Continuously Tunable Emission in Inverted Type-I CdS/CdSe Core/Crown Semiconductor Nanoplatelets. *Adv. Funct. Mater.* **2015**, *25*, 4282−4289.

(77)   Ithurria, S.; Bousquet, G.; Dubertret, B. Continuous Transition from 3D to 1D Confinement Observed during the Formation of CdSe Nanoplatelets. *J. Am. Chem. Soc.* **2011**, *133*, 3070–3077.

(78)   Bouet, C.; Tessier, M. D.; Ithurria, S.; Mahler, B.; Nadal, B.; Dubertret, B. Flat

Colloidal Semiconductor Nanoplatelets. *Chem. Mater.* **2013**, *25*, 1262–1271.

(79)   She, C.; Fedin, I.; Dolzhnikov, D. S.; Demortière, A.; Schaller, R. D.; Pelton, M.;

Talapin, D. V. Low-Threshold Stimulated Emission Using Colloidal Quantum Wells.

Nano Lett. **2014**, *14*, 2772–2777.

(80)   Efros, A. L.; Efros, A. L. Interband Absorption of Light in a Semiconductor Sphere.

Sov. Phys. Semicond. **1982**, *16*, 772–775.

(81)   Brus, L. E. Electron–electron and Electron–hole Interactions in Small Semiconductor

Crystallites: The Size Dependence of the Lowest Excited Electronic State. *J. Chem. Phys.*

1984, *80*, 4403–4409.

(82)   Ekimov, A. I.; Hache, F.; Schanne-Klein, M. C.; Ricard, D.; Flytzanis, C.;

Kudryavtsev, I. A.; Yazeva, T. V.; Rodina, A. V. Efros, A. L. Absorption and

Intensity-dependent Photoluminescence Measurements on CdSe Quantum Dots

Assignment of the First Electronic Transitions. *J. Opt. Soc. Am. B* **1998**, *10*, 100–107.

(83)   Hu, J.; Lin, W.; Liang, S. L.; Yang, W.; Alivisatos, A. P Semiempirical

Pseudopotential Calculation of Electronic States of CdSe Quantum Rods. *J. Phys. Chem.*

B, **2002**, *106*, 2447–2452.

(84)   Bose, S.; Song, Z.; Fan, W. J.; Zhang, D. H. Effect of Lateral Size and Thickness on

the Electronic Structure and Optical Properties of Quasi Two-dimensional CdSe and CdS

Nanoplatelets. *J. Appl. Phys*. **2016**, *119*, 143107.

(85)   Klimov, V. I.; McGuire, J. A.; Schaller, R. D.; Rupasov, V. I. Scaling of multiexciton

lifetimes in semiconductor nanocrystals. *Phys. Rev. B* **2008**, *77*, 195324.

(86)   Kobayashi, Y.; Tamai, N. Size-Dependent Multiexciton Spectroscopy and Moderate

Temperature Dependence of Biexciton Auger Recombination in Colloidal CdTe Quantum

Dots. *J. Phys. Chem. C* **2010**, *114*, 17550–17556.

(87)   Heyon–Deuk, K.; Kobayashi, Y.; Tamai, N. Evidence of Phonon-Assisted Auger

Recombination and Multiple Exciton Generation in Semiconductor Quantum Dots

Revealed by Temperature-Dependent Phonon Dynamics. *J. Phys. Chem. Lett.* **2014**, *5*,

99–105.

(88)   Barzykin, A. V.; Tachiya, M. Stochastic models of charge carrier dynamics in

semiconducting nanosystems. *J. Phys.: Condens. Matter.* **2007**, *19*, 065105.

(89)   Htoon, H.; Hollingsworth, J. A.; Dickerson, R.; Klimov, V. I.; Effect of Zero- to

One-Dimensional Transformation on Multiparticle Auger Recombination in

Semiconductor Quantum Rods Scaling of multiexciton lifetimes in semiconductor

nanocrystals. *Phys. Rev. Lett.* **2003**, *91*, 227401.

(90)   Aerts, M.; Spoor, F. C. M.; Grozema, F. C.; Houtepen, A. J.; Schins, J. M.; Siebbeles,

L. D. A. Cooling and Auger Recombination of Charges in PbSe Nanorods: Crossover

from Cubic to Bimolecular Decay. *Nano Lett.* **2013**, *13*, 4380–4386.

(91)   Ueda, A.; Tayagaki, T.; Kanemitsu, Y. Dynamics of Quantized Auger Recombination in CdSe Nanocrystals Studied by Femtosecond Intraband Pump–Probe Spectroscopy. *J. Phys. Soc. Jpn.* **2009**, *78*, 083706.

(92)   Bartnik, A. C.; Efros, A. L.; Koh, W.-K.; Murray, C. B.; Wise, F. W. Electronic States and Optical Properties of PbSe Nanorods and Nanowires. *Phys. Rev. B* **2010**, *82*, 195313.

(93)   Kunneman, L. T.; Tessier, M. D.; Heuclin, H.; Dubertret, B; Aulin, Y. V.; Grozema, F. C.; Schins, J. M.; Siebbeles, L. D. A. Bimolecular Auger Recombination of Electron−Hole Pairs in Two-Dimensional CdSe and CdSe/CdZnS Core/Shell Nanoplatelets. *J. Phys. Chem. Lett.* **2013**, *4*, 3574–3578.

(94)   Klimov, V. I.; McBranch, D. W.; Leatherdale, C. A.; Bawendi M. G. Electron and Hole Relaxation Pathways in Semiconductor Quantum Dots. *Phys. Rev. B* **1999**, *60*, 13740.

(95)   Yu, P.; Nedeljkovic, J. M.; Ahrenkiel, P. A.; Ellingson, R. J.; Nozik, A. J. Size Dependent Femtosecond Electron Cooling Dynamics in CdSe Quantum Rods. *Nano Lett.* **2004**, *4*, 1089–1092.

(96)   Sippel, P.; Albrecht, W.; Bok, J. C.; Dijk-Moes, R. J. A.; Hannappel, T.; Eichberger, R.; Vanmaekelbergh, D. Femtosecond Cooling of Hot Electrons in CdSe Quantum-Well Platelets. *Nano Lett.* **2015**, *15*, 2409–2416.

(97)   Miller, J. R.; Beitz, J. V.; Huddleston, R. K. Effect of Free Energy on Rates of

Electron Transfer between Molecules. *J. Am. Chem. Soc.* **1984**, *106*, 5057–5068.

(98)   Okuhata, T.; Kobayashi, Y.; Nonoguchi, Y.; Kawai, T.; Tamai, N. Ultrafast Carrier

Transfer and Hot Carrier Dynamics in PbS−Au Hybrid Nanostructures. *J. Phys. Chem. C*

2015, *119*, 2113–2120.

(99)   Tisdale, W. A.; Williams, K. J.; Timp, B. A.; Norris, D. J.; Aydil, E. S.; Zhu, X.-Y.

Hot−Electron Transfer from Semiconductor Nanocrystals. *Science* **2010**, *328*, 1543−1547.

(100)   Wang, Y.; Wang, H.; Li, Z.; Zhao, J.; Wang, L.; Chen, Q.; Wang, W.; Sun, H.

Electron Extraction Dynamics in CdSe and CdSe/CdS/ZnS Quantum Dots Adsorbed with

Methyl Viologen. *J. Phys. Chem. C* **2014**, *118*, 17240−17246.

(101)   Sagarzazu, G.; Inoue, K.; Saruyama, M.; Sakamoto, M.; Teranishi, T.; Tamai, N.

Hot-electron transfer in Au-CdSe nanorods. *Submitted.*
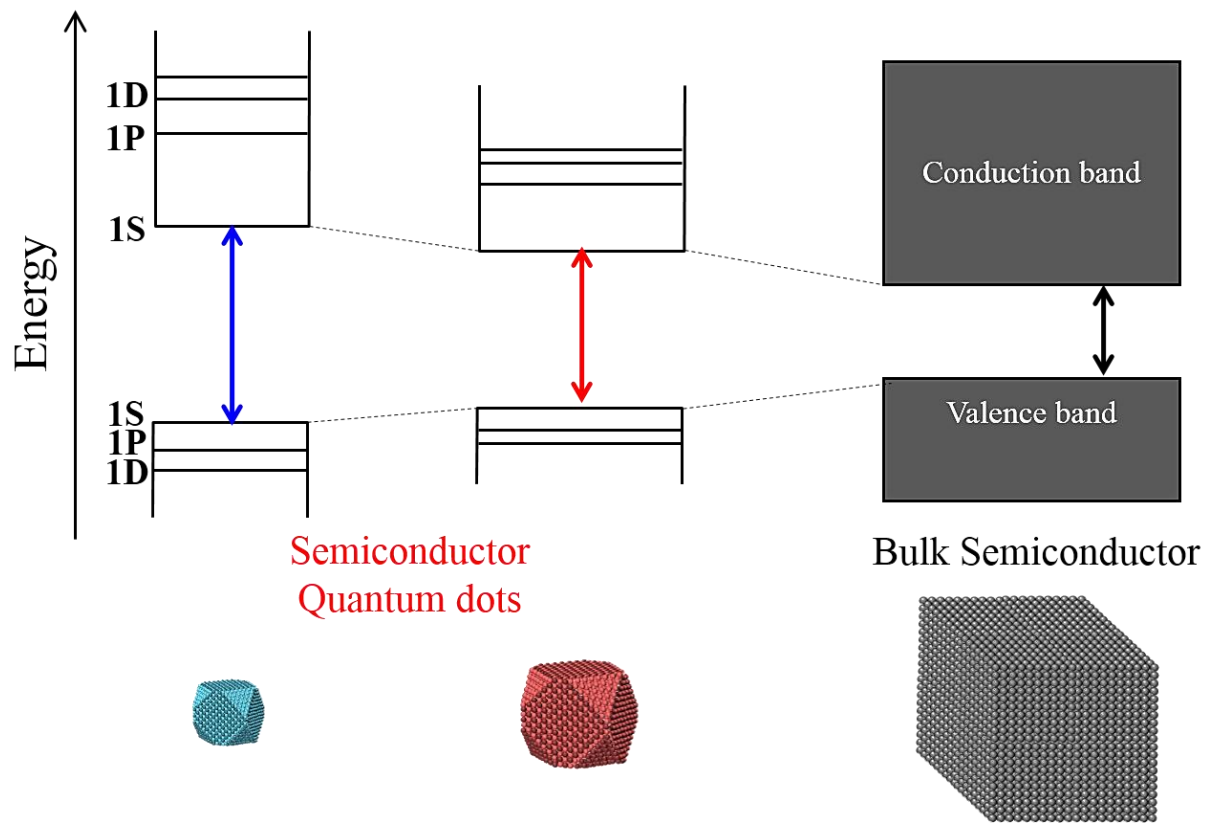
Figure 1.1 Size dependent electronic structures of semiconductor QDs and the band structure

of bulk semiconductors.
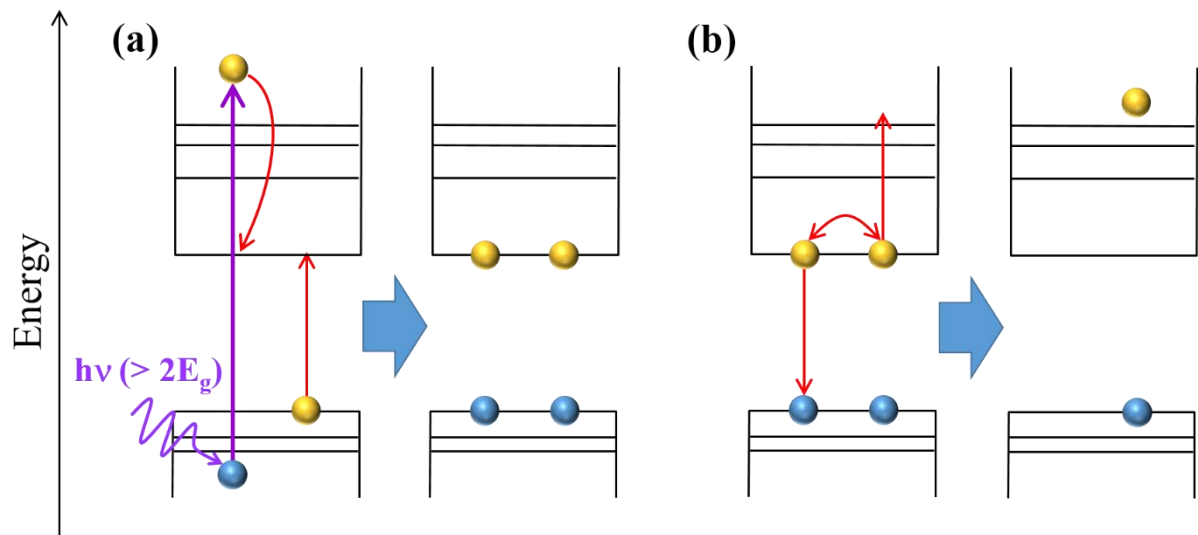
Figure 1.2 Schemes of the (a) multiple exciton generation process and (b) Auger recombination process.
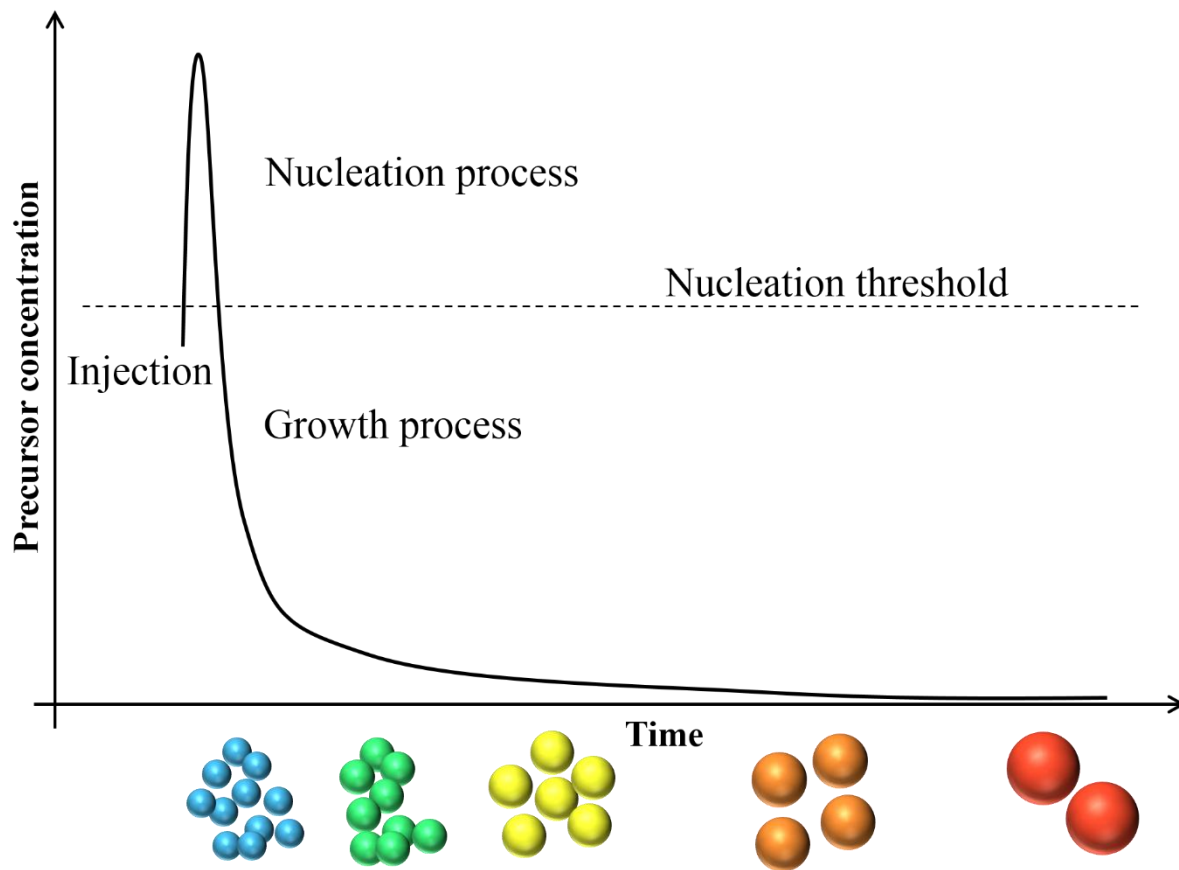
Figure 1.3 The scheme for a nucleation and growth of colloidal semiconductor nanocrystals based on La Mer's model.
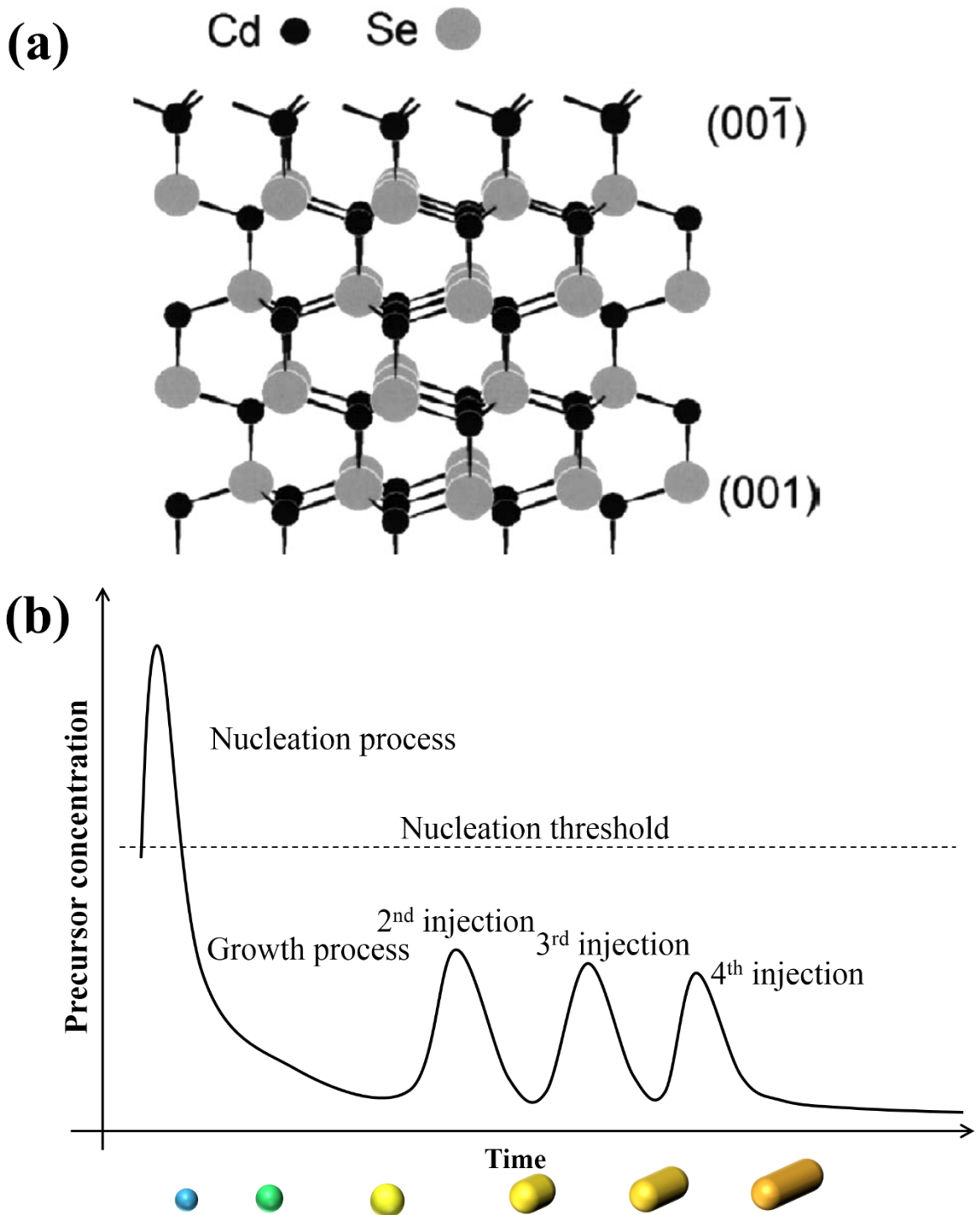
Figure 1.4 (a) The crystal structure of wrutzite CdSe[12] and (b) the scheme of anisotropic growth of colloidal semiconductor nanocrystals using a multiple injection method.
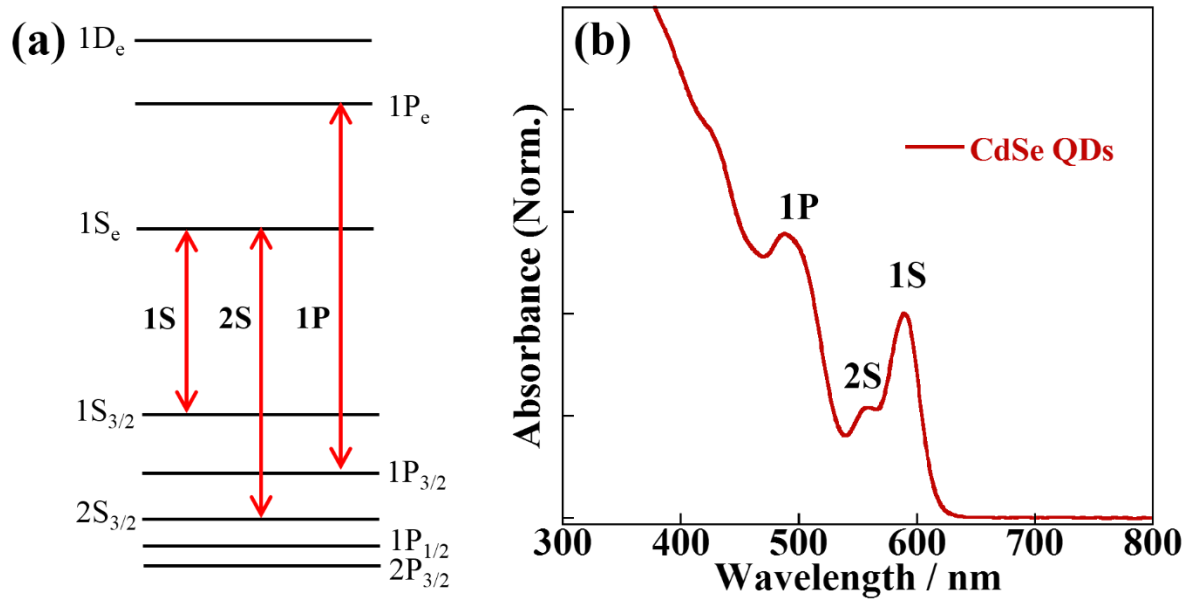
Figure 1.5 (a) The energy diagram and optical transitions of CdSe QDs and (b) absorption

spectrum of typical CdSe QDs.
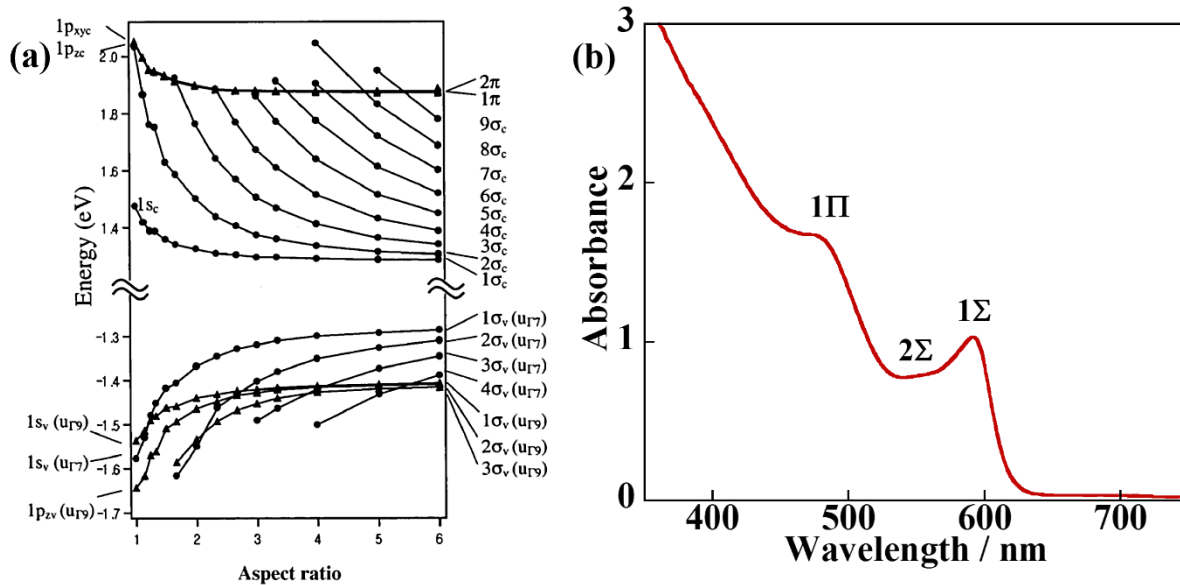
Figure 1.6 (a) The calculated electronic structure of CdSe nanocrystals with different aspect ratio[83] and (b) absorption spectrum of typical CdSe NRs.
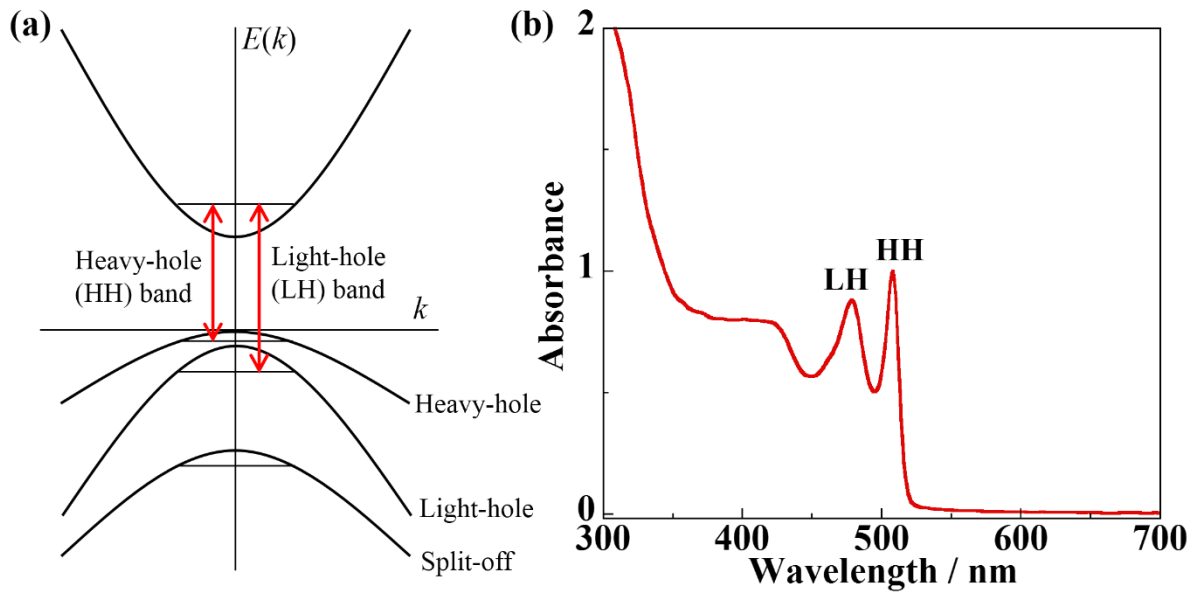
Figure 1.7 (a) The energy diagram and optical transitions of CdSe NPLs and (b) absorption

spectrum of typical CdSe NPLs.
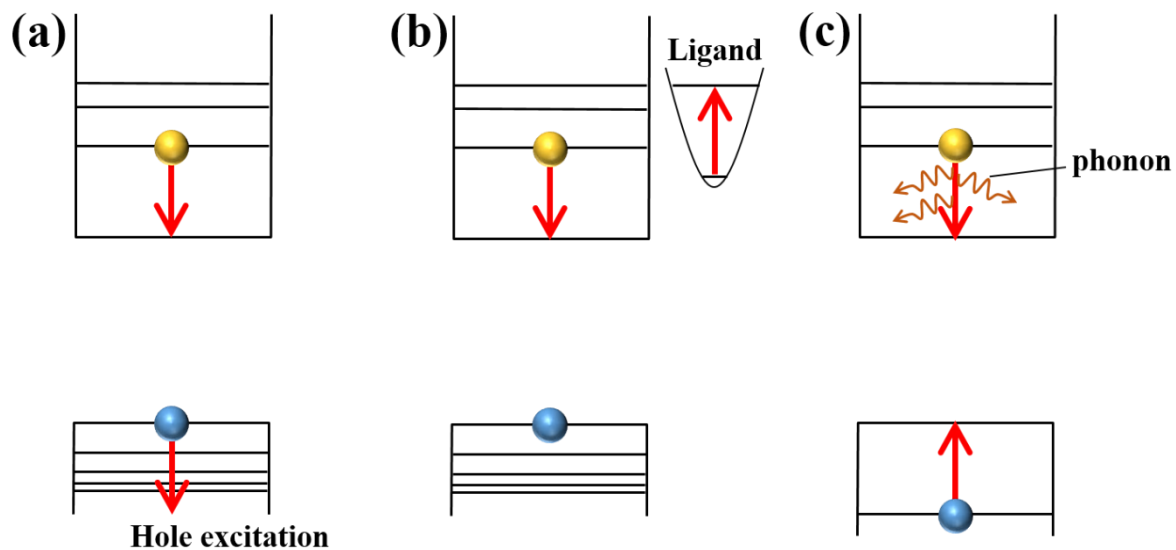
Figure 1.8 Schemes of hot electron relaxation in colloidal semiconductor nanocrystals via (a) Auger cooling process, (b) energy transfer to surface ligands, and (c) multiple phonon emission.
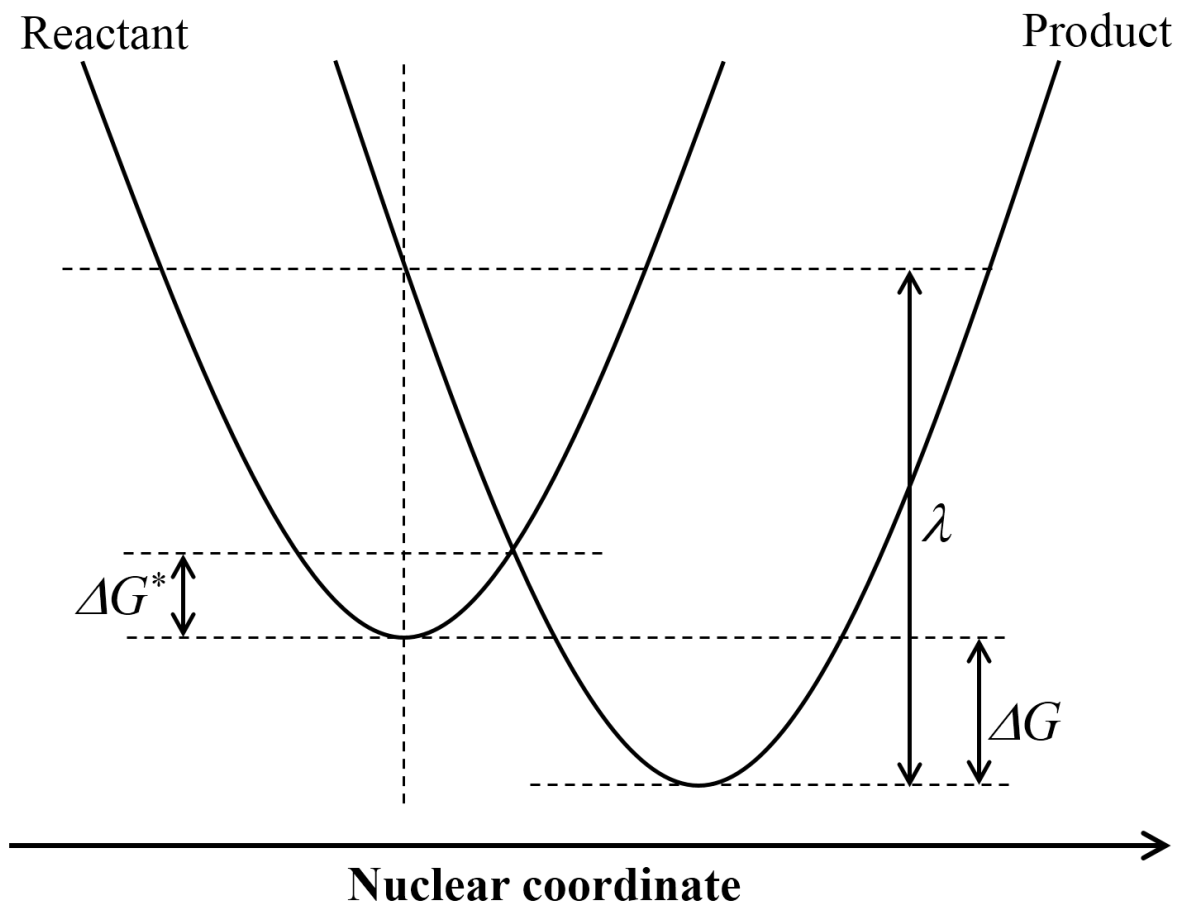
Figure 1.9 Potential energy curves of the reactant and product.
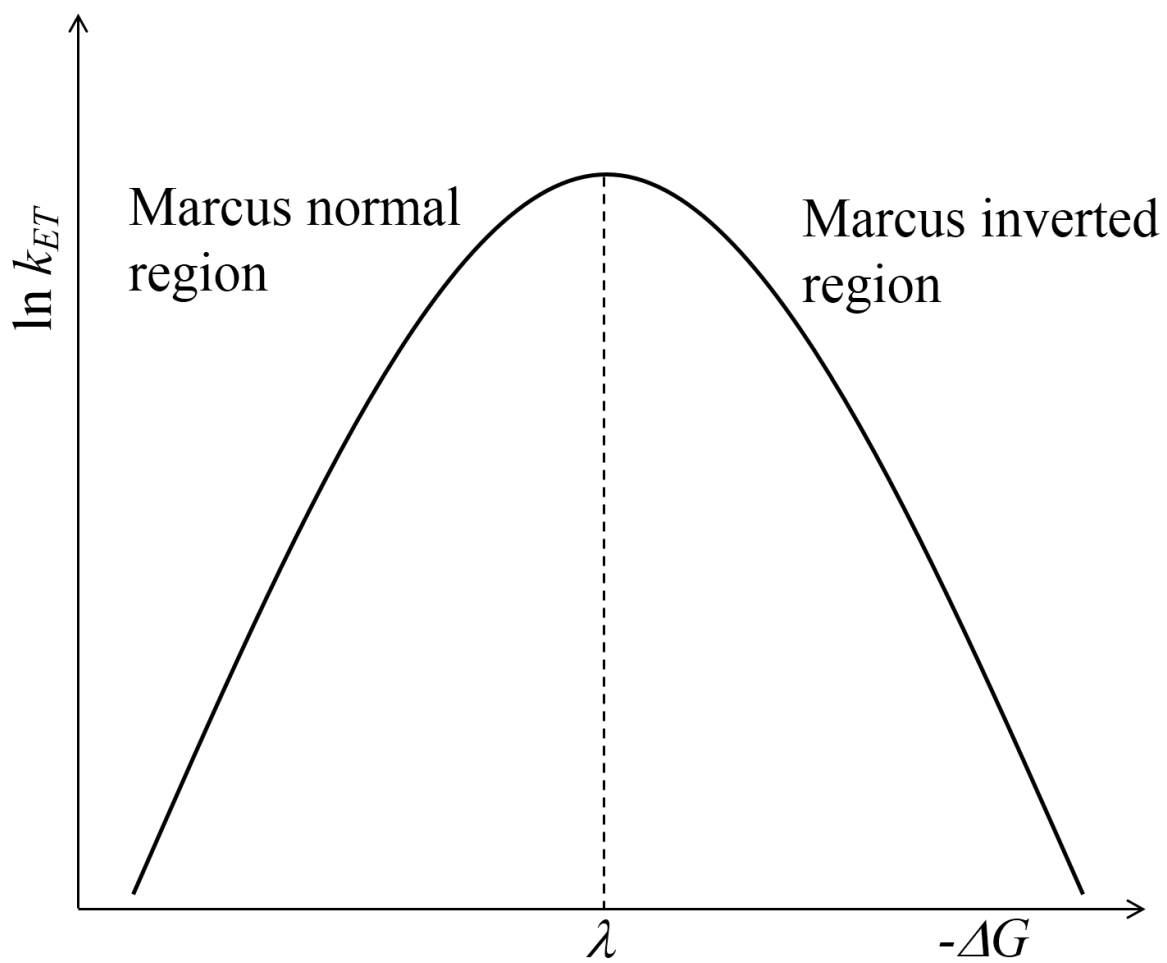
Figure 1.10 The energy gap dependence of electron transfer rates based on the Marcus theory.

Chapter 2

Synthesis of Colloidal Semiconductor Nanocrystals and Semiconductor-metal HNs

2.1   CdSe/CdS core/shell QDs and core/shell QD-MV^{2+} complexes

a) Synthesis of CdSe/CdS core/shell QDs

Trioctylphosphine (90%, TOP) and cadmium oxide (99%, CdO) were purchased from Alfa Aesar and Kanto Chemical Co., Inc., respectively. 1-octadecene (90%) and sulfur (S, 99.99%) were purchased from Tokyo Chemical Industry Co., Ltd. and Kojundo Chemical Laboratory, respectively. Tetradecylphosphonic acid (97%), Selenium powder (99.99%, Se), ocadecylamine (99%), oleic acid (90%), and trioctylphosphine oxide (99%) were purchased from Sigma-Aldrich. Ethanol (99.8%), hexane (96%), and chloroform (99%) were purchased from Kishida Chemical Co.

The core CdSe QDs capped with tetradecylphosphonic acid were synthesized with apparatuses shown in Figure 2.1 according to the method reported by Freitas et al.[1] Briefly, 0.11 g of CdO, 0.43 g of tetradecylphosphonic acid, and 7 g of trioctylphosphine oxide were introduced into the three-neck flask. The mixture was heated to 120 °C and degassed for 20 min. Then, the mixture was heated to 360 °C under argon atmosphere until the mixture became transparent. Then, the temperature was lowered to 270 °C and Se precursor solution prepared by dissolving the 79 mg of Se in 5 mL of trioctylphosphine was injected to the mixture. The reaction mixture was maintained at 270 °C for 7 minutes. After that, the reaction mixture was cooled to room temperature. Core CdSe QDs were purified by ethanol and redispersed in hexane.

The CdSe/CdS core/shell QDs were synthesized with apparatuses shown in Figure 2.1 according to the method reported by Zhang et al.[2] For the CdS shell growth, we prepared the Cd- and S-precursor solution. The Cd precursor solution was prepared by dissolving the 102 mg of cadmium oxide in 2 mL of oleic acid and 18 mL of 1-octadecene at 250 °C. The S precursor solution was prepared by dissolving the 13 mg of sulfur in 10 mL of 1-octadecene at 200 °C. The 3.7 mL of the presynthesized core CdSe QDs, 1.5 g of octadecylamine, and 6

48

mL of 1-octadecene were mixed in the three-neck flask. The mixture was heated to 60 °C and degassed for 30 min. Then, the mixture was heated to 240 °C under argon atmosphere. Cd- and S-precursor solution were alternately added to CdSe QDs solution with an interval of 10 minutes. We synthesized CdSe/CdS core/shell QDs A and B by adding two kinds of precursor solutions one and two times, respectively. CdSe/CdS core/shell QDs were purified and redispersed in chloroform.

b) Preparation of CdSe/CdS core/shell QD-MV^{2+} complexes

The CdSe/CdS core/shell QD-MV^{2+} complexes were prepared by adding a drop of highly concentrated MV^{2+} in methanol to the chloroform solution of CdSe/CdS core/shell QDs.[3] Then, any undissolved MV^{2+} and aggregation of NPLs were removed by filtration using a 1 μm syringe filter. Because of the insolubility of MV^{2+} in chloroform, all MV^{2+} present in the CdSe/CdS core/shell QD solution is considered to be adsorbed on the surface of the core/shell QDs.

2.2   4-monolayer CdSe NPLs and CdSe NPL-MV^{2+} complexes

a) Synthesis of CdSe NPLs with different lateral size

Selenium powder (99.99%, Se), oleic acid (90%) and methyl viologen dichloride hydrate (98%, MV^{2+}) were purchased from Sigma-Aldrich. Cadmium acetate dihydrate (98%) was purchased from Wako Pure Chemical Industries, Ltd. Sodium myristate (>98%) and 1-octadecene (90%) were purchased from Tokyo Chemical Industry Co., Ltd. Cadmium nitrate tetrahydrate (>98.5%), methanol (99.8%), hexane (96%), and chloroform (99%) were purchased from Kishida Chemical Co.

Cadmium myristate was prepared for the synthesis of CdSe NPLs.[4] 1.23 g of Cadmium nitrate tetrahydrate was dissolved in 40 mL of methanol. This methanol solution was added to the 250 mL of methanol containing 3.13 g of sodium myristate. The white

precipitate of cadmium myristate was filtered, and dried under vacuum overnight.

CdSe NPLs with the different lateral size were synthesized with apparatuses shown in Figure 2.1 according to the method reported by Tessier et al.[5] Briefly, 170 mg of cadmium myristate, 12 mg of Se, and 1-octadecene (15 mL) were mixed in a three-neck flask, and the mixture was degassed at room temperature. Then, the mixture was heated, and 80 mg of cadmium acetate was added at 195 °C. The reaction mixture was maintained at 240 °C for 4-20 minutes for the control of the lateral size. Subsequently, the mixture was cooled to 40 °C, and 2 mL of oleic acid and 15 mL of hexane were added. The mixture was centrifuged, and the precipitate containing CdSe NPLs was dispersed in chloroform.

b) Preparation of CdSe NPL-MV^{2+} complexes

The CdSe NPL-MV^{2+} complexes were prepared by adding a drop of highly concentrated MV^{2+} in methanol to the chloroform solution of CdSe NPLs.[3] Then, the solution was sonicated, and any undissolved MV^{2+} and aggregation of NPLs were removed by filtration using a 1 μm syringe filter. Because of the insolubility of MV^{2+} in chloroform, all MV^{2+} present in the CdSe NPL solution is considered to be adsorbed on the surface of the NPLs.

2.3   oleylamine capped PbS QDs and PbS QD-Au HNs

a) Synthesis of PbS QDs

Lead chloride (PbCl$_2$, 99.999%) and sulfur (S, 99.99%) were purchased from Kojundo Chemical Laboratory. Oleylamine (OLAm, 70%), Trioctylphosphine (TOP, 90%) and oleic acid (90%) were purchased from Sigma-Aldrich. 1,1,2,2-Tetrachloroethylene (TCE, 99.0%), methanol (99.8%), ethanol (99.8%), and toluene (99.5%) were purchased from Kishida Chemical Co.

OLAm capped PbS QDs were synthesized with apparatuses shown in Figure 2.1 according to the method reported by Moreels et al.[6] Briefly, 0.417 g (1.5 mmol) of $PbCl_2$ and 5 mL of OLAm were mixed in a three neck flask and degassed for 1 hour under vacuum at 120 °C. Sulfur precursor solution was prepared under a nitrogen atmosphere by heating a mixture of 24 mg (0.75 mmol) of S and 2.25 mL of OLAm for 30 min at 120 °C. 1.1 mL of S precursor solution was then injected into the Pb-OLAm suspension under a nitrogen atmosphere at 120 °C. After 2 min, the reaction mixture was cooled to room temperature. 6 mL of toluene was added to the reaction mixture and the reaction mixture was centrifuged to remove excess $PbCl_2$. PbS QDs in the supernatant was purified by ethanol and dispersed in a 20:3 mixture of toluene and oleic acid. PbS QDs with various sizes (reference A, B, and C) were synthesized by injecting the S precursor solution including 170 μL of TOP to the Pb-OLAm suspension and varying the reaction temperature (80-100 °C) and reaction time (3-15 min). All of PbS QDs were purified by methanol and dissolved in TCE for measurements in the near-IR region.

b) Synthesis of PbS QD-Au HNs

Didodecyldimethylammonium bromide (DDAB, 98%), gold chloride (AuCl₃, 99.99%), and dodecylamine (DDA, 98%) were purchased from Sigma-Aldrich. 1,1,2,2-Tetrachloroethylene (TCE, 99.0%), methanol (99.8%), ethanol (99.8%), and toluene (99.5%) were purchased from Kishida Chemical Co.

PbS QD-Au HNs were synthesized under a nitrogen atmosphere according to the some modifications of a previously reported method.[7] Briefly, a gold precursor solution was prepared by dissolving 65 mg (0.35 mmol) of DDA, 69 mg (0.15 mmol) of DDAB, and 2 mg (6.6 μmol) of $AuCl_3$ in toluene. Three kinds of PbS QD-Au HNs were synthesized by changing the concentration of Au precursor, in which $AuCl_3$ was dissolved in 4, 3, and 2 mL

of toluene for PbS QD-Au HNs A, B, and C, respectively. In each case, 2 mL of the precursor solution was injected into the toluene solution of PbS QDs at room temperature, after which the reaction mixture was stirred for 10 min. The reaction was stopped by adding methanol to the reaction mixture. All of PbS QD-Au HNs were redispersed in TCE for measurements in the near-IR region.

2.4 Au NPs attached CdSe nanocrystals with different quantum confinement dimensionality

a) Synthesis of CdSe QDs

Trioctylphosphine (90%, TOP) and cadmium oxide (99%, CdO) were purchased from Alfa Aesar and Kanto Chemical Co., Inc., respectively. 1-octadecene (90%) was purchased from Tokyo Chemical Industry Co., Ltd. Selenium powder (99.99%, Se), ocadecylamine (99%) and trioctylphosphine oxide (99%) were purchased from Sigma-Aldrich. Stearic acid (98%), methanol (99.8%) and toluene (99.5%) were purchased from Kishida Chemical Co.

Octadecylamine capped CdSe QDs were synthesized with apparatuses shown in Figure 2.1 according to the method reported by Goodman et al.[8] Briefly, 51.2 mg of CdO, 0.454 g of stearic acid and 16 mL of 1-octadecene were mixed in a three neck flask. The mixture was heated to 125 °C and degassed for 1 hour under vacuum. Then, the mixture was heated to 250 °C under argon atmosphere until the mixture became transparent. The mixture was cooled to room temperature, and 2 g of octadecylamine and 2 g of trioctylphosphine oxide were added to the mixture. After that, the mixture was heated to 125 °C and degassed for 1 hour under vacuum, and the mixture was heated to 300 °C. Se precursor solution prepared by dissolving 78 mg of Se in 1.7 mL of TOP was injected into the three neck flask. The reaction mixture was maintained at 300 °C for 20 minutes. Then, the mixture was cooled

to 80 °C, and toluene was added to the aliquot of reaction mixture containing CdSe QDs (reaction mixture:toluene = 1:2). CdSe QDs were precipitated by adding excess methanol and centrifugation. The purified CdSe QDs were redispersed in toluene.

b) Synthesis of CdSe NPLs

4-monolayer CdSe NPLs were synthesized according to the method of 2.2 a). The reaction time was 7 minutes, and the synthesized CdSe NPLs were dispersed in toluene.

c) Synthesis of CdSe QD-Au HNs and NPL-Au HNs

Didodecyldimethylammonium bromide (DDAB, 98%), gold chloride (AuCl$_3$, 99.99%), and dodecylamine (DDA, 98%) were purchased from Sigma-Aldrich. Methanol (99.8%), and toluene (99.5%) were purchased from Kishida Chemical Co.

CdSe QD-Au HNs were synthesized under a nitrogen atmosphere according to the previously reported method.[9] Briefly, a gold precursor solution was prepared by dissolving 9 mg of DDA, 10 mg of DDAB, and 3 mg of AuCl$_3$ in 1mL of toluene. The prepared Au precursor solution was added into toluene solution of CdSe QDs at 0 °C. Two kinds of CdSe QD-Au HNs were synthesized by changing the amount of Au precursor solution and reaction time. For the synthesis of CdSe QD-Au HNs A (B), 300 μL (500 μL) of Au precursor solution was added to the toluene solution of CdSe QDs, and the reaction mixture was stirred for 10 (20) minutes. After that, CdSe QD-Au HNs were precipitated by adding excess methanol and centrifugation, CdSe QD-Au HNs were redispersed in toluene.

CdSe NPL-Au HNs were synthesized according to the modifications of a method for CdSe QD-Au HNs. Briefly, a gold precursor solution was prepared by dissolving 9 mg of DDA, 10 mg of DDAB, and 1 mg of AuCl$_3$ in 10 mL of toluene. 100 μL of Au precursor solution was added into toluene solution of CdSe NPLs at room temperature, and the reaction mixture was stirred for 10 minutes. CdSe NPL-Au HNs were precipitated by adding excess methanol and centrifugation, and CdSe NPL-Au HNs were redispersed in toluene.

References

(1) Freitas, J. N.; Grova, I. R.; Akcelrud, A. C.; Arici, E.; Sariciftci, N. S.; Noqueira, A. F. The effects of CdSe incorporation into bulk heterojunction solar cells. *J. Mater. Chem.* **2010**, *20*, 4845–4853.

(2) Zhang, J.; Zhang, X.; Zhang, J. Y. Dependence of Microstructure and Luminescence on Shell Layers in Colloidal CdSe/CdS Core/Shell Nanocrystals. *J. Phys. Chem. C* **2010**, *114*, 3904–3908.

(3) Zhu, H.; Lian, T. Enhanced Multiple Exciton Dissociation from CdSe Quantum Rods: The Effect of Nanocrystal Shape. *J. Am. Chem. Soc.* **2012**, *134*, 11289–11297.

(4) Ithurria, S.; Bousquet, G.; Dubertret B. Continuous Transition from 3D to 1D Confinement Observed during the Formation of CdSe Nanoplatelets. *J. Am. Chem. Soc.* **2011**, *133*, 3070–3077.

(5) Tessier, M. D.; Biadala, L.; Bouet, C.; Ithurria, S.; Abecassis, B.; Dubertret, B. Phonon Line Emission Revealed by Self-Assembly of Colloidal Nanoplatelets. *ACS Nano* **2013**, *7*, 3332−3340.

(6) Moreels, I.; Justo, Y.; Geyter, B. D.; Haustraete, K.; Martins, J. C.; Hens, Z. Size-Tunable, Bright, and Stable PbS Quantum Dots: A Surface Chemistry Study. *ACS Nano* **2011**, *5*, 2004−2012.

(7) Yang, J.; Elim, H. I.; Zhang, Q.; Lee, J. Y.; Ji, W. Rational Synthesis, Self-Assembly, and Optical Properties of PbS−Au Heterogeneous Nanostructures via Preferential Deposition. *J. Am. Chem. Soc.* **2006**, *128*, 11921–11926.

(8) Goodman, S. M.; Singh, V.; Ribot, J. C.; Chatterjee, A.; Nagpal, P. Multiple Energy Exciton Shelves in Quantum-Dot–DNA Nanobioelectronics. *J. Phys. Chem. Lett.* **2014**, *5*, 3909–3913.

(9) Sagarzazu, G.; Inoue, K.; Saruyama, M.; Sakamoto, M.; Teranishi, T.; Masuo, S.; Tamai,

N. Ultrafast Dynamics and Single Particle Spectroscopy of Au–CdSe Nanorods. Phys. Chem. Chem. Phys. 2013, 15, 2141–2152.
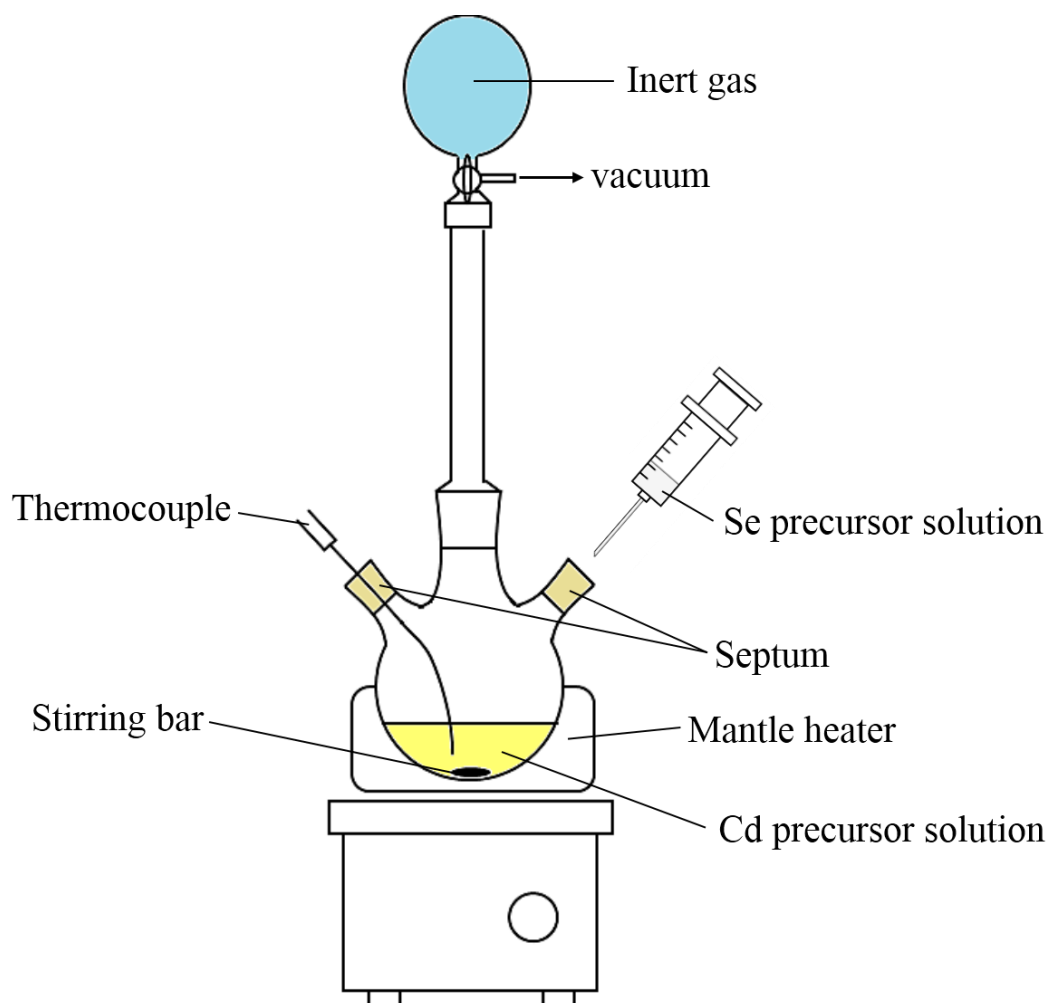
Figure 2.1 The illustration of apparatuses for the colloidal synthesis of semiconductor nanocrystals.

Chapter 3

Hot Electron Transfer from CdSe/CdS Core/shell QDs to Methyl Viologen

3.1 Abstract

The efficient hot electron transfer from colloidal semiconductor nanocrystals to the outside promotes the development of the highly efficient solar cells. However, the previous studies on the electron extraction from semiconductor nanocrystals have focused on the electron transfer from conduction band-edge state of semiconductor nanocrystals. In the present study, we prepared CdSe/CdS core/shell QD-methyl viologen (MV^{2+}) complexes with different shell thickness, and analyzed the shell thickness dependence on the hot electron transfer processes, as well as the electron transfer from the band-edge state, by using the femtosecond pump-probe spectroscopy with the state-selective excitation technique. The electron transfer from conduction band-edge state of CdSe/CdS core/shell QDs to MV^{2+} became slower with increasing the shell thickness, which was originated from the decrease of electronic coupling constant between QDs and MV^{2+} adsorbed on the surface. In contrast, the hot electron transfer from CdSe/CdS core/shell QDs to MV^{2+} did not depend on the shell thickness or became slightly faster as the shell thickness increased.

3.2 Introduction

The efficient charge separation from colloidal semiconductor nanocrystals is one of the most important processes for the application of light-energy conversion, such as the photovoltaics and photocatalysis. In particular, much attention has been paid to the development of next generation solar cells using the colloidal semiconductor nanocrystals. In bulk semiconductors, photoexcited carrier with excess energy (hot carrier) relaxes immediately to the band-edge states by a phonon emission because the bulk semiconductor have continuous band structures. As a result, the photon-to-current conversion efficiency of the conventional solar cells using bulk semiconductors is theoretically limited to 32.7% by fast relaxation of hot carrier, which is well known as the Shockley-Queisser limit.[1] In contrast,

semiconductor quantum dots (QDs) have the discrete energy states when electron and hole are confined in a size smaller than the exciton Bohr radius. For the II-VI semiconductor QDs, since the energy spacing between the conduction band-edge state ($1S_e$ state) and next higher energy state ($1P_e$ state) is 10 times larger than the LO phonon energy,[2] excited hot electron relaxes to the band-edge state by different processes from bulk semiconductors, such as the Auger cooling process, in which a electron relaxes from $1P_e$ to $1S_e$ state via energy transfer to hole, and energy transfer to surface ligands.[3-7] These discrete energy states and particular relaxation processes in QDs lead to the slower hot carrier relaxation compared to bulk semiconductors. In addition, the hot electron relaxation time in colloidal semiconductor nanocrystals can be controlled by surface ligands[7], charge separation[7,8], and temperature.[9] Actually, Pandey and Guyot-Sionnest have achieved the extremely slow hot electron relaxation with a lifetime longer than 1 ns in CdSe/ZnSe/ZnS/CdSe multishell nanoparticles (NPs).[8] Therefore, the efficient hot electron extraction from semiconductor QDs is expected. In a previous theoretical study, Ross and Nozik reported that the maximum conversion efficiency of QD solar cells could reach to ~67% by utilizing the excess energy of photoexcited hot carrier.[10] Consequently, colloidal semiconductor nanocrystals are one of the best candidate materials for the highly efficient solar cell.

The charge transfer from colloidal semiconductor nanocrystals to the outside has been examined using time-resolved fluorescence measurements and pump-probe spectroscopy. In the previous study on the electron transfer from band-edge state of cadmium chalcogenide QDs to acceptor molecules adsorbed on the surface of QDs, Zhu et al. reported the unique and efficient electron transfer process in which the Marcus inverted region does not exist, resulting from the hole excitation coincident with the electron transfer.[11] In addition, Zhu et al. reported the enhanced extraction of multiple excitons (~21 electrons) from CdSe nanorods (NRs) to methyl viologen (MV^{2+}) as compared with that from CdSe QDs to MV^{2+}(< ~4

electrons), which was due to the fast electron transfer (~60 fs) and slow Auger recombination process.[12,13] The efficient electron transfer dynamics in the semiconductor-metal hybrid nanostructures (HNs) was examined by several groups. Mongin et al. reported the ultrafast electron transfer from band-edge state of CdS NRs with the lifetime of sub-20 fs time scale in Au NP-attached CdS NRs.[14] In our previous studies, by using the femtosecond pump-probe spectroscopy, ultrafast (much faster than the instrumental response function) and ps-scale electron transfer from the band-edge state of PbS QDs and CdSe NRs to Au NPs were analyzed, respectively.[15,16] In addition, in PbS QDs strongly coupled with TiO_2 NPs systems, ultrafast electron transfer from the band-edge state of PbS QDs with the estimated lifetime of ~6 fs were suggested.[17] Furthermore, the hot electron transfer from semiconductor nanocrystals have been observed. Tisdale et al. analyzed the hot electron transfer from colloidal PbSe QDs to the single-crystalline TiO_2 (rutile) by using the femtosecond time-resolved second harmonic generation experiments.[18] In our previous study on the femtosecond pump-probe spectroscopy for CdSe NR-Au HNs with different size of Au NPs, hot electron transfer from CdSe NRs to Au NPs were revealed by analyses of rise time and initial bleach amplitudes of band-edge bleach band.[16] Moreover, the hot electron transfer from CdSe QDs and NRs to MV^{2+} were reported.[12,19-21]

In addition, the electron transfer dynamics from core/shell nanocrystals as well as from bare semiconductor nanocrystals were examined. The shell growth on the core semiconductor nanocrystals is a very effective method for the drastic increase of luminescence quantum yield and modification of electronic structures and carrier relaxation processes. Core/shell semiconductor nanocrystals can be classified into type I, quasi-type II, and type II (Figure 3.1) depending on the relative energy levels of core and shell materials. In the type I core/shell QDs (CSQDs), such as CdSe/ZnS CSQDs, electron and hole are confined in the core region and the increase of luminescence quantum yields is observed as compared

with the core only.[22] In type II CSQDs, such as CdTe/CdSe CSQDs, electron and hole are spacially separated into the core and shell regions and the charge recombination rate reduces.[23,24] In the intermediate electronic structure, the electron (or hole) wavefunction spreads out a whole CSQDs, although the another wavefunction confines in the core or shell region, which is referred as quasi-type II CSQDs. In the CdSe/CdS CSQDs, the electronic structures can be modified by changing the core diameter and shell thickness since the conduction band-edge energy of bulk CdSe (-4.04 V vs vacuum) is slightly lower than that of bulk CdS (-3.84 V vs vacuum).[11] The control of electronic structures in the CSQDs can leads to the change of the hot electron relaxation rate. In previous reports, the hot electron relaxation rate by Auger cooling and energy transfer to ligands depends on the overlap of wavefunction of electron and hole, and interaction between QDs and surface ligands, respectively.[3,7] Therefore, the modification of electronic structures and overlap of wavefunctions in CSQDs can potentially allow to suppress the fast hot electron relaxation.[8,25] Furthermore, the electron transfer dynamics from several kinds of CSQDs to acceptor molecules were examined. The shell thickness dependence of the rate of electron transfer from band-edge state was analyzed in the type I CdSe/ZnS CSQDs-anthraquinone and quasi-type II CdSe/CdS CSQDs-MV^{2+} complexes.[26,27] According to these studies, natural logarithm of electron transfer rate from the band-edge state decreases linearly with increasing the shell thickness, resulting from the decrease of electronic coupling strength between core/shell QDs and acceptor molecules adsorbed on the surface of QDs. Moreover, the multiple (~19) electron transfer from quasi-type II CdSe/CdS CSQDs to MV^{2+} were observed, which was due to the slow multiexciton annihilation and fast electron transfer in quasi-type II CSQDs.[20] However, the shell thickness dependence of the rate of hot electron transfer from CSQDs has not been examined yet and remains unclear.

In the present study, we prepared CdSe/CdS CSQDs and CSQD-MV^{2+} complexes

with different shell thickness. We analyzed the shell thickness dependence of hot electron transfer rates as well as electron transfer rates from $1S_e$ state by using the femtosecond pump-probe spectroscopy with a state-selective excitation technique.

3.3 Experimental section

Synthetic and preparation methods of CdSe/CdS CSQDs and CSQD-MV^{2+} complexes were described in Chapter 2, respectively. The size of CdSe QDs and CdSe/CdS CSQDs were characterized by scanning transmission electron microscopy (STEM, TECNAI 20, 200 keV, FEI) and energy dispersive X-ray spectrometry (EDX, ibid). UV−vis absorption and luminescence spectra of CSQDs and CSQD-MV^{2+} complexes were recorded using an U-4100 (Hitachi) and a Fluorolog-3 (Jobinyvon-Spex), respectively. The transient absorption spectra were measured using femtosecond pump-probe techniques. The samples were exited at 400 nm using the second harmonic of an amplified mode-locked Ti:sapphire laser (Spitfire and Tsunami, Spectra-Physics, repetition rate: 1 kHz), and the state-selective excitation experiments were performed by an optical parametric amplifier (OPA) (TOPAS, Light Conversion Ltd.). The pump pulse was focused to a spot with 0.7 mm diameter, and a repetition rate of 0.5 kHz was achieved by an optical chopper (Model 3501, New Focus, Inc.). The transient absorption was probed using the delayed pulses of a femtosecond white-light continuum generated by focusing the fundamental laser pulse into a D_2O cell. Detection was carried out using a polychromator-CCD combination (Spectra Pro-275, Acton Research Co., and Spec-10, Princeton Instruments). The temporal resolution for 400 nm and state-selective excitation were ~100 fs and ~60 fs, respectively.

3.4 Results and discussion

STEM images of CdSe QDs and CdSe/CdS CSQDs A and B were shown in Figure

3.2 and the shell thickness of CSQDs A and B were estimated to be ~0.4 nm and ~0.6 nm, respectively (Table 3.1). STEM image analyses revealed that the diameter of CdSe/CdS CSQDs became larger than that of core CdSe QDs by the growth of CdS shell on the core, and the shell thickness increased with increasing the number of precursor injection. Furthermore, as shown in Figure 3.3, the EDX data of CdSe/CdS CSQDs A clearly showed a S peak as well as Cd and Se peaks, suggesting the CdS shell growth on the CdSe core. Steady-state absorption and emission spectra of CdSe QDs and CdSe/CdS CSQDs were illustrated in Figure 3.4. In the absorption spectrum of CdSe QDs, 1S, 2S, and 1P absorption bands were observed centered at 547 nm, 512 nm, and 466 nm, respectively.[3,5] From the wavelength of a 1S absorption peak, the diameter of CdSe QDs was estimated to be 3.0 nm,[28] which is in good agreement with the STEM data. In the absorption spectra of CdSe/CdS CSQDs A and B, 1S absorption peak was shifted to the longer wavelength region as the shell thickness increased, resulting from the penetration of electron wavefunction of CdSe core to the CdS shell region.[29,30] In addition, the absorption of CdS shell was detected in the shorter wavelength region (<500 nm). The band-edge luminescence centered at 559 nm in CdSe QDs exhibited the red-shift with increasing the shell thickness. Luminescence quantum yields of CdSe/CdS CSQDs (A; 25%, B; 29%) were higher than that of CdSe QDs (15%), suggesting that the decrease of surface trap states by the shell growth on the core CdSe QDs.[27,29] The steady-state absorption and emission spectra of CdSe/CdS CSQDs-MV^{2+} complexes are illustrated in Figure 3.5. In the absorption spectra, the absorption of MV^{2+} is superposed on the spectrum of the CdSe/CdS CSQDs in the shorter wavelength region.[13,19] The band-edge luminescence of CSQDs are strongly quenched in CdSe/CdS CSQDs-MV^{2+} complexes, which is due to the electron transfer from CdSe/CdS CSQDs to MV^{2+}.

The transient absorption spectra of CdSe/CdS CSQDs A, B, and their MV^{2+} complexes excited at 400 nm are shown in Figure 3.6. In the CdSe/CdS CSQDs A and B, 1S

bleach bands were observed at 554 nm and 575 nm, corresponding to the wavelength of 1S absorption peak in steady-state absorption spectra of CSQDs A and B, respectively. As shown in Figure 3.6, though the spectral features of CdSe/CdS CSQDs-MV^{2+} A and CSQDs-MV^{2+} B complexes were very similar to those of CdSe/CdS CSQDs, the very fast relaxation in CSQD-MV^{2+} complexes was clearly observed. The fast relaxation was due to the electron transfer from CdSe/CdS CSQDs to MV^{2+}.[20,27] Moreover, the broad induced absorption corresponding to the absorption of methyl viologen cation radical (MV^{+} radical)[31] were detected at longer wavelength region (>600 nm) of transient absorption spectra in both CSQD-MV^{2+} complexes. The appearance of MV^{+} radical band indicates the electron transfer from CdSe/CdS CSQDs to MV^{2+}.

The 1S bleach band dynamics of each samples were illustrated in Figure 3.7. In the CdSe/CdS CSQDs, the ps-scale fast relaxation corresponding to the electron trapping to the surface defect does not detected. In contrast, the 1S bleach dynamics of CdSe/CdS CSQD-MV^{2+} complexes showed a very fast decay component corresponding to the electron transfer from the 1S$_e$ state of QDs to MV^{2+}. The 1S bleach dynamics were fitted with the sum of exponential functions by a deconvolution analysis. The electron transfer dynamics in CdSe/CdS CSQD-MV^{2+} complexes A (shell thickness: ~0.4 nm) were faster than that in CSQD-MV^{2+} complexes B (shell thickness: ~0.6 nm), and the lifetime of electron transfer from the 1S$_e$ state in CSQD-MV^{2+} complexes A and B were estimated to be ~400 fs and ~640 fs, respectively. In the previous studies on the CSQDs-acceptor molecules complexes, the electron transfer from the 1S$_e$ state of CSQDs to acceptor molecules became slower with increasing the shell thickness because of the decrease of electronic coupling constant between QDs and acceptor molecules adsorbed on the surface.[27,32] Therefore, the observed decrease of electron transfer rate from the 1S$_e$ state of CdSe/CdS CSQDs to MV^{2+} is consistent with these previous reports. According to the previous studies, the electron transfer rate depends on the

number of electron acceptors.[12,33-35] Morris-Cohen et al. reported that the electron transfer rate from CdS QDs increased linearly with the number of viologen molecules.[36] However, in the present study, the estimation of the average number of MV^{2+} adsorbed on the surface of a CSQD was not easy because the absorption coefficient of CdSe/CdS CSQDs was unclear. Thus, the average number of MV^{2+} on a QD was possible to contribute to the decrease of electron transfer rate as the shell thickness increase. On the other hand, the growth kinetics of 1S bleach band of semiconductor nanocrystals represents the hot carrier relaxation to the band-edge states.[2-6] Kambhampati group reported the hot electron relaxation mechanism in CdSe QDs with the state-selective excitation experiments.[3-6] According to their reports, when the pump pulse whose energy is much higher than the 1P transition is used for the excitation, the hot electron relaxation follows a sum of three signals convolved with the instrumental response function (IRF).[3,6]

$$\Delta OD(t) = \left[A_{1S} + A_{1p}e^{-k_1 t} + A_i \left\{ 1 + \frac{1}{k_2 - k_1} \times (k_1 e^{-k_2 t} - k_2 e^{-k_1 t}) \right\} \right] \otimes IRF \quad (1)$$

where i is the electronic states higher than $1P_e$ state, $k_2 \equiv k_{i \rightarrow 1P}$ and $k_1 \equiv k_{1P \rightarrow 1S}$. However, in our experiments, by considering the signal-to-noise ratio in transient absorption measurements, only one rise component is enough to analyze the 1S bleach dynamics. Therefore, a sequential relaxation process (i $\rightarrow$ 1P and 1P $\rightarrow$ 1S) can be approximately expressed as one process (i $\rightarrow$ 1S) with the rate constant of k_{int}. By using one exponential function with a deconvolution analysis, the rise time of 1S bleach band ($1/k_{int}$) in CdSe/CdS CSQDs A and B were estimated to be ~240 fs and ~550 fs, respectively. In addition, in the growth kinetics of both CSQDs, a fast rise component comparable to an instrumental response function was also detected. The fast rise component is likely due to electronic excitation from deep valence band states to the $1S_e$ state in the conduction band. The growth kinetics of 1S

bleach band of CdSe/CdS CSQD-MV^{2+} complexes A and B became much faster than those of CSQDs A and B. The rise times were estimated to be ~100 fs and ~90 fs for CSQD-MV^{2+} complexes A and B, respectively. By assuming the hot electron transfer from CSQDs to MV^{2+} with the rate constant of k_{HET}, the rise time of 1S bleach band in CSQD-MV^{2+} complexes can be expressed as the inverse of the sum of the rate constants of intraband relaxation and hot electron transfer $(1/(k_{int} + k_{HET}))$. Therefore, the observed faster growth kinetics in CdSe/CdS CSQD-MV^{2+} complexes strongly suggested the hot electron transfer from QDs to MV^{2+}. By using the estimated rise time of growth kinetics in each sample, the lifetime of hot electron transfer in CdSe/CdS CSQD-MV^{2+} complexes A and B were estimated to be ~170 fs and ~110 fs, respectively. Furthermore, the hot electron transfer yields defined as $k_{HET}/(k_{int} + k_{HET})$ were 0.59 and 0.82 for CdSe/CdS CSQD-MV^{2+} complexes A and B, respectively. In addition, as clearly shown in Figure 3.6, the 1S bleach amplitude of CdSe/CdS CSQDs-MV^{2+} complexes were smaller than those of CdSe/CdS CSQDs. Since the 1S bleach band of CdSe/CdS CSQDs is originated from the state filling of $1S_e$ level,[20] the lower 1S bleach amplitude of CSQDs-MV^{2+} suggests the hot electron transfer from CSQDs to MV^{2+}.

As mentioned above, MV$^+$ radical band were detected in the transient absorption spectra, suggesting the electron transfer from CdSe/CdS CSQDs to MV^{2+}. Therefore, the growth kinetics of MV$^+$ radical band, as well as the 1S bleach band dynamics, should represent the total electron transfer processes from $1S_e$ and higher excited states of QDs to MV^{2+}. The growth kinetics of MV$^+$ radical band in both CSQD-MV^{2+} complexes excited at 400 nm were shown in Figure 3.8. The growth kinetics of MV$^+$ radical band were analyzed using biexponential function including the electron transfer from $1S_e$ state and hot electron transfer. The fast rise times of MV$^+$ radical band in both samples were estimated to be ~120 fs and ~90 fs for CSQDs-MV^{2+} complexes A and B by fixing the slow rise time in the electron transfer time from the $1S_e$ state, respectively. These fast rise times of MV$^+$ radical band were

similar to the rise time of 1S bleach band for each CSQDs-MV^{2+} complexes (1/(k_{int} + k_{HET})), suggesting that analyses based on the hot electron transfer and electron transfer from 1S$_e$ state were valid..

In order to analyze electron transfer processes from CdSe/CdS CSQDs to MV^{2+} in more detail, the selective excitation of 1S transition of CSQDs was conducted using an OPA. In this experimental condition, the photoexcited electron occupies 1S$_e$ states directly and the hot electron does not generate. Transient absorption spectra of all samples excited at 1S absorption band (A: ~550 nm; B: ~570 nm) were illustrated in Figure 3.9. In all transient absorption spectra, 1S bleach band was clearly observed. In the CdSe/CdS CSQD-MV^{2+} complexes A and B, fast relaxation of transient absorption signal derived from CSQDs and the broad MV$^+$ radical band were observed, indicating the electron transfer from 1S$_e$ state of CdSe/CdS CSQDs to MV^{2+}. Transient absorption dynamics of 1S bleach band of each sample under 1S excitation were illustrated in Figure 3.10. As shown in Figure 3.10, the rise component of 1S bleach band was comparable to the instrumental response function (~60 fs), indicating that hot electron did not generate and hot electron transfer did not contribute to the transient absorption spectra and dynamics under 1S excitation. The lifetime of fast relaxation in the 1S bleach band of CSQD-MV^{2+} complexes A and B were estimated to be ~0.46 ps and ~1.0 ps, respectively. The growth kinetics of MV$^+$ radical band in CSQD-MV^{2+} complexes A and B under 1S and 400 nm excitation were shown in Figure 3.11. In contrast to 400 nm excitation experiments, the growth kinetics of MV$^+$ radical band was fitted with single exponential function, and the rise time of MV$^+$ radical band in QD-MV^{2+} complexes A and B were estimated to be ~0.43 ps and ~1.1 ps, which were similar to those of the fast decay component of 1S bleach dynamics. In 1S excitation experiments, the electron transfer process from 1S$_e$ state of QDs to MV^{2+} was only observed in the transient absorption spectra and dynamics, which leads to the excitation wavelength dependence of growth kinetics of MV$^+$

radical band dynamics.

As mentioned above, electron transfer time from $1S_e$ state of CdSe/CdS CSQDs to MV^{2+} became slower with increasing the shell thickness, which was similar to the previous reports.[27,32] On the other hand, the hot electron transfer time from CdSe/CdS CSQDs A (shell thickness: ~0.4 nm) to MV^{2+} was similar to (or slightly faster than) that from CdSe/CdS CSQDs B (shell thickness: ~0.6 nm). Consequently, in the CdSe/CdS CSQD-MV^{2+} complexes, the shell thickness dependence on the hot electron transfer rate were probably different from that on the electron transfer from $1S_e$ state of CdSe/CdS CSQDs. The electron transfer rate was expressed as the sum of the electron transfer rates to all possible accepting states as given in the equation,[37-40]

$$k_{ET} = \frac{2\pi}{\hbar} \int_{-\infty}^{\infty} dE \, \rho(E) |\overline{H}(E)|^2 \frac{1}{\sqrt{4\pi\lambda k_B T}} \times exp\left[-\frac{(\lambda + \Delta G_0 + E)^2}{4\lambda k_B T}\right] \qquad (2)$$

where k_{ET} is the total rate constant of electron transfer, $\rho(E)$ is the density of the MV^{2+} final state, ΔG_0 is the change in Gibbs energy corresponding to the energy difference between the electronic state of the CdSe/CdS CSQDs and the LUMO level of MV^{2+}, λ is the reorganization energy, which is the sum of the inner-sphere, λ_i, and outer-sphere, λ_o, components, and $|\overline{H}(E)|$ is the electronic coupling constant between the initial electronic state of the CdSe/CdS CSQDs and the final state of MV^{2+}. Since the solvent (chloroform) has a weak polarity, λ_o is very small and λ_i of MV^{2+} dominantly contributes to the total λ, indicating that the λ does not depends on shell thickness. Therefore, possible reasons for the different shell thickness dependence of hot electron transfer rate are the electronic coupling constant, Gibbs energy change, and the density of acceptor states. Firstly, the penetration of electron wave functions at higher excited states ($1P_e$, $1D_e$, etc.) are expected to be different from that at $1S_e$ state, suggesting the different shell thickness (or total diameter) dependence

of electronic coupling between higher excited states of CSQDs and MV^{2+}. Secondly, in the present study, the specific electronic state of CdSe/CdS CSQDs where hot electron transfer takes place is unclear. Therefore, the estimation of Gibbs energy change is not so easy. Zhu et al. reported the electron transfer rate from the $1S_e$ state of semiconductor QDs to acceptor molecules increases monotonically with increasing the Gibbs energy change.[11] According to this report, if the Gibbs energy change became larger (the energy level of initial state in a hot electron transfer process became higher) with increasing the shell thickness, the hot electron transfer could be faster in CdSe/CdS CSQDs-MV^{2+} complexes B. Therefore, the Gibbs energy change modified the hot electron transfer rate in CdSe/CdS CSQDs-MV^{2+} complexes. Thirdly, if the energy level of initial state for the hot electron transfer changed with changing the shell thickness, the density of MV^{2+} states whose energy levels are equal to the initial state could change. Consequently, these three reasons or their multiplier effects could lead to the unique shell thickness dependence of hot electron transfer from CdSe/CdS CSQDs to MV^{2+}. Further experiments such as 1P excitation experiments are necessary for the elucidation of shell thickness dependence of the hot electron transfer rate in CdSe/CdS CSQD-MV^{2+} complexes.

3.5 Conclusion

In conclusion, we synthesized the CdSe/CdS CSQDs with different shell thickness and prepared the CdSe/CdS CSQD-MV^{2+} complexes, and analyzed shell thickness dependence on the electron transfer from $1S_e$ state and higher excited states by femtosecond pump-probe spectroscopy with the state-selective excitation technique. Steady-state absorption and luminescence spectra shows the absorption of MV^{2+} and strong quenching of band-edge luminescence, respectively. In the transient absorption measurements for CdSe/CdS CSQD-MV^{2+} complexes under 400 nm excitation, the fast relaxation of transient

absorption bands of CSQDs and the growth of MV^+ radical band were observed, indicating the electron transfer from CSQDs to MV^{2+}. By analyzing the 1S bleach band dynamics of each sample, we estimated the rate of electron transfer from $1S_e$ state and hot electron transfer in CdSe/CdS CSQD-MV^{2+} complexes with different shell thickness. The electron transfer from $1S_e$ state of CdSe/CdS CSQD-MV^{2+} complexes became slower with increasing the shell thickness, which was similar to previous studies on the electron transfer in CSQD-MV^{2+} complexes. On the other hand, we found that the hot electron transfer time from CdSe/CdS CSQDs to MV^{2+} did not depend on the shell thickness or became slightly faster as the shell thickness increased, which is clearly different from the shell thickness dependence of electron transfer from $1S_e$ state. Furthermore, in the growth kinetics of MV^+ radical band, both electron transfer from $1S_e$ state and hot electron transfer were detected under 400 nm excitation, and only electron transfer from $1S_e$ state was detected under 1S excitation. Our experimental results will provide the new insight into the hot electron transfer process from semiconductor nanocrystals, and develop the highly efficient QDs solar cell utilizing the hot electron.

References

(1) Shockley, W.; Queisser, H. J. Detailed Balance Limit of Efficiency of p–n Junction Solar Cells. *J. Appl. Phys.* **1961**, *32*, 510.

(2) Klimov, V. I. Optical Nonlinearities and Ultrafast Carrier Dynamics in Semiconductor Nanocrystals. *J. Phys. Chem. B* **2000**, *104*, 6112–6123.

(3) Kambhampati, P. Hot Exciton Relaxation Dynamics in Semiconductor Quantum Dots: Radiationless Transitions on the Nanoscale. *J. Phys. Chem. C*, **2011**, *115*, 22089–22109.

(4) Kambhampati, P. Unraveling the Structure and Dynamics of Excitons in Semiconductor Quantum Dots. *Acc. Chem. Res.* **2011**, *44*, 1−13.

(5) Sewall, S. L.; Cooney, R. R.; Anderson, K. E. H.; Dias, E. A.; Kambhampati, P. State-to-State Exciton Dynamics in Semiconductor Quantum Dots. *Phys. Rev. B* **2006**, *74*, 235328.

(6) Cooney, R. R.; Sewall, S. L.; Dias, E. A.; Sagar, D. M.; Anderson, K. E. H.; Kambhampati, P. Unified Picture of Electron and Hole Relaxation Pathways in Semiconductor Quantum Dots. *Phys. Rev. B* **2007**, *75*, 245311.

(7) Guyot–Sionnest, P.; Wehrenberg, B.; Yu, D. Intraband Relaxation in CdSe Nanocrystals and the Strong Influence of the Surface Ligands. *J. Chem. Phys.* **2005**, *123*, 074709.

(8) Pandey, A.; Guyot–Sionnest, P. Slow Electron Cooling in Colloidal Quantum Dots. *Science* **2008**, *322*, 929–932.

(9) Schaller, R. D.; Pietryga, J. M.; Goupalov, S. V.; Petruska, M. A.; Ivanov, S. A.; Klimov, V. I. Breaking the Phonon Bottleneck in Semiconductor Nanocrystals via Multiphonon Emission Induced by Intrinsic Nonadiabatic Interactions. *Phys. Rev. Lett.* **2005**, *95*, 196401.

(10) Ross, R. T.; Nozik, A. J. Efficiency of hot–carrier solar energy converters. *J. Appl. Phys.* **1982**, *53*, 3813–3818.

(11) Zhu, H.; Yang, Y.; Hyeon–Deuk, K.; Califano, M.; Song, N.; Wang, Y.; Zhang, W.; Prezhdo, O. V.; Lian, T. Auger–Assisted Electron Transfer from Photoexcited Semiconductor Quantum Dots. *Nano Lett.* **2014**, *14*, 1263–1269.

(12) Zhu, H.; Lian, T. Enhanced Multiple Exciton Dissociation from CdSe Quantum Rods: The Effect of Nanocrystal Shape. *J. Am. Chem. Soc.* **2012**, *134*, 11289–11297.

(13) Matylitsky, V. V.; Dworak, L.; Breus, V. V.; Basché, T.; Wachtveitl, J. Ultrafast Charge Separation in Multiexcited CdSe Quantum Dots Mediated by Adsorbed Electron Acceptors. *J. Am. Chem. Soc.* **2009**, *131*, 2424–2425.

(14) Mongin, D.; Shaviv, E.; Maioli, P.; Crut, A. Banin, U.; Fatti, N. D.; Vallée, F. Ultrafast Photoinduced Charge Separation in Metal–Semiconductor Nanohybrids. *ACS Nano* **2012**, *6*, 7034–7043.

(15) Okuhata, T.; Kobayashi, Y.; Nonoguchi, Y.; Kawai, T.; Tamai, N. Ultrafast Carrier Transfer and Hot Carrier Dynamics in PbS−Au Hybrid Nanostructures. *J. Phys. Chem. C*

2015, *119*, 2113–2120.

(16)   Sagarzazu, G.; Inoue, K.; Saruyama, M.; Sakamoto, M.; Teranishi, T.; Masuo, S.; Tamai, N. Ultrafast Dynamics and Single Particle Spectroscopy of Au–CdSe Nanorods. *Phys. Chem. Chem. Phys.* **2013**, *15*, 2141–2152.

(17)   Yang, Y.; Rodríguez−Córdoba, W.; Xiang, X.; Lian, T. Strong Electronic Coupling and Ultrafast Electron Transfer between PbS Quantum Dots and TiO_2 Nanocrystalline Films. *Nano Lett*. **2012**, *12*, 303−309.

(18)   Tisdale, W. A.; Williams, K. J.; Timp, B. A.; Norris, D. J.; Aydil, E. S.; Zhu, X.-Y. Hot–Electron Transfer from Semiconductor Nanocrystals. *Science* **2010**, *328*, 1543–1547.

(19)   Wang, Y.; Wang, H.; Li, Z.; Zhao, J.; Wang, L.; Chen, Q.; Wang, W.; Sun, H. Electron Extraction Dynamics in CdSe and CdSe/CdS/ZnS Quantum Dots Adsorbed with Methyl Viologen. *J. Phys. Chem. C* **2014**, *118*, 17240–17246.

(20)   Zhu, H.; Song, N.; Rodríguez–Córdoba, W.; Lian, T. Wave Function Engineering for Efficient Extraction of up to Nineteen Electrons from One CdSe/CdS Quasi–Type II Quantum Dot. *J. Am. Chem. Soc.* **2012**, *134*, 4250–4257.

(21)   Jiang, Z.–J.; Kelley, D. F. Hot and Relaxed Electron Transfer from the CdSe Core and Core Shell Nanorods. *J. Phys. Chem. C* **2011**, *115*, 4594–4602.

(22)   (CdSe)ZnS Core−Shell Quantum Dots: Synthesis and Characterization of a Size Series of Highly Luminescent Nanocrystallites. *J. Phys. Chem. B* **1997**, *101*, 9463–9475.

(23)   Chuang, C.–H.; Lo, S. S.; Scholes, G. D.; Bruda, C. Charge Separation and

Recombination in CdTe/CdSe Core/Shell Nanocrystals as a Function of Shell Coverage:

Probing the Onset of the Quasi Type–II Regime. *J. Phys. Chem. Lett.* **2010**, *1*, 2530–2535.

(24)   Ma, X.; Mews, A.; Kipp, T. Determination of Electronic Energy Levels in Type–II

CdTe–Core/CdSe–Shell   and   CdSe–Core/CdTe–Shell   Nanocrystals   by   Cyclic

Voltammetry and Optical Spectroscopy. *J. Phys. Chem. C* **2013**, *117*, 16698–16708.

(25)   Cirloganu, C. M.; Padilha, L. A.; Lin, Q.; Makarov, N. S.; Velizhanin, K. A.; Luo,

H.; Robel, I.; Pietryga, J. M.; Klimov, V. I. Enhanced carrier multiplication in engineered

quasi–type–II quantum dots. *Nat. Commun.* **2014**, *5*, 4148.

(26)   Zhu, H.; Song, N.; Lian, T. Controlling Charge Separation and Recombination Rates

in CdSe/ZnS Type I Core−Shell Quantum Dots by Shell Thicknesses. *J. Am. Chem. Soc.*

2010, *132*, 15038–15045.

(27)   Jia, Y.; Chen, J.; Wu, K.; Kaledin, A.; Musaev, D. G.; Xie, Z.; Lian, T. Enhancing

Photo-reduction Quantum Efficiency Using Quasi−Type II Core/Shell Quantum Dots.

Chem. Sci. **2016**, *7*, 4125−4133.

(28)   Yu, W.W.; Qu, L.; Guo, W.; Peng, X. Experimental Determination of the Extinction

Coefficient of CdTe, CdSe, and CdS Nanocrystals. *Chem. Mater.* **2003**, *15*, 2854–2860.

(29)   Mekis, I.; Talapin, D. V.; Kornowski, A.; Haase, M.; Weller, H. One-Pot Synthesis

of Highly Luminescent CdSe/CdS Core-Shell Nanocrystals via Organometallic and

"Greener" Chemical Approaches. *J. Phys. Chem. B* **2003**, *107*, 7454–7462.

(30)   Bae, W. K.; Padilha, L. A.; Park, Y.–S.; McDaniel, H.; Robel, I.; Pietryga, J. M.;

Klimov, V. I. Controlled Alloying of the Core_Shell Interface in CdSe/CdS Quantum

Dots for Suppression of Auger Recombination. *ACS Nano* **2013**, *7*, 3411–3419.

(31)   Vuckovic, M.; Mentus, S. V.; Janata, E.; Milosavljevic, B. H. Fast Dimerisation of

the Triparaquat Radical Dication. *Phys. Chem. Chem. Phys.* **2001**, *3*, 4310–4315.

(32)   Dworak, L.; Matylisky, V. V.; Braun, M.; Basché, T.; Wachtveitl, J. Ultrafast Charge

Separation at the CdSe/CdS Core/Shell Quantum Dot/Methylviologen Interface:

Implications for Nanocrystal Solar Cells. *J. Phys. Chem. C* **2011**, *115*, 3949–3955.

(33)   Tachiya, M. Application of a Generating Function to Reaction Kinetics in Micelles.

Kinetics of Quenching of Luminescent Probes in Micelles. *Chem. Phys. Lett.*, **1975**, *33*,

289–292.

(34)   Rodgers, M. A. J.; Wheeler, M. F. D. S. E; Quenching of Fluorescence from Pyrene

in Micellar Solutions by Cationic Quenchers. *Chem. Phys. Lett.* **1978**, *53*, 165–169.

(35)   Peterson, M. D.; Jensen, S. C.; Weinberg, D. J.; Weiss, E. A. Mechanisms for

Adsorption of Methyl Viologen on CdS Quantum Dots. *ACS Nano* **2014**, *8*, 2826–2837.

(36)   Morris–Cohen, A. J.; Frederick, M. T.; Cass, L. C.; Weiss, E. A. Simultaneous

Determination of the Adsorption Constant and the Photoinduced Electron Transfer Rate

for a CdS Quantum Dot–Viologen Complex. *J. Am. Chem. Soc.* **2011**, *133*, 10146–10154.

(37)   Asbury, J. B.; Hao, E.; Wang, Y.; Ghosh, H. N.; Lian, T. Ultrafast Electron Transfer Dynamics from Molecular Adsorbates to Semiconductor Nanocrystalline Thin Films. *J. Phys. Chem. B* **2001**, *105*, 4545–4557.

(38)   Gao, Y. Q.; Marcus, R. A. On the Theory of Electron Transfer Reactions at Semiconductor/Liquid Interfaces. II. A Free Electron Model. *J. Chem. Phys.* **2000**, *113*, 6351–6360.

(39)   Gosavi, S.; Marcus, R. A. Nonadiabatic Electron Transfer at Metal Surfaces. *J. Phys. Chem. B* **2000**, *104*, 2067–2072.

(40)   Gao, Y. Q.; Georgievskii, Y.; Marcus, R. A. On the Theory of Electron Transfer Reactions at Semiconductor Electrode/Liquid Interfaces. *J. Chem. Phys.* **2000**, *112*, 3358–3369.
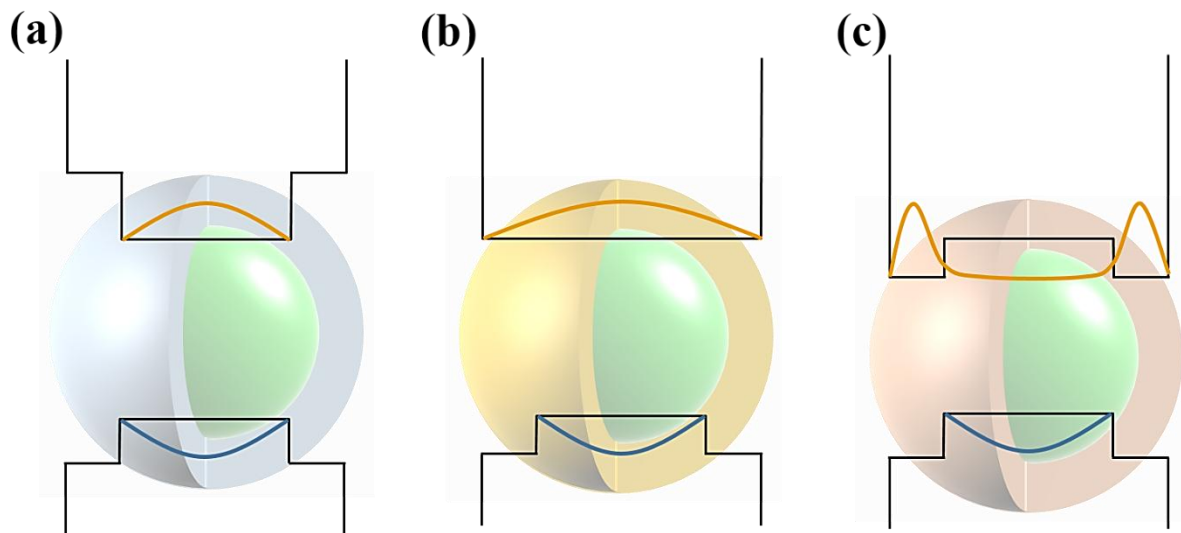
Figure 3.1 The electronic structures of (a) type I, (b) quasi-type II, and (c) type II CSQDs.
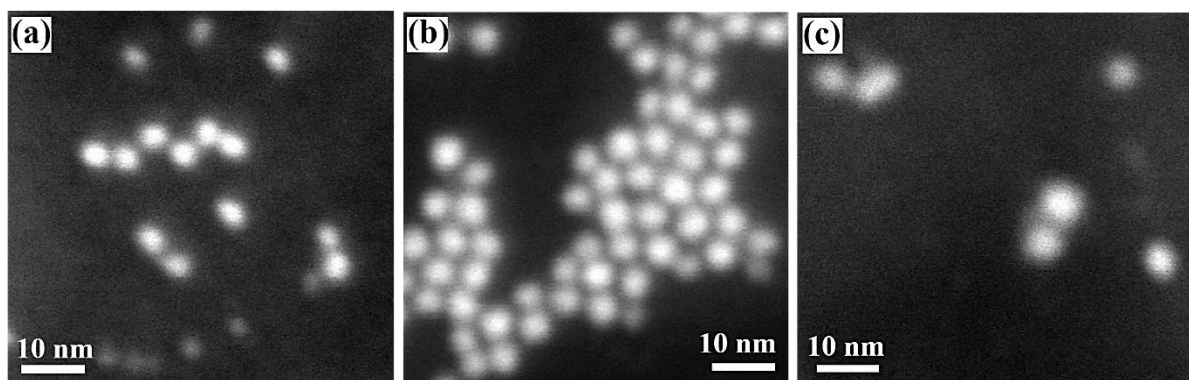
Figure 3.2 STEM images of (a) CdSe QDs, (b) CdSe/CdS CSQDs A, and (c) B.

Table 3.1 The diameter of each samples.

Sample	Diameter / nm	Shell thickness / nm
CdSe QDs	2.9 ± 0.2	
CdSe/CdS CSQDs A	3.7 ± 0.4	~0.4
CdSe/CdS CSQDs B	4.1 ± 0.6	~0.6
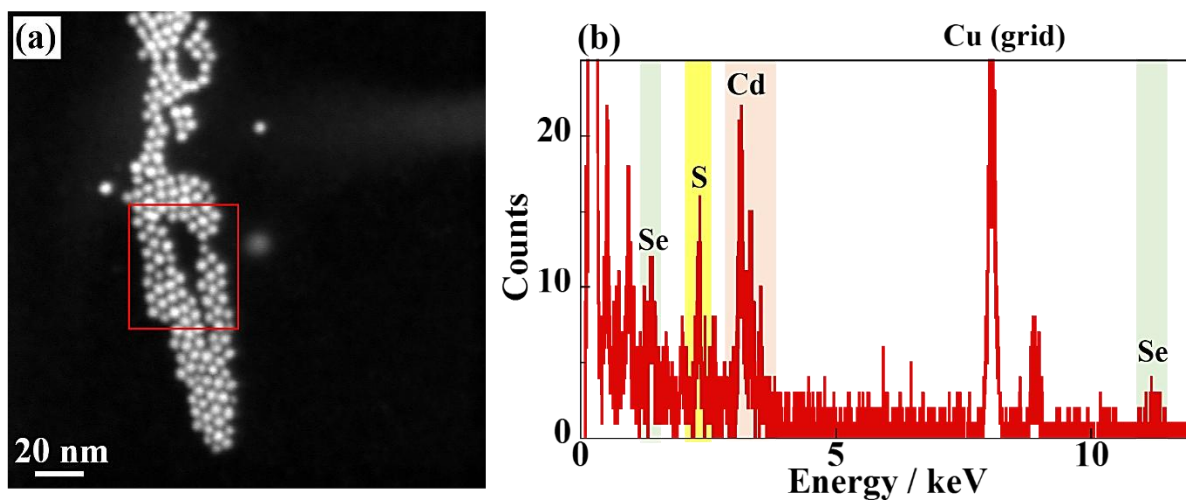
Figure 3.3 (a) STEM image of CdSe/CdS CSQDs A and (b) EDX data obtained at red square region in Figure 3.3a.
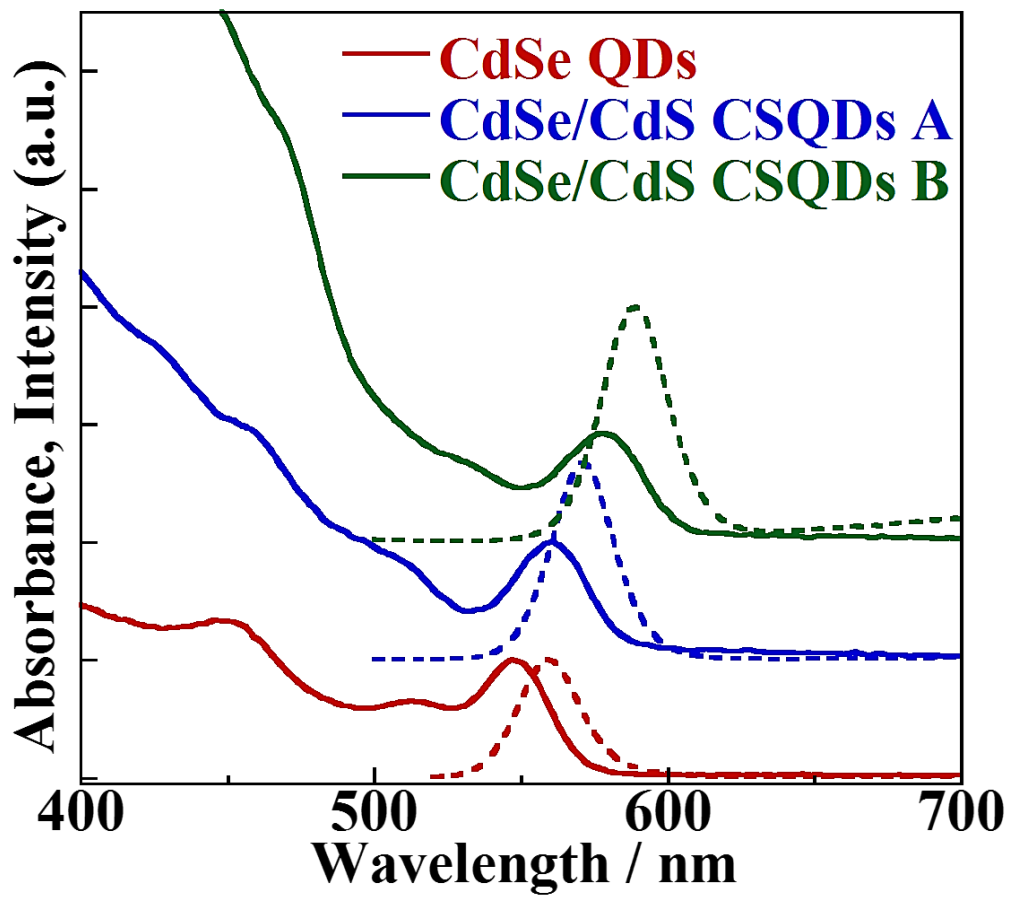
Figure 3.4 Steady-state absorption (solid line) and emission spectra (dashed line) of CdSe QDs and CdSe/CdS CSQDs.
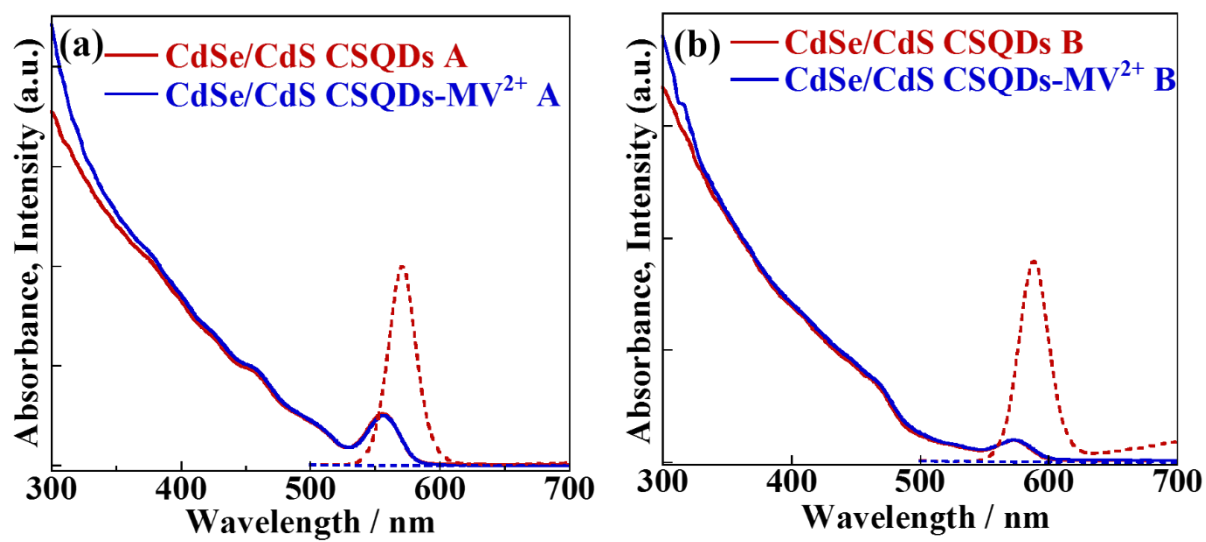
Figure 3.5 Steady-state absorption (solid) and emission (dashed) spectra of CdSe/CdS CSQDs and CSQD-MV^{2+} complexes.
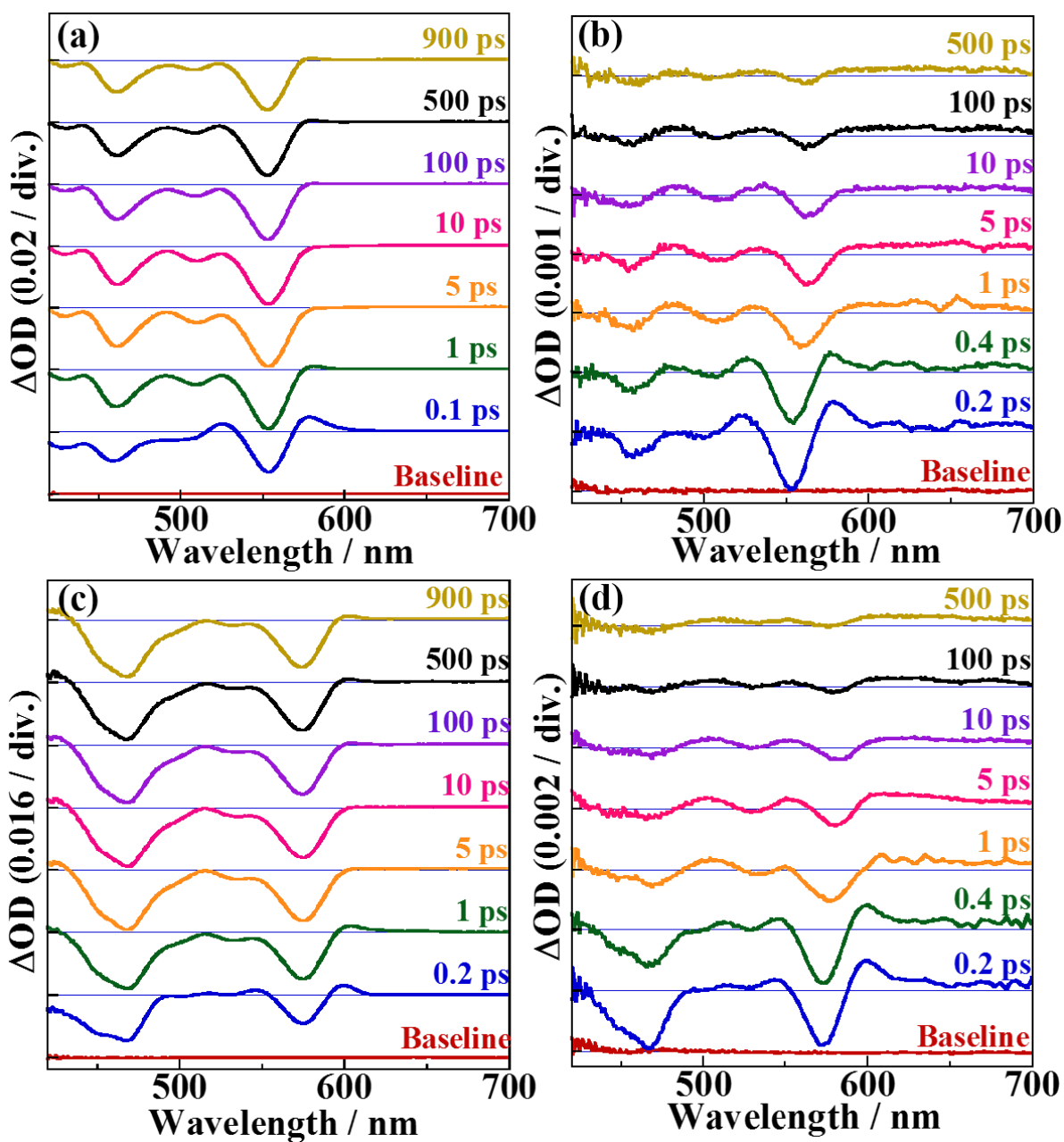
Figure 3.6 Transient absorption spectra of (a) CdSe/CdS CSQDs A, (b) CSQD-MV^{2+} complexes A, (c) CdSe/CdS CSQDs B, and (d) CSQD-MV^{2+} complexes B excited at 400 nm (excitation intensity for A and B were 10 μW and 20 μW, respectively).
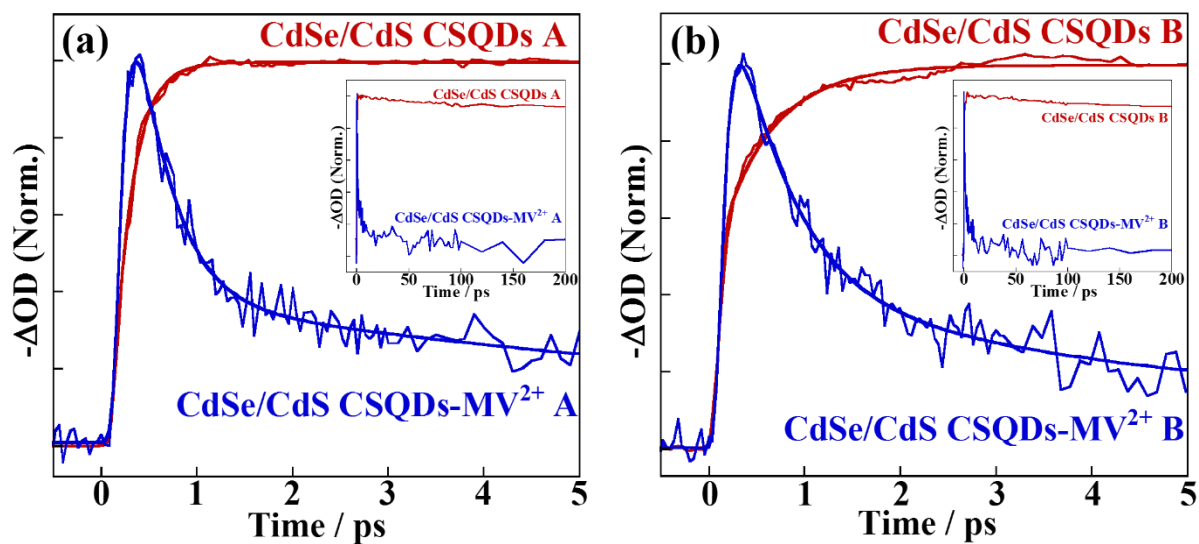
Figure 3.7 Transient absorption dynamics at the 1S bleach band of CdSe/CdS CSQDs and MV^{2+} complexes (a) A (λ_{obs}: 554 nm) and (b) B (λ_{obs}: 575 nm) excited at 400 nm. The inset shows the 1S bleach dynamics of each sample in the long time region.
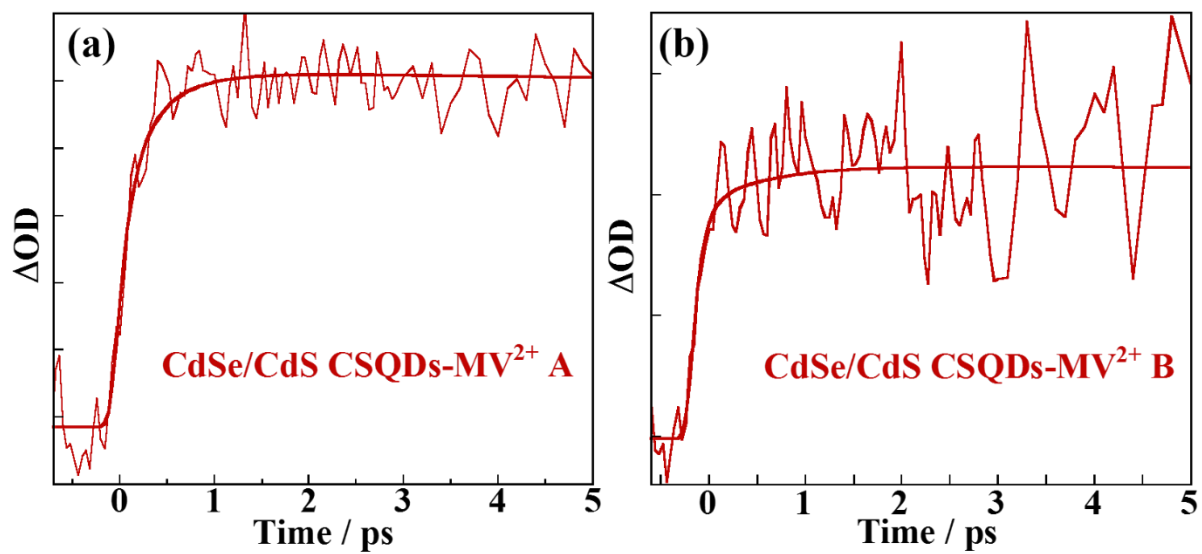
Figure 3.8 Growth kinetics of MV^+ radical band in (a) CdSe/CdS CSQDs MV^{2+} complexes A and (b) B (λ_{ex}: 400 nm, λ_{obs}: 630 nm).
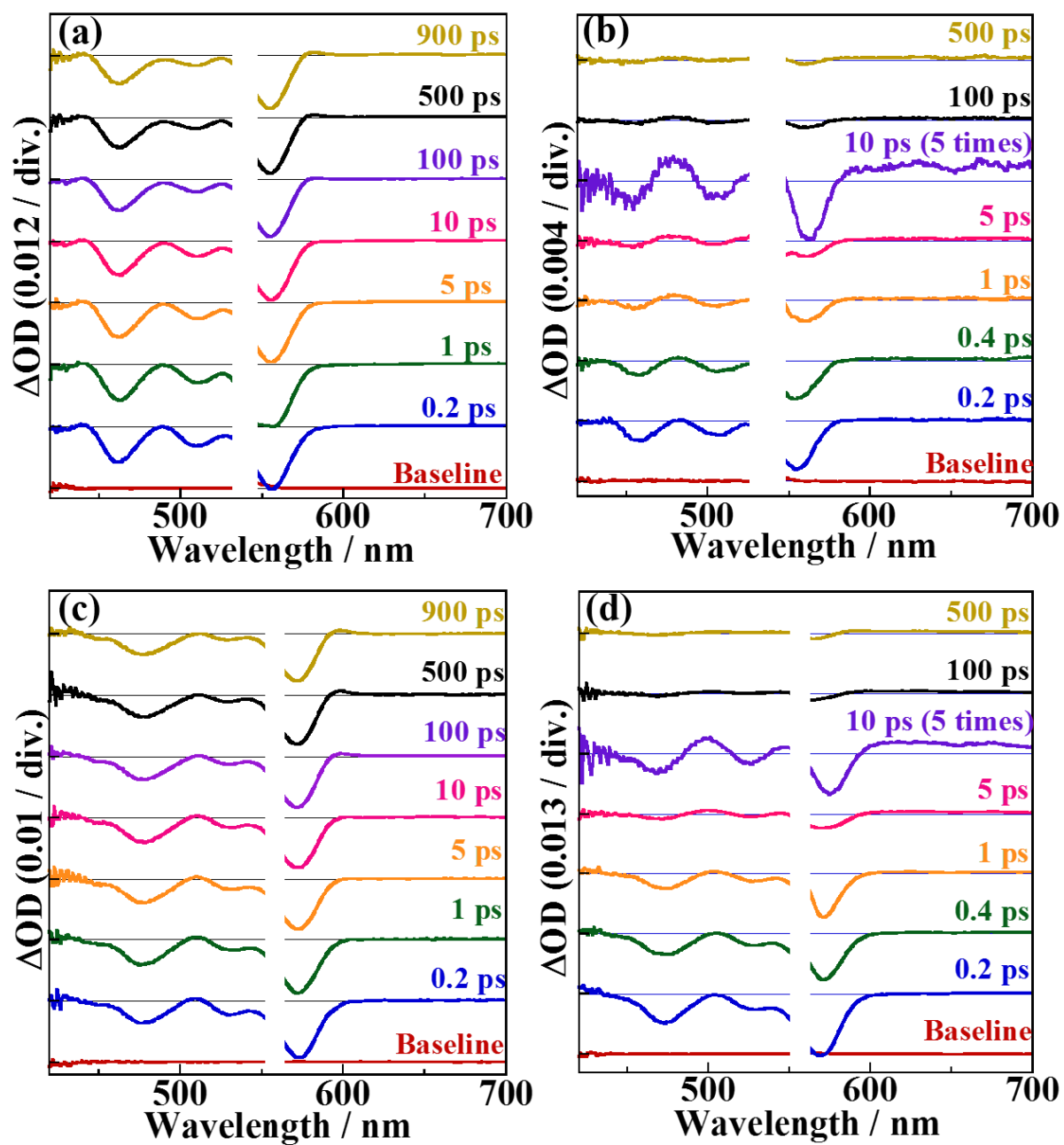
Figure 3.9 Transient absorption spectra of (a) CdSe/CdS CSQDs A, (b) CSQD-MV^{2+} complexes A, (c) CdSe/CdS CSQDs B, and (d) CSQD-MV^{2+} complexes B excited at 1S absorption peak (λ_{ex} for A: 550 nm, λ_{ex} for B: 570 nm).
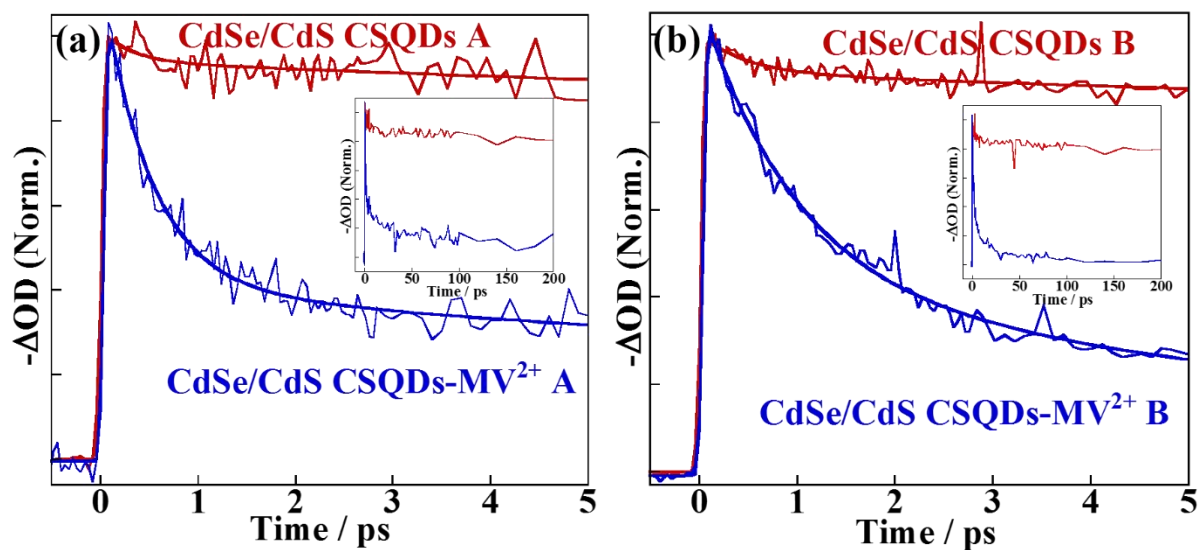
Figure 3.10 Transient absorption dynamics at 1S bleach band of (a) CdSe/CdS CSQDs A and CSQDs-MV^{2+} A, and (b) CdSe/CdS CSQDs B and CSQDs-MV^{2+} B excited at 1S absorption band (λ_{ex} for A: 550 nm, λ_{ex} for B: 570 nm).
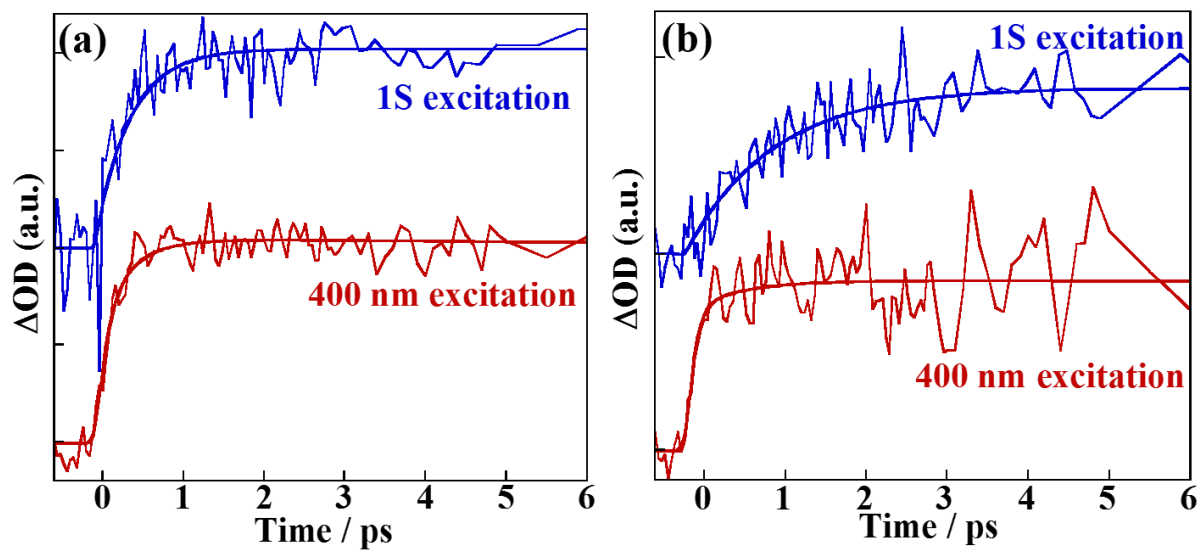
Figure 3.11 The excitation wavelength dependence of growth kinetics of MV$^+$ radical band in CdSe/CdS CSQDs-MV^{2+} complexes (a) A and (b) B (λ_{obs}: 630 nm).

Chapter 4

Elementary Electron Transfer Processes from CdSe NPL to Methyl Viologen

4.1 Abstract

Charge separation in colloidal semiconductor nanocrystals is one of the key processes for the development of highly efficient solar cells. Several types of colloidal semiconductor nanocrystals have been recently synthesized with controlled quantum confinement dimensionality such as quantum dots (QDs), nanorods (NRs), and nanoplatelets (NPLs). However, previous studies on the carrier extraction dynamics from colloidal semiconductor nanocrystals have focused on QDs and NRs. Here, we analyzed the electron transfer process from colloidal CdSe NPLs to methyl viologen (MV^{2+}, electron acceptor) using luminescence decay measurements and femtosecond pump-probe spectroscopy. We examined the dependence of the electron transfer dynamics on the lateral size of CdSe NPLs and found that the rate of electron transfer from CdSe NPLs to MV^{2+} depends on the NPL face where MV^{2+} adsorbs. In addition, we analyzed the growth kinetics and initial bleach amplitude at the band-edge bleach of CdSe NPLs and CdSe NPL-MV^{2+} complexes and found that, in contrast with the behavior of CdSe QD-MV^{2+} and NR-MV^{2+} complexes, hot electron transfer does not occur. This result is a consequence of fast intraband relaxation in CdSe NPLs and the relatively slow electron transfer process.

4.2 Introduction

Recent progress in the colloidal synthesis of semiconductor nanocrystals allows control over the quantum confinement dimensionality, for example, quantum dots[1] (QDs, three dimensional confinement), nanorods[2,3] (NRs, two dimensional confinement), and nanopletelets[4,5] (NPLs, one dimensional confinement). Colloidal semiconductor NPLs have been synthesized with atomic-layer precision. Furthermore, core/shell[6-8] and core/crown[9-11] colloidal semiconductor NPLs have also been synthesized. In semiconductor NPLs, electrons and holes are strongly confined only in the thickness direction, and the absorption and

emission features are almost independent of the lateral size of NPLs.[12] Colloidal semiconductor NPLs exhibit tunable, bright luminescence with narrow line widths[5,13] and large absorption cross sections.[14,15] Therefore, colloidal semiconductor NPLs are of interest for various applications, such as light-harvesting materials and lasers, owing to their lower threshold of amplified spontaneous emission and higher gain saturation.[8,13]

The carrier dynamics of photoexcited colloidal NPLs were investigated using luminescence decay measurements,[5] single particle spectroscopy,[7,16] and transient absorption spectroscopy.[11,15,17] Ithurria et al. synthesized CdE (E = S, Se, Te) NPLs and measured the luminescence lifetimes of CdSe NPLs at various temperature (6-300 K).[5] They found that CdSe NPLs exhibited an increase of luminescence intensity and decrease of luminescence lifetime as the temperature decreased, which was a unique signature observed only in quantum wells. The multiple exciton dynamics of CdSe NPLs were examined using time-resolved photoluminescence[8,13,18] and transient absorption measurements.[8] The multiple exciton annihilation in colloidal NPLs was described by a bimolecular process,[18] and slow biexciton Auger recombination with a lifetime from hundreds of ps to 10 ns was observed.[18] Furthermore, Rowland et al. reported picosecond energy transfer from 4-monolayer NPLs to 5-monolayer NPLs in a self-assembled CdSe NPL system, suggesting the potential for multiexciton extraction.[19] In CdSe/CdTe core/crown type-II NPLs, the charge separation dynamics between the core and crown were analyzed using transient absorption spectroscopy.[17]

Efficient charge extraction to the outside of a nanocrystal is very important for the application of semiconductor nanocrystals to photovoltaics and photocatalysis. The charge separation dynamics from various semiconductor nanocrystals to several kinds of acceptor molecules (methyl viologen (MV^{2+}), methylene blue, anthraquinone, etc.)[20-26] and metal nanoparticles[27-31] have been reported. MV^{2+} is especially well known as an efficient electron

90

acceptor for CdSe nanocrystals. Furthermore, in contrast with molecular chromophores and bulk semiconductors, the recent work in semiconductor QD-acceptor molecule complexes has revealed a unique electron transfer process in which the Marcus inverted regime does not exist.[20] In metal nanoparticle–tipped CdSe and CdS NRs, photoinduced electron transfer from the semiconductor to metal (or metal to semiconductor) was analyzed using luminescence decay measurements, transient absorption spectroscopy, and single particle spectroscopy.[28-31] Furthermore, Wu et al. synthesized Pt nanoparticle-attached CdSe NPLs and examined their carrier dynamics using transient absorption spectroscopy.[31] In these nanostructures, ultrafast energy transfer (<150 fs) and ps-scale electron transfer (~9.4 ps) from the band-edge state of CdSe NPLs to the Pt nanoparticles were reported. However, as far as we know, this is the only report analyzing the carrier extraction dynamics from colloidal NPLs to the outside. Moreover, in contrast to metal-attached semiconductor nanocrystal systems, the transient absorption spectra of semiconductor nanocrystal-acceptor molecule complexes show growth kinetics of the radical species of the acceptor molecules, as well as decay kinetics of the semiconductor nanocrystals. Therefore, in semiconductor nanocrystal-acceptor molecule complexes, the electron transfer dynamics can be analyzed in more detail.

In addition, hot electron extraction is a very important process for the development of highly efficient solar cells that are beyond the Shockley-Queisser limit.[32] In a previous theoretical study by Ross and Nozik, the maximum conversion efficiency was reported to reach ~67% when the excess energy of photoexcited hot carriers was utilized.[33] In contrast with bulk semiconductors, semiconductor nanocrystals have discrete electronic states because of the strong confinement of electrons and holes. Consequently, the energy separation between the $1S_e$ and $1P_e$ states is much larger than the LO phonon energy,[34] which leads to different intraband relaxation processes from bulk semiconductors such as Auger cooling and energy transfer to surface ligands.[35-38] Pandey et al. reported extremely slow electron cooling

with a time constant of ~1 ns in CdSe/ZnSe/ZnS/CdSe multishell nanocrystals.[39] Therefore, hot electrons in semiconductor nanocrystals show potential for extraction to the outside. In the work of Tisdale et al., hot electron transfer from colloidal PbSe QDs on single-crystalline (110) TiO_2 (rutile) was observed in femtosecond time-resolved second harmonic generation experiments.[40] Wang et al. reported hot electron transfer from CdSe QDs and CdSe/CdS core/shell QDs to MV^{2+} by analyzing the growth kinetics at the band-edge bleach.[21] Zhu et al. examined ultrafast hot electron transfer in CdSe NR-MV^{2+} complexes.[25] In this report, the electron transfer from CdSe NRs to MV^{2+} was comparable to or faster than that in CdSe QD-MV^{2+} complexes because transfer of the excited electron to MV^{2+} occurred along the radial direction of the NRs, where the electron is strongly confined. Moreover, Sagarzazu et al. examined the carrier dynamics of Au-tipped CdSe NRs and suggested the existence of hot electron transfer from CdSe NRs to Au NPs.[29] However, the occurrence of hot electron transfer in colloidal semiconductor NPLs remains unclear.

In this study, we prepared several kinds of CdSe NPLs with different lateral sizes and CdSe NPL-MV^{2+} complexes. We examined the electron transfer dynamics from CdSe NPLs to MV^{2+} adsorbed on their surfaces using luminescence decay measurements and femtosecond transient absorption spectroscopy. Using the transient absorption measurements, we analyzed the lateral size dependence of the electron transfer dynamics. Furthermore, the hot electron dynamics of the CdSe NPL-MV^{2+} complexes were analyzed by comparing the growth kinetics and initial transient bleach amplitude at the band-edge bleach of CdSe NPLs with those of CdSe NPL-MV^{2+} complexes.

4.3   Experimental section

Synthetic and preparation methods of CdSe NPLs and CdSe NPL-MV^{2+} complexes were described in Chapter 2, respectively. The lateral size and thickness of CdSe NPLs were

characterized by scanning transmission electron microscopy (STEM, TECNAI 20, 200 keV, FEI). UV-vis absorption and luminescence spectra of CdSe NPLs and CdSe NPL-MV^{2+} complexes were recorded using an U-4100 (Hitachi) and a Fluorolog-3 (Jobinyvon-Spex), respectively. Luminescence decays were measured using a time-correlated single-photon counting system. The samples were excited by the second harmonic (415 nm) of a cavity-dumped Ti:sapphire laser (Kapteyn-Murnane, Cascade), and the luminescence signal was detected with a monochromator-microchannel plate photomultiplier combination (JASCO, CT-10, and Hamamatsu, R2809U). The transient absorption spectra were measured using femtosecond pump-probe techniques. The samples were exited at 400 nm using the second harmonic of an amplified mode-locked Ti:sapphire laser (Spitfire and Tsunami, Spectra-Physics, repetition rate: 1 kHz). The pump pulse was focused to a spot with 0.7 mm diameter, and a repetition rate of 0.5 kHz was achieved by using an optical chopper (Model 3501, New Focus, Inc.). The transient absorption was probed using the delayed pulses of a femtosecond white-light continuum generated by focusing the fundamental laser pulse into a D$_2$O cell. Detection was carried out using a polychromator−CCD combination (Spectra Pro-275, Acton Research Co., and Spec-10, Princeton Instruments). The temporal resolution was ~100 fs.

4.4   Results and discussion

4.4.1   Elementary electron transfer processes from CdSe NPL to MV^{2+}

STEM images of CdSe NPLs with different lateral size were shown in Figure 4.1 and their lateral size were summarized in Table 4.1. The thickness of CdSe NPLs was estimated to be ~1.4 nm from STEM image analyses. Steady-state absorption and emission spectra of CdSe NPLs with different size were illustrated in Figure 4.2. CdSe NPLs with different lateral size have similar spectral features, suggesting that all CdSe NPLs have the same thickness.[12]

CdSe NPLs exhibited two narrow absorption band at ~510 nm and ~480 nm, which correspond to the electronic transitions from heavy-hole and light-hole valence bands to the conduction band edge (heavy-hole band and light-hole band), respectively.[4,5] The very narrow band-edge luminescence was observed at ~511 nm, and the luminescence quantum yield of CdSe NPLs were determined by comparing the integrated emission intensity of the CdSe NPLs and that of coumarin343 in ethanol. The absolute quantum yield of coumarin343 in ethanol was measured by QE-2000 (Otsuka Electronics Co., Ltd). Steady-state absorption and emission spectra of CdSe NPLs and CdSe NPL-MV^{2+} complexes were illustrated in Figure 4.3. In the CdSe NPL-MV^{2+} complexes, the absorption of MV^{2+} were superposed on the spectra of CdSe NPLs in the shorter wavelength region (<320 nm).[21,23] Moreover, the band-edge emission of CdSe NPLs were strongly quenched in the CdSe NPL-MV^{2+} complexes (Table 4.2). This luminescence quenching is due to electron transfer from CdSe NPLs to MV^{2+}, as illustrated in the energy diagram shown in Figure 4.3e.[20]

The luminescence decays monitored at the band-edge luminescence peak of CdSe NPLs and CdSe NPL-MV^{2+} complexes are illustrated in Figure 4.4. The luminescence decay of the CdSe NPL-MV^{2+} complexes became much faster than that of the CdSe NPLs, indicating that the excited electron in the band-edge state of CdSe NPLs is transferred to MV^{2+}. As shown in Table 4.3, the electron transfer time in all CdSe NPL-MV^{2+} complexes could not be accurately estimated from the luminescence decay measurements because the estimated lifetime of the excited state of CdSe NPL-MV^{2+} complexes was much shorter than the instrumental response function (~30 ps).

The transient absorption spectra of typical CdSe NPLs C and CdSe NPL-MV^{2+} complexes C excited at 400 nm are shown in Figure 4.5a and 5b. As shown in Figure 4.6, multiexcitons did not contribute to the transient absorption spectra and dynamics because of the low excitation intensity (1.6 μJ/cm^2) in these measurements. In each samples, two bleach

peaks were observed, corresponding to the heavy-hole and light-hole bands in the steady-state spectra. The transient absorption dynamics at heavy-hole and light-hole bands in the typical CdSe NPLs C are illustrated in Figure 4.5c. In the light-hole band dynamics, a fast relaxation component with a lifetime of 240 fs was detected, whereas this fast relaxation was not detected in the heavy-hole band dynamics. This fast relaxation component was probably due to the hole relaxation from light-hole to heavy-hole state. As shown in Figure 4.5b, a very fast relaxation in CdSe NPL-MV^{2+} complexes were clearly observed though the spectral features were similar to those of CdSe NPLs. We assigned the origin of transient absorption bands in CdSe NPLs using the electron and hole acceptor molecules. The detailed results are described in section 4. 4. 2. From these results, the excited electron predominantly contributed to the heavy-hole band dynamics, and both electron and hole contributed to the light-hole band dynamics in CdSe NPLs. Consequently, the fast relaxation at the heavy-hole band of CdSe NPL-MV^{2+} complexes was due to the electron transfer from band-edge state of CdSe NPLs to MV^{2+}. Furthermore, as shown in Figure 4.7, a broad absorption band centered at ~620 nm corresponding to the methyl viologen cation radical (MV^{+} radical) was observed in the transient absorption spectra, further supporting the electron transfer from CdSe NPLs to MV^{2+}.[41] As the formation of the MV^{+} radical originated from the electron transfer from the CdSe NPLs to MV^{2+}, the rise components of the MV^{+} radical band, as well as the decay components of the heavy-hole band, should represent the electron transfer processes. However, the growth kinetics of the MV^{+} radical band could not be accurately analyzed because of the weak transient absorption signal at the very low excitation intensity of 1.6 μJ/cm^2. Therefore, we used somewhat higher excitation intensity (10 μJ/cm^2) for the analysis of the electron transfer dynamics in MV^{+} radical band (the growth kinetics of the MV^{+} radical band with both excitation intensities are very similar).[42] The transient absorption dynamics at heavy-hole band and MV^{+} radical band in all CdSe NPL-MV^{2+} complexes obtained using an

excitation intensity of 10 μJ/cm^2 were shown in Figure 4.8, and the fitting results were summarized in Table 4.4. Two rise and two decay components were detected in MV$^+$ radical band and heavy-hole band, respectively. However, the amplitudes of two rise and decay components does not match well with each other. In the heavy-hole band dynamics of CdSe NPLs, the intrinsic fast relaxation component with the lifetime of a few picoseconds exists. Therefore, the electron transfer rate analyzed from heavy-hole band dynamics included some uncertainty, which leads to the difference of the amplitudes. For the clarification of two electron transfer rates, we analyzed the lateral size dependence of the electron transfer dynamics from CdSe NPLs to MV^{2+}. In previous studies on QD-MV^{2+} complexes, the electron transfer rate depends on the number of acceptor molecules adsorbed on each QD.[43] To analyze the number of MV^{2+} molecules on the surface of each CdSe NPLs, the absorption cross section (σ_{NPL}) of the CdSe NPLs was estimated by assuming that the σ_{NPL} value of CdSe NPLs with the same thickness is proportional to the physical cross section and comparing with the reported value (3.91 × 10^{-14} cm^2 at 400 nm for a lateral size of 230 nm^2).[14] By analyzing the steady-state absorption (Figure 4.3), the ratio of MV^{2+} to CdSe NPL was estimated to be ~80 for each of the CdSe NPL-MV^{2+} complexes. The time constants of the two electron transfer processes obtained by fitting the growth kinetics of the MV$^+$ (Table 4.4) became longer as the lateral dimension of the CdSe NPLs increased (τ_{fast}: from 370 to 580 fs; τ_{slow}: from 2.4 to 6.2 ps). In addition, A biexponential decay was observed in the long-time region for the MV$^+$ radical band, corresponding to the charge recombination between the electron in the MV$^+$ radical and the hole in the valence band of the CdSe NPLs (back electron transfer from the MV$^+$ radical to CdSe NPLs). Both lifetimes became slower as the lateral size of CdSe NPLs increased.

The electron transfer rate was expressed as the sum of the electron transfer rates to all possible accepting states as given in the following equation[44-47]

$$k_{ET} = \frac{2\pi}{\hbar} \int_{-\infty}^{\infty} dE \, \rho(E) |\bar{H}(E)|^2 \frac{1}{\sqrt{4\pi\lambda k_B T}} \times exp\left[-\frac{(\lambda + \Delta G + E)^2}{4\lambda k_B T}\right] \qquad (1)$$

where k_{ET} is the total rate constant of electron transfer, $\rho(E)$ is the density of the MV^{2+} final state, ΔG_0 is the change in Gibbs energy corresponding to the energy difference between the band-edge state of the CdSe NPLs and the LUMO level of MV^{2+}, λ is the reorganization energy, which is the sum of the inner-sphere, λ_i, and outer-sphere, λ_o, components, and $|\bar{H}(E)|$ is the electronic coupling constant between the initial conduction band-edge state of the CdSe NPLs and the final state of MV^{2+}. As shown in Figure 4.2, each of the CdSe NPLs with a different lateral size had a similar absorption peak wavelength, indicating that all CdSe NPLs have comparable bandgap energies and conduction band edge energies. Therefore, ΔG_0 does not change with the lateral size of the CdSe NPLs. In addition, the inner-sphere term of the reorganization energy, λ_i, has contributions from both the CdSe NPLs and acceptor molecules. According to previous studies, the contribution from acceptor molecules (a few hundreds of meV)[20] to λ_i is dominant, whereas that from semiconductor nanocrystals (~10 meV)[48] is negligible. The outer-sphere term, λ_o, which is related to the dielectric response of the solvent and ligand, depends on the size of nanocrystals.[49-51] However, the change in λ_o with the size of the CdSe NPLs is not very large (~10 meV) because of the relatively large size of the CdSe NPLs and the small difference between the static and optical dielectric constants of chloroform. As a result, the overall change in the reorganization energy ($\lambda_i + \lambda_o$) with lateral size does not significantly affect the electron transfer rate from the CdSe NPLs to MV^{2+}. The electronic coupling constant, $|\bar{H}(E)|$, depends on the degree of overlap between the penetrated wave function of the conduction band-edge state of CdSe NPLs and MV^{2+} adsorbed on the NPL surface. Zhu et al. reported that the electronic coupling strength is proportional to the amplitude of the electron density at

the surface of QDs, with the density increasing as the size of the QDs decreases (~10 times larger with a decrease of the radius from 2 to 1 nm),[20] indicating that the electronic coupling between QDs and acceptor molecules is stronger in smaller QDs. Therefore, the lateral size dependence of the electron transfer time from CdSe NPLs to MV^{2+} probably originated from a change in the electronic coupling strength.

Since the shape of the CdSe NPLs was highly anisotropic, with a large lateral size (short axis of 5.1−7.5 nm and long axis of 15.0−22.8 nm) and small thickness (1.4 nm), the electronic coupling strength between the CdSe NPLs and MV^{2+} should be different at the different CdSe NPLs faces. Therefore, the two electron transfer rates observed probably originate MV^{2+} adsorbed on different CdSe NPLs faces. We deduced that MV^{2+} likely adsorbed on the faces perpendicular to the short and long axes in the lateral dimension of the CdSe NPLs for the following reasons. If MV^{2+} were adsorbed on the face perpendicular to the thickness direction (the plane of CdSe NPLs), the electronic coupling strength would not change with the lateral size because all the CdSe NPLs have the same thickness. Thus, electron transfer from the CdSe NPLs to MV^{2+} adsorbed on the face perpendicular to the thickness direction is expected to be similar for all the CdSe NPL-MV^{2+} complexes. However, in our results, the time constants of the fast and slow electron transfer depend clearly on the lateral size of the CdSe NPLs. Furthermore, previous studies have reported that the faces perpendicular to the thickness direction are well passivated by carboxylic acid groups.[6,16,52,53] Moreover, these faces are terminated with cadmium atoms.[6,16,52,53] Peterson et al. reported that MV^{2+} tends to adsorb to the anionic surface (S-terminated) of CdS QDs because MV^{2+} is a cationic molecule.[43] For these reasons, MV^{2+} cannot be adsorbed on the faces perpendicular to the thickness direction of the CdSe NPLs. In addition, as mentioned above, electron transfer from semiconductor nanocrystals to acceptor molecules adsorbed on the surface is faster in the smaller nanocrystals because of differences in the electronic coupling at the surface.

Therefore, the observed fast and slow electron transfer from the CdSe NPLs to MV^{2+} can be assigned to electron transfer at the faces perpendicular to the short and long axes in the lateral dimension, respectively (Figure 4.9). The fast and slow electron transfer rates are plotted against the length of the short and long axes in the lateral dimension of the CdSe NPLs, as shown in Figure 4.10. A good correlation was shown between two electron transfer rates and the length of the short and long axes.

In previous studies, the electron transfer dynamics in semiconductor nanocrystal-acceptor molecule complexes was fitted by a kinetic model derived from the Poisson distribution.[20,22,43] This model assumes that the number of acceptor molecules adsorbed on the surface of a nanocrystal follows Poisson statistics and the observed electron transfer rate increases linearly with the number of adsorbed acceptor molecules. Therefore, the observed electron transfer kinetics is written as $\sum_{n=1}^{\infty} A_n e^{-nk_{ET,int}t}$, where $k_{ET,int}$ is the intrinsic electron transfer rate of one semiconductor nanocrystal with one adsorbed acceptor molecule and A_n is the amplitude of the nth electron transfer component. This sum of exponential functions can be converted to the following function[20,22,43,54]

$$\sum_{n=1}^{\infty} A_n e^{-nk_{ET,int}t} = e^{\left[m\left(e^{-k_{ET,int}t}-1\right)\right]} \qquad (2)$$

where m is the average number of acceptor molecules adsorbed on the surface of a semiconductor nanocrystal which can be estimated from UV-vis absorption spectra. We simulated the growth kinetics of the MV^+ radical band using the Poisson-derived function with a m value of 80 (Figure 4.11). However, as shown in Figure 4.11, the growth kinetics cannot be well fitted by this function. In this expression, when the value of $k_{ET,int}t$ is small, $e^{-k_{ET,int}t}$ is approximated as $1 - k_{ET,int}$, indicating that the Poisson-derived function approaches a single-exponential function.[22,55] In our simulation of the dynamics of the MV^+

radical band, the product $k_{ET,int}t$ is very small for all the CdSe NPL-MV^{2+} complexes in the initial time region ($k_{ET,int}t < 0.15$ at t $\leq$ 10 ps). Therefore, the biexponential-like growth kinetics of the MV$^+$ radical band can be explained by the adsorption of MV^{2+} on different faces of the CdSe NPLs.

By assuming hot electron transfer, the rise time of the heavy-hole band in the CdSe NPL-MV^{2+} complexes can be expressed as the inverse of the sum of the rate constants of intraband relaxation and hot electron transfer, indicating that the rise time of the heavy-hole band in the CdSe NPL-MV^{2+} complexes should be faster than that in the CdSe NPLs. The growth kinetics of the CdSe NPLs and CdSe NPL-MV^{2+} complexes at the heavy-hole band are illustrated in Figure 4.12. As clearly shown, the rise times of both samples are very similar (~70 fs), and the initial amplitudes of the transient bleach at the heavy-hole band divided by the ground state absorbance value (ΔOD/OD) were also very similar. These results indicate that the rate of hot electron relaxation in the CdSe NPL-MV^{2+} complexes is very similar to that in the CdSe NPLs, indicating that hot electron transfer does not occur. In contrast to our results, hot electron transfer from CdSe QDs[21,24] and CdSe NRs[25] to MV^{2+} has been observed in previous studies. As QDs have a discrete electronic state, the hot electron relaxes to the band-edge state through energy transfer to the hole (Auger cooling).[35-37] The hot electron in QDs relaxes to the band-edge (1S$_e$) state with a lifetime of a few hundreds of fs to several ps.[34,38,56,57] Yu et al.[58] and Spann et al.[59] reported hot electron relaxation in CdSe NRs with similar time scales to that in CdSe QDs. On the other hand, semiconductor NPLs have relatively continuous electronic states in the conduction band because of the large lateral dimension. Therefore, the hot electron in CdSe NPLs relaxes to the band-edge state via these continuous electronic states by immediate phonon emission.[60] Indeed, the intraband relaxation time of the hot electron in the CdSe NPLs with different lateral sizes was much faster (~60-70 fs) than that in CdSe QDs and NRs. In previous studies, ultrafast electron transfer was

observed from CdSe QDs to MV^{2+} within tens of fs.[20,23] Furthermore, in the case of CdSe NR-MV^{2+} complexes, ultrafast electron transfer (~60 fs) to MV^{2+} occurred along the short axis (3.2 nm) because of strong electronic coupling.[25] In the CdSe NPL-MV^{2+} complexes, the electron transfer processes were slower than those in CdSe QD-MV^{2+} and NR-MV^{2+} complexes, owing to the relatively weak electronic coupling along the short and long axes in the lateral dimension. Because of the fast intraband relaxation and slow electron transfer, hot electron transfer did not occur from the CdSe NPLs to MV^{2+}.

4.4.2 The assignment of transient absorption bands of CdSe NPLs

Transient absorption spectra at visible and near-IR region, and dynamics at each band of CdSe NPLs B are illustrated in Figure 4.13. In the transient absorption spectra of CdSe NPLs B, the induced absorption peak in the near-IR region (~1060 nm) was clearly observed as well as heavy-hole and light-hole bands in the visible region. As shown in Figure 4.13c, the fast decay component corresponding to the hole relaxation with a lifetime of 240 fs was observed only in the light–hole band dynamics. Moreover, the decay kinetics of induced absorption band at near-IR region was nearly identical with that of heavy-hole band, suggesting that the origin of near-IR band was the absorption of excited electron or hole at the band-edge states.[15] In order to assign these transient absorption bands of CdSe NPLs, we examined the transient absorption dynamics of CdSe NPLs B with electron acceptor (MV^{2+}) and hole acceptor (phenothiazine, PTZ) molecules.[25] Steady-state absorption and luminescence spectra of these samples were illustrated in Figure 4.14a and 14b, where the absorption of acceptor molecules at shorter wavelength region (<400 nm) and luminescence quenching in CdSe NPL-acceptor molecule complexes were observed. In addition, luminescence decays of CdSe NPL-acceptor molecules complexes monitored at the band-edge luminescence peak (inset of Figure 4.14b) became faster than that of CdSe NPLs,

resulting from electron and hole transfer from CdSe NPLs to acceptor molecules.[61,62] As shown in Figure 4.15, transient absorption spectra of CdSe NPL-MV^{2+} and CdSe NPL-PTZ complexes in visible and near-IR region have similar features to those of CdSe NPLs. Transient absorption dynamics at each band are shown in Figure 4.16. In CdSe NPL-MV^{2+} complexes, transient absorption dynamics at each band showed much faster relaxation than those of CdSe NPLs, corresponding to the electron transfer from the conduction band-edge of CdSe NPLs to MV^{2+}. This fast relaxation in CdSe NPL-MV^{2+} complexes indicates that excited electron in conduction band-edge contributes to all transient absorption band of CdSe NPLs. In contrast, transient absorption dynamics of CdSe NPL-PTZ complexes were similar to those of CdSe NPLs, though the luminescence decay of CdSe NPL-PTZ complexes was faster than that of CdSe NPLs. The similar transient absorption dynamics of CdSe NPLs and CdSe NPL-PTZ complexes indicates that the hole transfer from CdSe NPLs to PTZ did not affect to all transient absorption band of CdSe NPLs. However, as mentioned above, hot hole relaxation with the time constant of 240 fs were observed at the light-hole band of CdSe NPLs, suggesting that excited hole in the valence band contributes to the light-hole band. As a result, although the excited hole contributes to the light-hole band, hole transfer dynamics from CdSe NPLs to PTZ could not be observed because of the very fast hole relaxation. These comparisons of transient absorption dynamics between CdSe NPLs and CdSe NPL-acceptor molecule complexes revealed that excited electron in conduction band predominantly contributed to the heavy-hole and near-IR band, and both electron and hole contributed to the light-hole band.

Benchamekh et al. calculated the electronic structure of colloidal CdSe NPLs by tight-binding approximation, where the energy spacing between the conduction band-edge and next higher electronic state was ~1.2 eV.[63] Therefore, induced absorption peak observed in the near-IR region (~1.17 eV) was assigned to the electronic transition between conduction

band-edge and next higher electronic state.

4.5 Conclusion

In conclusion, we prepared CdSe NPLs with different lateral sizes and the corresponding CdSe NPL-MV^{2+} complexes and examined their carrier dynamics using luminescence decay measurements and femtosecond transient absorption spectroscopy. Transient absorption spectroscopy of the CdSe NPL-MV^{2+} complexes revealed fast recovery of the heavy-hole band and growth of the MV^{+} radical band due to electron transfer from the CdSe NPLs to MV^{2+}. An analysis of the transient absorption dynamics revealed the existence of fast and slow electron transfer processes from the band-edge state of CdSe NPLs to MV^{2+}. The time constants of these fast and slow electron transfer processes decreased in the larger CdSe NPL-MV^{2+} complexes. This dependence of the electron transfer on the lateral size is due to a change in the electronic coupling strength between the penetrated wave function of the CdSe NPLs and MV^{2+} adsorbed on the surface. Furthermore, the two electron transfer processes originated from the different faces of the CdSe NPLs where MV^{2+} adsorbed, with fast and slow electron transfer occurring along the short and long axes in the lateral dimension, respectively. The analysis of the initial bleach amplitude and growth kinetics at the heavy-hole band indicates that hot electron transfer does not occur from the CdSe NPLs to MV^{2+}. This is probably due to the faster hot electron relaxation and relatively slow electron transfer time in CdSe NPL-MV^{2+} complexes when compared with CdSe QD-MV^{2+} and NR-MV^{2+} complexes. Our experimental results will provide the new insight into the electron extraction mechanism from colloidal semiconductor nanocrystals.

References

(1) Murray, C. B.; Norris, D. J.; Bawendi, M. G. Synthesis and Characterization of Nearly Monodisperse CdE (E = Sulfur, Selenium, Tellurium) Semiconductor Nanocrystallites. *J. Am. Chem. Soc.* **1993**, *115*, 8706–8715.

(2) Peng, X.; Manna, L.; Yang, W.; Wickham, J.; Scher, E.; Kadavanich, A.; Alivisatos, A. P. Shape control of CdSe nanocrystals. *Nature* **2000**, *404*, 59–61.

(3) Manna, L.; Scher, E.; Alivisatos, A. P. Synthesis of Soluble and Processable Rod–, Arrow–, Teardrop–, and Tetrapod–Shaped CdSe Nanocrystals. *J. Am. Chem. Soc.* **2000**, *122*, 12700–12706.

(4) Ithurria, S.; Dubertret, B. Quasi 2D Colloidal CdSe Platelets with Thicknesses Controlled at the Atomic Level. *J. Am. Chem. Soc.* **2008**, *130*, 16504–16505.

(5) Ithurria, S.; Tessier, M. D.; Mahler, B.; Lobo, R. P. S. M.; Dubertret, B.; Efros, Al. L. Colloidal Nanoplatelets with Two–dimensional Electronic Structure. *Nature* **2011**, *10*, 936–941.

(6) Mahler, B.; Nadal, B.; Bouet, C.; Patriarche, G.; Dubertret, B. Core/Shell Colloidal Semiconductor Nanoplatelets. *J. Am. Chem. Soc.* **2012**, *134*, 18591–18598.

(7) Tessier, M. D.; Mahler, B.; Nadal, B.; Heuclin, H.; Pedetti, S.; Dubertret, B. Spectroscopy of Colloidal Semiconductor Core/Shell Nanoplatelets with High Quantum Yield. *Nano Lett.* **2013**, *13*, 3321–3328.

104

(8) She, C.; Fedin, I.; Dolzhnikov, D. S.; Demortière, A.; Schaller, R. D.; Pelton, M.; Talapin, D. V. Low–Threshold Stimulated Emission Using Colloidal Quantum Wells. *Nano Lett.* **2014**, *14*, 2772–2777.

(9) Pedetti, S.; Ithurria, S.; Heuclin, H.; Patriarche, G.; Dubertret, B. Type–II CdSe/CdTe Core/Crown Semiconductor Nanoplatelets. *J. Am. Chem. Soc.* **2014**, *136*, 16430–16438.

(10) Kelestemur, Y.; Olutas, M.; Delikanli, S.; Guzelturk, B.; Akgul, M. Z.; Demir, H. V. Type–II Colloidal Quantum Wells: CdSe/CdTe Core/Crown Heteronanoplatelets. *J. Phys. Chem. C* **2015**, *119*, 2177–2185.

(11) Li, Q.; Wu, K.; Chen, J.; Chen, Z.; McBride, J. R.; Lian, T. Size–Independent Exciton Localization Efficiency in Colloidal CdSe/CdS Core/Crown Nanosheet Type–I Heterostructures. *ACS Nano* **2016**, *10*, 3843–3851.

(12) Olutas, M.; Guzelturk, B.; Kelestemur, Y.; Yeltik, A.; Delikanli, S.; Demir, H. V. Lateral Size–Dependent Spontaneous and Stimulated Emission Properties in Colloidal CdSe Nanoplatelets. *ACS Nano* **2015**, *9*, 5041–5050.

(13) She, C.; Fedin, I.; Dolzhnikov, D. S.; Dahlberg, P. D.; Engel G. S.; Schaller, R. D.; Talapin, D. V. Red, Yellow, Green, and Blue Amplified Spontaneous Emission and Lasing Using Colloidal CdSe Nanoplatelets. *ACS Nano* **2015**, *9*, 9475–9485.

(14) Baghani, E.; O'Leary, S. K.; Fedin, I.; Talapin, D. V.; Pelton, M. Auger–Limited Carrier Recombination and Relaxation in CdSe Colloidal Quantum Wells. *J. Phys. Chem.*

Lett. **2015**, *6*, 1032–1036.

(15)   Pelton, M.; Ithurria, S.; Schaller, R. D.; Dolzhnikov, D. S.; Talapin, D. V. Carrier

Cooling in Colloidal Quantum Wells. *Nano Lett.* **2012**, *12*, 6158–6163.

(16)   Tessier, M. D.; Javaux, C.; Maksimovic, I.; Loriette, V.; Dubertret, B. Spectroscopy

of Single CdSe Nanoplatelets. *ACS Nano* **2012**, *6*, 6751–6758.

(17)   Wu, K.; Li, Q.; Jia, Y.; McBride, J. R.; Xie, Z.; Lian, T. Efficient and Ultrafast

Formation of Long–Lived Charge–Transfer Exciton State in Atomically Thin Cadmium

Selenide/Cadmium Telluride Type–II Heteronanosheets. *ACS Nano* **2015**, *9*, 961–968.

(18)   Kunneman, L. T.; Tessier, M. D.; Heuclin, H.; Dubertret, B.; Aulin, Y. V.; Grozema,

F. C.; Schins, J. M.; Siebbeles, L. D. A. Bimolecular Auger Recombination of

Electron–Hole Pairs in Two–Dimensional CdSe and CdSe/CdZnS Core/Shell

Nanoplatelets. *J. Phys. Chem. Lett.* **2013**, *4*, 3574–3578.

(19)   Rowland, C. E.; Fedin, I.; Zhang, H.; S. K. Gray, Govorov, A. O.; Talapin, D. V.;

Schaller, R. D. Picosecond Energy Transfer and Multiexciton Transfer Outpaces Auger

Recombination in Binary CdSe nanoplatelet Solids. *Nature Materials* **2015**, *14*, 484–489.

(20)   Zhu, H.; Yang, Y.; Hyeon–Deuk, K.; Califano, M.; Song, N.; Wang, Y.; Zhang, W.;

Prezhdo, O. V.; Lian, T. Auger–Assisted Electron Transfer from Photoexcited

Semiconductor Quantum Dots. *Nano Lett.* **2014**, *14*, 1263–1269.

(21)   Wang, Y.; Wang, H.; Li, Z.; Zhao, J.; Wang, L.; Chen, Q.; Wang, W.; Sun, H.

Electron Extraction Dynamics in CdSe and CdSe/CdS/ZnS Quantum Dots Adsorbed with Methyl Viologen. *J. Phys. Chem. C* **2014**, *118*, 17240–17246.

(22)   Morris–Cohen, A. J.; Frederick, M. T.; Cass, L. C.; Weiss, E. A. Simultaneous Determination of the Adsorption Constant and the Photoinduced Electron Transfer Rate for a CdS Quantum Dot–Viologen Complex. *J. Am. Chem. Soc.* **2011**, *133*, 10146–10154.

(23)   Matylitsky, V. V.; Dworak, L.; Breus, V. V.; Basché, T.; Wachtveitl, J. Ultrafast Charge Separation in Multiexcited CdSe Quantum Dots Mediated by Adsorbed Electron Acceptors. *J. Am. Chem. Soc.* **2009**, *131*, 2424–2425.

(24)   Zhu, H.; Song, N.; Rodríguez–Córdoba, W.; Lian, T. Wave Function Engineering for Efficient Extraction of up to Nineteen Electrons from One CdSe/CdS Quasi–Type II Quantum Dot. *J. Am. Chem. Soc.* **2012**, *134*, 4250–4257.

(25)   Zhu, H.; Lian, T. Enhanced Multiple Exciton Dissociation from CdSe Quantum Rods: The Effect of Nanocrystal Shape. *J. Am. Chem. Soc.* **2012**, *134*, 11289–11297.

(26)   Zhu, H.; Song, N.; Lian, T. Controlling Charge Separation and Recombination Rates in CdSe/ZnS Type I Core−Shell Quantum Dots by Shell Thicknesses. *J. Am. Chem. Soc.* **2010**, *132*, 15038–15045.

(27)   Khon, E.; Mereshchenko, A.; Tarnovsky, A. N.; Acharya, K.; Klinkova, A.; Hewa–Kasakarage, N. N.; Nemitz, I.; Zamkov, M. Suppression of the Plasmon Resonance in Au/CdS Colloidal Nanocomposites. *Nano Lett.* **2011**, *11*, 1792–1799.

(28) Wu, K.; Chen, J.; McBride, J. R.; Lian, T. Efficient Hot–Electron Transfer by a

Plasmon–Induced Interfacial Charge-Transfer Transition. *Science* **2015**, *349*, 632-635.

(29) Sagarzazu, G.; Inoue, K.; Saruyama, M.; Sakamoto, M.; Teranishi, T.; Masuo, S.;

Tamai, N. Ultrafast Dynamics and Single Particle Spectroscopy of Au–CdSe Nanorods.

Phys. Chem. Chem. Phys. **2013**, *15*, 2141-2152.

(30) Mongin, D.; Shaviv, E.; Maioli, P.; Crut, A. Banin, U.; Fatti, N. D.; Vallée, F.

Ultrafast Photoinduced Charge Separation in Metal–Semiconductor Nanohybrids. *ACS*

Nano **2012**, *6*, 7034–7043.

(31) Wu, K.; Li, Q.; Du, Y; Chen, Z.; Lian, T. Ultrafast Exciton Quenching by Energy

and Electron Transfer in Colloidal CdSe Nanosheet–Pt Heterostructures. *Chem. Sci.* **2015**,

6, 1049-1054.

(32) Shockley, W.; Queisser, H. J. Detailed Balance Limit of Efficiency of p–n Junction

Solar Cells. *J. Appl. Phys.* **1961**, *32*, 510.

(33) Ross, R. T.; Nozik, A. J. Efficiency of hot–carrier solar energy converters. *J. Appl.*

Phys. **1982**, *53*, 3813–3818.

(34) Klimov, V. I. Optical Nonlinearities and Ultrafast Carrier Dynamics in

Semiconductor Nanocrystals. *J. Phys. Chem. B* **2000**, *104*, 6112–6123.

(35) Cooney, R. R.; Sewall, S. L.; Anderson, K. E. H.; Dias, E. A.; Kambhampati, P.

Breaking the Phonon Bottleneck for Holes in Semiconductor Quantum Dots. *Phys. Rev.*

Lett. **2007**, *98*, 177403.

(36)   Cooney, R. R.; Sewall, S. L.; Dias, E. A.; Sagar, D. M.; Anderson, K. E. H.;

Kambhampati, P. Unified Picture of Electron and Hole Relaxation Pathways in

Semiconductor Quantum Dots. *Phys. Rev. B* **2007**, *75*, 245311.

(37)   Sewall, S. L.; Cooney, R. R.; Anderson, K. E. H.; Dias, E. A.; Kambhampati, P.

State-to-State Exciton Dynamics in Semiconductor Quantum Dots. *Phys. Rev. B* **2006**, *74*,

235328.

(38)   Guyot–Sionnest, P.; Wehrenberg, B.; Yu, D. Intraband Relaxation in CdSe

Nanocrystals and the Strong Influence of the Surface Ligands. *J. Chem. Phys.* **2005**, *123*,

074709.

(39)   Pandey, A.; Guyot–Sionnest, P. Slow Electron Cooling in Colloidal Quantum Dots.

Science **2008**, *322*, 929–932.

(40)   Tisdale, W. A.; Williams, K. J.; Timp, B. A.; Norris, D. J.; Aydil, E. S.; Zhu, X.-Y.

Hot–Electron Transfer from Semiconductor Nanocrystals. *Science* **2010**, *328*, 1543–1547.

(41)   Vuckovic, M.; Mentus, S. V.; Janata, E.; Milosavljevic, B. H. Fast Dimerisation of

the Triparaquat Radical Dication. *Phys. Chem. Chem. Phys.* **2001**, *3*, 4310-4315.

(42)   Yang, Y.; Rodríguez–Córdoba, W.; Lian T.   Multiple Exciton Generation and

Dissociation in PbS Quantum Dot–Electron Acceptor Complexes. Nano Lett., 2012, 12,

4235–4241.

(43)   Peterson, M. D.; Jensen, S. C.; Weinberg, D. J.; Weiss, E. A. Mechanisms for

Adsorption of Methyl Viologen on CdS Quantum Dots. *ACS Nano* **2014**, *8*, 2826–2837.

(44)   Asbury, J. B.; Hao, E.; Wang, Y.; Ghosh, H. N.; Lian, T. Ultrafast Electron Transfer

Dynamics from Molecular Adsorbates to Semiconductor Nanocrystalline Thin Films. *J.

Phys. Chem. B* **2001**, *105*, 4545–4557.

(45)   Gao, Y. Q.; Marcus, R. A. On the Theory of Electron Transfer Reactions at

Semiconductor/Liquid Interfaces. II. A Free Electron Model. *J. Chem. Phys.* **2000**, *113*,

6351–6360.

(46)   Gosavi, S.; Marcus, R. A. Nonadiabatic Electron Transfer at Metal Surfaces. *J. Phys.

Chem. B* **2000**, *104*, 2067–2072.

(47)   Gao, Y. Q.; Georgievskii, Y.; Marcus, R. A. On the Theory of Electron Transfer

Reactions at Semiconductor Electrode/Liquid Interfaces. *J. Chem. Phys.* **2000**, *112*,

3358–3369.

(48)   Tvrdy, K.; Frantsuzov, P. A.; Kamat, P. V. Photoinduced Electron Transfer from

Semiconductor Quantum Dots to Metal Oxide Nanoparticles. *Proc. Natl. Acad. Sci. USA*

2011, *108*, 29–34.

(49)   Parker, J. F.; Choi, J.–P.; Wang, W.; Murray, R. W. Electron Self–exchange

Dynamics of the Nanoparticle Couple $[Au_{25}(SC_2Ph)_{18}]^{0/1-}$ By Nuclear Magnetic

Resonance Line–Broadening. *J. Phys. Chem. C* **2008**, *112*, 13976–13981.

(50)   Marcus, R. A. On the Theory of Electron–Transfer Reactions. VI. Unified Treatment

for Homogeneous and Electrode Reactions. *J. Chem. Phys.* **1965**, *43*, 679–701.

(51)   Marcus, R. A.; Sutin, N. Electron Transfers in Chemistry and Biology. *Biochimica et*

Biophysica Acta, **1985**, *811*, 265–322.

(52)   Lhuillier, E.; Pedetti, S.; Ithurria, S.; Nadal, B.; Heuclin, H.; Dubertret, B.

Two-Dimensional Colloidal Metal Chalcogenides Semiconductors: Synthesis,

Spectroscopy, and Applications. *Acc. Chem. Res.* **2015**, *48*, 22–30.

(53)   Li, Z.; Peng, X. Size/Shape–Controlled Synthesis of Colloidal CdSe Quantum Disks:

Ligand and Temperature Effects. J. Am. Chem. Soc. 2011, 133, 6578–6586.

(54)   Tachiya, M. Application of a Generating Function to Reaction Kinetics in Micelles.

Kinetics of Quenching of Luminescent Probes in Micelles. *Chem. Phys. Lett.*, **1975**, *33*,

289–292.

(55)   Rodgers, M. A. J.; Wheeler, M. F. D. S. E; Quenching of Fluorescence from Pyrene

in Micellar Solutions by Cationic Quenchers. *Chem. Phys. Lett.* **1978**, *53*, 165–169.

(56)   Guyot–Sionnest, P.; Shim, M.; Matranga, C.; Hines, M. Intraband Relaxation in

CdSe Quantum Dots. *Phys. Rev. B* **1999**, *60*, R2181–2184.

(57)   Kambhampati, P. Hot Exciton Relaxation Dynamics in Semiconductor Quantum

Dots: Radiationless Transitions on the Nanoscale. *J. Phys. Chem. C*, **2011**, *115*,

22089–22109.

(58)   Yu, P.; Nedeljkovic, J. M.; Ahrenkiel, P. A.; Ellingson, R. J.; Nozik, A. J. Size

Dependent Femtosecond Electron Cooling Dynamics in CdSe Quantum Rods. *Nano Lett.*

2004, *4*, 1089–1092.

(59)   Spann, B. T.; Xu, X. Ultrafast Spectroscopy of CdSe Nanocrystals: Morphological

and Environmental Effects on Nonradiative and Nonadiabatic Relaxation. *J. Phys. Chem.*

C **2014**, *118*, 2844–2850.

(60)   Sippel, P.; Albrecht, W.; van der Bok, J. C.; Van Dijk–Moes, R. J. A.; Hannappel, T.;

Eichberger, R.; Vanmaekelbergh, D. Femtosecond Cooling of Hot Electrons in CdSe

Quantum–Well Platelets. *Nano Lett.* **2015**, *15*, 2409–2416.

(61)   Zhu, H.; Yang, Y.; Hyeon–Deuk, K.; Califano, M.; Song, N.; Wang, Y.; Zhang, W.;

Prezhdo, O. V.; Lian, T. Auger–Assisted Electron Transfer from Photoexcited Semiconductor

Quantum Dots. *Nano Lett.* **2014**, *14*, 1263–1269.

(62)   Wu, K.; Du, Y.; Tang, H.; Chen, Z.; Lian, T. Efficient Extraction of Trapped Holes from

Colloidal CdS Nanorods. *J. Am. Chem. Soc.* **2015**, *137*, 10224–10230.

(63)   Benchamekh, R.; Gippius, N. A.; Even, J.; Nestoklon, M. O.; Jancu, J. M.; Ithurria,

S.; Dubertret, B.; Eflos, A. L.; Voisin, P. Tight–binding Calculations of Image-charge

Effects in Colloidal Nanoscale Platelets of CdSe. *Phys. Rev. B* **2014**, *89*, 035307.
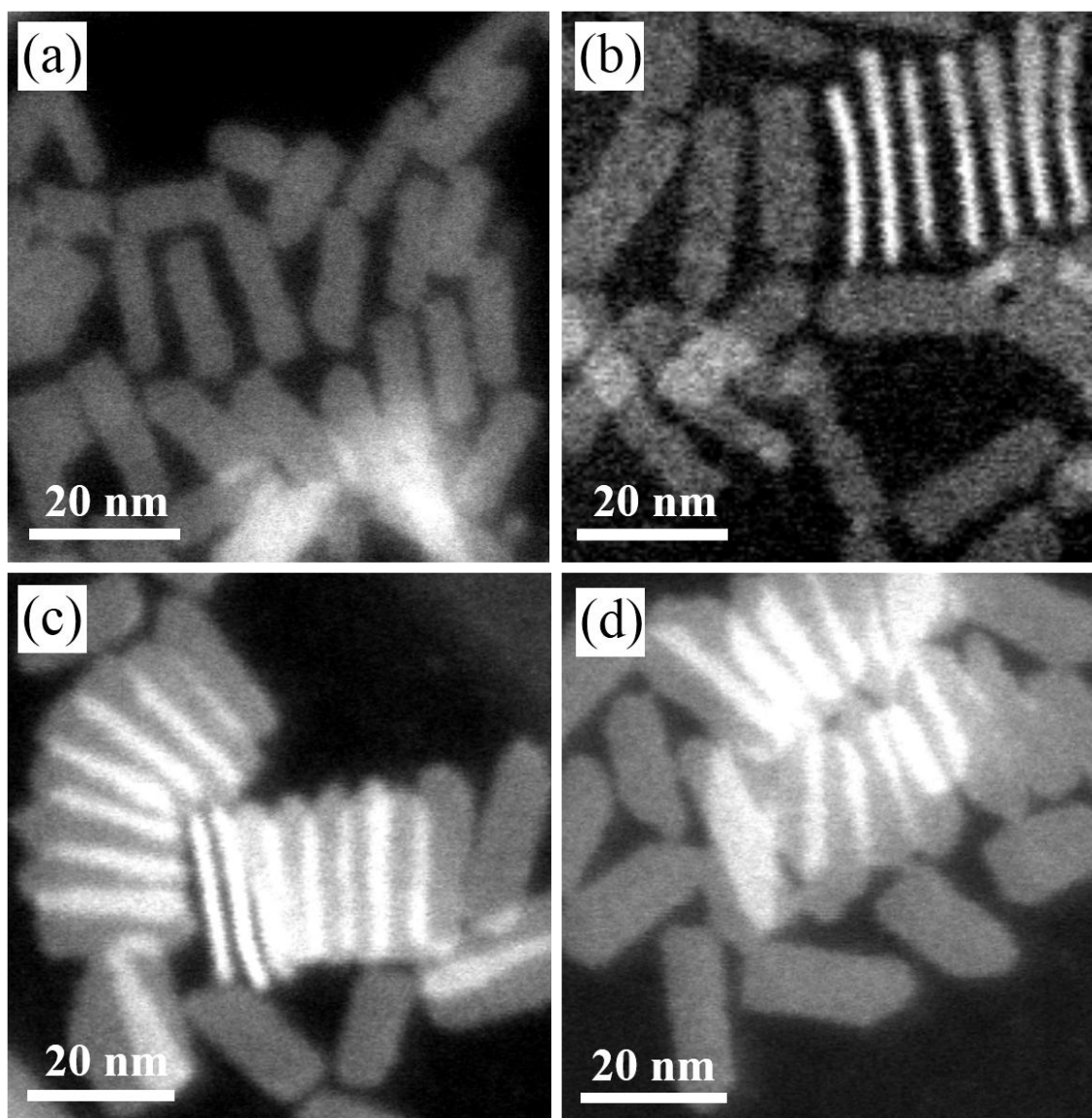
Figure 4.1 STEM images of CdSe NPLs (a) A, (b) B, (c) C, and (d) D.

Table 4.1 Lateral size of each CdSe NPLs

Sample	Reaction time / min	Short axis / nm	Long axis / nm
CdSe NPLs A	4	15.0 ± 2.2	5.1 ± 0.7
CdSe NPLs B	7	21.3 ± 2.7	5.8 ± 0.8
CdSe NPLs C	15	21.7 ± 3.0	6.7 ± 0.8
CdSe NPLs D	20	22.8 ± 3.0	7.5 ± 0.9
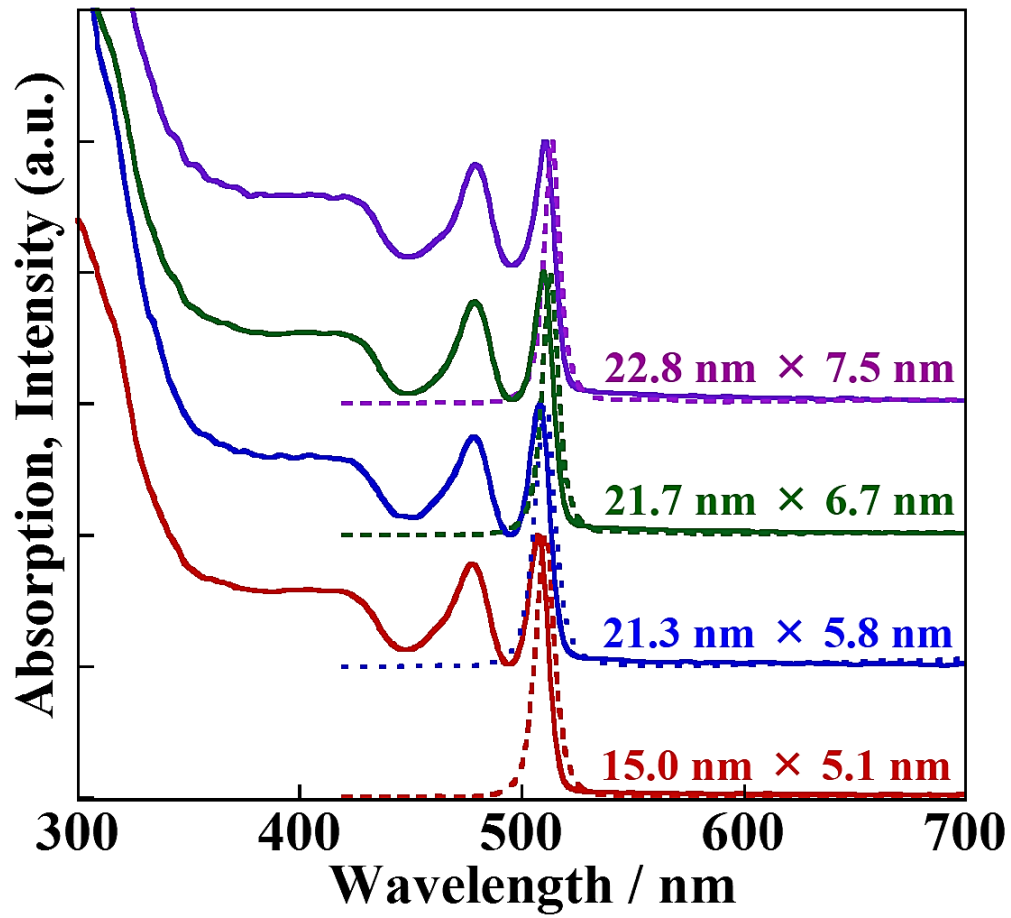
Figure 4.2 Steady-state absorption (solid) and emission (dashed) spectra of each sample.
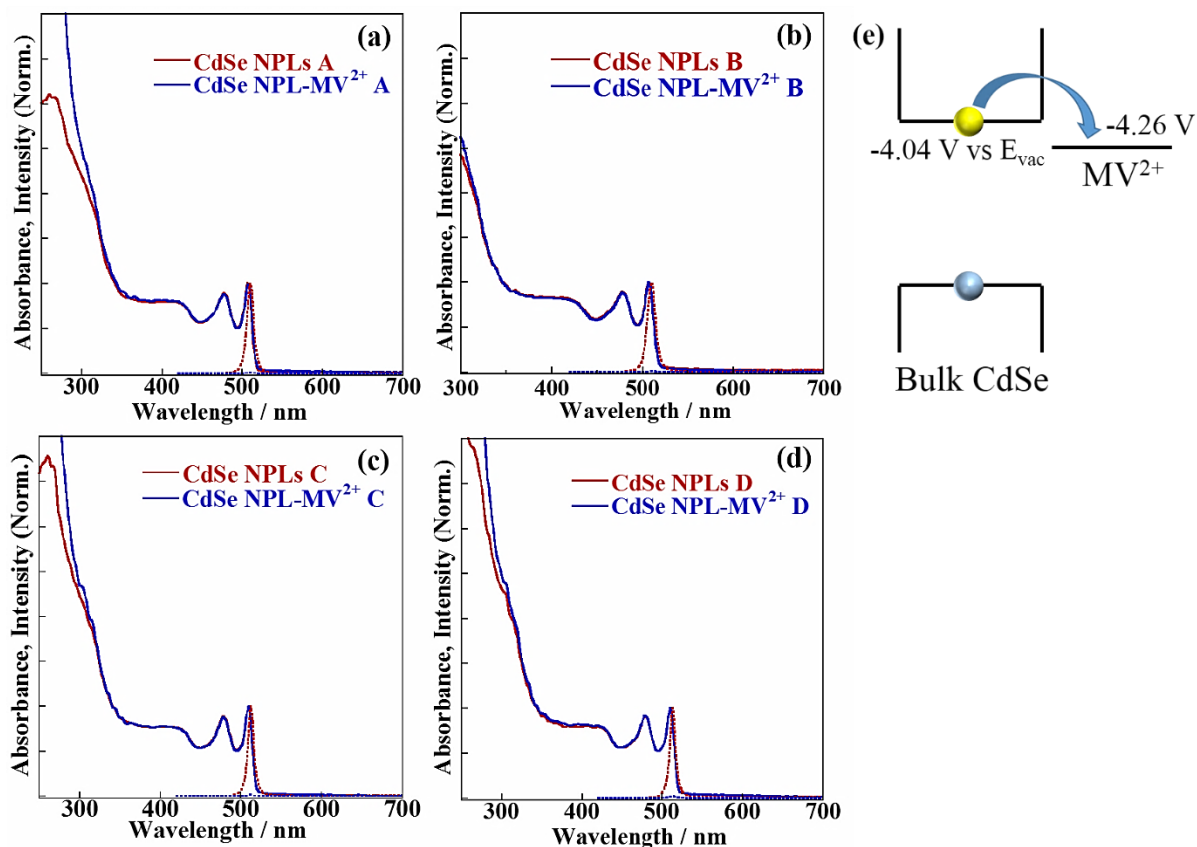
Figure 4.3 Steady-state absorption (solid) and emission (dashed) spectra of CdSe NPLs and

NPL-MV^{2+} (a) A, (b) B, (c) C, and (d) D. (e) The diagram of the conduction band edge of

bulk CdSe and reduction potential of MV^{2+}.[20]

Table 4.2 Luminescence quantum yields of CdSe NPLs and CdSe NPL-MV^{2+} complexes

Sample	CdSe NPLs	CdSe NPL-MV^{2+} complexes
A (15.0 nm × 5.1 nm)	0.34	1.2×10^{-3}
B (21.3 nm × 5.8 nm)	0.35	2.7×10^{-3}
C (21.7 nm × 6.7 nm)	0.20	1.7×10^{-3}
D (22.8 nm × 7.5 nm)	0.19	2.1×10^{-3}
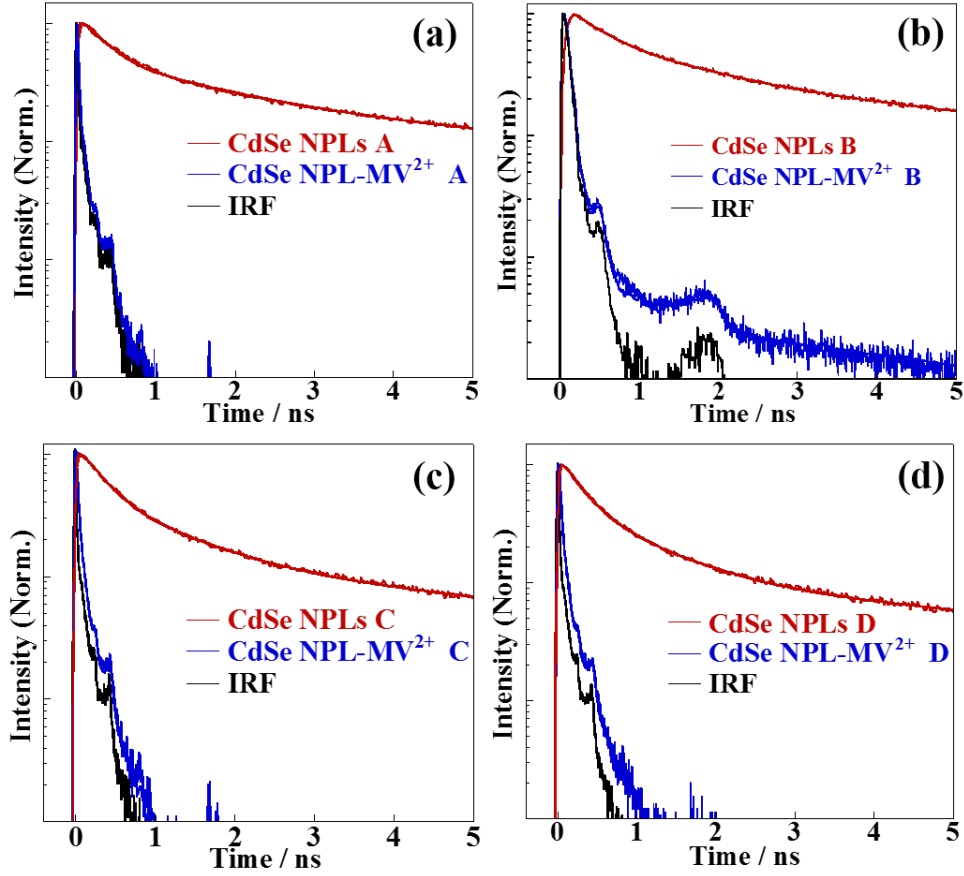
Figure 4.4 Luminescence decay monitored at a luminescence peak of CdSe NPLs and CdSe

NPL-MV^{2+} complexes (a) A, (b) B, (c) C, and (d) D.

Table 4.3 Luminescence lifetimes of CdSe NPLs and CdSe NPL-MV^{2+} complexes

Sample	τ_1 / ns (%)	τ_2 / ns (%)	τ_3 / ns (%)	τ_{ave} / ns
CdSe NPLs A	0.22 ± 0.03 (65.5)	1.7 ± 0.2 (24.5)	13.0 ± 0.3 (10.0)	1.86
CdSe NPL-MV^{2+} A	0.009 ± 0.002 (99.9)	1.7 ± 0.1 (0.10)		0.010
CdSe NPLs B	0.26 ± 0.03 (41.4)	1.2 ± 0.1 (38.8)	8.1 ± 0.2 (19.8)	2.18
CdSe NPL-MV^{2+} B	0.009 ± 0.002 (99.9)	3.3 ± 0.1 (0.1)		0.010
CdSe NPLs C	0.19 ± 0.04 (64.5)	0.97 ± 0.07 (27.8)	7.9 ± 0.3 (7.7)	1.01
CdSe NPL-MV^{2+} C	0.017 ± 0.002 (99.9)	1.2 ± 0.1 (0.1)		0.018
CdSe NPLs D	0.16 ± 0.04 (66.8)	0.85 ± 0.05 (26.7)	7.6 ± 0.4 (6.5)	0.83
CdSe NPL-MV^{2+} D	0.020 ± 0.002 (99.9)	0.62 ± 0.05 (0.1)		0.020
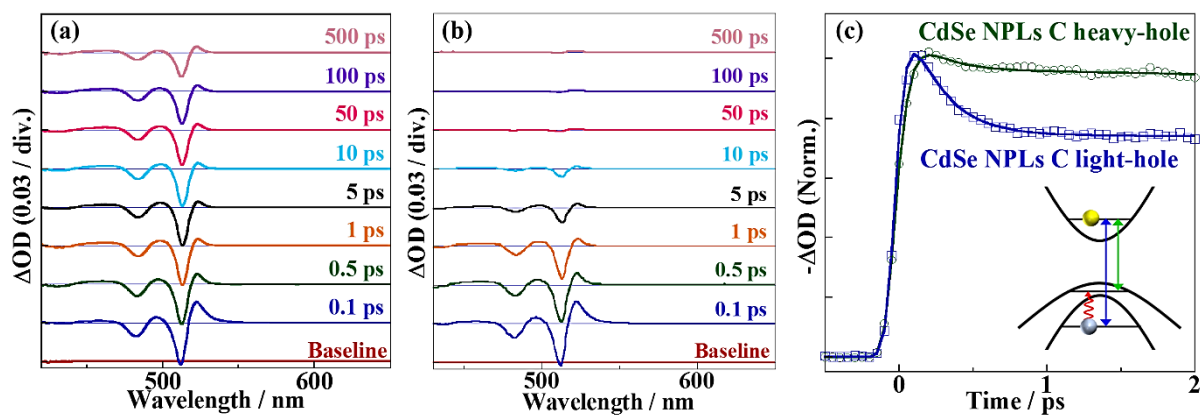
Figure 4.5 Transient absorption spectra of (a) CdSe NPLs C and (b) CdSe NPL-MV^{2+} complexes C and (c) transient absorption dynamics at the heavy-hole and light-hole bands of CdSe NPLs C (λ_{ex}: 400 nm). The inset of (c) shows the electronic structure of CdSe NPLs and the heavy-hole (green) and light-hole (blue) band transitions.
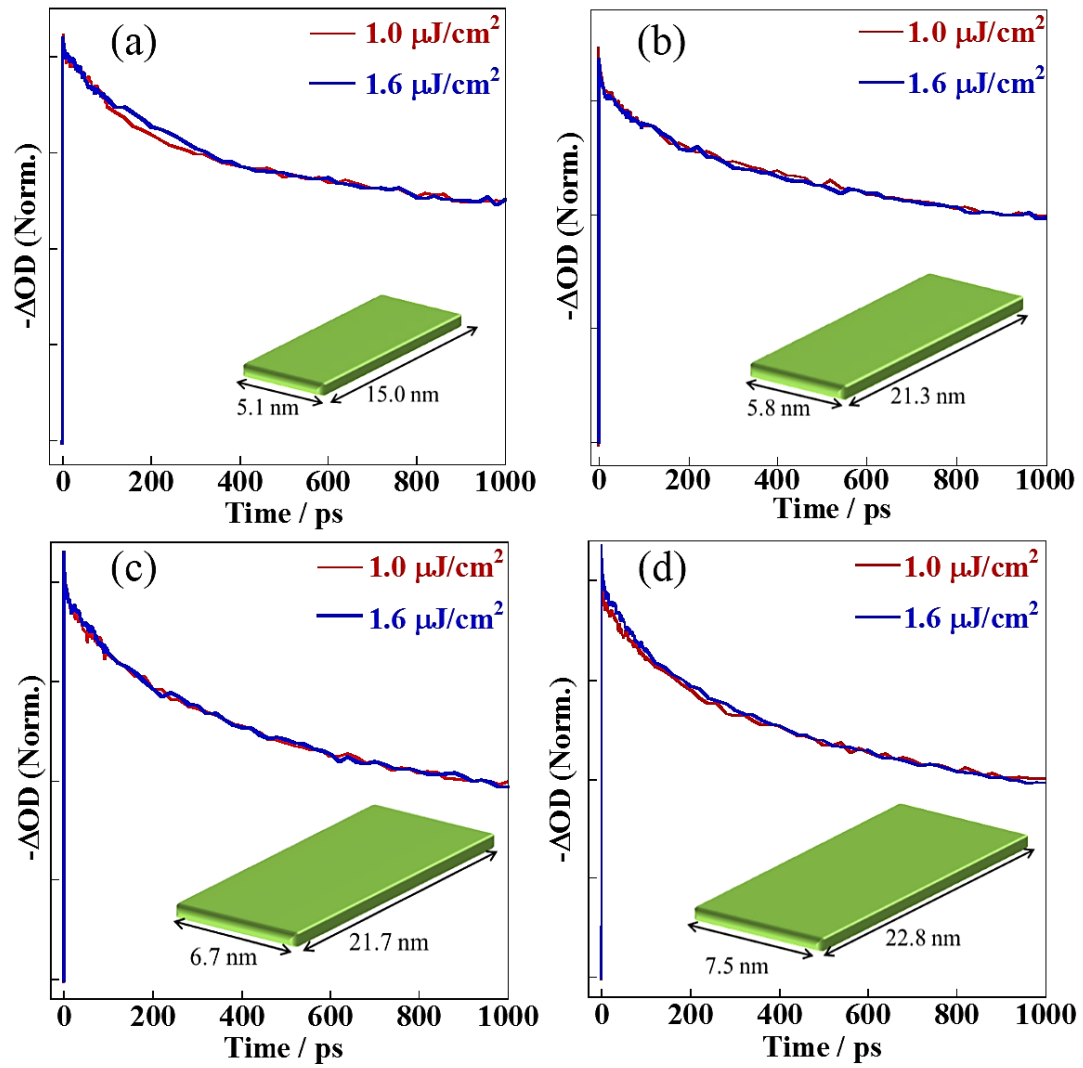
Figure 4.6 Single-exciton dynamics at heavy-hole bleach of CdSe NPLs (a) A, (b) B, (c) C, and (d) D.
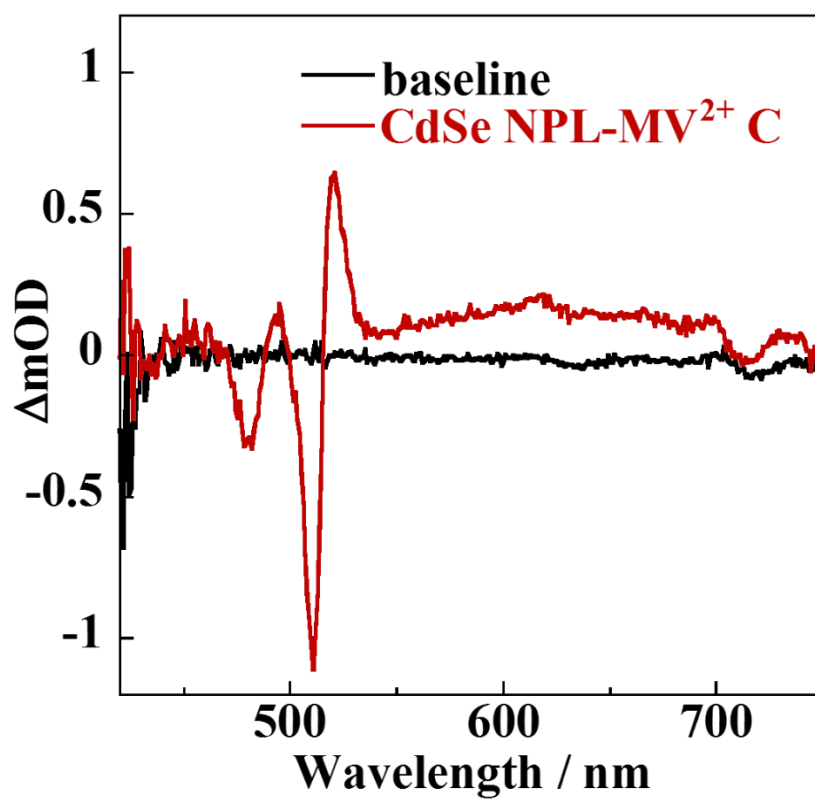
Figure 4.7 Transient absorption spectrum of CdSe NPL-MV^{2+} C at the delay time of 100 ps

with the low excitation intensity (1.6 μJ/cm^2).
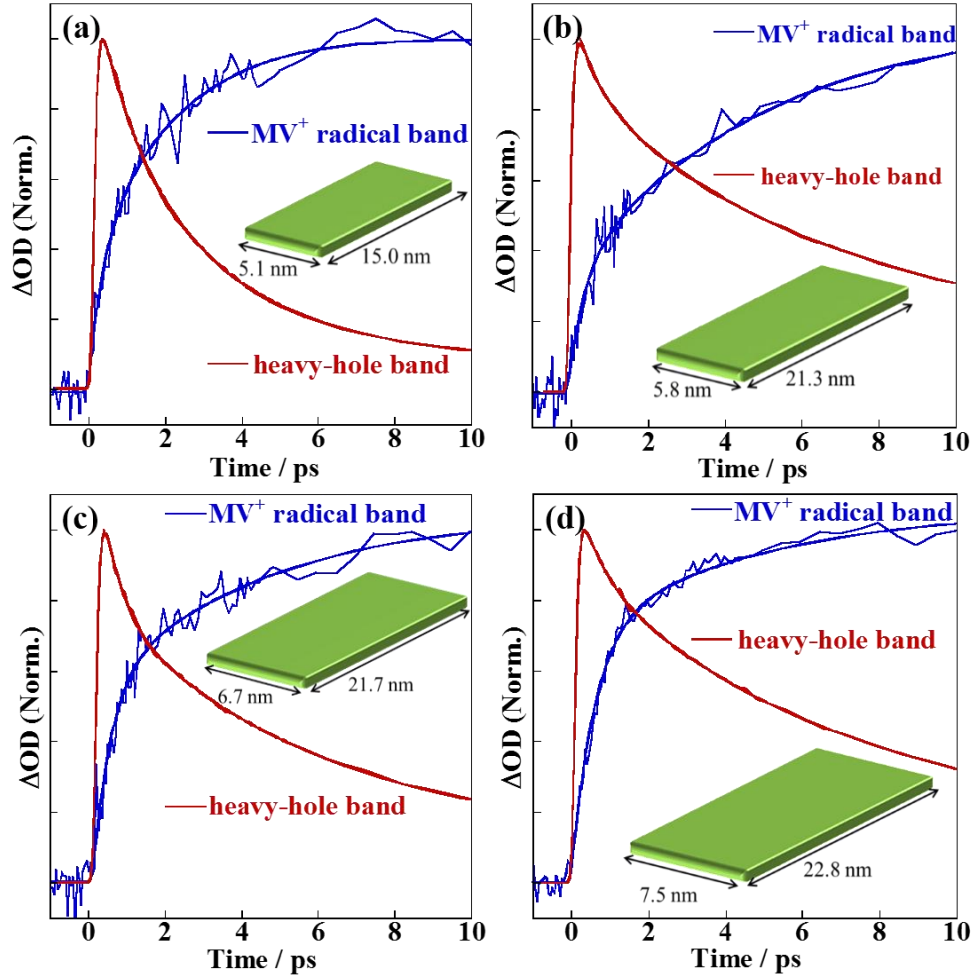
Figure 4.8 Transient absorption dynamics of the heavy-hole band (red) and MV[+] radical band

at 620 nm (blue) in CdSe NPL-MV^{2+} complexes (a) A, (b) B, (c) C, and (d) D (excitation

intensity: 10 μJ/cm^2).

Table 4.4 Electron transfer times for each CdSe NPL-MV^{2+} complexes.

Sample	Lateral size / nm^2	MV[+] radical band		Heavy-hole band	
		τ_{fast} / fs	τ_{slow} / ps	τ_{fast} / fs	τ_{slow} / ps
CdSe NPL-MV^{2+} A	15.0 × 5.1	370 ± 30 (34%)	2.4 ± 0.2 (66%)	390 ± 20 (15%)	2.1 ± 0.3 (85%)
CdSe NPL-MV^{2+} B	21.3 × 5.8	420 ± 20 (31%)	5.3 ± 0.3 (69%)	500 ± 30 (32%)	5.2 ± 0.4 (68%)
CdSe NPL-MV^{2+} C	21.7 × 6.7	470 ± 20 (49%)	5.5 ± 0.4 (51%)	450 ± 20 (44%)	5.3 ± 0.3 (56%)
CdSe NPL-MV^{2+} D	22.8 × 7.5	580 ± 30 (61%)	6.2 ± 0.3 (39%)	600 ± 30 (30%)	5.7 ± 0.3 (70%)
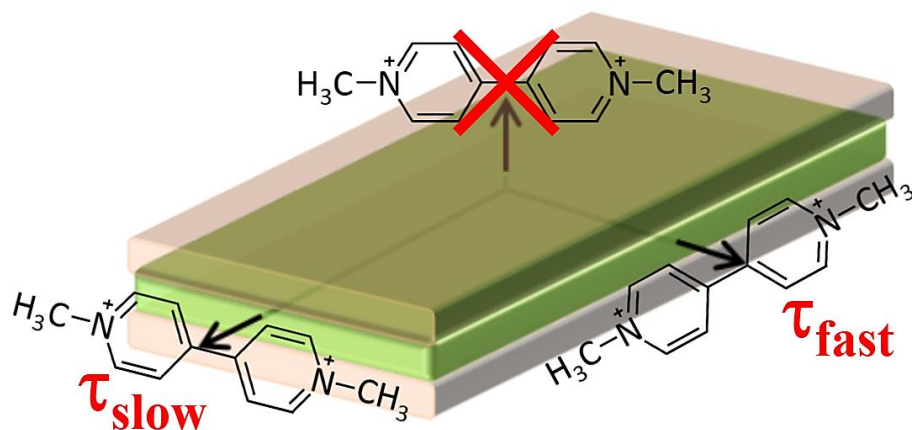
Figure 4.9 Origin of different electron transfer rates from the CdSe NPLs to MV^{2+} adsorbed

on the surface. The green and transparent red rectangles represent CdSe NPL and surface

ligands, respectively.
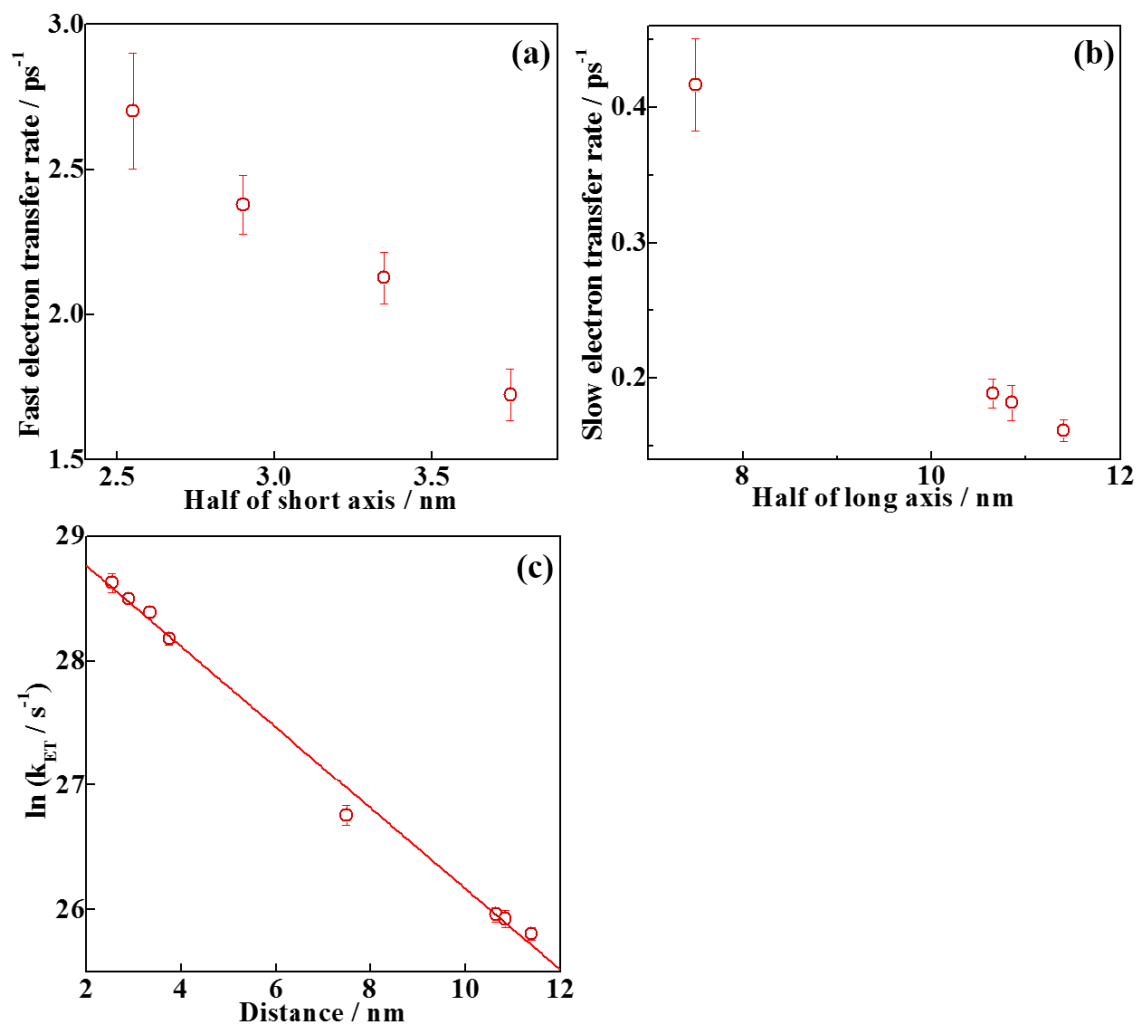
Figure 4.10 Lateral size dependence on the (a) fast and (b) slow electron transfer rates. (c)

The natural logarithm of fast and slow electron transfer rates were plotted against the distance

(the half of short and long axis) and the linear dependence of ln k_{ET} against the distance was

experimentally obtained.
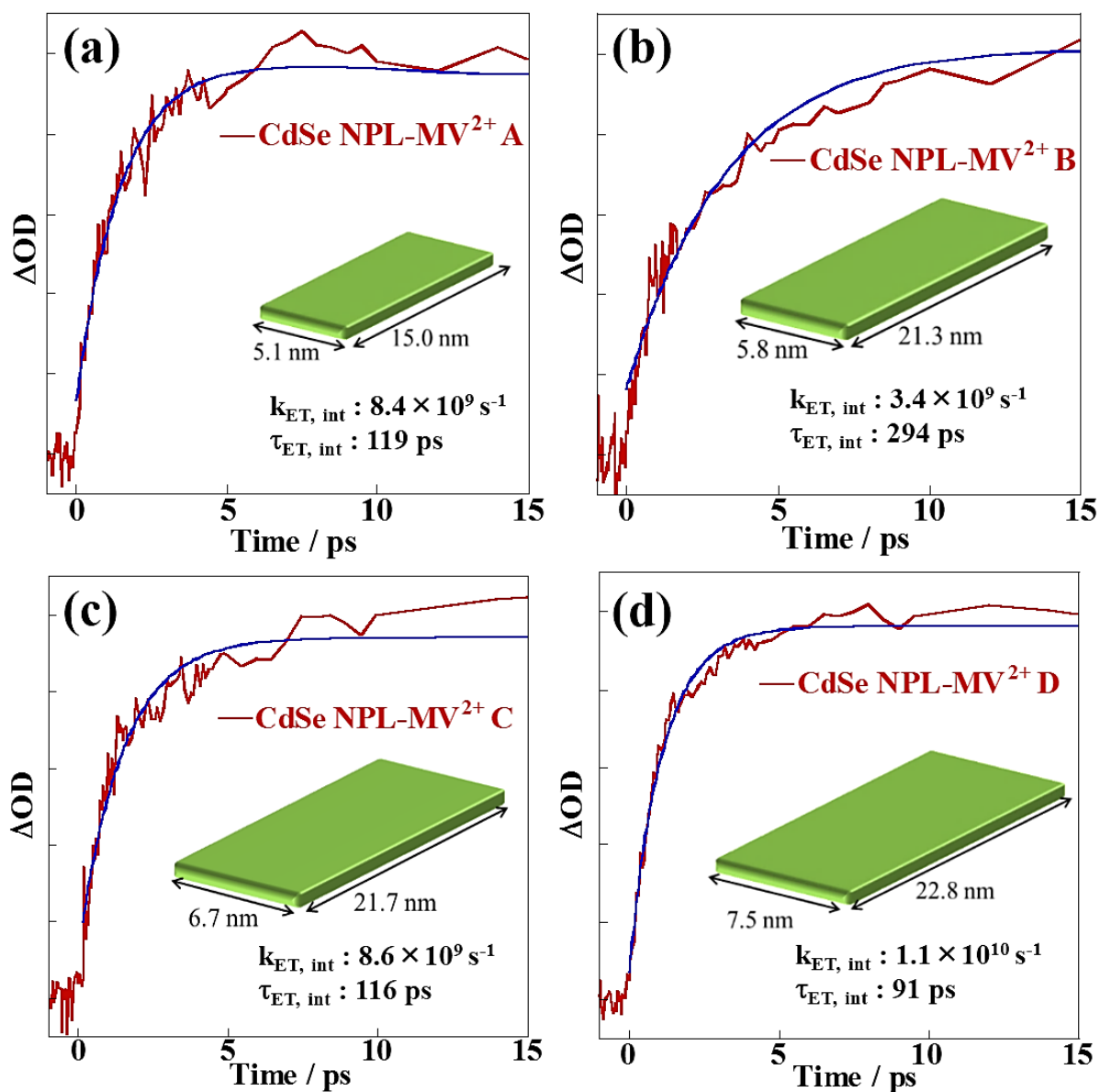
Figure 4.11 Fitting results of MV^+ radical band at 620 nm of CdSe NPL–MV^{2+} (a) A, (b) B, (c) C and (d) D by the Poisson-derived function (*m* was fixed to 80). As compared with the fitting by the biexponential function (Figure 4.8), the growth kinetics of MV^+ radical band could not be well fitted by the Poisson-derived function.
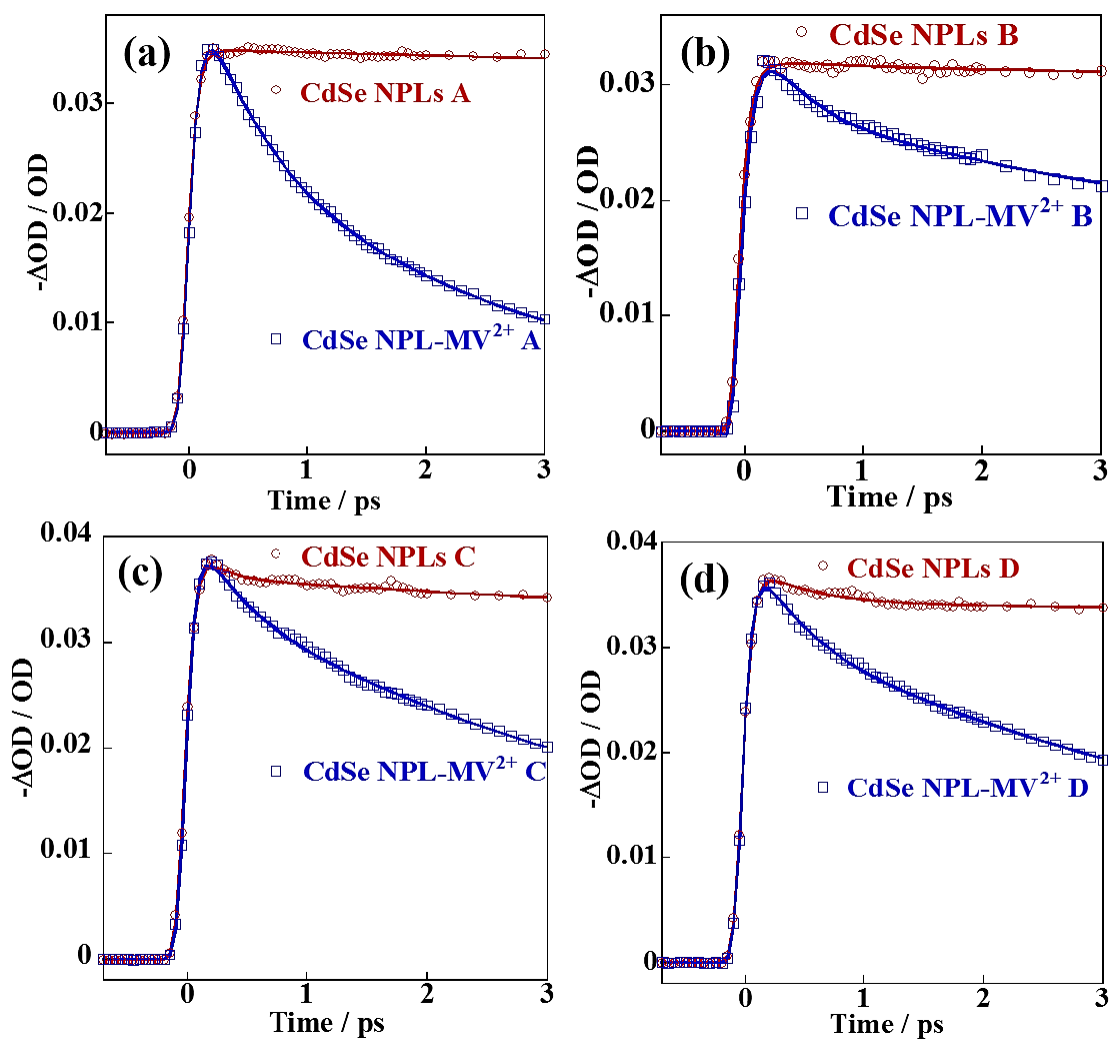
Figure 4.12 Transient absorption signal and growth kinetics of the heavy-hole band bleach in CdSe NPLs and CdSe NPL-MV^{2+} complexes (a) A, (b) B, (c) C and (d) D under low excitation intensity (1.6 μJ/cm^2).
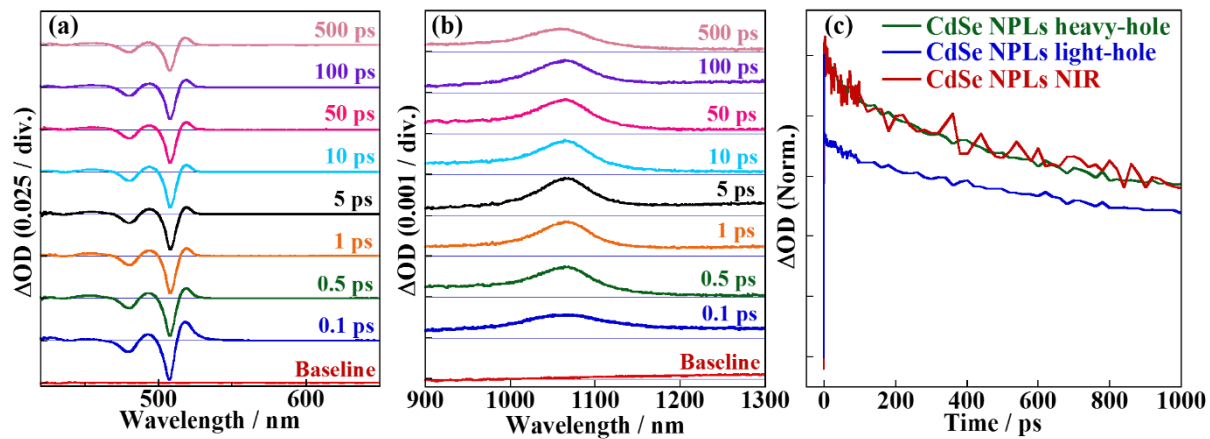
Figure 4.13 Transient absorption spectra of CdSe NPLs B (λ_{ex} : 400 nm) with low excitation intensity (1.6 μJ/cm^2) at (a) visible and (b) near–IR region. (c) Transient absorption dynamics at each band.
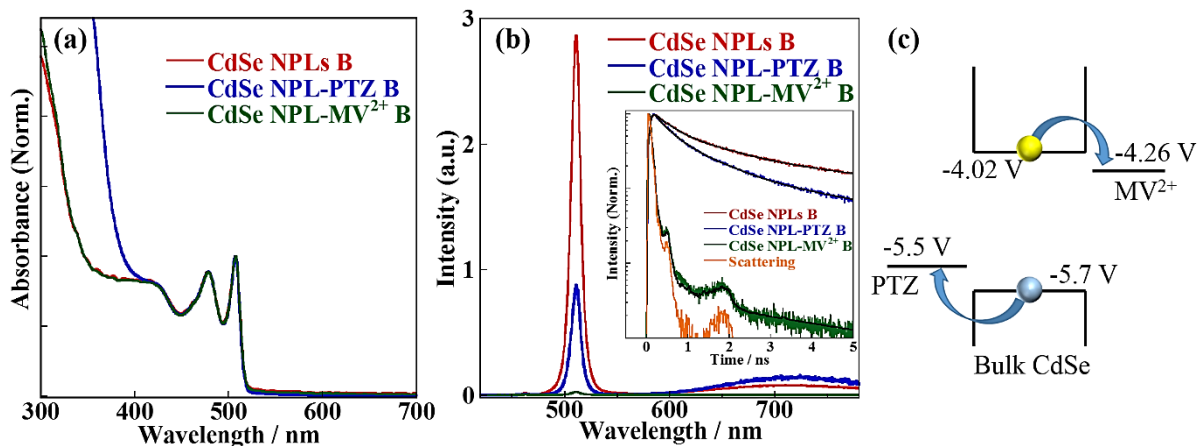
Figure 4.14 Steady–state (a) absorption and (b) luminescence spectra of CdSe NPLs, CdSe NPL-PTZ, and CdSe NPL-MV^{2+} complexes. The inset of Figure S5b shows the luminescence decay of these samples observed at 511 nm. (c) The energy diagram of bulk CdSe, reduced potential of methyl viologen, and oxidation potential of phenothiazine.[61,62]
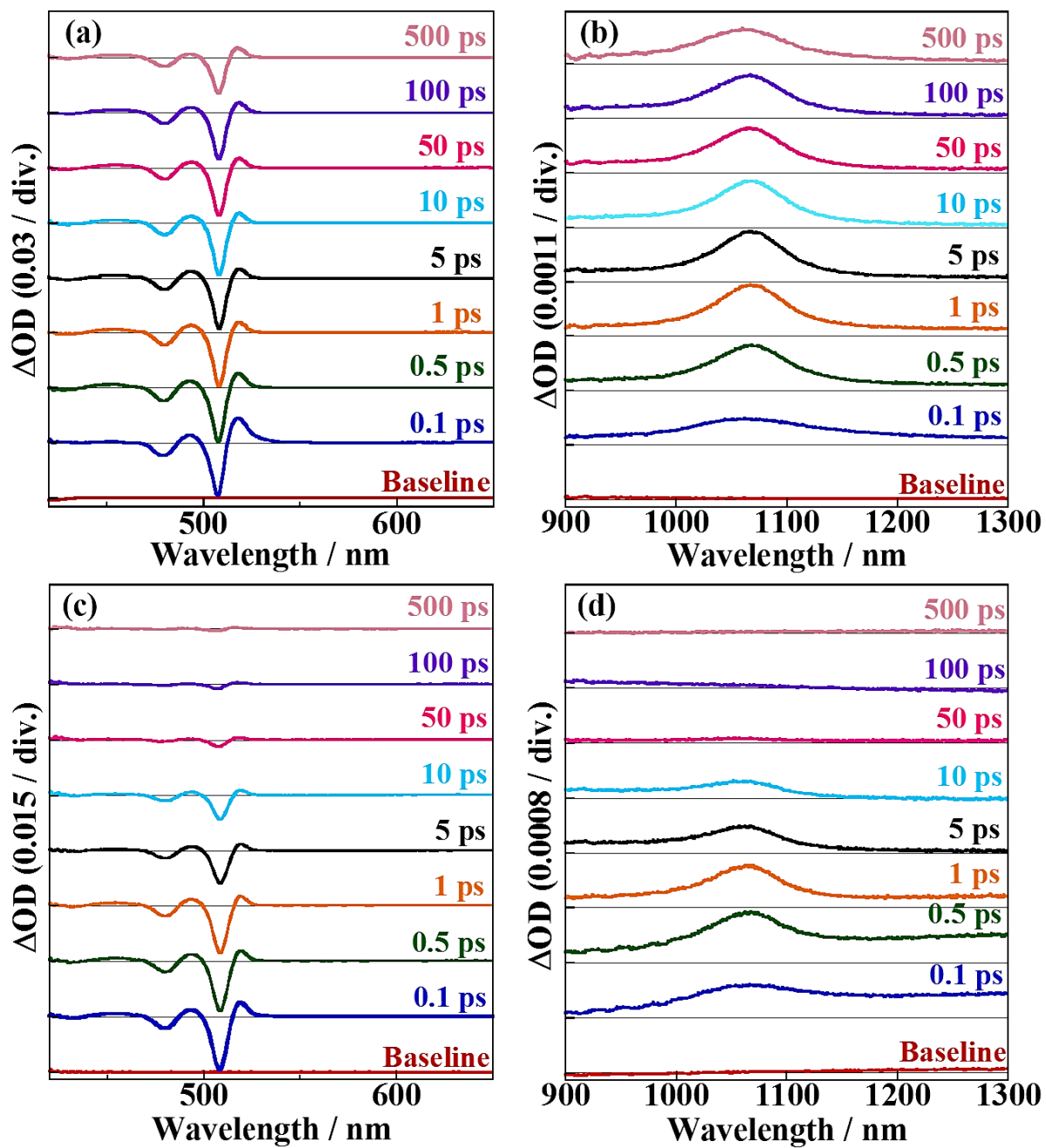
Figure 4.15 Transient absorption spectra at visible and near–IR region of (a and b) CdSe NPL-PTZ and (c and d) CdSe NPL-MV^{2+} complexes under the low excitation intensity (1.6 µJ/cm^2).
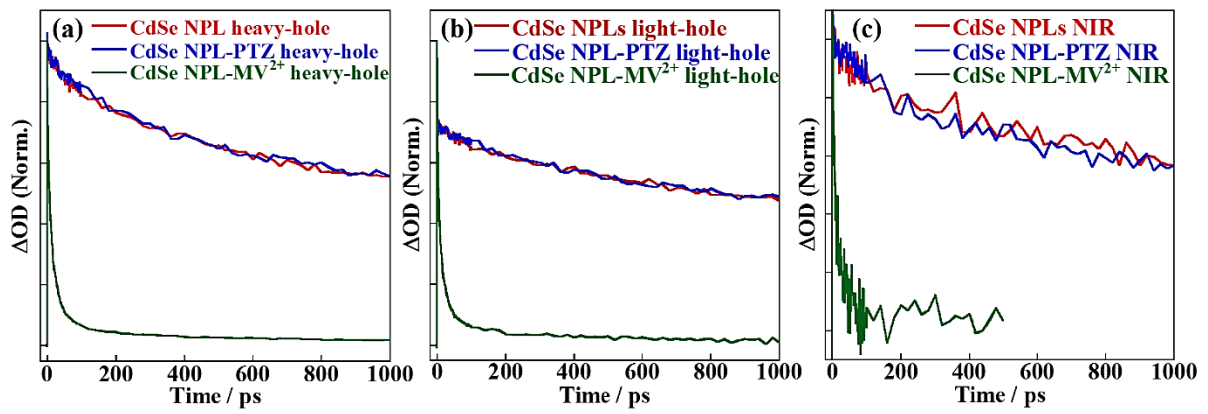
Figure 4.16 The comparison of transient absorption dynamics at each band of all samples

under the low excitation intensity (1.6 μJ/cm^2).

Chapter 5

Ultrafast and Hot Carrier Dynamics in PbS QD-Au HNs

5.1 Abstract

Semiconductor-metal hybrid nanostructures (HNs) are promising materials for photovoltaics and photocatalysis because of their efficient charge separation in the excited state. However, analysis of their carrier dynamics has been limited to only a handful of HNs, such as CdSe-Au and CdS-Au. Herein, we synthesized and characterized PbS QD-Au HNs and examined their carrier dynamics by femtosecond near-IR pump-probe spectroscopy. A decrease in band-edge (1S) bleach yields was clearly observed in PbS QD-Au HNs as compared to PbS QDs under 1S excitation, suggesting the existence of ultrafast carrier transfer from the 1S states of PbS QDs to Au NPs that was faster than the instrumental response function. A rise time analysis of 1S bleach dynamics determined that no hot carrier transfer was present. In addition to ultrafast carrier transfer, picosecond-scale carrier transfer was observed, with the rate constants increasing with Au NPs diameter. This difference between ultrafast and picosecond-scale carrier transfer is likely due to a difference in rate constants between electron and hole transfer.

5.2 Introduction

Semiconductor nanocrystals strongly confine electrons and holes, resulting in significant enhancement of electron-hole Coulomb interaction. This enhancement can lead to highly efficient multiple exciton generation (MEG),[1] a process whereby multiple excitons result from the absorption of only one photon. This process has been observed in several kinds of quantum dots (QDs)[2-5] and could be applied to the development of highly efficient solar cells. However, this strong confinement effect also result in highly efficient Auger recombination, reducing the lifetime of these semiconductor QD excitons to the order of tens of picoseconds.[6] Therefore, it is essential to extract multiple excitons from QDs before Auger recombination for the highly efficient solar cells.

In addition, semiconductor QDs have discrete electronic structures while bulk semiconductors have continuous band structures. Since energy separation between 1S and 1P states of CdSe QDs is 10-fold larger than the LO phonon energy,[7] excited carriers in semiconductor nanocrystals relax to band-edge state through different processes from bulk semiconductors such as Auger cooling.[8] The mechanism of intraband relaxation in CdSe QDs has been reported with the state-selective excitation experiments by Kambhampati et al.[9-12] According to these reports, excited electrons relax primarily via Auger process from the 1P to 1S state, and holes relax primarily by a surface ligand mediated nonadiabatic process. In addition, they reported the hot carrier trapping in CdSe QDs competing with the hot carrier relaxation.[13-15] For bulk semiconductors, excited carriers relax to the band-edge state by phonon emission, and this fast relaxation is an origin of the theoretical efficiency limit of solar cell (Shockley-Queisser limit).[16] In contrast, intraband relaxation time in semiconductor nanocrystals can be controlled by capping reagents,[17] spatial separation between electron and hole,[18] and changing temperature.[19] An extreme example of this increased relaxation time can be observed in the work of Gyot-Sionnest et al., who reported very slow electron cooling (over 1 ns) in CdSe/ZnSe/ZnS/CdSe multishell nanoparticles (NPs).[18] This effect could potentially allow for efficient hot carrier extraction.

Lead chalcogenide QDs (PbS, PbSe, etc.) in particular have a great potential for use in solar energy conversion because of their small bandgap energies that lead to large exciton absorption in the near-IR to UV region and the easy generation of hot carriers. In addition, many researchers have reported MEG in lead chalcogenide QDs by transient absorption spectroscopy, fluorescence decay measurements, and photonto-current efficiency measurements.[3,20-22]

Multiple excitons and hot carriers should be extracted from semiconductor nanocrystals to the outside for efficient energy conversion. Semiconductor-metal hybrid

nanostructures (HNs) are one of the best candidate materials for photovoltaics[23-26] and photocatlysis[27-30] because of the ultrafast carrier transfer from the semiconductor to metal. Recent progress in the synthesis of colloidal nanocrystals has allowed for the synthesis of various kinds of semiconductor-metal HNs, including metal-tipped CdSe and CdS nanorods (NRs)[31-33], Au-attached CdSe and PbS quantum dots (QDs),[34,35] and Au/PbS core/shell hybrid nanoparticles.[36] Their carrier dynamics have been examined by transient absorption spectroscopy, luminescence decay, and single-particle spectroscopy. Khon et al. reported the Au NPs size dependence on carrier dynamics of Au-tipped CdS NRs,[37] showing that transient absorption signal of the smallest (2.7 nm) and largest (15.4 nm) Au-tipped CdS NRs showed only excitonic and plasmonic features, respectively. However, in middle size (5.3 nm) Au-tipped CdS NRs, both of these features were suppressed because of the mixing of electronic states at the semiconductor-metal domain interface. Ultrafast electron transfer (sub-20 fs) from band-edge state ($1\sigma_e$ state) of CdS NRs to Au NPs has been reported.[26] Furthermore, one of our previous studies analyzed the electron transfer dynamics from both higher excited states (hot electron transfer) and the $1\sigma_e$ state of CdSe NRs to Au NPs (1.5−2.2 nm).[23]

Yang et al. reported the synthesis and carrier dynamics of Au attached PbS QDs,[35] where electron transfer dynamics from PbS QDs to Au NPs was studied by femtosecond pump−probe measurements at a particular wavelength of 700 nm. However, excited carrier dynamics in specific electronic states ($1S_e$, $1P_e$, etc.) could not be analyzed because of the lack of spectral information. In addition, excitonic transition of PbS QDs was not clearly observed in the steady-state absorption spectrum. In our previous experiments on Au/PbS core/shell hybrid nanoparticles (diameter of the Au core = 5.1 ± 1.3 nm, thickness of the PbS shell = 2.2 ± 0.7 nm), coherent acoustic phonon dynamics for the Au/PbS nanoparticles as a whole was clearly observed through transient absorption spectroscopy.[38] However, excitonic features were not observed in the steady-state and transient absorption spectra because of the

significantly larger extinction coefficient of Au NPs as compared to that of the PbS shell. Therefore, in order to understand the excited carrier dynamics of PbS in PbS QD-Au HNs, it is essential to synthesize PbS QD-Au HNs with clear excitonic features and examine their carrier dynamics.

In the present study, we synthesized PbS QD-Au HNs showing clear excitonic features and characterized them by transmission electron microscopy (TEM) and energy dispersive X-ray spectroscopy (EDX). Moreover, carrier dynamics of PbS QD-Au HNs was examined by femtosecond near-IR transient absorption spectroscopy. In order to evaluate hot carrier and   ultrafast carrier transfer, we analyzed the rise time of 1S bleach dynamics and 1S bleach yields in state-selective excitation experiments.

5.3   Experimental section

Synthetic methods of OLAm capped PbS QDs and PbS QD-Au HNs were described in Chapter 2. The structures of PbS QDs and PbS QD-Au HNs were characterized by transmission electron microscopy (TEM, TECNAI 20, 200 keV, FEI), scanning TEM (STEM, ibid), and energy dispersive X-ray spectrometry (EDX, ibid). UV-vis absorption and luminescence spectra of PbS QDs and PbS QD-Au HNs were recorded using an U-4100 (Hitachi) and a Fluorolog-3 (Jobinyvon-Spex), respectively. Near-IR transient absorption spectra were measured using femtosecond pump-probe experiments. In 800 nm excitation experiments, PbS QDs and PbS QD-Au HNs were excited with fundamental wave of an amplified mode-locked Ti:sapphire laser (Spitfire and Tsunami, Spectra-Physics, repetition rate: 1 kHz). The state selective excitation experiments were performed by an optical parametric amplifier (OPA) (TOPAS, Light Conversion Ltd.). Excitation intensity was 7.1-213 μJ/cm^2 with a repetition rate of 0.5 kHz by using a chopper (Model 3501, NEW FOCUS, Inc.). Absorption transients were probed by delayed pulses of a femtosecond

white-light continuum generated by focusing a fundamental laser pulse into a sapphire plate and were detected by an InGaAs detector (Princeton Instruments, OMA V). The temporal resolution in 800 nm excitation and state-selective excitation experiments were 100 fs and 60 fs, respectively.

5.4   Results and discussion

TEM and STEM images of PbS QDs and PbS QD-Au HNs were shown in Figure 5.1. In the STEM images, PbS QD-Au HNs were constructed in two clearly contrasting parts. As shown in Figure 5.2, the EDX data of PbS QD-Au HNs A confirm that the bright and dark parts corresponded to Au NPs and PbS QDs, respectively. The average diameter of PbS QDs and Au NPs were summarized in Table 5.1. The average diameter of PbS QDs became smaller with increasing the concentration of Au precursor solution. The decrease of PbS QDs diameter was probably due to the etching during the synthesis which has been reported in CdSe NR-Au HNs.[27,39] Steady-state absorption and luminescence spectra of PbS QDs and PbS QD-Au HNs are shown in Figures 5.3, respectively. The band-edge (1S) absorption band was clearly observed in the absorption spectra of both PbS QDs and PbS QD-Au HNs. The 1S absorption band shifted to the shorter wavelength (Table 5.2) and became broader with increasing the diameter of Au NPs. As mentioned above, the blueshift of 1S absorption band was due to the etching of PbS QDs diameter. Indeed, the diameter of PbS QDs in PbS QD-Au HNs estimated from 1S absorption peak[40] were in good agreement with those from STEM images. In addition to the blueshift, the absorption spectra of PbS QD-Au HNs became broader as compared with that of PbS QDs. This observed broadening is likely due to either the size distribution of the PbS QDs or contribution of ultrafast carrier transfer between the PbS QDs and Au NPs under strong electronic coupling. Yang et al. have reported that the absorption spectrum of PbS QDs strongly coupled to TiO_2 NPs became broader by ultrafast

134

electron transfer (~6 fs) from PbS QDs to TiO_2 NPs.[41] In the luminescence spectra of PbS QD-Au HNs, wavelengths of luminescence peak slightly shifted to shorter wavelength region, and the luminescence intensity decreased with increasing the diameter of Au NPs. This luminescence quenching is likely due primarily to the interaction between PbS QDs and Au NPs. Steady-state absorption and emission spectra of PbS QDs with various sizes (reference A, B, and C) were illustrated in Figure 5.4. The wavelengths of 1S absorption peak in reference PbS QDs A, B, and C were nearly identical to those of PbS QD-Au HNs A, B, and C, respectively, indicating that the diameter of each set of QDs and PbS QD-Au HNs were very similar.

Figure 5.5a shows the transient absorption spectra of PbS QDs under 800 nm excitation with weak excitation intensity of 14.2 $\mu J/cm^2$. The average number of excitons in a PbS QD, $<N_0>$, is estimated to be ~0.1 at 14.2 $\mu J/cm^2$ by the equation $<N_0> = j_p\sigma$, where j_p is the pump photon fluence and σ is the QD absorption cross section at the excitation wavelength.[42] In the Figure 5.5a, 1S bleach peak was clearly observed at ~1400 nm, which is the expected wavelength from the 1S exciton peak in the steady-state absorption spectrum. The excitation intensity dependence of 1S bleach dynamics in PbS QDs is illustrated in Figure 5.5b. At low excitation intensity, the almost single exponential decay was observed in 1S bleach dynamics. However, an additional relaxation component with the lifetime of ~120 ps was detected at higher excitation intensity, corresponding to the Auger recombination. The estimated Auger lifetime was slightly longer than that of oleic acid-capped PbS QDs with similar diameters (τ_{Auger}: 80−90 ps for 5.5 nm).[21]

Transient absorption spectra of PbS QD-Au HNs A, B, and C are illustrated in Figure 5.6. In these measurements, multiexcitons did not contribute to the transient absorption spectra and dynamics, because of the low excitation intensity ($<N_0> \leq 0.1$). The 1S bleach peak was clearly observed in each sample, and shifted to the shorter wavelength region with

increasing the diameter of Au NPs. The 1S bleach dynamics of all samples, which were illustrated in Figure 5.7, were fitted by the biexponential decay function, and the results were summarized in Table 5.3. The ps-scale fast relaxation component was observed in the PbS QD-Au HNs and became clearly faster as the diameter of Au NPs increased. The fast relaxation component was probably due to the carrier transfer from 1S states of PbS QDs to Au NPs. In the nonadiabatic limit, the total rate of electron transfer from the donor state of PbS QDs to the acceptor states of Au NPs can be expressed as the sum of electron transfer rates to all possible accepting states as given in the following equation,[43-46]

$$k_{ET} = \frac{2\pi}{\hbar} \int_{-\infty}^{\infty} dE\ \rho(E)|\bar{H}(E)|^2 \frac{1}{\sqrt{4\pi\lambda k_B T}} \times exp\left[-\frac{(\lambda + \Delta G + E)^2}{4\lambda k_B T}\right] \qquad (1)$$

where k_{ET} is the total rate constant of electron transfer, $\rho(E)$ is the density of the final states of the Au NPs, $|\bar{H}(E)|$ is the electronic coupling constant between the initial 1S state of PbS QDs and the final states of the Au NPs, λ is the reorganization energy, and ΔG is the variation of Gibbs energy corresponding to the energy difference between the band edge state of PbS QDs and the Fermi level of Au NPs. This equation suggests that total carrier transfer rate strongly depends on the density of final states of Au NPs. In the small Au NPs whose diameter is less than 2 nm, the localized surface plasmon resonance band could not be observed.[47] In addition, at room temperature, Coulomb blockade effect was clearly observed in Au NPs with the diameter of 1.8 nm.[48] This phenomenon was only observed if the energy spacing is larger than the thermal energy. In contrast with small Au NPs (1.8 nm), larger Au NPs with the diameter of 5 nm exhibited Coulomb blockade effect at only low temperature (10 K).[49] These results strongly suggested that the electronic structure of Au NPs becomes discrete drastically as the diameter decreases below 2 nm, indicating that the total carrier transfer rate from 1S state of PbS QDs to Au NPs becomes slower as the diameter of Au NPs

decrease. Therefore, the observed Au NPs size dependence of carrier transfer rate can be interpreted in terms of the change of $\rho(E)$ in Au NPs. Moreover, the change of the electronic coupling constant, $|\bar{H}(E)|$, between PbS QDs and Au NPs can contribute to the Au NPs size dependence of the total carrier transfer rate. The electronic coupling constant depends on the degree of overlap between the penetrated wave function of the 1S state of PbS QDs and Au NPs on the PbS QDs surface, which is known to increase in smaller QDs.[50] In our experiments, the diameter of PbS QDs became smaller with increasing the Au NPs size. Therefore, the change of the electronic coupling constant can contribute to the total carrier transfer rate from 1S state of PbS QDs to Au NPs.

Reorganization energy, λ, is expressed as the sum of the inner-sphere (λ_{inner}) and the outer-sphere component (λ_{outer}). λ_{inner} comes from the nuclear displacement of the reactants and products, and the λ_{inner} in semiconductor QDs is known to be negligibly small (a few tens of meV).[51,52] Though the effect of the Au NPs size to λ_{inner} is still unclear, in this study, we assume that the effect of nuclear displacement in Au NPs associated with single electron transfer is very small because there are a lot of electrons in Au NPs. λ_{outer} comes from the dielectric response of the solvent and ligand.[53] In our PbS QD-Au HNs systems, λ_{outer} is very small (a few meV) because of the small difference between static (ε_s) and optical (ε_{op}) dielectric constants of tetrachloroethylene (ε_s: 2.30, ε_{op}: 2.28).[54] Therefore, in the PbS QD-Au HNs, we expect that the change in total λ associated with the change in diameter of Au NPs is not so large.

In addition to ps-scale carrier transfer from 1S state, we analyzed the hot carrier dynamics in PbS QD-Au HNs. In our previous study on CdSe NR-Au HNs, both hot electron transfer and electron transfer from band-edge state were clearly observed.[23] In previous studies by Kambhampati et al., when the pump pulse with the excess energy is used for the

excitation, hot electron relaxation follows a sum of three signals with the instrumental response function (IRF).[8,10]

$$\Delta OD(t) = \left[A_{1S} + A_{1p}e^{-k_1 t} + A_i\left\{1 + \frac{1}{k_2 - k_1} \times (k_1 e^{-k_2 t} - k_2 e^{-k_1 t})\right\}\right] \otimes IRF \qquad (2)$$

where i is the electronic states higher than 1P state, $k_2 \equiv k_{i \to 1P}$ and $k_1 \equiv k_{1P \to 1S}$. This equation should be used to analyze the intraband relaxation from highly excited initial state to band-edge state. However, in our experiments, by considering the signal-to-noise ratio in transient absorption measurements, only one rise component is enough to analyze the 1S bleach dynamics. Therefore, a sequential relaxation process ($i \to$ 1P and 1P $\to$ 1S) can be approximately expressed as one process ($i \to$ 1S) with the rate constant of k_{int}. Therefore, assuming that the hot electron transfer from PbS QDs to Au NPs, the rise time of 1S bleach band is expressed as the inverse of the sum of the rate constants of intraband relaxation (k_{int}) and hot electron transfer (k_{hot}).

$$\tau_{rise} = \frac{1}{k_{int} + k_{hot}} \qquad (3)$$

This equation indicates that the rise time of 1S bleach band in PbS QD-Au HNs should become faster than that in bare PbS QDs ($1/k_{int}$) when the hot electron transfer occur. However, in our experiments, the diameter of PbS QDs decreased with increasing the size of Au NPs, suggesting that the intraband relaxation time could be different in each sample. Consequently, we compared rise times of 1S bleach band in PbS QD-Au HNs to those of PbS QDs with the similar diameter (reference A, B, and C).The comparison of growth kinetics of 1S bleach band were illustrated in Figure 5.8. In addition to the slow rise component, the reference samples show a fast rise component comparable to an IRF. The fast rise time is

likely due to electronic excitation from high valence band states to the $1S_e$ state in the conduction band. Therefore, the slow rise component was used as the time constant for intraband transition to the 1S states. Fitting results of 1S bleach band for all samples were summarized in Table 5.4. The observed rise time of PbS QDs becomes slower from 190 to 520 fs as PbS QDs diameter increases because of the generation of higher excited states in larger QDs that exhibit smaller bandgap energies. From the fitting results, there is no significant between the rise time in PbS QD-Au HNs and their corresponding reference samples, indicating that hot carrier transfer does not occur in PbS QD-Au HNs.

In order to analyze the carrier transfer dynamics from PbS QDs to Au NPs in more detail, state selective excitation experiments were conducted using an optical parametric amplifier. In these experiments, PbS QD-Au HNs A and B and their counterpart were excited at 1310 nm and 1200 nm, corresponding to the 1S absorption peak of each samples, respectively. In 1S excitation experiments, excited carrier occupy the band-edge states ($1S_e$ and $1S_h$) directly. 1S bleach band dynamics in the initial time region were illustrated in Figure 5.9a and 9b. The growth kinetics of 1S bleach dynamics were comparable to the instrumental response function (~ 60 fs), suggesting the no existence of hot carrier under 1S excitation. However, as shown in Figures 5.9c and 9d, initial 1S bleach amplitude corrected by the ground-state absorption at excitation wavelength (-ΔOD/OD) of both PbS QD-Au HNs decreased as compared with their counterparts, although band-edge states were occupied directly by the pump pulse. In addition, the larger decrease of initial 1S bleach amplitude for PbS QD-Au HNs B (D_{Au}: 1.7 nm) was clearly observed as compared with PbS QD-Au HNs A (D_{Au}: 1.3 nm). The lower initial bleach amplitude in semiconductor-metal HNs can be originated from hot carrier transfer or ultrafast carrier transfer from band-edge states whose lifetime is much faster than the instrumental response function. In the previous study on the CdSe NR-Au HNs, not only faster growth kinetics of band-edge bleach dynamics but also the

decrease of initial band-edge bleach amplitude under 400 nm excitation was observed, which was originated from hot electron transfer from CdSe NRs to Au NPs.[23] However, in the present study, the initial 1S bleach amplitude of PbS QD-Au HNs decreased, though the hot carrier does not generate in 1S excitation experiments. Another possible reason is the contribution of ultrafast carrier transfer. As mentioned above, Yang et al. reported that the transient bleach amplitude for PbS QDs coupled with TiO_2 NPs decreased as compared to PbS QDs on a sapphire plate by ultrafast electron transfer (~6 fs).[41] Moreover, Mongin et al. reported the similar results for CdS NR-Au HNs excited at band-edge absorption band.[26] Therefore, it is likely that the observed decrease in 1S bleach yields of PbS QD-Au HNs is due to the ultrafast carrier transfer that takes places on a faster time scale than our temporal resolution (~60 fs).

In this study, we discussed two types of carrier transfer processes in PbS QD-Au HNs. The first one is ultrafast carrier transfer analyzed from the decrease of the initial 1S bleach amplitude under the 1S excitation, and the second one is ps-scale carrier transfer determined by the fast decay component in the 1S bleach dynamics. In our PbS QD-Au HNs, since the energy level of valence band-edge of PbS QDs is almost the same as the Fermi level of Au NPs,[55,56] both electron and hole transfer from the PbS QDs to the Au NPs are possible. Furthermore, both electron and hole in the 1S state contribute to the 1S bleach signal in PbS QDs because of the similarity in the effective masses of electron and hole ($m_e^* = m_h^* = 0.085$).[57,58] Therefore, the observed 1S bleach dynamics of PbS QD-Au HNs includes electron and hole transfer from PbS QDs to Au NPs. Recently, Kaushik et al. have calculated the electron and hole coupling constants between PbSe QDs.[59] They found significant differences between these coupling constants because the HOMO wave function ($1S_h$) does not penetrate into the outside of PbSe QDs as much as the LUMO wave function ($1S_e$), suggesting that electron coupling and hole coupling between PbS QDs and Au NPs should be different.

Consequently, the ultrafast carrier transfer much faster than the the instrumental response function (~60 fs) and picosecond scale carrier transfer are probably attributed to the electron and hole transfer from PbS QDs to Au NP, respectively.

5.5 Conclusion

We synthesized PbS QD-Au HNs with clear excitonic absorption peaks and characterized these HNs by TEM and EDX. The 1S exciton absorption peak in the steady state spectra shifted to a shorter wavelength while the luminescence quantum yields decreased as Au NPs size increased. The carrier transfer dynamics from PbS QDs to Au NPs was analyzed by femtosecond near-IR transient absorption spectroscopy. The decrease of initial 1S bleach amplitude in PbS QD-Au HNs under 1S excitation suggests the existence of ultrafast carrier transfer beyond the time scale of the instrumental response function (~60 fs). However, the hot carrier transfer was not directly observed from the growth kinetics of the 1S bleach band in PbS QD-Au HNs. In addition to ultrafast carrier transfer, slow carrier transfer was also observed with time constants decreasing from 110 to 1.9 ps as Au NPs diameter increased from 1.3 to 2.6 nm. This size dependence was mainly interpreted in terms of the difference of density of state in Au NPs. The observed difference between ultrafast and ps-scale carrier transfer is probably attributed to the electron and hole transfer rates from 1S states of PbS QDs to Au NPs, respectively, which may be originated from the difference of penetration in $1S_e$ and $1S_h$ wave functions.

References

(41)   McGuire, J. A.; Joo, J.; Pietryga, J. M.; Schaller, R. D.; Klimov, V. I. New Aspects

of Carrier Multiplication in Semiconductor Nanocrystals. *Acc. Chem. Res.* **2008**, *41*,

1810−1819.

(42)   Kobayashi, Y.; Udagawa, T.; Tamai, N. Carrier Multiplication in CdTe Quantum

Dots by Single−Photon Timing Spectroscopy. *Chem. Lett.* **2009**, *38*, 830−831.

(43)   Schaller, R. D.; Klimov, V. I. High Efficiency Carrier Multiplication in PbSe

Nanocrystals: Implications for Solar Energy Conversion. *Phys. Rev. Lett.* **2004**, *92*,

186601.

(44)   Scheller, R. D.; Petruska, M. A.; Klimov, V. I. Effect of Electronic Structure on

Carrier Multiplication Efficiency: Comparative Study of PbSe and CdSe Nanocrystals.

Appl. Phys. Lett. **2005**, *87*, 253102.

(45)   Scheller, R. D.; Pietryga, J. M.; Klimov, V. I. Carrier Multiplication in InAs

Nanocrystal Quantum Dots with an Onset Defined by the Energy Conservation Limit.

Nano Lett. **2007**, *7*, 3469− 3476.

(46)   Klimov, V. I.; Mikhailovsky, A. A.; McBranch, D. W.; Leatherdale, C. A.; Bawendi,

M. G. Quantization of Multiparticle Auger Rates in Semiconductor Quantum Dots.

Science **2000**, *287*, 1011−1013.

(47)   Klimov, V. I. Optical Nonlinearities and Ultrafast Carrier Dynamics in

Semiconductor Nanocrystals. *J. Phys. Chem. B* **2000**, *104*, 6112−6123.

(48)   Kambhampati, P. Hot Exciton Relaxation Dynamics in Semiconductor Quantum

Dots: Radiationless Transitions on the Nanoscale. *J. Phys. Chem. C* **2011**, *115*,

22089−22109.

(49)   Kambhampati, P. Unraveling the Structure and Dynamics of Excitons in

Semiconductor Quantum Dots. *Acc. Chem. Res.* **2011**, *44*, 1−13.

(50)   Cooney, R. R.; Sewall, S. L.; Dias, E. A.; Sagar, D. M.; Anderson, K. E. H.;

Kambhampati, P. Unified Picture of Electron and Hole Relaxation Pathways in

Semiconductor Quantum Dots. *Phys. Rev. B* **2007**, *75*, 24531.

(51)   Cooney, R. R.; Sewall, S. L.; Anderson, K. E. H.; Dias, E. A.; Kambhampati, P.

Breaking the Phonon Bottleneck for Holes in Semiconductor Quantum Dot. *Phys. Rev.*

Lett. **2007**, *98*, 177403.

(52)   Sewall, S. L.; Cooney, R. R.; Anderson, K. E. H.; Dias, E. A.; Kambhampati, P.

State-to-State Exciton Dynamics in Semiconductor Quantum Dots. *Phys. Rev. B* **2006**, *74*,

235328.

(53)   Sewall, S. L.; Cooney, R. R.; Anderson, K. E. H.; Dias, E. A.; Kambhampati, P.

State-Resolved Studies of Biexcitons and Surface Trapping Dynamics in Semiconductor

Quantum Dots. *J. Chem. Phys.* **2008**, *129*, 084701.

(54)   Tyagi, P.; Cooney, R. R.; Sewall, S. L.; Sagar, D. M.; Saari, J. I.; Kambhampati, P.

Controlling Piezoelectric Response in Semiconductor Quantum Dots via Impulsive Charge Localization. *Nano Lett.* **2010**, *10*, 3062−3067.

(55)   Tyagi, P.; Kambhampati, P. False Multiple Exciton Recombination and Multiple Exciton Generation Signals in Semiconductor Quantum Dots Arise from Surface Charge Trapping. *J. Chem. Phys.* **2011**, *134*, 094706.

(56)   Shockley, W.; Queisser, H. J. Detailed Balance Limit of Efficiency of p−n Junction Solar Cells. *J. Appl. Phys.* **1961**, *32*, 510−519.

(57)   Guyot−Sionnest, P.; Wehrenberg, B.; Yu, D. Intraband Relaxation in CdSe Nanocrystals and the Strong Influence of the Surface Ligands. *J. Chem. Phys.* **2005**, *123*, 074709.

(58)   Pandey, A.; Guyot-Sionnest, P. Slow Electron Cooling in Colloidal Quantum Dots. *Science* **2008**, *322*, 929−932.

(59)   Schaller, R. D.; Pietryga, J. M.; Goupalov, S. V.; Petruska, M. A.; Ivanov, S. A.; Klimov, V. I. Breaking the Phonon Bottleneck in Semiconductor Nanocrystals via Multiphonon Emission Induced by Intrinsic Nonadiabatic Interactions. *Phys. Rev. Lett.* **2005**, *95*, 196401.

(60)   Nair, G.; Geyer, S. M.; Chang, L. Y.; Bawendi, M. G. Carrier Multiplication Yields in PbS and PbSe Nanocrystals Measured by Transient Photoluminescence. *Phys. Rev. B* **2008**, *78*, 125325.

(61)   Stewart, J. T.; Padilha, L. A.; Qazilbash, M. M.; Pietryga, J. M.; Midgett, A. G.;

Luther, J. M.; Beard, M. C.; Nozik, A. J.; Klimov, V. I. Comparison of Carrier

Multiplication Yields in PbS and PbSe Nanocrystals: The Role of Competing

Energy-Loss Processes. *Nano Lett.* **2012**, *12*, 622−628.

(62)   Sambur, J. B.; Novet, T.; Parkinson, B. A. Multiple Exciton Collection in a

Sensitized Photovoltaic System. *Science* **2010**, *330*, 63−66.

(63)   Sagarzazu, G.; Inoue, K.; Saruyama, M.; Sakamoto, M.; Teranishi, T.; Masuo, S.;

Tamai, N. Ultrafast Dynamics and Single Particle Spectroscopy of Au−CdSe Nanorods.

Phys. Chem. Chem. Phys. **2013**, *15*, 2141−2152.

(64)   Menagen, G.; Macdonald, J. E.; Shemesh, Y.; Popov, I.; Banin, U. Au Growth on

Semiconductor Nanorods: Photoinduced versus Thermal Growth Mechanisms. *J. Am.*

Chem. Soc. **2009**, *131*, 17406−17411.

(65)   Wu, K.; Zhu, H.; Liu, Z.; Rodríguez−Córdoba, W.; Lian, T. Ultrafast Charge

Separation and Long-Lived Charge Separated State in Photocatalytic CdS−Pt Nanorod

Heterostructures. *J. Am. Chem. Soc.* **2012**, *134*, 10337−10340.

(66)   Mongin, D.; Shaviv, E.; Maioli, P.; Crut, A.; Banin, U.; Fatti, N. D.; Vallée, F.

Ultrafast Photoinduced Charge Separation in Metal−Semiconductor Nanohybrids. *ACS*

Nano **2012**, *6*, 7034−7043.

(67)   Costi, R.; Saunders, A. E.; Elmalem, E.; Salant, A.; Banin, U. Visible Light-Induced

Charge Retention and Photocatalysis with Hybrid CdSe−Au Nanodumbbells. *Nano Lett.* **2008**, *8*, 637−641.

(68)   Yang, T. T.; Chen, W. T.; Hsu, Y. J.; Wei, K. H.; Lin, T. Y.; Lin, T. W. Interfacial Charge Carrier Dynamics in Core−Shell Au−CdS Nanocrystals. *J. Phys. Chem. C* **2010**, *114*, 11414−11420.

(69)   Bang, J. U.; Lee, S. J.; Jang, J. S.; Choi, W.; Song, H. Geometric Effect of Single or Double Metal-Tipped CdSe Nanorods on Photocatalytic H_2 Generation. *J. Phys. Chem. Lett.* **2012**, *3*, 3781−3785.

(70)   Kim, S. M.; Lee, S. J.; Kim, S. H.; Kwon, S.; Yee, K. J.; Song, H.; Somorjai, G. A.; Park, J. Y. Hot Carrier-Driven Catalytic Reactions on Pt−CdSe−Pt Nanodumbbells and Pt/GaN under Light Irradiation. *Nano Lett.* **2013**, *13*, 1352−1358.

(71)   Mokari, T.; Rothenberg, E.; Popov, I.; Costi, R.; Banin, U. Selective Growth of Metal Tips onto Semiconductor Quantum Rods and Tetrapods. *Science* **2004**, *304*, 1787−1790.

(72)   Yu, P.; Wen, X.; Lee, Y.; Lee, W.; Kang, C.; Tang, J. Photoinduced Ultrafast Charge Separation in Plexcitonic CdSe/Au and CdSe/Pt Nanorods. *J. Phys. Chem. Lett.* **2013**, *4*, 3596−3601.

(73)   Saunders, A. E.; Popov, I.; Banin, U. Synthesis of Hybrid CdS−Au Colloidal Nanostructures. *J. Phys. Chem. B* **2006**, *110*, 25421−25429.

(74)   Mokari, T.; Sztrum, C. G.; Salant, A.; Rabani, E.; Banin, U. Formation of

Asymmetric One-Sided Metal-Tipped Semiconductor Nanocrystal Dots and Rods. *Nat.*

Mater. **2005**, *4*, 855−863.

(75)   Yang, J.; Elim, H. I.; Zhang, Q.; Lee, J. Y.; Ji, W. Rational Synthesis, Self-Assembly,

and Optical Properties of PbS−Au Heterogeneous Nanostructures via Preferential

Deposition. *J. Am. Chem. Soc.* **2006**, *128*, 11921−11926.

(76)   Lee, J. S.; Shevchenko, E. V.; Talapin, D. V. Au−PbS Core−Shell Nanocrystals:

Plasmonic Absorption Enhancement and Electrical Doping via Intra-Particle Charge

Transfer. *J. Am. Chem. Soc.* **2008**, *130*, 9673−9675.

(77)   Khon, E.; Mereshchenko, A.; Tarnovsky, A. N.; Acharya, K.; Klinkova, A.;

Hewa-Kasakarage, N. N.; Nemitz, I.; Zamkov, M. Suppression of the Plasmon Resonance

in Au/CdS Colloidal Nanocomposites. *Nano Lett.* **2011**, *11*, 1792−1799.

(78)   Kobayashi, Y.; Nonoguchi, Y.; Wang, L.; Kawai, T.; Tamai, N. Dual Transient

Bleaching of Au/PbS Hybrid Core/Shell Nanoparticles. *J. Phys. Chem. Lett.* **2012**, *3*,

1111−1116.

(79)   Carbone, L.; Kudera, S.; Giannini, C.; Ciccarella, G.; Cingolani, R.; Cozzoli, P. D.;

Manna, L. Selective Reactions on the Tips of Colloidal Semiconductor Nanorods. *J.*

Mater. Chem. **2006**, *16*, 3952−3956.

(80)   Ushakova, E. V.; Litvin, A. P.; Parfenov, P. S.; Fedorov, A. V.; Artemyev, M.;

Prudnikau, A. V.; Rukhlenko, I. D.; Baranov, A. V. Anomalous Size-Dependent Decay of Low-Energy Luminescence from PbS Quantum Dots in Colloidal Solution. *ACS Nano* **2012**, *6*, 8913−8921.

(81)   Yang, Y.; Rodríguez−Córdoba, W.; Xiang, X.; Lian, T. Strong Electronic Coupling and Ultrafast Electron Transfer between PbS Quantum Dots and TiO2 Nanocrystalline Films. *Nano Lett.* **2012**, *12*, 303−309.

(82)   Klimov, V. I.; McBranch, D. W.; Leatherdale, C. A.; Bawendi, M. G. Electron and Hole Relaxation Pathways in Semiconductor Quantum Dots. *Phys. Rev. B* **1999**, *60*, 13740−13749.

(83)   Asbury, J. B.; Hao, E.; Wang, Y.; Ghosh, H. N.; Lian, T. Ultrafast Electron Transfer Dynamics from Molecular Adsorbates to Semiconductor Nanocrystalline Thin Films. *J. Phys. Chem. B* **2001**, *105*, 4545−4557.

(84)   Gao, Y. Q.; Marcus, R. A. On the Theory of Electron Transfer Reactions at Semiconductor/Liquid Interfaces. II. A Free Electron Model. *J. Chem. Phys.* **2000**, *113*, 6351−6360.

(85)   Gosavi, S.; Marcus, R. A. Nonadiabatic Electron Transfer at Metal Surfaces. *J. Phys. Chem. B* **2000**, *104*, 2067−2072.

(86)   Gao, Y. Q.; Georgievskii, Y.; Marcus, R. A. On the Theory of Electron Transfer Reactions at Semiconductor Electrode/Liquid Interfaces. *J. Chem. Phys.* **2000**, *112*,

3358−3369.

(87)   Alvarez, M. M.; Khoury, J. T.; Schaaff, T. G.; Shafigullin, M. N.; Vezmar, I.;

Whetten, R. L. Optical Absorption Spectra of Nanocrystal Gold Molecules. *J. Phys. Chem.*

B **1997**, *101*, 3706−3712.

(88)   Kano, S.; Azuma, Y.; Kanehara, M.; Teranishi, T.; Majima, Y. Room-Temperature

Coulomb Blockade from Chemically Synthesized Au Nanoparticles Stabilized by

Acid−Base Interaction. *Appl. Phys. Express* **2010**, *3*, 105003.

(89)   Negishi, R.; Hasegawa, T.; Tanaka, H.; Terabe, K.; Ozawa, H.; Ogawa, T.; Aono, M.

Size-Dependent Single Electron Tunneling Effect in Au Nanoparticles. *Surf. Sci.* **2007**,

601, 3907−3911.

(90)   Koole, R.; Liljeroth, P.; Donegá, C. M.; Vanmaekelbergh, D.; Meijerink, A.

Electronic Coupling and Exciton Energy Transfer in CdTe Quantum-Dot Molecules. *J.*

Am. Chem. Soc. **2006**, *128*, 10436−10441.

(91)   Tvrdy, K.; Frantsuzov, P. A.; Kamat, P. V. Photoinduced Electron Transfer from

Semiconductor Quantum Dots to Metal Oxide Nanoparticles. *Proc. Natl. Acad. Sci. U. S.*

A. **2011**, *108*, 29−34.

(92)   Zhu, H.; Yang, Y.; Hyeon−Deuk, K.; Calidano, M.; Song, N.; Wang, Y.; Zhang, W.;

Prezhdo, O. V.; Lian, T. Auger-Assisted Electron Transfer from Photoexcited

Semiconductor Quantum Dots. *Nano Lett.* **2014**, *14*, 1263−1269.

(93)   Tisdale, W. A.; Zhu, X. Y. Artificial Atoms on Semiconductor Surfaces. *Proc. Natl.*

Acad. Sci. U. S. A. **2011**, *108*, 965−970.

(94)   Hyun, B.; Bartnik, A. C.; Lee, J.; Imoto, H.; Sun, L.; Choi, J. J.; Chujo, Y.; Hanrath,

T.; Ober, C. K.; Wise, F. W. Role of Solvent Dielectric Properties on Charge Transfer

from PbS Nanocrystals to Molecules. *Nano Lett.* **2010**, *10*, 318−323.

(95)   Hyun, B. R.; Zhong, Y. W.; Bartnik, A. C.; Sun, L.; Abruña, H. D.; Wise, F. W.;

Goodreau, J. D.; Matthews, J. R.; Leslie, T. M.; Borrell, N. F. Electron Injection from

Colloidal PbS Quantum Dots into Titanium Dioxide Nanoparticles. *ACS Nano* **2008**, *2*,

2206−2212.

(96)   Koch, N.; Kahn, A.; Ghijsen, J.; Pireaux, J. J.; Schwartz, J.; Johnson, R. L.; Elschner,

A. Conjugated Organic Molecules on Metal versus Polymer Electrodes: Demonstration of

a Key Energy Level Alignment Mechanism. *Appl. Phys. Lett.* **2003**, *82*, 70.

(97)   Nanda, K. K.; Kruis, F. E.; Fissan, H.; Behera, S. N. Effective mass approximation

for two extreme semiconductors: Band gap of PbS and CuBr nanoparticles. *J. Appl. Phys.*

2004, *95*, 5035.

(98)   Wehrenberg, B. L.; Guyot-Sionnest, P. Electron and Hole Injection in PbSe Quantum

Dot Films. *J. Am. Chem. Soc.* **2003**, *125*, 7806−7807.

(99)   Kaushik, A. P.; Lukose, B.; Clancy, P. The Role of Shape on Electronic Structure

and Charge Transport in Faceted PbSe Nanocrystals. *ACS Nano* **2014**, *8*, 2302−2317.
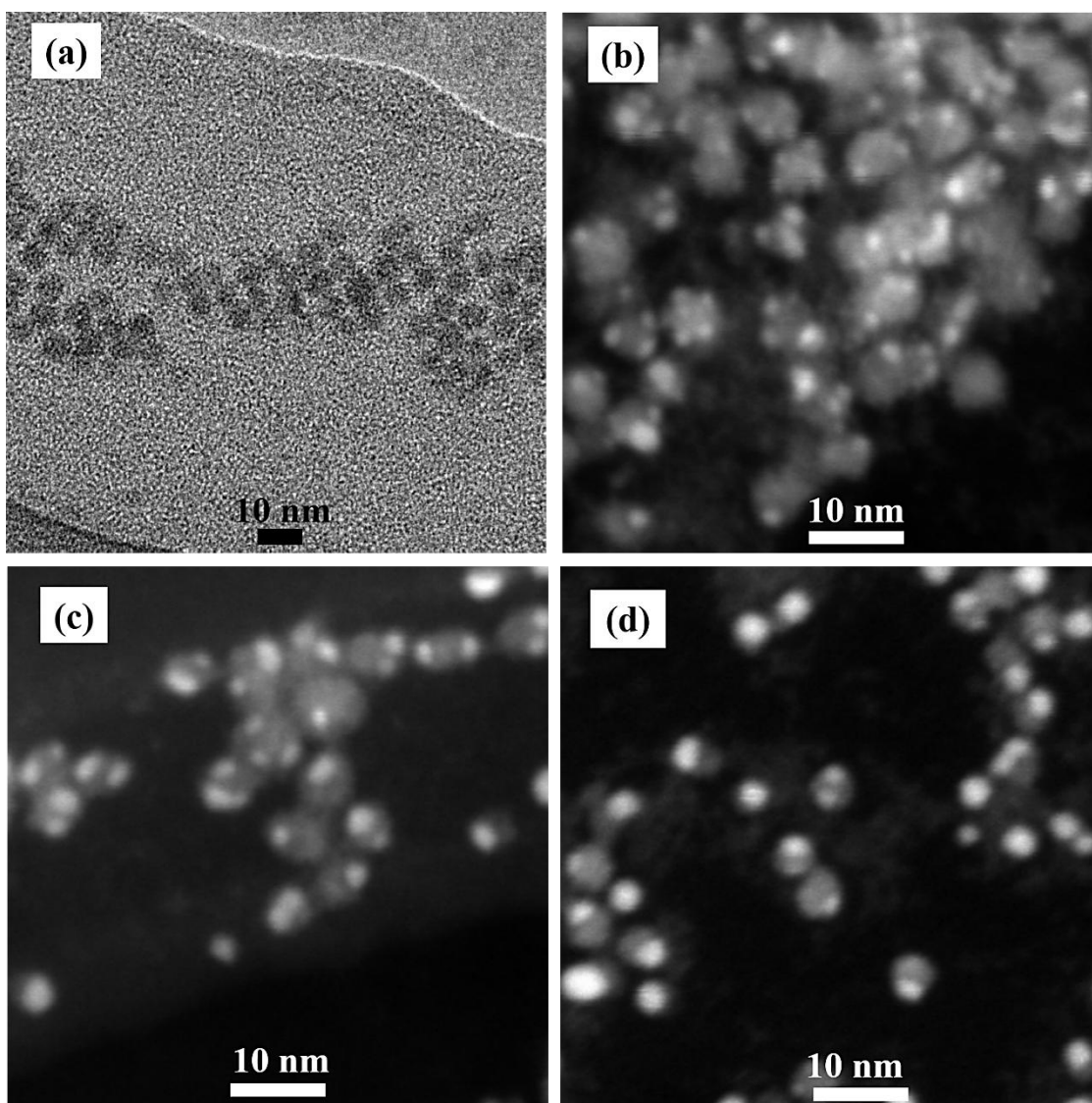
Figure 5.1 TEM image of (a) PbS QDs and STEM images of PbS QD-Au HNs (b) A, (c) B, and (d) C.

Table 5.1 Estimated diameter of PbS QDs and Au NPs

Sample	Diameter of PbS QDs / nm	Diameter of Au NPs / nm
PbS QDs	5.5 ± 0.4	
PbS QD-Au HNs A	5.1 ± 0.5	1.3 ± 0.3
PbS QD-Au HNs B	4.7 ± 0.5	1.7 ± 0.4
PbS QD-Au HNs C	4.4 ± 0.6	2.6 ± 0.5
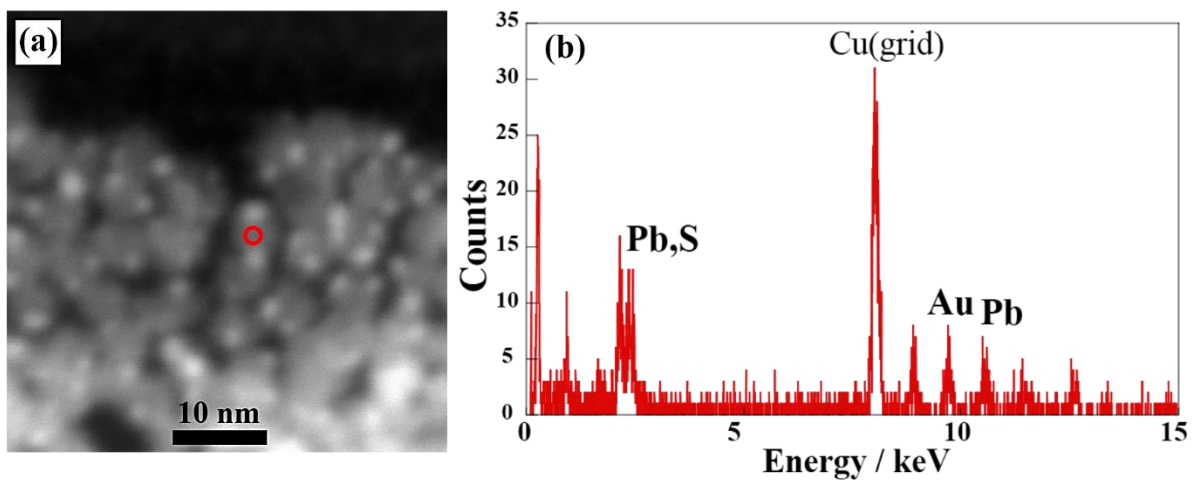
Figure 5.2 (a) STEM image of PbS QD-Au HNs and (b) the result of EDX measured at the red circle point in (a).
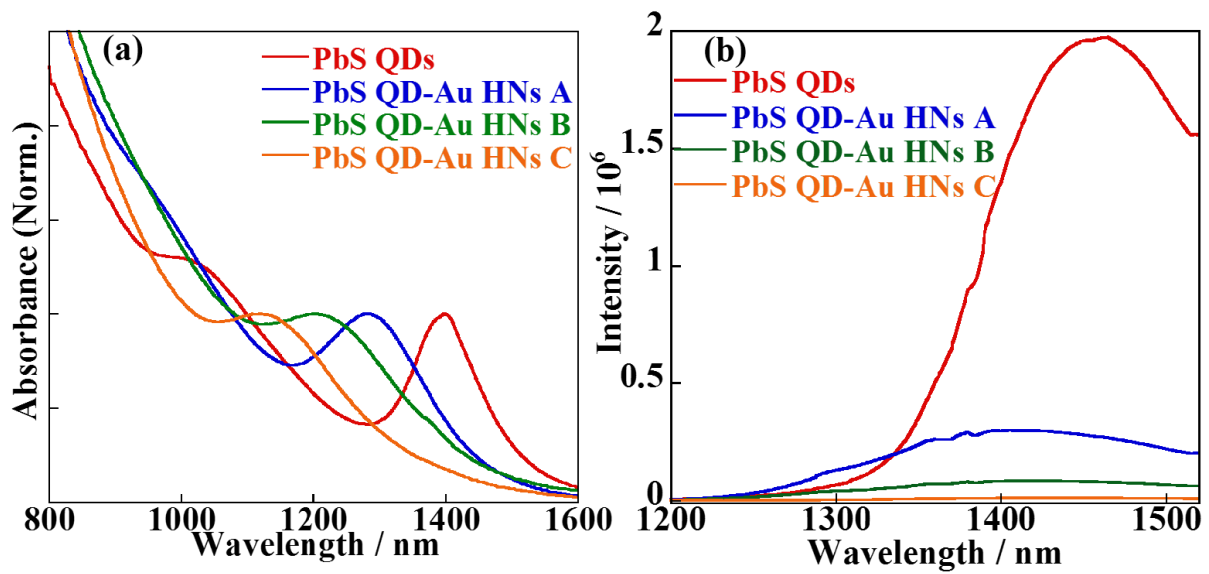
Figure 5.3 (a) Absorption spectra and (b) luminescence spectra (λ_{ex} =800 nm) of PbS QDs and PbS QD-Au HNs.

Table 5.2 Peak wavelength of 1S absorption and luminescence, and relative luminescence intensity of PbS QDs and PbS-Au HNs.

Sample	1S absoption peak / nm	Luminescence peak / nm	Relative luminescence intensity
PbS QDs	1400	1460	1
PbS QD-Au HNs A	1290	1430	0.20
PbS QD-Au HNs B	1200	1420	0.06
PbS QD-Au HNs C	1120	1430	0.01
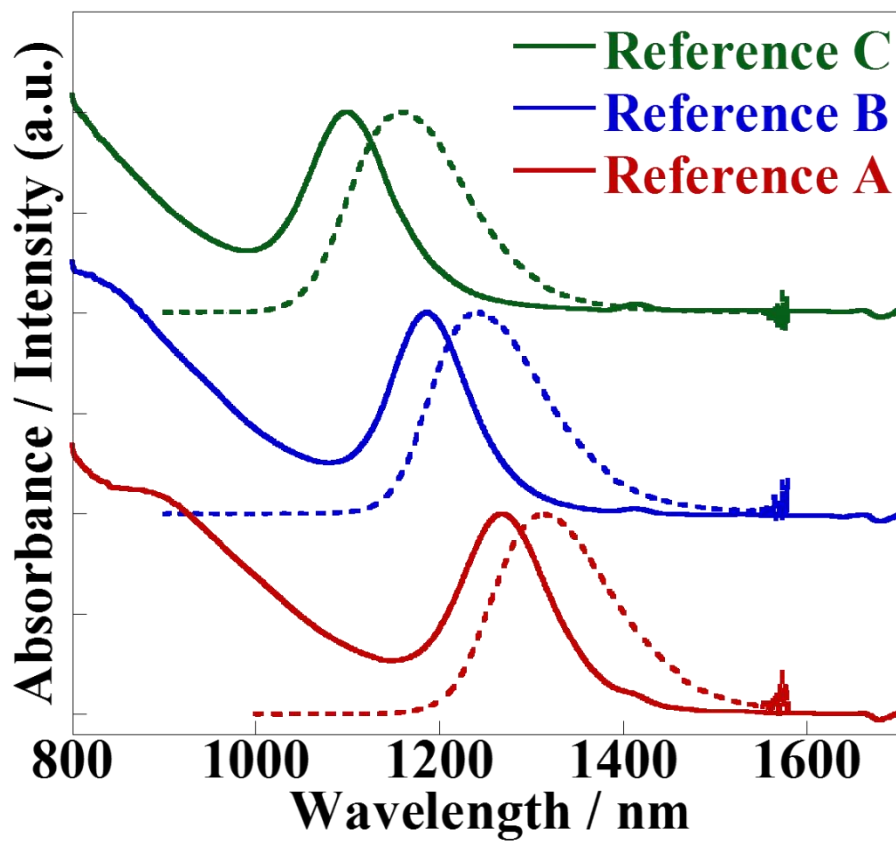
Figure 5.4 Absorption (solid line) and luminescence (dashed line) spectra of PbS QDs with various sizes (Reference A, B, and C).
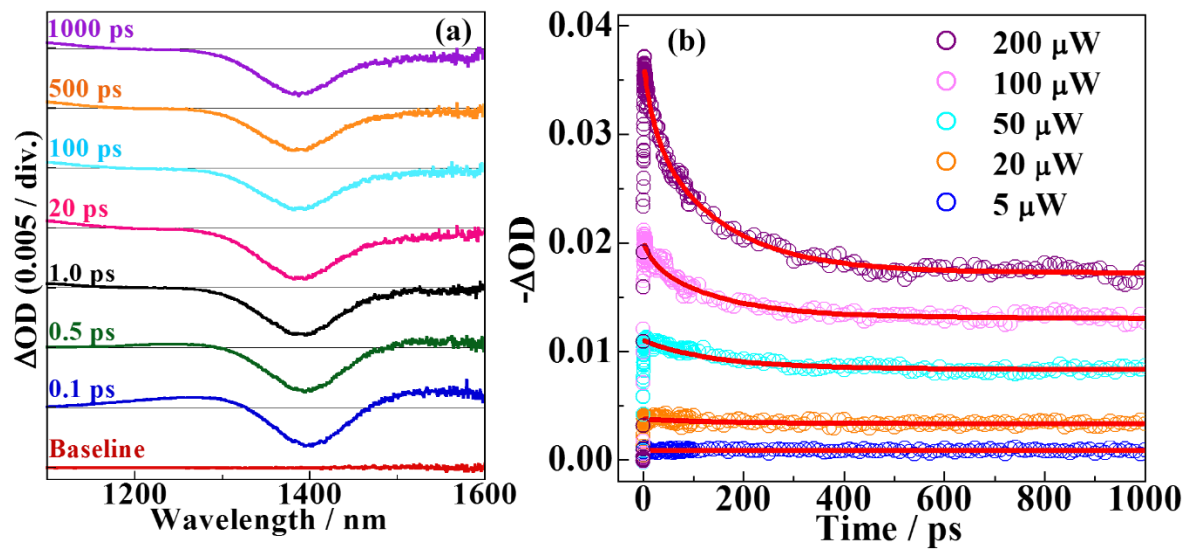
Figure 5.5 (a) Transient absorption spectra (λ_{ex} = 800 nm, $\langle N_0 \rangle$ = 0.1) and (b) excitation intensity dependence of 1S bleach dynamics of PbS QDs.
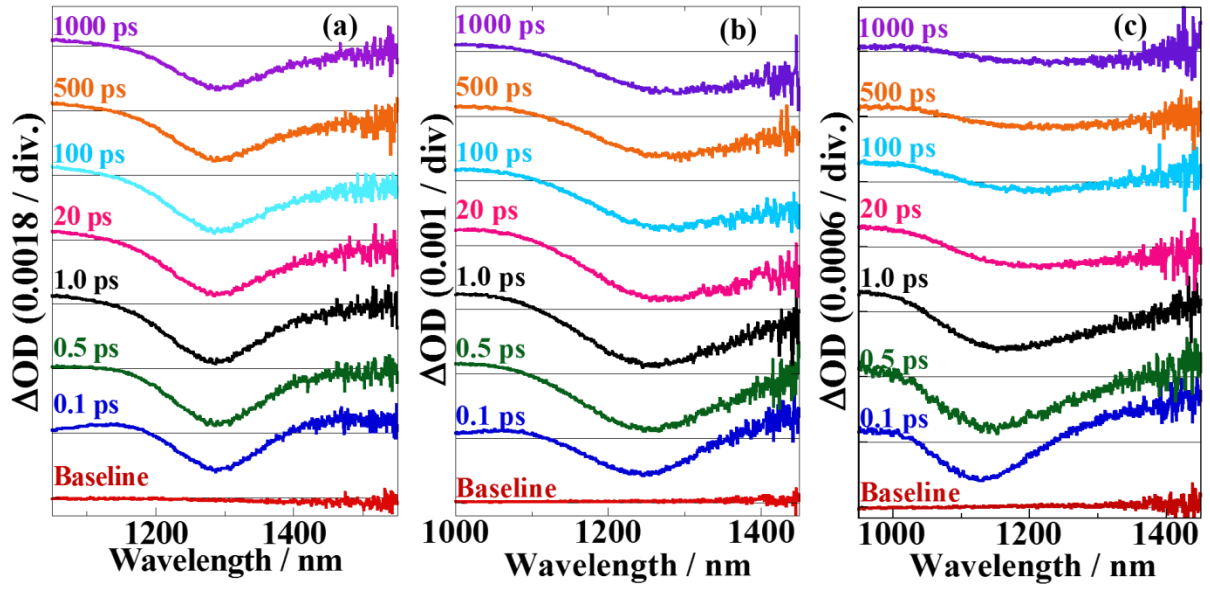
Figure 5.6 Transient absorption spectra of (a) PbS QD-Au HNs A, (b) PbS QD-Au HNs B, and (c) PbS QD-Au HNs C.
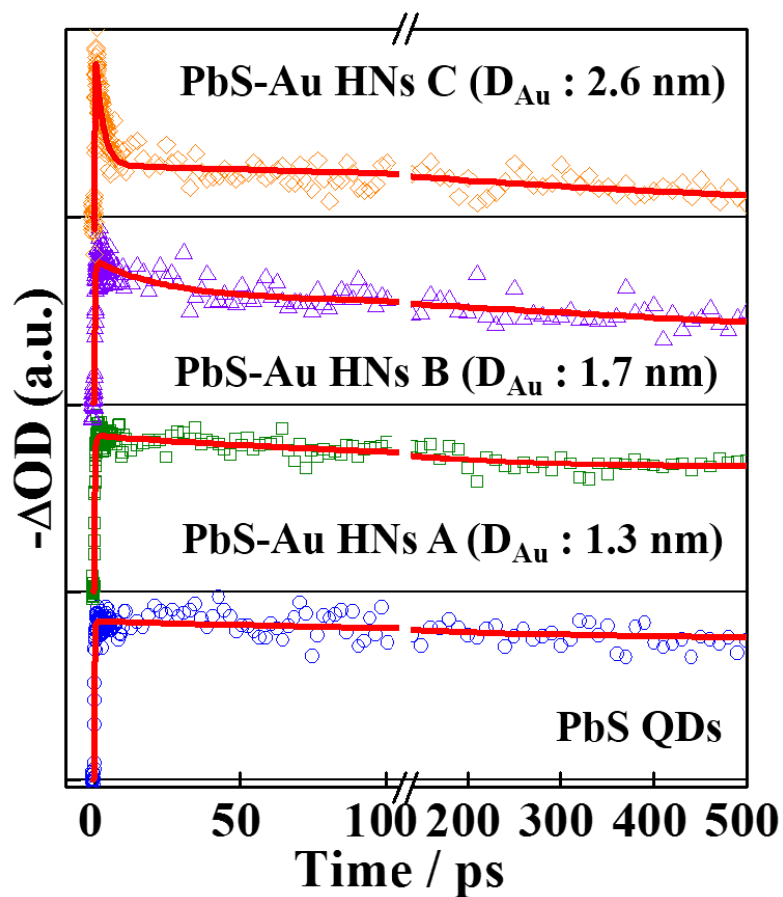
Figure 5.7 1S bleach dynamics of PbS QDs and PbS QD-Au HNs excited at 800 nm ($<N_0> \leq$ 0.1).

Table 5.3 Fitting results of the 1S bleach dynamics with a biexponentia decay function.

Sample	τ_1 / ps	τ_2 / ns
PbS QDs	200 (6%)	Over 10 ns (94%)
PbS QD-Au HNs A	110 (16%)	8.0 (84%)
PbS QD-Au HNs B	34 (29%)	3.1 (71%)
PbS QD-Au HNs C	1.9 (71%)	1.0 (29%)
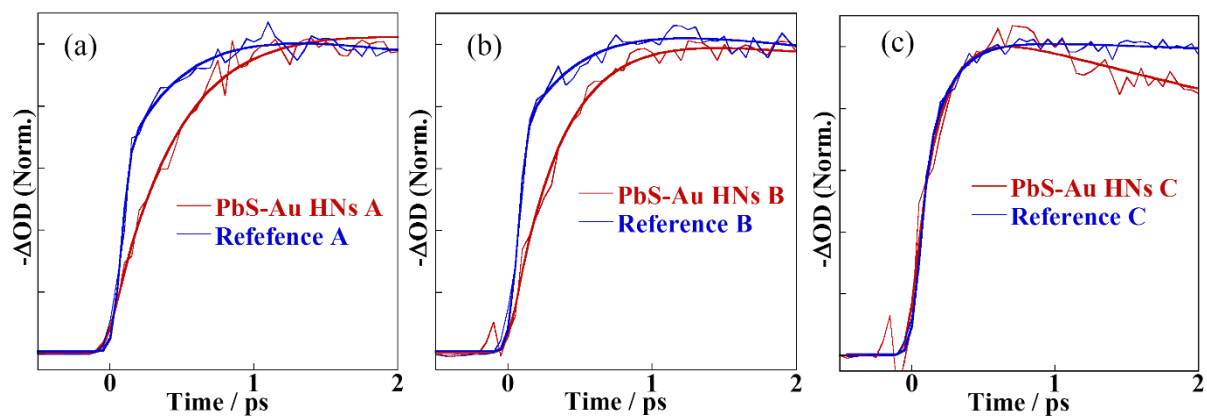
Figure 5.8 Transient absorption dynamics at 1S bleach of corresponding PbS QD-Au HNs and references (a) A, (b) B, and (c) C under 800 nm excitation.

Table 5.4 Rise time of 1S bleach band in each sample.

Sample	τ_{rise} / fs	Sample	τ_{rise} / fs
PbS QDs	520		
Reference A	440	PbS QD-Au HNs A	460
Reference B	400	PbS QD-Au HNs B	350
Reference C	190	PbS QD-Au HNs C	180
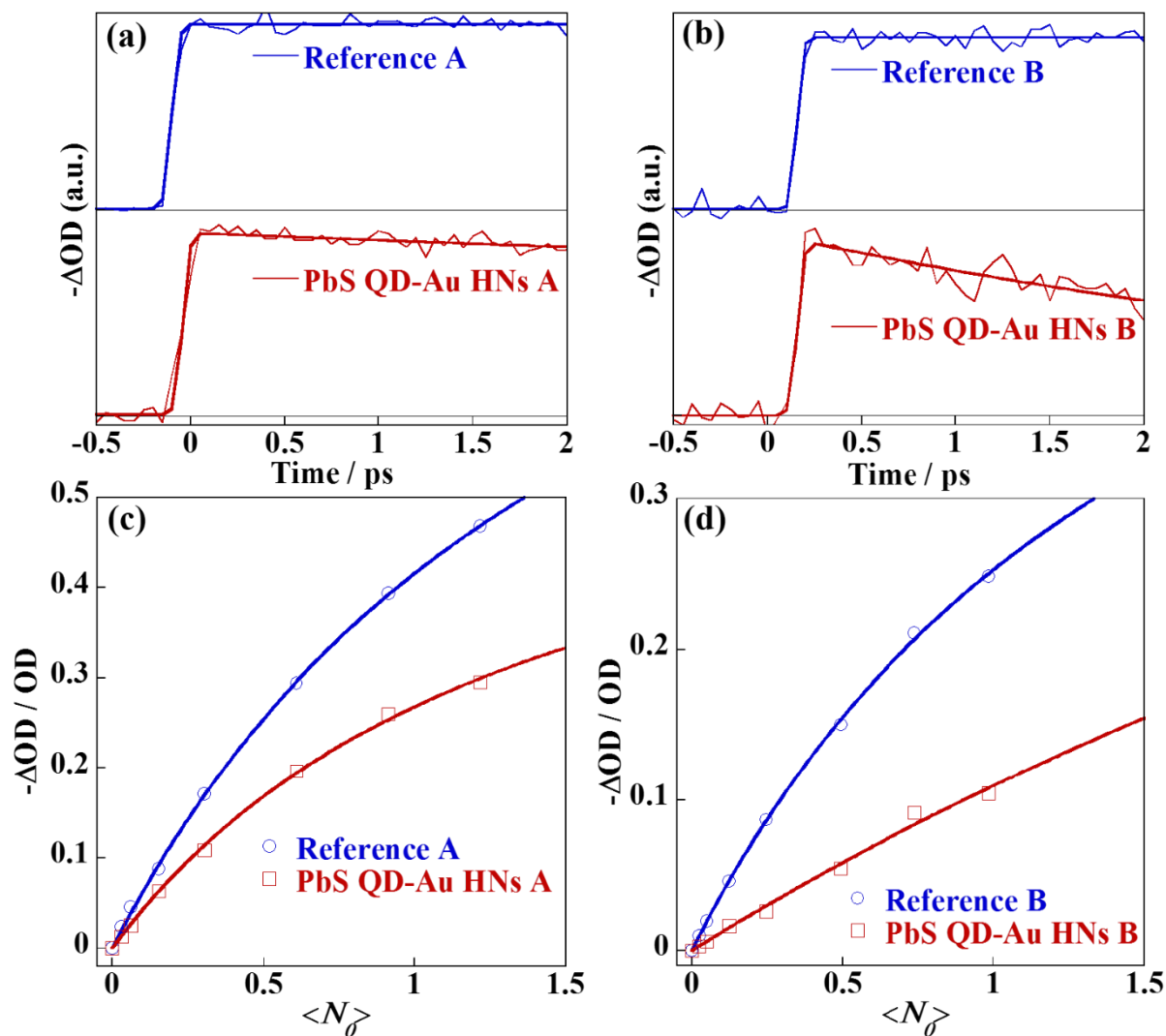
Figure 5.9 Transient absorption dynamics at 1S bleach of corresponding PbS QD-Au HNs and references (a) A and (b) B and 1S bleach yields of PbS QD-Au HNs and references (c) A and (d) B under 1S excitation.

Chapter 6

Ultrafast and Hot Electron Transfer Processes from CdSe QDs to Au NPs

6.1 Abstract

Recently, much attention has been paid for semiconductor-metal hybrid nanostructures (HNs) in terms of efficient electron transfer from semiconductor to metal, and semiconductor-metal HNs are one of the best candidate materials for photovoltaics and photocatlysis. However, the analyses of electron transfer processes in semiconductor-metal HNs have focused on the electron transfer from band-edge state in metal attached semiconductor nanorods (NRs). Here, we synthesized and characterized CdSe quantum dots (QDs) attached with different size of Au nanoparticles (NPs), and examined electron transfer from band-edge (1S(e)) and higher excited states using femtosecond pump-probe spectroscopy with state-selective excitation. We analyzed growth kinetics, decay dynamics, and initial bleach amplitude at the 1S bleach band, and found the existence of the hot electron transfer from 1P(e) state and ultrafast electron transfer with the lifetime much faster than the instrumental response function from 1S(e) state of CdSe QDs to Au NPs. We found that the rates and yields of hot electron transfer in CdSe QD-Au HNs became faster and larger than those in CdSe NR-Au HNs, although these properties does not change irrespective of the size of Au NPs. In addition, the yield of ultrafast electron transfer ($\ll$ 60 fs) from 1S(e) state in CdSe QD-Au HNs increased with increasing the Au NPs size, in contrast with CdSe NR-Au HNs.

6.2 Introduction

Semiconductor nanocrystals are promising materials for the photovoltaics because of their unique photophysical properties resulting from the strong confinement of electron and hole. The semiconductor quantum dots (QDs), where electron and hole are confined along three dimensional directions, exhibit the size-tunable absorption and luminescence spectra,[1,2] highly efficient multiple exciton generation (MEG),[3-6] and discrete electronic states.[2] MEG

process in semiconductor QDs, a process that multiple excitons are generated by the absorption of only one photon, is noticeable phenomenon for the development of highly efficient solar cells. However, multiple excitons in semiconductor QDs disappear with the time scale of tens of ps by Auger recombination process.[2,7-9] Therefore, the efficient extraction of multiple excitons from semiconductor QDs is very important for the application of light-energy conversion. In addition to the MEG process, slow relaxation of excited electron with excess energy (hot electron) in semiconductor QDs can potentially allow to increase the conversion efficiency of QDs solar cells. Semiconductor QDs have the discrete electronic structures while bulk semiconductor have the continuous band structures, and the energy spacing between 1S(e) and 1P(e) states in CdSe QDs is 10 times larger than the LO phonon energy.[2] Therefore, the hot electron in QDs relaxes to the band-edge state by different processes from bulk semiconductors such as Auger cooling process and energy transfer to surface ligands.[10-14] Kambhampati's group analyzed the size dependence of intraband transition rate in CdSe QDs using the state-selective excitation experiments and revealed that dominant hot carrier relaxation process from 1P(e) to 1S(e) and $2S_{3/2}$(h) to $1S_{3/2}$(h) were Auger cooling and energy transfer to surface ligands, respectively.[10-13] Moreover, Guyot-sionnest's group examined the role of surface ligands to the intraband transition of CdSe QDs capped with different ligands using the infrared pump-probe spectroscopy.[14] According to these previous studies, intraband relaxation rate from 1P(e) state to 1S(e) state can be modified by the separation of electron and hole wavefunction and surface ligands. Actually, the extremely slow hot electron relaxation in CdSe/ZnSe/ZnS/CdSe nanoparticles (NPs) have been achieved by Pandey et al.[15] For the conventional solar cells using bulk semiconductors, hot carrier relaxes immediately to the band-edge state by phonon emission through continuous electronic states. This fast relaxation of hot carriers limits the conversion efficiency to ~32.7%, which is well known as Shockley-Queisser limit.[16] On the other hand,

162

the slower intraband relaxation in semiconductor QDs can lead to the efficient extraction of hot carriers. In a previous theoretical study, Ross and Nozik reported that the maximum conversion efficiency of QD solar cells could reach ~67% by utilizing the excess energy of hot carriers.[17]

The efficient extraction of multiple and hot carriers from semiconductor nanocrystals to the outside is the key for the development of highly efficient QDs solar cells. In PbSe QDs strongly coupled with the TiO$_2$, the ultrafast electron transfer (~ 6 fs) from PbSe QDs to TiO$_2$ was suggested,[18] and the multiple excitons collection was detected by measurements of excitation wavelength dependence of photon-to-current conversion efficiency.[19,20] Moreover, electron transfer processes from semiconductor nanocrystals to acceptor molecules were examined by several groups. Matylitsky et al. examined the multiple electron ($\leq$ ~4 electrons) transfer from CdSe QDs to methyl viologen (MV^{2+}) that is known as an efficient electron acceptor molecule.[21] In the quasi-type II CdSe/CdS core/shell QDs-MV^{2+} complexes, the slow Auger recombination and fast electron transfer lead to very efficient multiple electron extraction up to ~19 electrons.[22] Furthermore, in nanorods (NRs) systems, Zhu and Lian reported the ~21 electrons extraction from CdSe NRs to MV^{2+}.[23] In addition to the multiple exciton extraction, hot electron transfer from CdSe QDs to MV^{2+} was examined by Wang et al.[24]

Since metal nanoparticles are well known as an electron acceptor for the semiconductor nanocrystals, semiconductor-metal hybrid nanostructures (HNs) are promising materials for the development of highly efficient solar cells in terms of the efficient charge separation. In the semiconductor-metal HNs, the ultrafast electron transfer from semiconductor nanocrystals to metal nanoparticles whose lifetime was much faster than the instrumental response function was reported.[25,26] In our previous study on PbS QD-Au HNs (Chapter 5), ultrafast electron transfer and ps-scale hole transfer from the band-edge states of

PbS QDs to Au NPs were examined by the state-selective excitation experiments.[25] Mongin et al, reported the sub-20 fs electron transfer from CdS NRs to Au NPs.[26]   Furthermore, in our previous study, the hot electron transfer from CdSe NRs to Au NPs were analyzed by state-selective excitation experiments.[27,28] For the analyses of growth kinetics of band-edge bleach band and initial bleach amplitude in CdSe NR-Au HNs with the Au NPs diameter of 2.2 nm, the rate and yield of hot electron transfer were estimated to be $\sim(0.5\text{-}1.0\text{ ps})^{-1}$ and ~23%, respectively. The most of previous studies on the charge separation in semiconductor-metal HNs have focused on the electron transfer from the band-edge state of cadmium chalcogenide NRs to Au NPs. However, semiconductor NRs have more complicated electronic structures compared with those of semiconductor QDs, in which additional electronic states derived from a weak quantum confinement along the long axis exist.[29] Therefore, the detailed analysis of electron transfer processes from semiconductor QDs to metal NPs is very important for the understanding of elementary electron transfer processes in semiconductor-metal HNs.

In the present study, we synthesized and characterized CdSe QD-Au HNs with different diameter of Au NPs. The electron transfer from CdSe QDs to Au NPs were examined by femtosecond pump-probe spectroscopy with the state-selective excitation technique. The hot electron transfer and ultrafast electron transfer much faster than the instrumental response function were analyzed by comparing the growth kinetics and initial bleach amplitude at 1S bleach band of CdSe QD-Au HNs with those of CdSe QDs. Furthermore, we compared the observed electron transfer dynamics in CdSe QD-Au HNs with that of CdSe NR-Au HNs.

6.3   Experimental section

Synthetic methods of CdSe QDs and CdSe QD-Au HNs were described in Chapter 2.

The structures of CdSe QDs and CdSe QD-Au HNs were characterized by scanning transmission electron microscopy (STEM, TECNAI 20, 200 keV, FEI) and energy dispersive X-ray spectrometry (EDX, ibid). UV−vis absorption and luminescence spectra of CdSe QDs and CdSe QD-Au HNs were recorded using an U-4100 (Hitachi) and a Fluorolog-3 (Jobinyvon-Spex), respectively. The femtosecond transient absorption spectra were measured using an amplified mode-locked Ti:sapphire laser system (Spitfire and Tsunami, Spectra-Physics, repetition rate: 1 kHz). In 400 nm excitation experiments, CdSe QDs and CdSe QD-Au HNs were excited by the second harmonic of fundamental wave. State selective excitation experiments were performed by an optical parametric amplifier (OPA) (TOPAS, Light Conversion Ltd.), in which excitation wavelengths were 574 nm, 555 nm and 496 nm. A repetition rate of 0.5 kHz was achieved by an optical chopper (Model 3501, New Focus, Inc.). Absorption transients were probed by delayed pulses of a femtosecond white-light continuum generated by focusing a fundamental laser pulse into a D_2O cell and were detected by a polychromator-CCD combination (Spectra Pro-275, Acton Research Co., and Spec-10, Princeton Instruments). The temporal resolution for 400 nm excitation and state-selective excitation experiments were 100 fs and 60 fs, respectively.

6.4 Results and discussion

6.4.1 Electron transfer processes from CdSe QDs to Au NPs

STEM images of CdSe QDs and CdSe QD-Au HNs A and B were shown in Figure 6.1. The average diameter of CdSe QDs was estimated to be 4.2 ± 0.3 nm from the STEM image analysis. In the STEM images of CdSe QD-Au HNs, two clearly contrasting parts exist, in which bright and gray parts can be assigned to Au NPs and CdSe QDs, respectively, as shown in the EDX data (Figure 6.2). From the STEM images of CdSe QD-Au HNs, the average diameters of Au NPs were estimated to be 1.3 ± 0.4 nm and 2.0 ± 0.4 nm in CdSe

QD-Au HNs A and B, respectively. Steady-state absorption and luminescence spectra of CdSe QDs and CdSe QD-Au HNs were illustrated in Figure 6.3. In the absorption spectrum of CdSe QDs, several absorption peaks were clearly observed, in which absorption bands centered at ~589 nm, ~555 nm and ~495 nm were due to the transition of $1S(e)-1S_{3/2}(h)$, $1S(e)-2S_{3/2}(h)$, and $1P(e)-1P_{3/2}(h)$, respectively.[10,30] From $1S(e)-1S_{3/2}(h)$ absorption peak wavelength, the diameter of CdSe QDs can be estimated to be ~4.2 nm, which is in good agreement with STEM images.[31] In the CdSe QD-Au HNs, absorption bands slightly shifted to the shorter wavelength and became broader with increasing the diameter of Au NPs. In the previous studies on PbS QD-Au HNs (Chapter 3)[25] and PbS QDs adsorbed on the TiO_2 NPs[18], the broadening of steady-state absorption bands of PbS QDs is originated from the strong electronic coupling. It is also known that Au NPs smaller than 2 nm in diameter exhibit the very broad steady-state absorption, in which the localized surface plasmon resonance band cannot be observed.[32] Therefore, the broad absorption spectra of CdSe QD-Au HNs were likely arised from both strong electronic coupling and absorption of small Au NPs attached to CdSe QDs. In the luminescence spectra, the band-edge emission of CdSe QDs centered at 593 nm was strongly quenched in CdSe QD-Au HNs (Figure 6.3b), suggesting the existence of efficient carrier transfer from CdSe QDs to Au NPs.

The transient absorption spectra of CdSe QDs and CdSe QD-Au HNs excited at 400 nm with the excitation intensity of 3.5 $\mu J/cm^2$ were shown in Figure 6.4. In all samples, transient absorption bleach bands corresponding to $1S(e)-1S_{3/2}(h)$, $1S(e)-2S_{3/2}(h)$, and $1P(e)-1P_{3/2}(h)$ transitions in steady-state spectra were observed. As clearly shown, the amplitude of transient absorption signal of CdSe QD-Au HNs at initial time region became lower with increasing the size of Au NPs attached to CdSe QDs. In this excitation intensity, multiple excitons does not contribute to the transient absorption spectra and dynamics because of the low excitation intensity, which is supported by the excitation intensity dependence of

1S bleach dynamics as shown in Figure 6.5. Although the spectral features of all samples were very similar with each other, fast relaxation of transient absorption signal were clearly observed in CdSe QD-Au HNs. The band-edge (1S) bleach dynamics of CdSe QDs and CdSe QD-Au HNs is shown in Figure 6.6. In the previous studies, the 1S bleach of CdSe nanocrystals was due to the state-filling of the band-edge state in conduction band (1S(e) state).[33] Therefore, fast relaxation of 1S bleach dynamics in CdSe QD-Au HNs were probably due to the electron transfer from 1S(e) state of CdSe QDs to Au NPs. Furthermore, the electron transfer from 1S(e) state of CdSe QDs became faster with increasing the diameter of Au NPs. The 1S bleach dynamics were fitted using sum of exponential functions by a deconvolution analysis, and the results were summarized in Table 6.1. The fitting results show that electron transfer from 1S(e) state to Au NPs became faster with increasing the size of Au NPs as similar to PbS QD-Au HNs (Chapter 3) and CdSe NR-Au HNs.[25,27]

In the nonadiabatic limit, the total rate of electron transfer from the donor state of CdSe QDs to the acceptor states of Au NPs can be expressed as the sum of electron transfer rates to all possible accepting states as given in the following equation,[34-37]

$$k_{ET} = \frac{2\pi}{\hbar} \int_{-\infty}^{\infty} dE \, \rho(E) |\bar{H}(E)|^2 \frac{1}{\sqrt{4\pi\lambda k_B T}} \times exp\left[-\frac{(\lambda + \Delta G + E)^2}{4\lambda k_B T}\right] \qquad (1)$$

where k_{ET} is the total rate constant of electron transfer, $\rho(E)$ is the density of the final states of the Au NPs, $|\bar{H}(E)|$ is the electronic coupling constant between the initial 1S(e) state of CdSe QDs and the final states of the Au NPs, λ is the reorganization energy, which is the sum of the inner-sphere, λ_i, and outer-sphere, λ_o, components, and ΔG_0 is the variation of Gibbs energy corresponding to the energy difference between the 1S(e) state of CdSe QDs and the Fermi level of Au NPs. The eq. 1 indicates that the electron transfer rate depends on the density of final states of Au NPs. According to previous studies, the localized surface plasmon

resonance band cannot be observed in the steady-state spectrum of the Au NPs whose diameter is less than 2 nm.[32] Furthermore, the small Au NPs within the diameter of 2 nm exhibit the Coulomb blockade effect at room temperature.[38,39] These results suggests the electronic states of Au NPs become discrete as the diameter decreases below 2 nm. Consequently, the observed Au NPs size dependence of electron transfer rate in CdSe QD-Au HNs was interpreted in terms of the change of the density of final states, $\rho(E)$, of Au NPs. The other parameters in eq. 1 such as $|\bar{H}(E)|$, ΔG_0, and λ may have small contribution on the size-dependent electron transfer rate because of the following reasons. As shown in Figure 6.3, 1S absorption peak wavelengths of CdSe QDs is similar to those of CdSe QD-Au HNs, suggesting that CdSe QDs in each samples have similar band gap energy and diameter irrespective of Au NPs attachment. The electronic coupling constant, $|\bar{H}(E)|$, depends on the degree of overlap between the penetrated wavefunction of the 1S(e) state of CdSe QDs and Au NPs, and is proportional to the amplitude of the electron density at the surface of QDs which increases as the size of the QDs decreases.[40] In the present study, since the diameter of QDs is similar in all samples, the change of electronic coupling strength with increasing the size of Au NPs is not so large. Moreover, the similar band gap energy suggests that all samples have comparable conduction band-edge energies. Therefore, the change of ΔG_0 with increasing the Au NPs size does not significantly contribute to the change of electron transfer rate. In addition, the inner-sphere term of reorganization energy (λ_i,) comes from the nuclear displacement of the reactants and products, and the value of λ_i in semiconductor QDs is known to be negligibly small (a few tens of meV).[40,41] Since the contribution of Au NPs to λ_i is still unclear, we assume that the effect of nuclear displacement in Au NPs associated with single electron transfer is very small because Au NPs contains many electrons. The λ_o comes from the dielectric response of the solvent and ligand.[42,43] In the present study, because of the small difference between static and optical dielectric constants of toluene (ε_s: 2.41, ε_{op}: 2.23)[44,]

the change of λ_o with the change of Au NPs size is very small (< 10 meV). Therefore, the total reorganization energy does not contribute to the Au NPs size dependence of electron transfer rate.

In addition to the electron transfer with a lifetime of sub-ps scale from the conduction band-edge state, we examined hot electron transfer from CdSe QDs to Au NPs by the analyses of growth kinetics of 1S bleach band. Assuming that the hot electron transfer occurred, the rise time of 1S bleach band can be expressed as the inverse of the sum of the rate constants of intraband relaxation (k_{int}) and hot electron transfer (k_{hot}). Thus, the faster growth kinetics of 1S bleach band can be expected in CdSe QD-Au HNs as compared to CdSe QDs. The initial dynamics at the 1S bleach band of CdSe QDs and CdSe QD-Au HNs excited at 400 nm are illustrated in Figure 6.7a. As clearly shown, the rise time of CdSe QD-Au HNs A and B became faster than that of CdSe QDs, strongly suggesting the existence of hot electron transfer from CdSe QDs to Au NPs. The rise time at the 1S bleach band of CdSe QDs and the both of CdSe QD-Au HNs A and B were estimated to be ~300 fs ($1/k_{int}$) and ~150 fs ($1/(k_{int} + k_{hot})$), respectively. From these results, the hot electron transfer time ($1/k_{hot}$) was calculated to be ~300 fs, and the hot electron transfer yield, defined as $\Phi_{hot} = k_{hot} / (k_{int} + k_{hot})$, to be ~0.5 in both CdSe QD-Au HNs A and B.

In addition to the growth kinetics of 1S bleach band, the initial bleach amplitude at the 1S bleach band should be affected by the hot electron transfer. The initial 1S bleach amplitudes corrected with the steady-state absorption at the excitation wavelength ($\Delta OD/OD_{400\ nm}$) in CdSe QDs and CdSe QD-Au HNs were plotted against the excitation intensity in Figure 6.7b. The hot electron in CdSe QDs relaxes to the 1S(e) state in competition with the hot electron transfer to Au NPs. As mentioned above, the 1S bleach band is due to the state filling of the 1S(e) state. Therefore, the decrease of the probability of electron relaxing to the 1S(e) state from higher excited states leads to the smaller initial

bleach amplitude of the 1S bleach in CdSe QD-Au HNs. By considering the three-level system including the $<i|$, 1S(e) state and Fermi level of Au (Figure 6.8), the initial bleach amplitude of 1S band in CdSe QD-Au HNs (B_{HNs}) can be expressed as the following equation,

$$B_{HNs} = [k_{int}/(k_{int} + k_{hot})] \times B_{QDs} \qquad (2)$$

where B_{QDs} is the initial bleach amplitude of 1S band in CdSe QDs. The 1S bleach amplitude of CdSe QD-Au HNs A and B estimated from Φ_{hot} was ~50% of CdSe QDs. However, as shown in Figure 6.7b, the observed 1S bleach amplitude of CdSe QD-Au HNs A and B were ~31% and ~15% of CdSe QDs, respectively. Therefore, the lower initial 1S bleach amplitude in CdSe QD-Au HNs as compared with the estimated value from Φ_{hot} is originated from not only hot electron transfer but also other processes. Mongin et al. reported the decrease of the initial transient absorption signal at a band-edge bleach band in CdS NR-Au HNs compared with that of CdS NRs.[26] According to this report, the decrease of initial amplitude of band-edge bleach was ascribed to the ultrafast electron transfer from band-edge state of CdS NRs to Au NPs with the sub-20 fs time scale, which was much faster than the instrumental response function. Therefore, the drastic decrease of the initial 1S bleach amplitude observed in our experiments is probably due to ultrafast electron transfer from the 1S(e) state of CdSe QDs to Au NPs.

In order to analyze the elementary electron transfer processes from CdSe QDs to Au NPs in more detail, state-selective excitation experiments were conducted with an OPA. In these experiments, samples were excited at 574 nm, 555 nm, and 496 nm, corresponding to the selective excitation of 1S(e)-1S$_{3/2}$(h) (1S), 1S(e)-2S$_{3/2}$(h) (2S), and 1P(e)-1P$_{3/2}$(h) (1P) transition, respectively. As mentioned in section 1.2.3, in the case of 1S and 2S excitation experiments, excited electron was occupied the band-edge state in conduction band directly

from different hole states. In contrast, in 1P excitation experiments, the electron is excited from $1P_{3/2}(h)$ state to $1P(e)$ state, generating the hot electron. The transient absorption spectra of CdSe QDs and CdSe QD-Au HNs under the 1S excitation were shown in Figure 6.9. In CdSe QDs, although transient absorption bands were similar to those under 400 nm excitation, positive absorption band around 610 nm observed at 400 nm excitation experiments (Figure 6.4a) did not appear under the 1S excitation. In previous studies, the positive absorption band longer than 1S bleach band was attributed to the shift of 1S transition arised from the biexciton effect between hot carrier and 1S exciton generatred by the probe pulse.[10] On the other hand, the positive absorption band was also formed by the charge separation from semiconductor nanocrystals to the outside because the charge separation induces the electric fields and exciton peak shift by a Stark effect.[22,23,45] In our experiments, the positive absorption band was clearly observed in transient absorption spectra of CdSe QD-Au HNs under 1S excitation in contrast with CdSe QDs, suggesting the charge separation between CdSe QDs and Au NPs. In the transient absorption dynamics at 1S bleach band illustrated in Figure 6.10a, the growth kinetics comparable to the instrumental response function were observed in all samples, indicating that hot electron was not generated under 1S excitation. Consequently, the hot electron transfer could not occur in this experimental condition. Nevertheless, as shown in Figure 6.10b, the decrease of initial bleach amplitude in CdSe QD-Au HNs was clearly observed. Moreover, the 1S bleach amplitude became lower with increasing the diameter of Au NPs. In our previous study on PbS QD-Au HNs (Chapter 5), the decrease of initial 1S bleach amplitude was clearly observed under 1S excitation. In the CdS NR-Au HNs[26] and PbS QDs on the TiO_2 NPs[18], similar results have been reported. Thus, the lower band-edge bleach amplitudes observed in CdSe QD-Au HNs are due to the ultrafast electron transfer from $1S(e)$ state much faster than the instrumental response function (~60 fs).

The lower initial 1S bleach amplitude under 400 nm excitation as illustrated in Figure 6.7b should be also contributed from ultrafast electron transfer from 1S(e) state.

Transient absorption spectra under 2S excitation (555 nm) and 1P excitation (496 nm) were shown in Figure 6.11. The 1S bleach dynamics, and initial 1S bleach amplitude with 2S and 1P excitation were shown in Figure 6.12. In the transient absorption spectra, spectral features of each samples were very similar for all excitation wavelength. In the 2S excitation experiments, the electron is excited from $2S_{3/2}$(h) state in valence band to 1S(e) state in conduction band, indicating that hot electron did not generate. However, 1S bleach dynamics of CdSe QDs under 2S excitation (Figure 6.12a) slightly showed rise component with the lifetime of ~60 fs, suggesting the existence of hot electron. The generation of hot electron was likely due to the excitation of the tail of 1P absorption band or a weak absorption band, such as a forbidden transition to an energy state higher than 1S(e) state. The growth kinetics of CdSe QD-Au HNs were comparable to the instrumental response function, and the 1S bleach amplitude of CdSe QD-Au HNs under 2S excitation (Figure 6.12b) became lower as compared with that of CdSe QDs with increasing the diameter of Au NPs.

In the 1P excitation, the electron is excited from $1P_{3/2}$(h) state in valence band to 1P(e) state in conduction band, indicating the generation of hot electron. In the transient absorption dynamics at 1S bleach band of CdSe QDs (Figure 6.12c), the rise component with the lifetime of 150 fs was clearly observed. In the previous studies by Kambhampati et al., hot electron relaxation processes in CdSe QDs were analyzed by using state-selective excitation experiments.[10-13] According to these reports, the Auger cooling predominantly contribute to the hot electron relaxation process from 1P(e) state to 1S(e) state, and the similar time constant of Auger cooling process was detected in CdSe QDs with the similar diameter to our sample (~4.2 nm).[10,13] In the CdSe QD-Au HNs A and B, faster rise time with the lifetime of ~90 fs were clearly observed, suggesting the hot electron transfer from 1P(e) state of CdSe

172

QD to Au NPs. Hot electron transfer times in both CdSe QD-Au HNs were estimated to be ~230 fs from rise time analyses, which is slightly faster than the hot electron transfer time in 400 nm excitation experiments (~300 fs). Furthermore, the initial 1S bleach amplitude of CdSe QD-Au HNs decreased with increasing the diameter of Au NPs (Figure 6.12d). The decrease of 1S bleach amplitude in CdSe QD-Au HNs resulted from both hot electron transfer from 1P(e) state and ultrafast electron transfer from 1S(e) state as similar to the results under 400 nm excitation.

Furthermore, we discussed the electron transfer processes from CdSe QD to Au NPs in terms of the change of initial 1S bleach amplitude with different excitation wavelength. At first, we defined the bleach yield as the ratio of initial bleach amplitude of CdSe QD-Au HNs and CdSe QDs (B_{HNs}/B_{QDs}). The 1S bleach yield of all samples with different excitation wavelength were plotted against excitation intensity in Figure 6.13. In these figures, 1S bleach yields did not depend on the excitation intensity. Since the multiple excitons were generated in higher excitation intensity experiments, the excitation intensity dependence of 1S bleach yields suggested that hot and ultrafast electron transfer yields were not affected by the number average of excitons in a QD. In 1S excitation experiments, 1S bleach yields of CdSe QD-Au HNs A and B were estimated to be ~0.71 and ~0.28, respectively. As mentioned above, the decrease of 1S bleach yields under 1S excitation were originated from the ultrafast electron transfer from 1S(e) state. Therefore, the ultrafast electron transfer yields (Φ_{ult}) in CdSe QD-Au HNs A and B were estimated to be ~0.29 and ~0.72, respectively. In the 400 nm and 1P excitation experiments, the 1S bleach yields of CdSe QD-Au HNs A and B became lower as compared with those in 1S excitation experiments. From rise time analyses, the hot electron transfer was clearly observed under 400 nm and 1P excitation. Therefore, much lower 1S bleach yields under 400 nm and 1P excitation were due to both hot electron transfer and ultrafast electron transfer from 1S(e) state. Furthermore, the observed 1S bleach yields of

CdSe QD-Au HNs A and B under 400 nm excitation (~0.31 in HNs A and ~0.13 in HNs B) were nearly identical to those under 1P excitation (~0.36 in HNs A and ~0.15 in HNs B). From these comparisons, we can conclude that hot electron transfer occurred from 1P(e) state of CdSe QDs to Au NPs after the hot electron relaxation from initial photoexcited state ($< i|$) to 1P(e) state. As mentioned above, the hot electron transfer yields (Φ_{hot}) in CdSe QD-Au HNs A and B were estimated to be ~0.50 by the rise time analyses in the 400 nm excitation experiments. The 1S bleach signal is originated from the electron without hot electron transfer from 1P(e) state and ultrafast electron transfer much faster than the instrumental response function from 1S(e) state. Consequently, the 1S bleach yields of CdSe QD-Au HNs A and B can be calculated by using the products of (1-Φ_{hot}) and (1-Φ_{ult}). The calculated 1S bleach yields were very similar to the observed 1S bleach yields for each samples, as summarized in Table 6.2, indicating that the decrease of 1S bleach yields in CdSe QD-Au HNs were originated from the hot electron transfer and ultrafast electron transfer from the 1S(e) state.

6.4.2 Electron transfer processes from CdSe NRs to Au NPs

Previously, in our group, Sagarzazu *et al*. examined the electron transfer dynamics from CdSe NRs (4.0 nm × 14.0 nm) to Au NPs.[27,28] Figure 6.14a shows absorption spectra of CdSe NRs and CdSe NR-Au HNs. According to the electronic structure of CdSe NRs (Figure 6.14b)[29], Absorption bands of CdSe NRs at 590 nm, 550 nm, and 480 nm were due to transitions of $1\sigma_e$-$1\sigma_h$ (1Σ band), $2\sigma_e$-$2\sigma_h$ (2Σ band), and $1\pi_e$-$1\pi_h$ (1Π band) respectively. In our study, the wavelength of 1Σ absorption peak of CdSe NRs and CdSe NR-Au HNs were similar to those of CdSe QDs and CdSe QD-Au HNs. The average diameter of Au NPs were 1.5 nm, 1.6 nm, and 2.2 nm in CdSe NR-Au HNs A, B, and C, respectively. Transient absorption spectra of CdSe NRs and CdSe NR-Au HNs C excited at 400 nm were shown in Figure 6.15, where spectral features of CdSe NR-Au HNs were similar to those of CdSe NRs.

The 1Σ bleach dynamics of all samples were illustrated in Figure 6.16. In CdSe NR-Au HNs, the relaxation of 1Σ bleach band became faster with increasing the diameter of Au NPs, and lifetimes of these decay components were summarized in Table 6.3. Ps-scale fast relaxations in the 1Σ bleach band was probably originated from the electron transfer from $1\sigma_e$ state to Au NPs. The electron transfer dynamics from conduction band-edge state detected in CdSe NR-Au HNs were slower as compared to that in CdSe QD-Au HNs. In CdSe NR-Au HNs, Au NPs attached to the tip of CdSe NRs. Since the long axis of CdSe NRs (14.0 nm) are much larger than the diameter of CdSe QDs (4.2 nm) and exciton Bohr radius in CdSe (~5.6 nm), the electronic coupling in CdSe NR-Au HNs is much weaker than that in CdSe QD-Au HNs. Therefore, the weak electronic coupling between long axis of CdSe NRs and Au NPs probably induces the slower electron transfer from $1\sigma_e$ state in CdSe NR-Au HNs. Moreover, growth kinetics and initial bleach amplitude of 1Σ bleach band excited at 400 nm in all samples were illustrated in Figure 6.17. As clearly shown in Table 6.4, the rise time of 1Σ bleach became faster as the diameter of Au NPs increased, indicating the hot electron transfer from CdSe NRs to Au NPs. By comparing the rise time of CdSe NR-Au HNs with that of CdSe NRs, hot electron transfer time was estimated to be ~2.7 ps, ~2.0 ps, and ~1.0 ps in CdSe NR-Au HNs A, B, and C, respectively. The Φ_{hot} of CdSe NR-Au HNs estimated from rise time analyses were 0.10, 0.14, and 0.23 in CdSe NR-Au HNs A, B, and C, respectively. As with the experimental data of CdSe QD-Au HNs, the initial bleach amplitude of 1Σ band in CdSe NR-Au HNs became lower with increasing the diameter of Au NPs. The initial bleach amplitude in CdSe NR-Au HNs A, B, and C (Figure 6.17b) decreased by 10%, 19%, and 23% as compared to that in CdSe NRs, respectively. In contrast with CdSe QD-Au HNs, these decrease of initial bleach amplitude of CdSe NR-Au HNs are in good agreement with the Φ_{hot}.

The growth kinetics and initial bleach amplitude of 1Σ bleach band excited at 1Σ absorption band for CdSe NRs and CdSe NR-Au HNs were illustrated in Figure 6.18. Since the hot carrier was not generated under the 1Σ excitation, the rise components of all samples were comparable to the instrumental response function, and initial bleach amplitudes of all CdSe NR-Au HNs were similar to that of CdSe NRs. The latter revealed that the ultrafast electron transfer much faster than the instrumental response function from $1\sigma_e$ state of CdSe NRs does not exist in CdSe NR-Au HNs. Non-existence of ultrafast electron transfer in CdSe NR-Au HNs is in contrast with CdSe QD-Au HNs, which is likely due to the relatively weak electronic coupling between CdSe NRs and Au NPs.

In addition, the growth kinetics of 1Σ bleach band and initial 1Σ bleach amplitude in CdSe NRs and CdSe NR-Au HNs under 2Σ (550 nm) and 1Π (488 nm) excitation were shown in Figure 6.19.[28] According to the previous study on the theoretical calculation of electronic structure in CdSe NRs, 2Σ and 1Π absorption bands were assigned to transitions of $2\sigma_h$-$2\sigma_e$ and $1\pi_h$-$1\pi_e$, respectively.[29] Since the hot electron generated in these experiments, the fast rise component corresponding to the hot electron relaxation with the lifetime of ~140 fs was observed in 1Σ bleach band of CdSe NRs. In CdSe NR-Au HNs, rise times became faster (Table 6.4) and initial bleach amplitudes of 1Σ bleach band became lower with increasing the diameter of Au NPs, indicating the hot electron transfer from CdSe NRs to Au NPs. The rate of hot electron transfer (k_{hot}) in each sample were estimated by comparing the rise time of CdSe NR-Au HNs with that of CdSe NRs, and plotted against the excitation wavelength in Figure 6.20. Hot electron transfer from CdSe NRs to Au NPs became faster as the diameter of Au NPs increased and the excitation wavelength became longer. The excitation wavelength dependence of hot electron transfer time observed in CdSe NR-Au HNs indicates that the larger excess energy of electron leads to the slower hot electron transfer.

The excitation wavelength dependence of the Φ_{hot} in CdSe NR-Au HNs estimated from rise time analyses (solid line) and initial 1Σ bleach amplitude (dashed line) were illustrated in Figure 6.21.[28] As clearly shown, the Φ_{hot} of each CdSe NR-Au HNs estimated from rise time analyses are in good agreement with those from initial 1Σ bleach amplitude. These results strongly suggest that lower initial bleach amplitude of CdSe NR-Au HNs can be interpreted only by the hot electron transfer process. This is in contrast with CdSe QD-Au HNs where both hot and ultrafast electron transfer exist. Furthermore, the Φ_{hot} of each CdSe NR-Au HNs were independent of excitation wavelengths from 400 to 550 nm, indicating that the hot electron transfer occurred from $2\sigma_e$ state of CdSe NRs to Au NPs after the intraband relaxation from initial excited state (higher than the $2\sigma_e$ state) to $2\sigma_e$ state. The Φ_{hot} and the rate of hot electron transfer in CdSe NR-Au HNs increased as the diameter of Au NPs increased, and the Φ_{hot} and rate of hot electron transfer reached to ~23% and ~$(0.5\text{-}1.0 \text{ ps})^{-1}$ in CdSe NR-Au HNs C (the diameter of Au NPs: ~2.2 nm), respectively. The slower rate of hot electron transfer and lower Φ_{hot} in CdSe NR-Au HNs as compared to CdSe QD-Au HNs are likely due to the difference of electronic coupling constant, because the wavefunction penetration of CdSe NRs is smaller than that of CdSe QDs. The origin of the Au NPs size independence of hot electron transfer process in CdSe QD-Au HNs are still unclear.

6.5 Conclusion

In summary, we synthesized and characterized CdSe QD-Au HNs with different diameter of Au NPs. The electron transfer from band-edge state and higher excited states of CdSe QDs to Au NPs were analyzed using the femtosecond pump-probe spectroscopy with the state-selective excitation technique. In the transient absorption measurements of CdSe QD-Au HNs excited at 400 nm, sub ps-scale fast relaxation components of 1S bleach band dynamics were observed, which is probably attributed to the electron transfer from the 1S(e)

state of CdSe QDs to Au NPs. The observed sub ps-scale electron transfer process became faster as the diameter of Au NPs increased, resulting from the change of density of states of Au NPs. In addition, the growth kinetics of CdSe QD-Au HNs under 400 nm excitation became faster than that of CdSe QDs. By analyzing the rise time of 1S bleach band, the rate and yields of hot electron transfer in both CdSe QD-Au HNs were estimated to be $\sim(300 \text{ fs})^{-1}$ and ~50%, respectively. Under the 400 nm excitation, the initial 1S bleach amplitudes of CdSe QD-Au HNs became much lower compared with that of CdSe QDs, however, these lower bleach amplitudes of CdSe QD-Au HNs could not be explained by the hot electron transfer. In the 1S excitation experiments, the decrease of 1S bleach yields in CdSe QD-Au HNs were clearly observed, revealing the existence of ultrafast electron transfer with a lifetime much faster than the instrumental response function from 1S(e) state of CdSe QDs to Au NPs. In CdSe QD-Au HNs B (diameter of Au NPs: ~2.0 nm), the yield of ultrafast electron transfer was estimated to be ~72%. Moreover, 1P excitation experiments revealed that the hot electron transfer occurred from 1P(e) state of CdSe QDs, which was confirmed by the similar initial bleach amplitudes at 400 nm and 1P excitation. The observed decrease of initial 1S bleach amplitudes in CdSe QD-Au HNs was originated from not only the hot electron transfer but also the ultrafast electron transfer. The rate and yield of hot electron transfer in CdSe NR-Au HNs C (diameter of Au NPs: ~2.2 nm) were estimated to be $\sim(0.5\text{-}1.0 \text{ ps})^{-1}$ and ~23%, respectively. In addition, the ultrafast electron transfer from $1\sigma_e$ state of CdSe NRs to Au NPs could not be observed. These difference of hot and ultrafast electron transfer dynamics for CdSe QD-Au HNs and NR-Au HNs is probably due to the difference of electronic coupling constant between CdSe nanocrystals and Au NPs. For these results, the electron transfer from band-edge state and higher excited states in CdSe QD-Au HNs is more efficient than those in CdSe NR-Au HNs.

References

(1) R. Rossetti, S. Nakahara, and L. Brus, Quantum Size Effects in the Redox Potentials, Resonance Raman Spectra, and Electronic Spectra of CdS Crystallites in Aqueous Solution. *J. Chem. Phys.* **1983**, *79*, 1086−1088.

(2) Klimov, V. I. Optical Nonlinearities and Ultrafast Carrier Dynamics in Semiconductor Nanocrystals. *J. Phys. Chem. B* **2000**, *104*, 6112−6123.

(3) Schaller, R. D.; Klimov, V. I. High Efficiency Carrier Multiplication in PbSe Nanocrystals: Implications for Solar Energy Conversion. *Phys. Rev. Lett.* **2004**, *92*, 186601.

(4) Kobayashi, Y.; Udagawa, T.; Tamai, N. Carrier Multiplication in CdTe Quantum Dots by Single−Photon Timing Spectroscopy. *Chem. Lett.* **2009**, *38*, 830−831.

(5) McGuire, J. A.; Joo, J.; Pietryga, J. M.; Schaller, R. D.; Klimov, V. I. New Aspects of Carrier Multiplication in Semiconductor Nanocrystals. *Acc. Chem. Res.*, **2008**, *41*, 1810–1819.

(6) Klimov, V. I. Spectral and Dynamical Properties of Multiexcitons in Semiconductor Nanocrystals. *Annu Rev Phys Chem.* **2007**, *58*, 635–673.

(7) Klimov, V. I.; Mikhailovsky, A. A.; McBranch, D. W.; Leatherdale, C. A.; Bawendi, M. G. Quantization of Multiparticle Auger Rates in Semiconductor Quantum Dots. *Science* **2000**, *287*, 1011−1013.

(8) Kobayashi, Y.; Pan, L.; Tamai, N. Effects of Size and Capping Reagents on Biexciton

Auger Recombination Dynamics of CdTe Quantum Dots. *J. Phys. Chem. C* **2009**, *113*,

11783–11789.

(9) Kobayashi, Y.; Nishimura, T.; Yamagushi, H.; Tamai, N. Effect of Surface Defects on

Auger Recombination in Colloidal CdS Quantum Dots. *J. Phys. Chem. Lett.*, **2011**, *2*,

1051–1055.

(10) Kambhampati, P. Hot Exciton Relaxation Dynamics in Semiconductor Quantum

Dots: Radiationless Transitions on the Nanoscale. *J. Phys. Chem. C* **2011**, *115*,

22089−22109.

(11) Kambhampati, P. Unraveling the Structure and Dynamics of Excitons in

Semiconductor Quantum Dots. *Acc. Chem. Res.* **2011**, *44*, 1−13.

(12) Sewall, S. L.; Cooney, R. R.; Anderson, K. E. H.; Dias, E. A.; Kambhampati, P.

State-to-State Exciton Dynamics in Semiconductor Quantum Dots. *Phys. Rev. B: Condens.

Matter Mater. Phys.* **2006**, *74*, 235328.

(13) Cooney, R. R.; Sewall, S. L.; Dias, E. A.; Sagar, D. M.; Anderson, K. E. H.;

Kambhampati, P. Unified Picture of Electron and Hole Relaxation Pathways in

Semiconductor Quantum Dots. *Phys. Rev. B: Condens. Matter Mater. Phys.* **2007**, *75*,

245311.

(14) Guyot−Sionnest, P.; Wehrenberg, B.; Yu, D. Intraband Relaxation in CdSe

Nanocrystals and the Strong Influence of the Surface Ligands. *J. Chem. Phys.* **2005**, *123*, 074709.

(15)   Pandey, A.; Guyot-Sionnest, P. Slow Electron Cooling in Colloidal Quantum Dots. *Science* **2008**, *322*, 929−932.

(16)   Shockley, W.; Queisser, H. J. Detailed Balance Limit of Efficiency of p−n Junction Solar Cells. *J. Appl. Phys.* **1961**, *32*, 510−519.

(17)   Ross, R. T.; Nozik, A. J. Efficiency of hot−carrier solar energy converters. *J. Appl. Phys.* **1982**, *53*, 3813−3818.

(18)   Yang, Y.; Rodríguez−Córdoba, W.; Xiang, X.; Lian, T. Strong Electronic Coupling and Ultrafast Electron Transfer between PbS Quantum Dots and TiO$_2$ Nanocrystalline Films. *Nano Lett.* **2012**, *12*, 303−309.

(19)   Sambur, J. B.; Novet, T.; Parkinson, B. A. Multiple Exciton Collection in a Sensitized Photovoltaic System. *Science* **2010**, *330*, 63−66.

(20)   Semonin, O. E.; Luther, J. M.; Choi, S.; Chen, H.-Y.; Gao, J.; Nozik, A. J.; Beard, M. C. Peak External Photocurrent Quantum Efficiency Exceeding 100% via MEG in a Quantum Dot Solar Cell. *Science* **2011**, *334*, 1530−1533.

(21)   Matylitsky, V. V.; Dworak, L.; Breus, V. V.; Basché, T.; Wachtveitl, J. Ultrafast Charge Separation in Multiexcited CdSe Quantum Dots Mediated by Adsorbed Electron Acceptors. *J. Am. Chem. Soc.* **2009**, *131*, 2424–2425.

(22)   Zhu, H.; Song, N.; Rodríguez–Córdoba, W.; Lian, T. Wave Function Engineering for

Efficient Extraction of up to Nineteen Electrons from One CdSe/CdS Quasi–Type II

Quantum Dot. *J. Am. Chem. Soc.* **2012**, *134*, 4250–4257.

(23)   Zhu, H.; Lian, T. Enhanced Multiple Exciton Dissociation from CdSe Quantum

Rods: The Effect of Nanocrystal Shape. *J. Am. Chem. Soc.* **2012**, *134*, 11289−11297.

(24)   Wang, Y.; Wang, H.; Li, Z.; Zhao, J.; Wang, L.; Chen, Q.; Wang, W.; Sun, H.

Electron Extraction Dynamics in CdSe and CdSe/CdS/ZnS Quantum Dots Adsorbed with

Methyl Viologen. *J. Phys. Chem. C* **2014**, *118*, 17240−17246.

(25)   Okuhata, T.; Kobayashi, Y.; Nonoguchi, Y.; Kawai, T.; Tamai, N. Ultrafast Carrier

Transfer and Hot Carrier Dynamics in PbS−Au Hybrid Nanostructures. *J. Phys. Chem. C*

2015, *119*, 2113–2120.

(26)   Mongin, D.; Shaviv, E.; Maioli, P.; Crut, A. Banin, U.; Fatti, N. D.; Vallée, F.

Ultrafast Photoinduced Charge Separation in Metal−Semiconductor Nanohybrids. *ACS*

Nano **2012**, *6*, 7034–7043.

(27)   Sagarzazu, G.; Inoue, K.; Saruyama, M.; Sakamoto, M.; Teranishi, T.; Masuo, S.;

Tamai, N. Ultrafast Dynamics and Single Particle Spectroscopy of Au−CdSe Nanorods.

Phys. Chem. Chem. Phys. **2013**, *15*, 2141–2152.

(28)   Sagarzazu, G.; Inoue, K.; Saruyama, M.; Sakamoto, M.; Teranishi, T.; Tamai, N.

Hot-electron transfer in Au-CdSe nanorods. *Submitted.*

(29)   Hu, J.; Lin, W.; Liang, S. L.; Yang, W.; Alivisatos, A. P Semiempirical

Pseudopotential Calculation of Electronic States of CdSe Quantum Rods. *J. Phys. Chem.

B*, **2002**, *106*, 2447–2452.

(30)   Efros, A. L.; Rosen, M. The Electronic Structure of Semiconductor Nanocrystals.

Annu Rev Phys Chem. 2000, 30, 475–521.

(31)   Yu, W. W.; Qu, L.; Guo, W.; Peng, X. Experimental Determination of the Extinction

Coefficient of CdTe, CdSe, and CdS Nanocrystals. *Chem. Mater.* **2003**, *15*, 2854–2860.

(32)   Alvarez, M. M.; Khoury, J. T.; Schaaff, T. G.; Shafigullin, M. N.; Vezmar, I.;

Whetten, R. L. Optical Absorption Spectra of Nanocrystal Gold Molecules. *J. Phys. Chem.

B* **1997**, *101*, 3706−3712.

(33)   Klimov, V. I.; McBranch, D. W.; Leatherdale, C. A.; Bawendi M. G. Electron and

Hole Relaxation Pathways in Semiconductor Quantum Dots. *Phys. Rev. B* **1999**, *60*,

13740.

(34)   Asbury, J. B.; Hao, E.; Wang, Y.; Ghosh, H. N.; Lian, T. Ultrafast Electron Transfer

Dynamics from Molecular Adsorbates to Semiconductor Nanocrystalline Thin Films. *J.

Phys. Chem. B* **2001**, *105*, 4545–4557.

(35)   Gao, Y. Q.; Marcus, R. A. On the Theory of Electron Transfer Reactions at

Semiconductor/Liquid Interfaces. II. A Free Electron Model. *J. Chem. Phys.* **2000**, *113*,

6351–6360.

(36)   Gosavi, S.; Marcus, R. A. Nonadiabatic Electron Transfer at Metal Surfaces. *J. Phys. Chem. B* **2000**, *104*, 2067–2072.

(37)   Gao, Y. Q.; Georgievskii, Y.; Marcus, R. A. On the Theory of Electron Transfer Reactions at Semiconductor Electrode/Liquid Interfaces. *J. Chem. Phys.* **2000**, *112*, 3358–3369.

(38)   Kano, S.; Azuma, Y.; Kanehara, M.; Teranishi, T.; Majima, Y. Room-Temperature Coulomb Blockade from Chemically Synthesized Au Nanoparticles Stabilized by Acid−Base Interaction. *Appl. Phys. Express* **2010**, *3*, 105003.

(39)   Negishi, R.; Hasegawa, T.; Tanaka, H.; Terabe, K.; Ozawa, H.; Ogawa, T.; Aono, M. Size-Dependent Single Electron Tunneling Effect in Au Nanoparticles. *Surf. Sci.* **2007**, *601*, 3907−3911.

(40)   Zhu, H.; Yang, Y.; Hyeon−Deuk, K.; Calidano, M.; Song, N.; Wang, Y.; Zhang, W.; Prezhdo, O. V.; Lian, T. Auger-Assisted Electron Transfer from Photoexcited Semiconductor Quantum Dots. *Nano Lett.* **2014**, *14*, 1263−1269.

(41)   Tvrdy, K.; Frantsuzov, P. A.; Kamat, P. V. Photoinduced Electron Transfer from Semiconductor Quantum Dots to Metal Oxide Nanoparticles. *Proc. Natl. Acad. Sci. U. S. A.* **2011**, *108*, 29−34.

(42)   Marcus, R. A. On the Theory of Electron−Transfer Reactions. VI. Unified Treatment for Homogeneous and Electrode Reactions. *J. Chem. Phys.* **1965**, *43*, 679−701.

(43)   Marcus, R. A.; Sutin, N. Electron Transfers in Chemistry and Biology. *Biochim.*

Biophys. Acta, Rev. Bioenerg. **1985**, *811*, 265−322.

(44)   Hyun, B.; Bartnik, A. C.; Lee, J.; Imoto, H.; Sun, L.; Choi, J. J.; Chujo, Y.; Hanrath,

T.; Ober, C. K.; Wise, F. W. Role of Solvent Dielectric Properties on Charge Transfer

from PbS Nanocrystals to Molecules. *Nano Lett.* **2010**, *10*, 318−323.

(45)   Norris, D. J.; Sacra, A.; Murray, C. B.; Bawendi, M. G. Measurement of the Size

Dependent Hole Spectrum in CdSe Quantum Dots. *Phys. Rev. Lett.* **1994**, *72*, 2612.
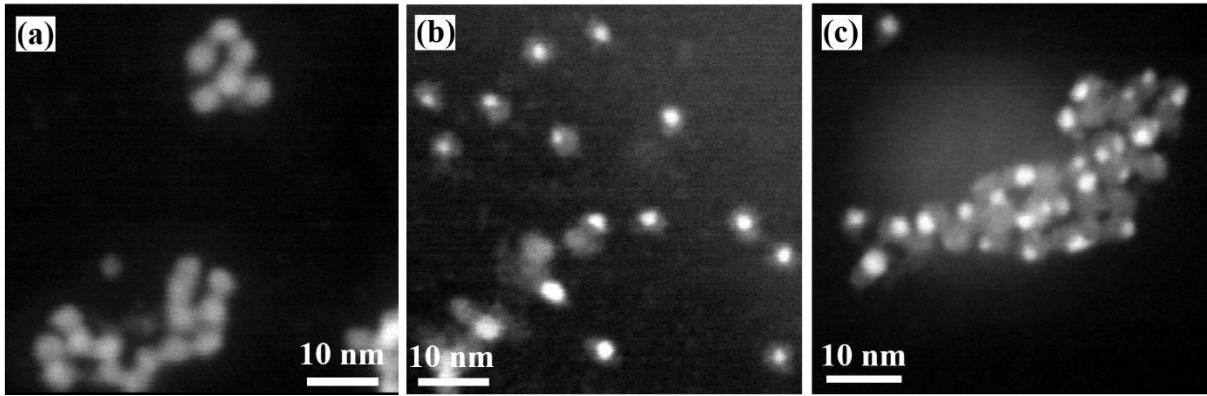
Figure 6.1 STEM images of (a) CdSe QDs, (b) CdSe QD-Au HNs A, and (c) CdSe QD-Au

HNs B.
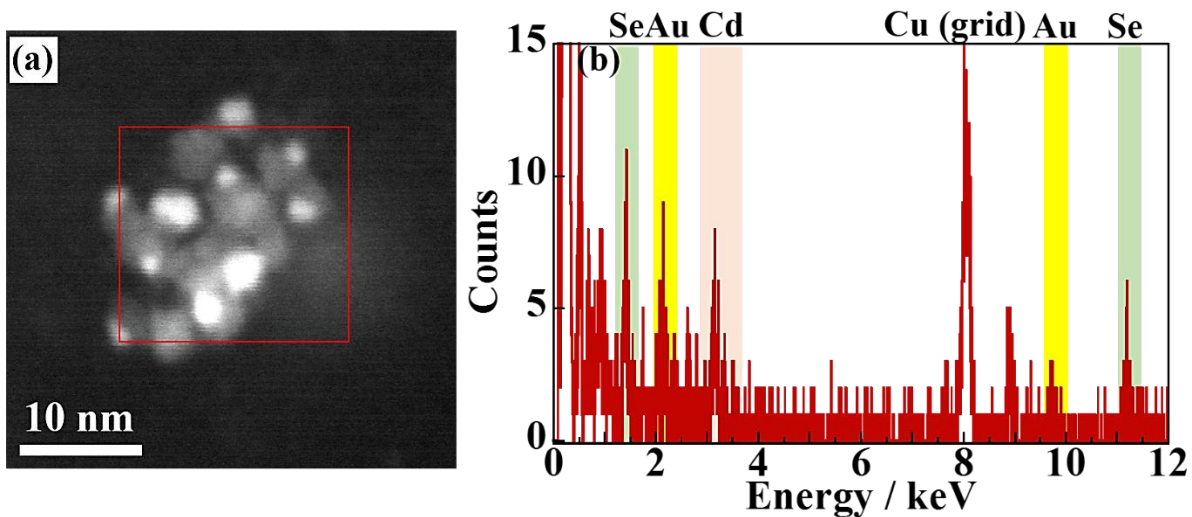
Figure 6.2 (a) STEM image of CdSe QD-Au HNs A and (b) the EDX data at the red square

region in (a).
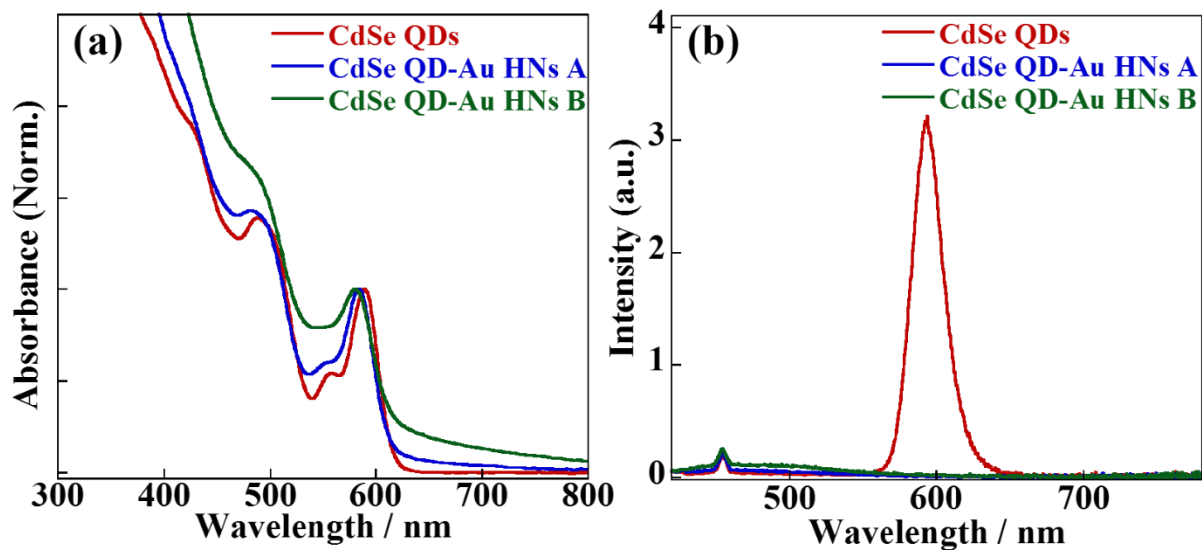
Figure 6.3 Steady-state (a) absorption and (b) luminescence spectra of CdSe QDs and CdSe QD-Au HNs.
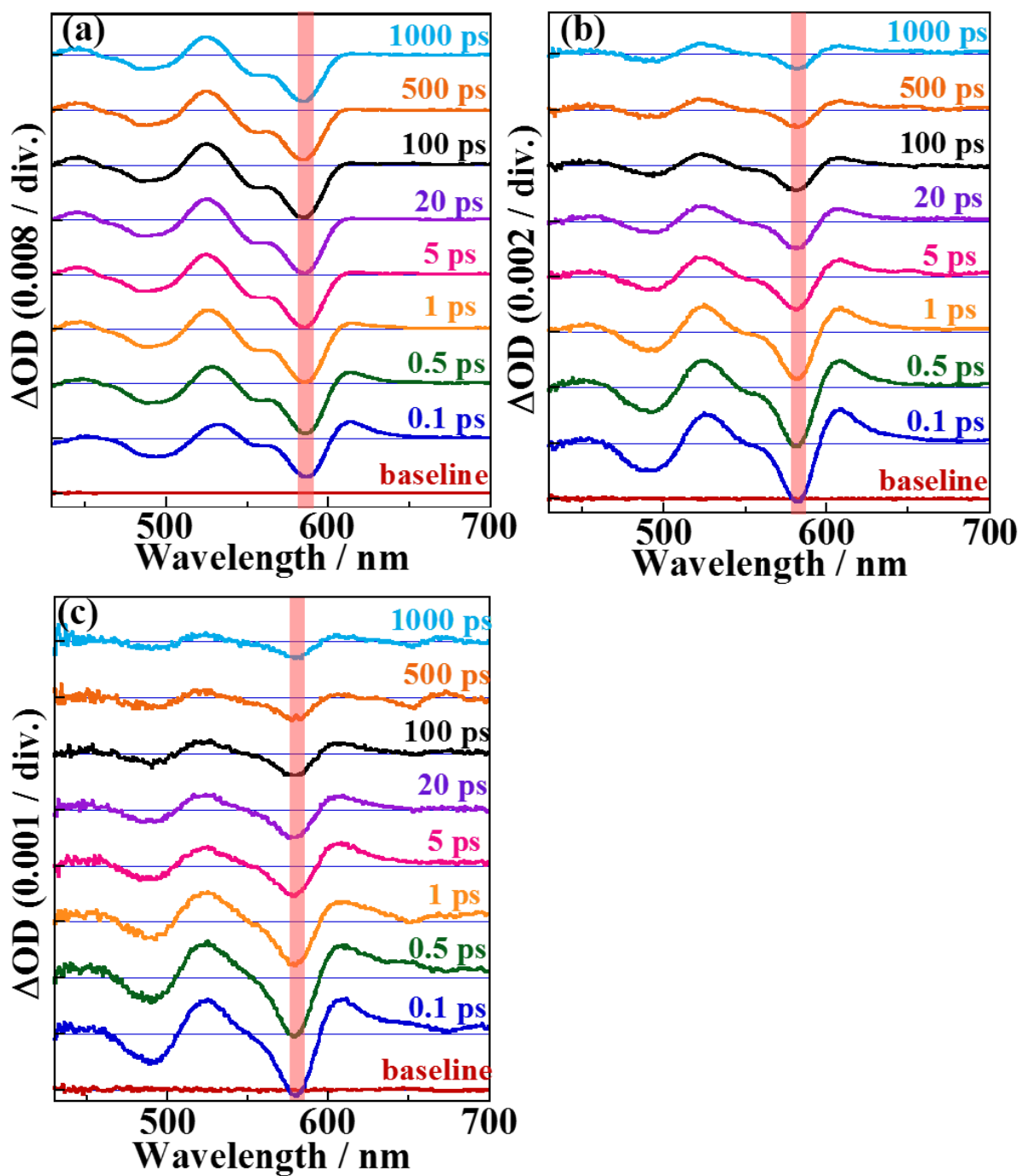
Figure 6.4 Transient absorption spectra of (a) CdSe QDs, (b) CdSe QD-Au HNs A, and (c)

CdSe QD-Au HNs B excited at 400 nm.
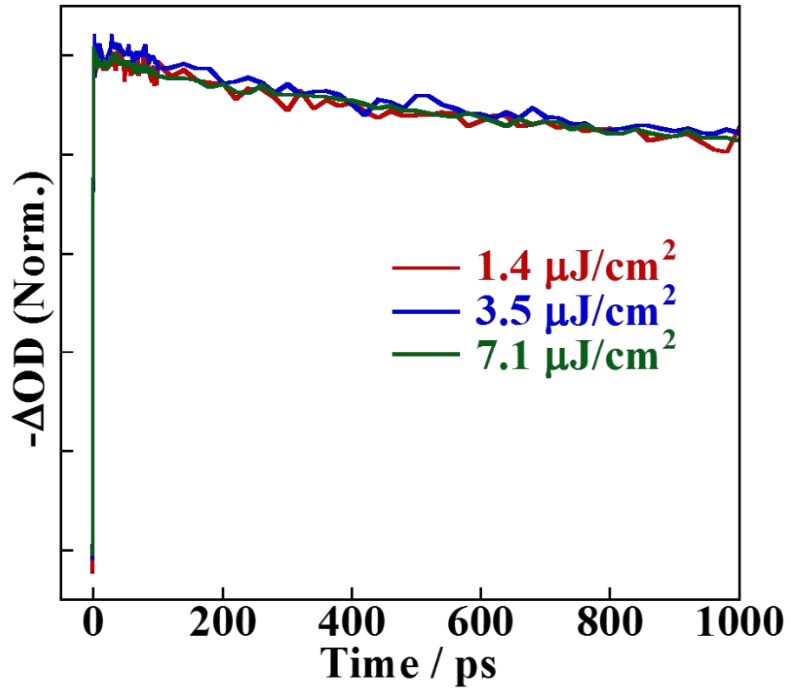
Figure 6.5 The excitation intensity dependence of 1S bleach dynamics for CdSe QDs.
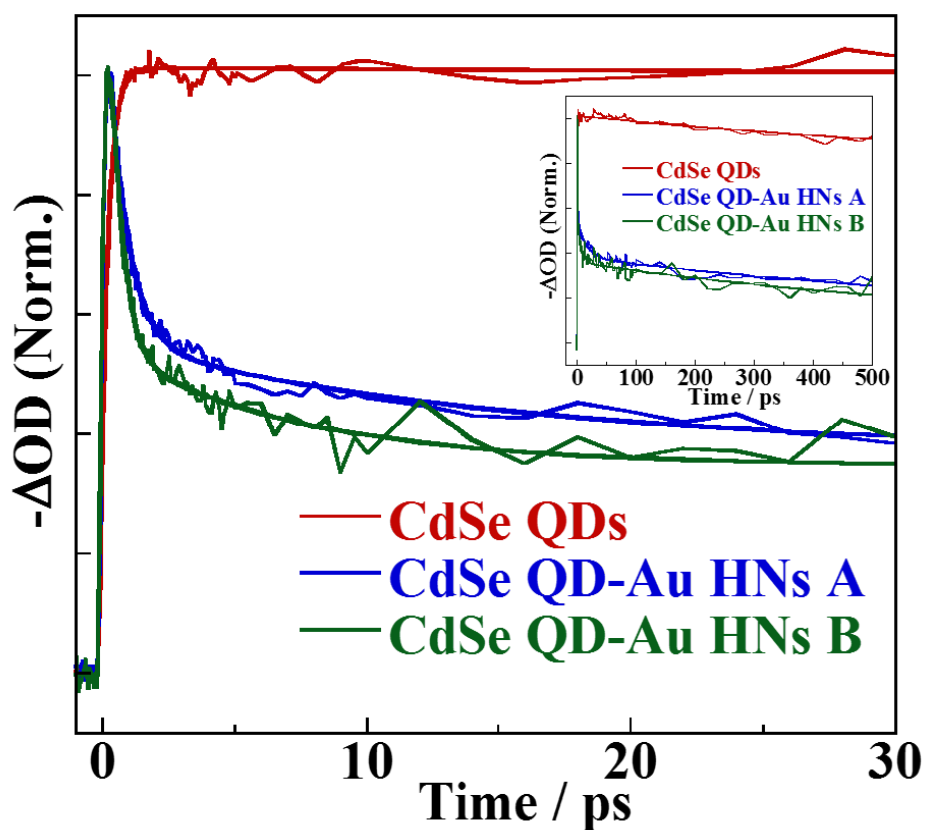
Figure 6.6 Transient absorption dynamics at 1S bleach band of CdSe QDs and CdSe QD-Au

HNs excited at 400 nm.

Table 6.1 Fitting results of 1S bleach dynamics for each sample

Sample	τ_1 / ps	τ_2 / ps	τ_3 / ns
CdSe QDs		670 (11%)	10 (89%)
CdSe QD-Au HNs A	0.75 (60%)	20 (14%)	1.8 (26%)
CdSe QD-Au HNs B	0.45 (78%)	10 (8%)	1.5 (14%)
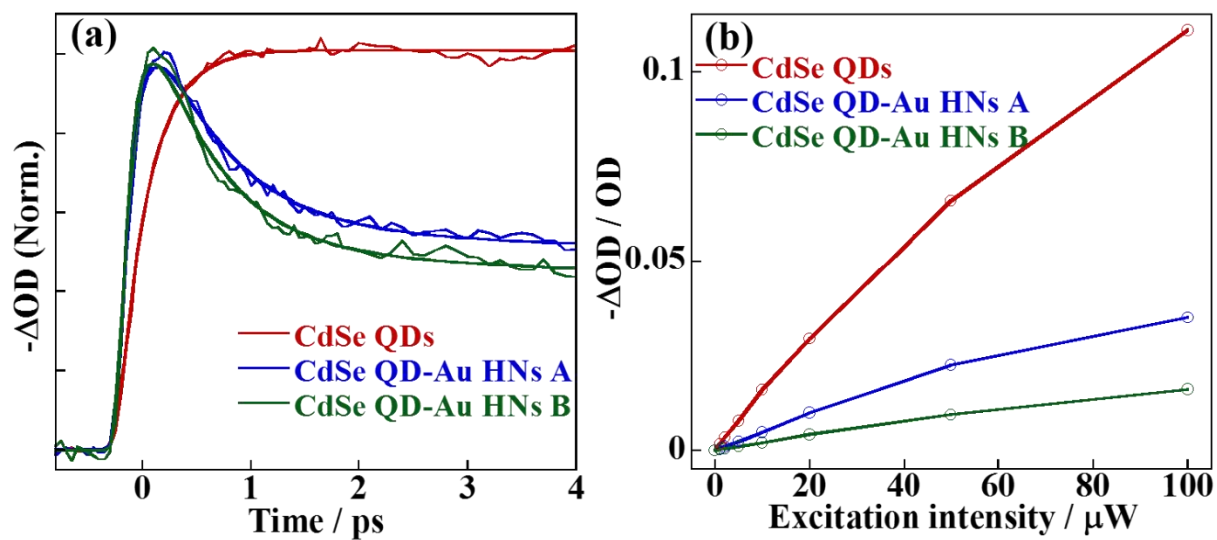
Figure 6.7 (a) The growth kinetics of 1S bleach band and (b) excitation intensity dependence

of initial 1S bleach amplitudes for each sample excited at 400 nm.
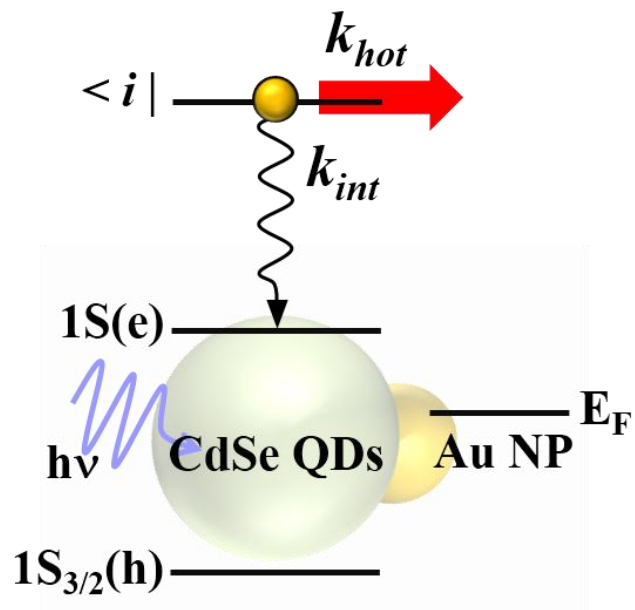
Figure 6.8 The scheme of a hot electron transfer process.
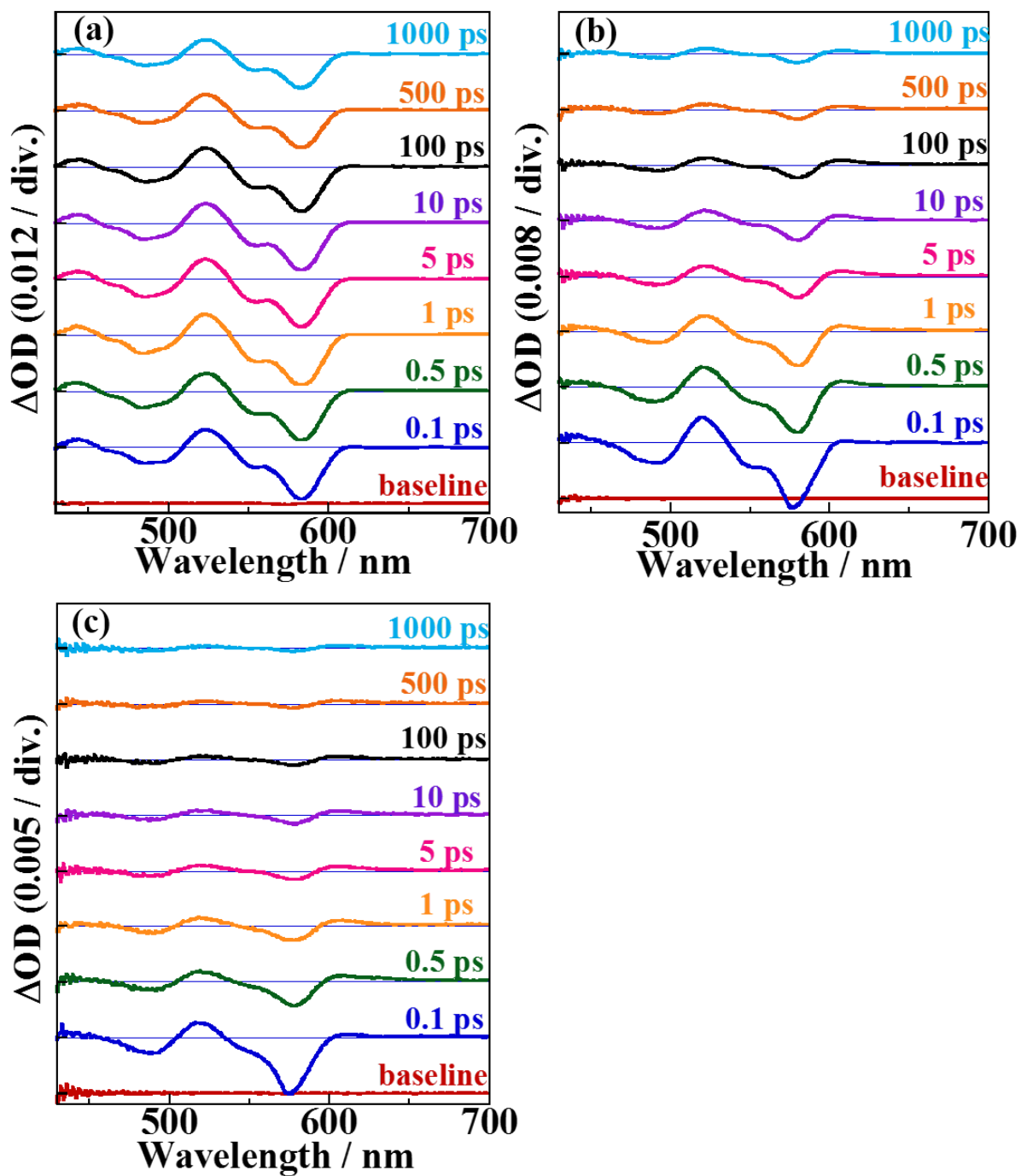
Figure 6.9 Transient absorption spectra of (a) CdSe QDs, (b) CdSe QD-Au HNs A, and (c)

CdSe QD-Au HNs B excited at 1S absorption band.
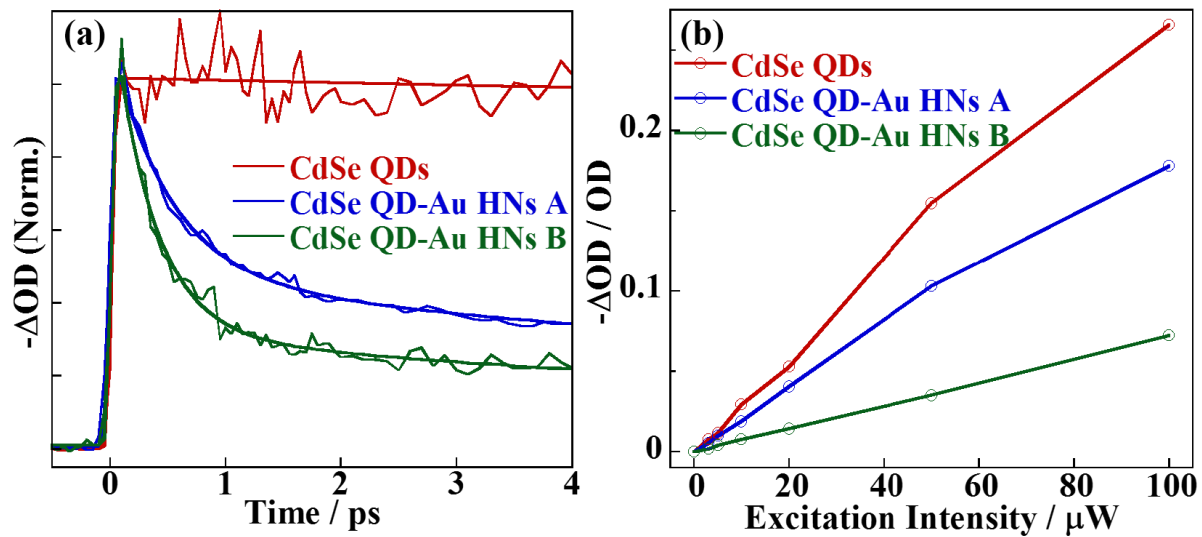
Figure 6.10 (a) 1S bleach dynamics in initial time region and (b) initial 1S bleach amplitude

for each sample excited at 1S absorption band.
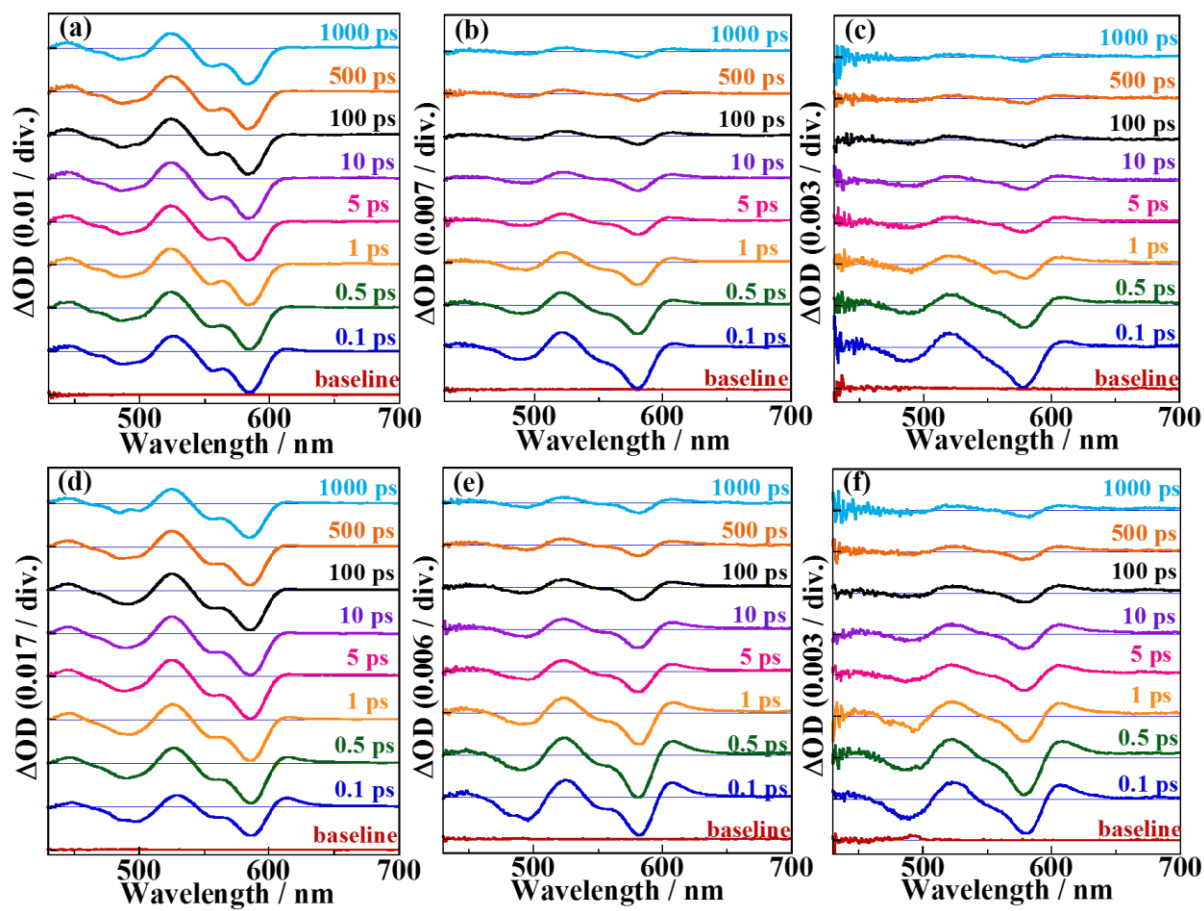
Figure 6.11 Transient absorption spectra excited at (a-c) 2S absorption band and (d-f) 1P

absorption band for (a, d) CdSe QDs, (b, e) CdSe QD-Au HNs A, and (c, f) CdSe QD-Au

HNs B.
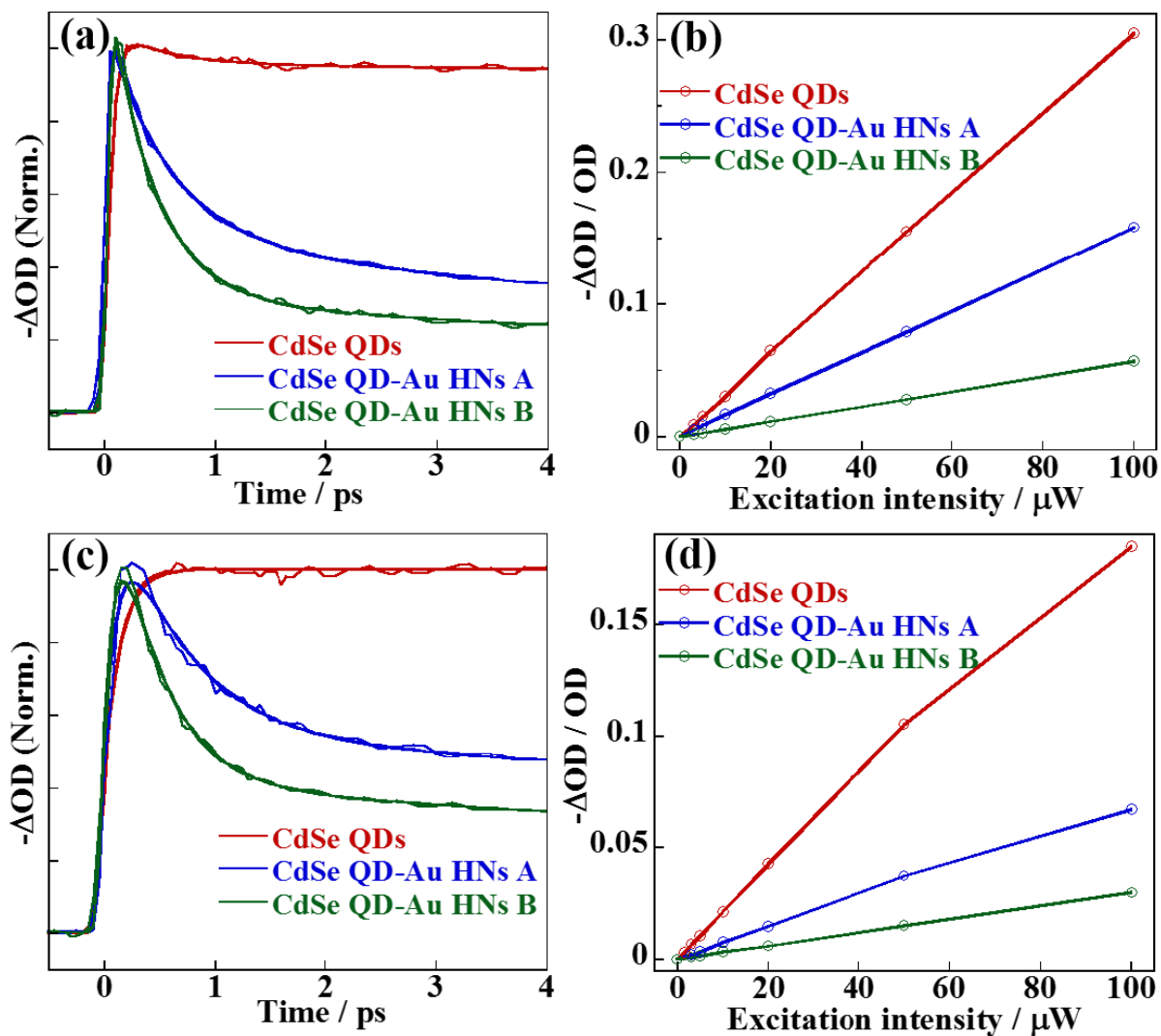
Figure 6.12 (a, c) Growth kinetics and (b, d) initial 1S bleach amplitude for CdSe QDs and

CdSe QD-Au HNs excited at (a, b) 2S and (c, d) 1P absorption band.
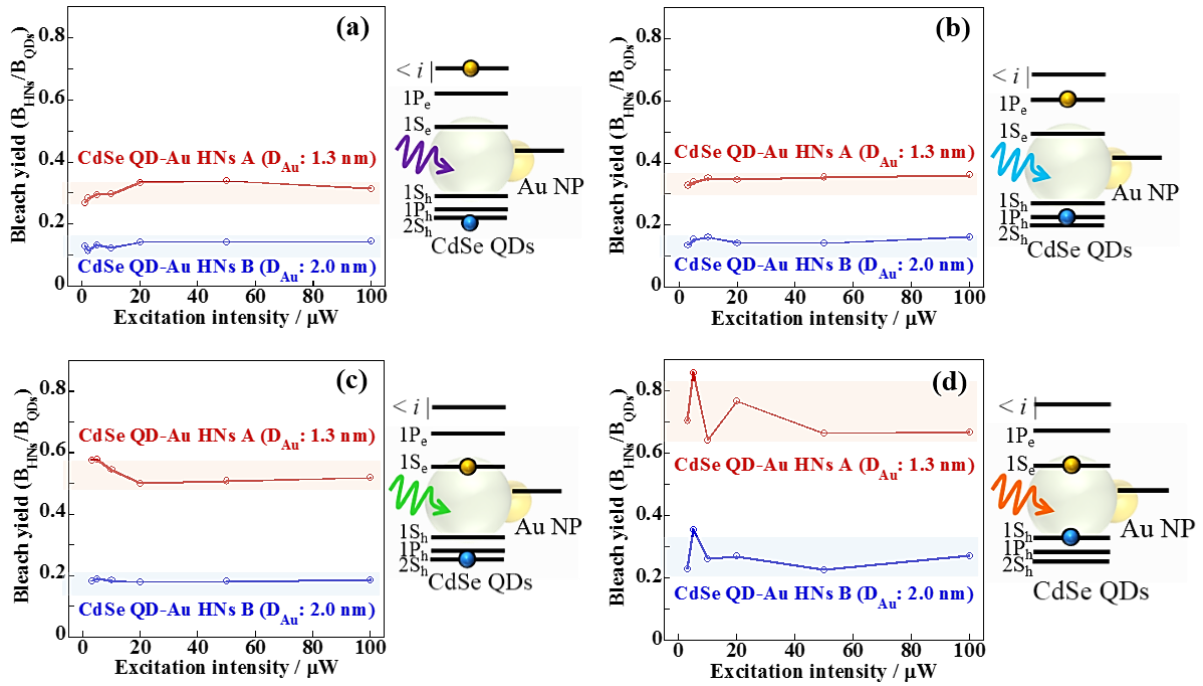
Figure 6.13 1S bleach yields of CdSe QD-Au HNs and schemes of the electronic transition in

(a) 400 nm, (b) 1P, (c) 2S, and (d) 1S excitation experiments.

Table 6.2 Observed and calculated bleach yields of CdSe QD-Au HNs excited at 400 nm.

Sample	Bleach yield	Φ_{hot}	Φ_{ult}	$(1-\Phi_{hot})\times(1-\Phi_{ult})$
CdSe QD-Au HNs A (D_{Au}: 1.3 nm)	0.31	0.50	0.29	0.36
CdSe QD-Au HNs B (D_{Au}: 2.0 nm)	0.13	0.50	0.72	0.14
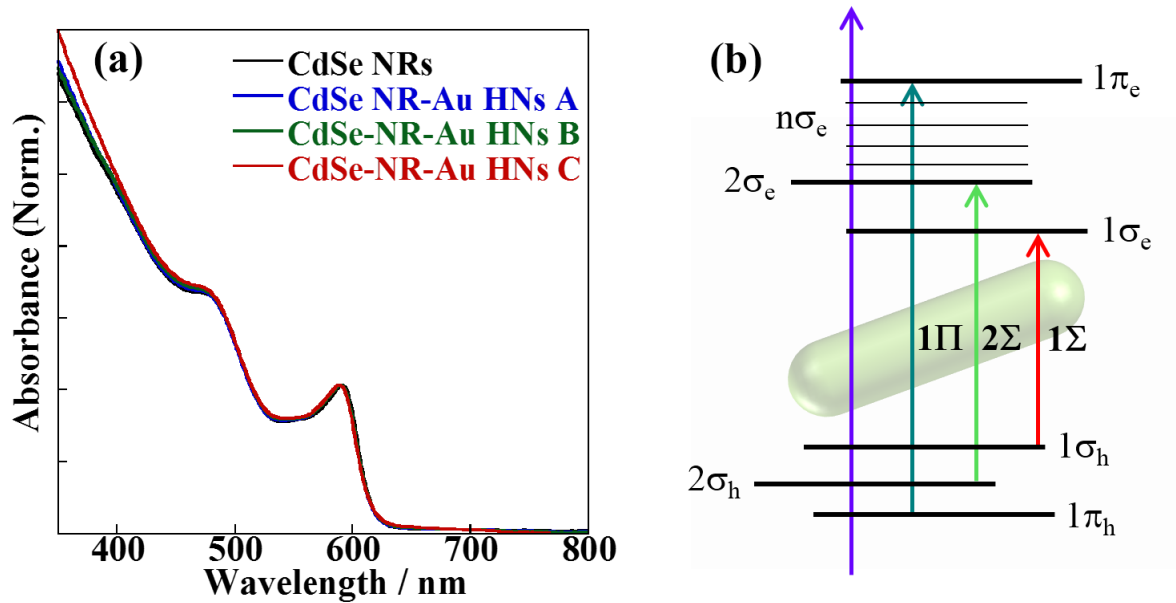
Figure 6.14 (a) Absorption spectra of CdSe NRs (4.0 nm × 14.0 nm) and CdSe NR-Au HNs,

and (b) electronic structures and transitions of CdSe NRs.[29]
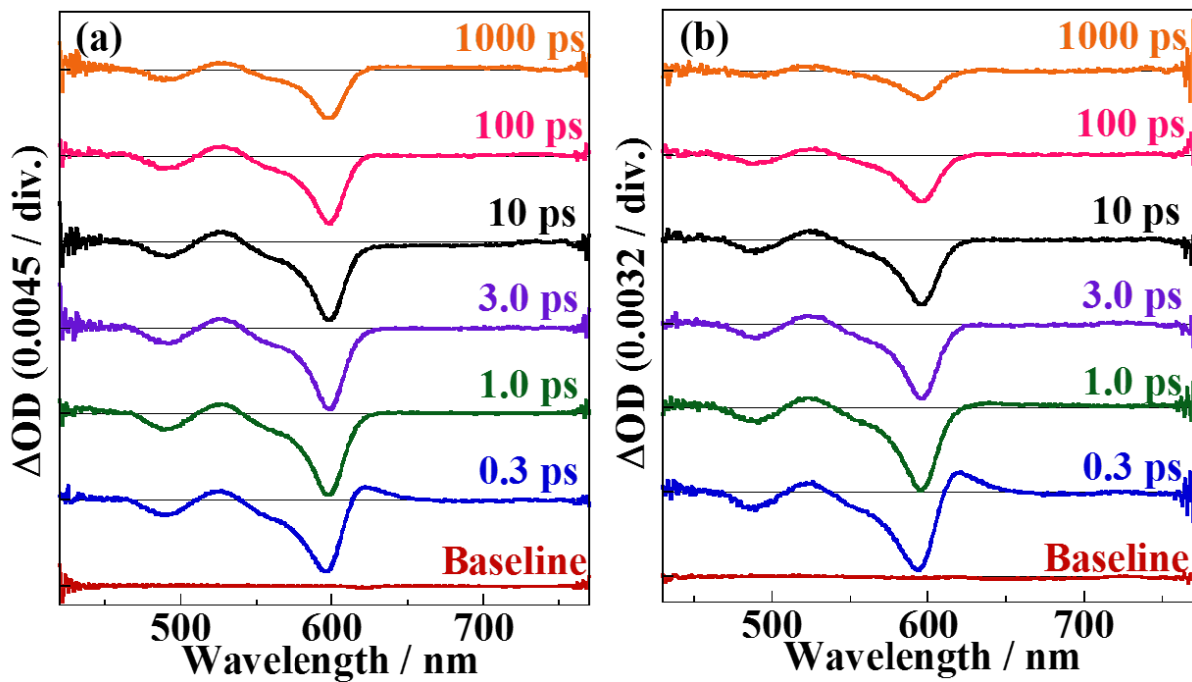
Figure 6.15 Transient absorption spectra of (a) CdSe NRs and (b) CdSe NR-Au HNs (the

diameter of Au NPs: ~2.2 nm).[27]
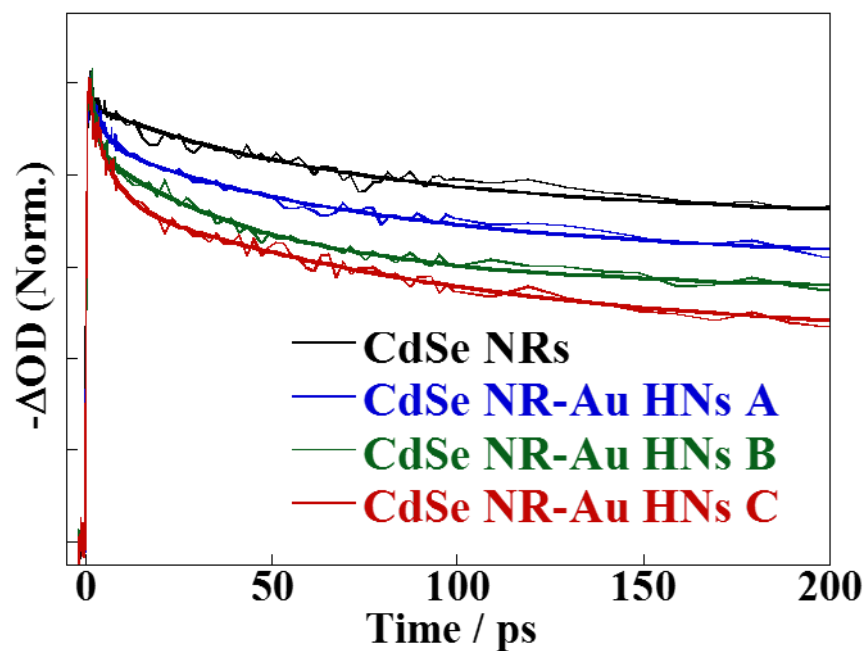
Figure 6.16 Transient absorption dynamics at 1Σ bleach band of each sample.[27]

Table 6.3 Fitting results of 1Σ bleach dynamics for each sample.[27]

Sample	τ_1 / ps	τ_2 / ps	τ_3 / ns
CdSe NRs	4.2 (5%)	76 (18%)	4.5 (76%)
CdSe NR-Au HNs A	3.8 (10%)	65 (21%)	3.4 (69%)
CdSe NR-Au HNs B	1.8 (15%)	44 (26%)	3.0 (60%)
CdSe NR-Au HNs C	2.0 (15%)	56 (32%)	2.3 (52%)
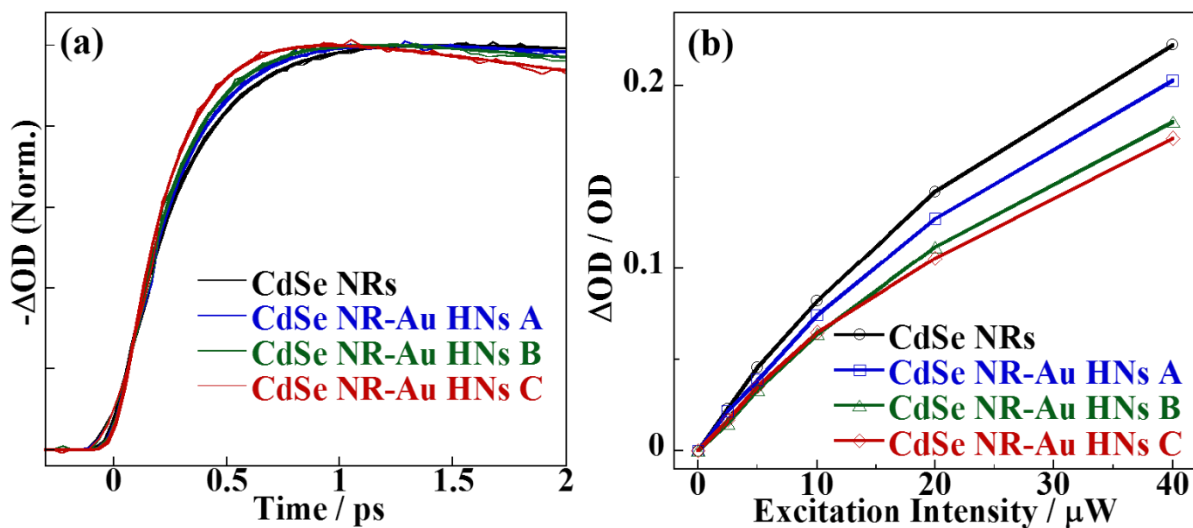
Figure 6.17 (a) The growth kinetics and (b) initial bleach amplitude at the 1Σ bleach band for

CdSe NRs and CdSe NR-Au HNs excited at 400 nm.[27,28]

Table 6.4 Excitation wavelength dependence of Rise times at 1S bleach band for CdSe NRs

and CdSe NR-Au HNs.[28]

Sample	2Σ excitation	1Π excitation	400 nm excitation
	τ_{rise} / ps	τ_{rise} / ps	τ_{rise} / ps
CdSe NRs	0.14	0.14	0.30
CdSe NR-Au HNs A	0.12	0.13	0.27
CdSe NR-Au HNs B	0.11	0.11	0.26
CdSe NR-Au HNs C	0.11	0.10	0.23
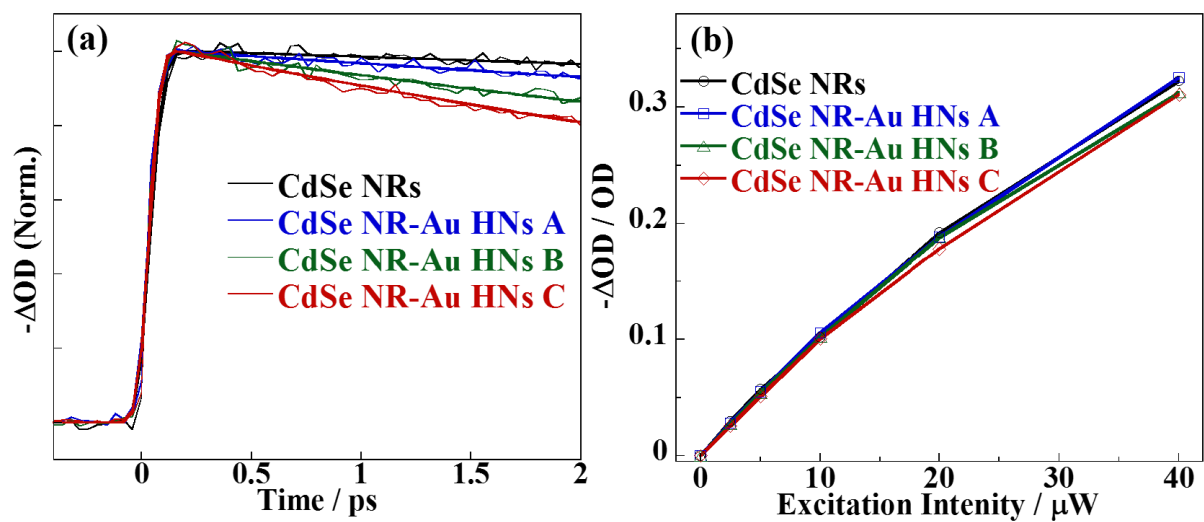
Figure 6.18 (a) 1Σ bleach dynamics in initial time region and (b) initial 1Σ bleach amplitude

for each sample excited at 1Σ absorption band.[28]
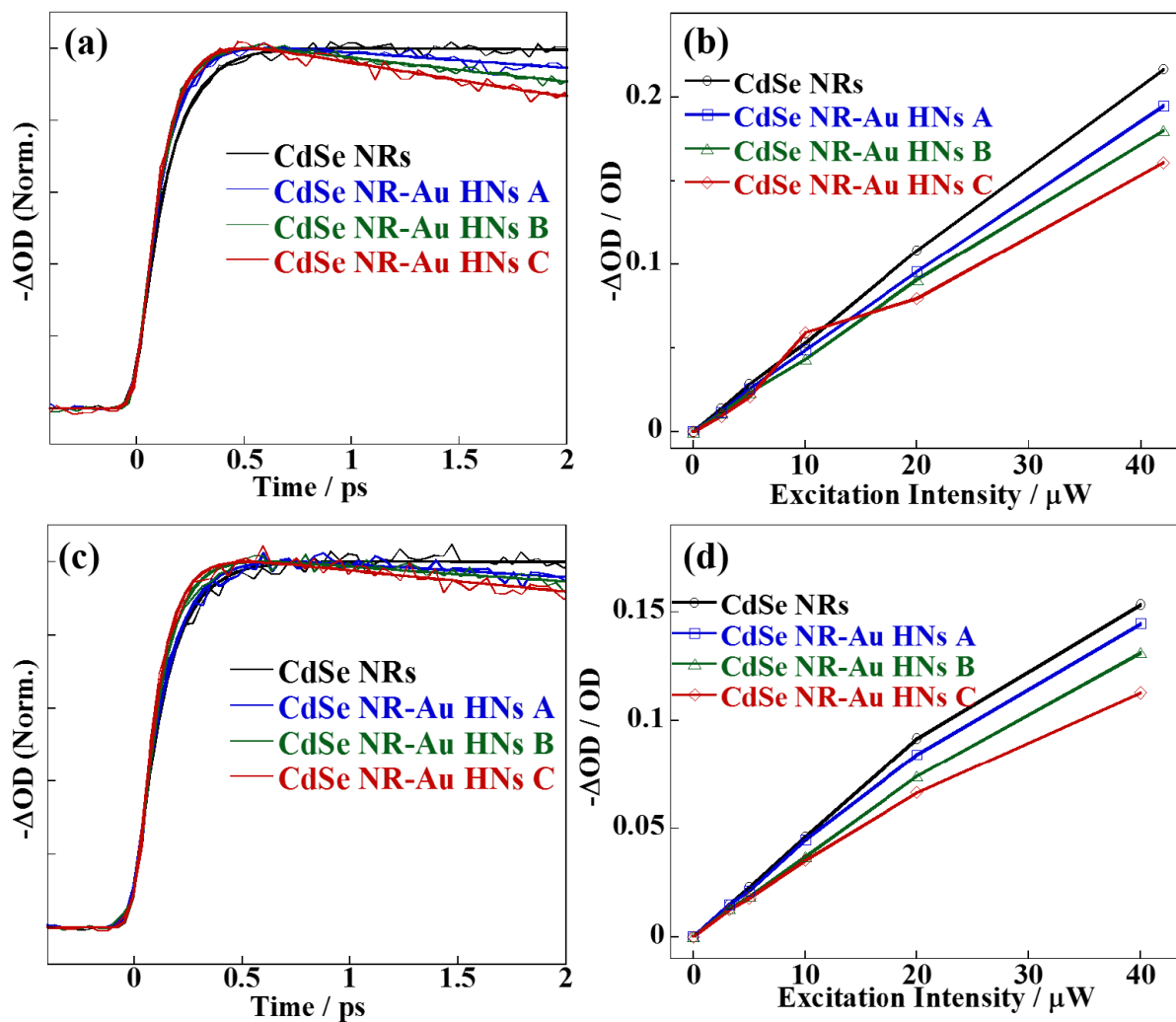
Figure 6.19 (a, c) Growth kinetics and (b, d) initial 1S bleach amplitude for CdSe NRs and

CdSe NR-Au HNs excited at (a, b) 2Σ and (c, d) 1Π absorption band.[28]
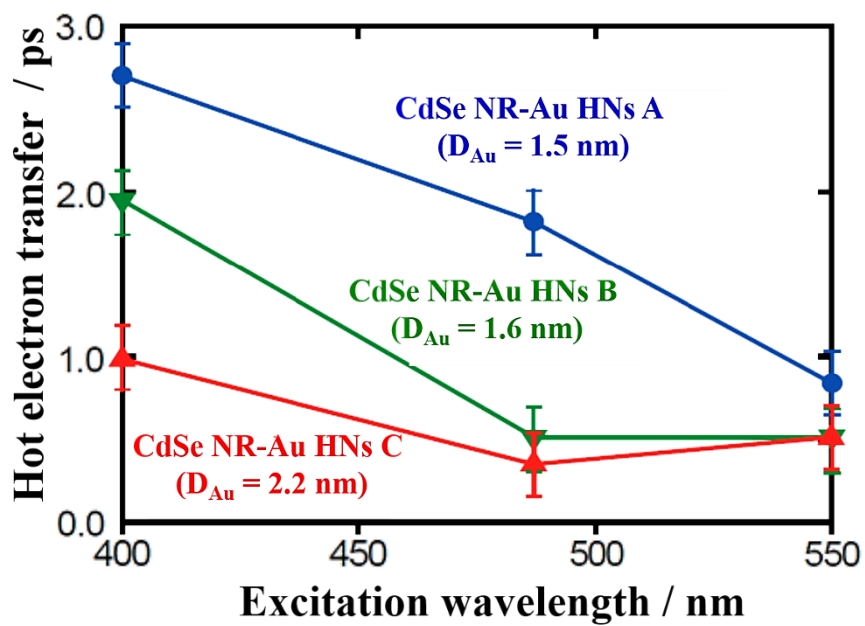
Figure 6.20 Excitation wavelength dependence of hot electron transfer times for each CdSe
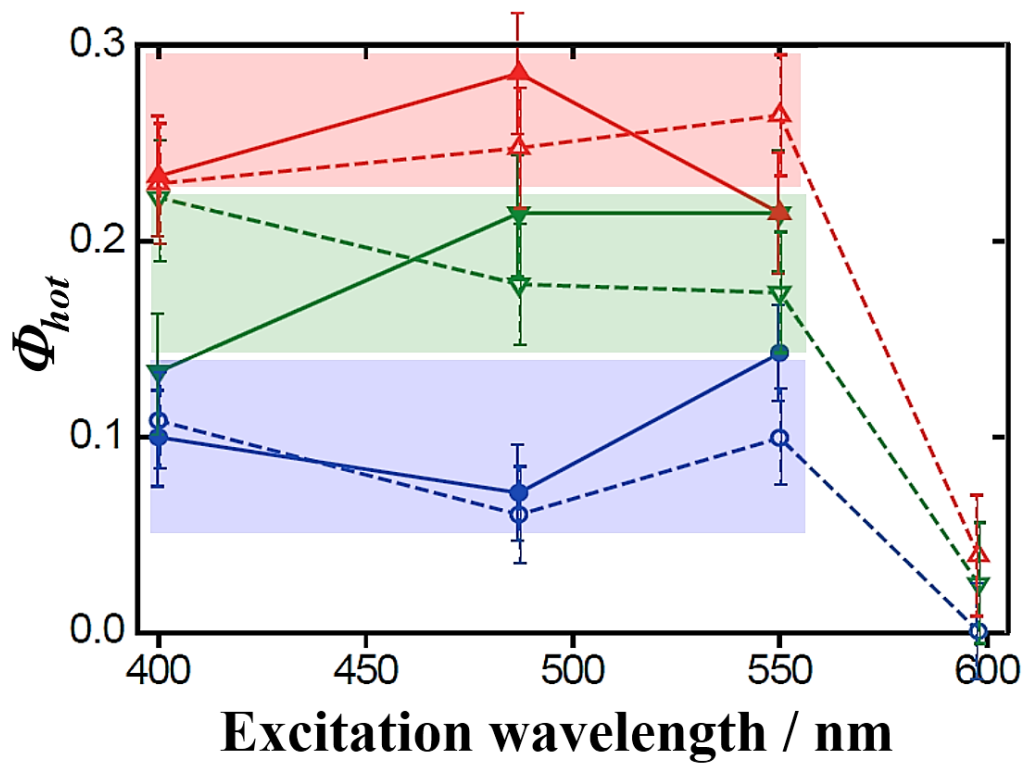
NR-Au HNs.[28]

Figure 6.21 Φ_{hot} estimated from rise time analyses (solid) and initial 1Σ bleach amplitudes (dashed) of CdSe NR-Au HNs A (blue), B (green), and C (red).[28]

Chapter 7

Electron Transfer Processes from CdSe NPLs to Au NPs

7.1 Abstract

Recently, quantum confinement dimensionality of semiconductor nanocrystals could be controlled by colloidal synthetic method. This control leads to the variation of electronic states and carrier relaxation processes. For the application of light-energy conversion devices, charge separation in semiconductor nanocrystals is very important process. Much attention has been paid for semiconductor-metal hybrid nanostructures (HNs) in terms of efficient charge extraction from semiconductor to metal. Therefore, semiconductor-metal HNs are one of the best candidate materials for photovoltaics and photocatlysis. However, the analyses of electron transfer processes in semiconductor-metal HNs have focused on the electron transfer from bend-edge state in semiconductor nanorods attached with metal nanoparticles. Here, we synthesized and characterized CdSe nanoplatelets (NPLs)-Au HNs. In our sample, Au nanoparticles (NPs) with the diameter of ~1.1 nm attached to the corner of CdSe NPLs. We analyzed electron transfer from band-edge and higher excited states of CdSe NPLs to Au NPs using femtosecond pump-probe spectroscopy. In transient absorption measurements of CdSe NPL-Au HNs, the electron transfer from the band-edge state of CdSe NPLs to Au NPs takes place with a time constant of a few ps. By analyzing the rise time and initial bleach amplitude of band-edge bleach band, hot electron transfer and ultrafast electron transfer faster than the instrumental response function does not exist in CdSe NPL-Au HNs.

7.2 Introduction

Recently, the progress in colloidal synthesis of semiconductor nanocrystals allow us to control the quantum confinement dimensionality, such as quantum dots (QDs, three dimensional confinement),[1] nanorods (NRs, two dimensional confinement),[2,3] and nanoplatelets (NPLs, one dimensional confinement).[4,5] The control of quantum confinement dimensionality induces the variation of electronic structures and carrier relaxation processes.

The primary synthetic method of colloidal CdSe NPLs, in which the exciton is confined only in the thickness direction, have been reported in 2008 by Dubertret's group.[4] After this report, several kinds of semiconductor NPLs have been synthesized, for example, CdS and CdTe NPLs,[5] core/shell and core/crown heterostructure-NPLs.[6-8] Semiconductor NPLs shows the thickness-dependent absorption and luminescence spectra with the narrow band width,[4,5] and the large absorption cross section.[9,10] Carrier dynamics of colloidal semiconductor NPLs were examined using luminescence decay measurements and transient absorption measurements. Ithurria et al. examined the single exciton dynamics of CdSe NPLs with different temperature (6-300 K) using luminescence decay measurements.[5] They showed an increase of luminescence intensity and decrease of luminescence lifetime with decreasing the temperature, which were interpreted in terms of the coherent motion of the exciton leading to the giant oscillation strength (GOST). Kunneman et al. analyzed the dynamics of multiple exciton annihilation for CdSe NPLs and CdSe/CdZnS core/shell NPLs, and showed the very slow bimolecular Auger recombination process with the lifetime of ~14 ns and ~8.3 ns, respectively.[11]

The slow Auger recombination of semiconductor NPLs potentially allow the efficient carrier extraction. In our previous study on the electron transfer from CdSe NPLs to methyl viologen (MV^{2+}), we found that the rate of electron transfer depended on the NPL face where MV^{2+} adsorbed and hot electron transfer from CdSe NPLs to MV^{2+} did not occur (Chapter 4). On the other hand, metal NPs such as Au and Pt NPs can become the electron acceptor and the charge transfer dynamics in semiconductor-metal hybrid nanostructures (HNs) have been studied by several groups.[12-17] In Chapter 6, we analyzed the elementary electron transfer processes in CdSe QD-Au HNs by transient absorption measurements with state-selective excitation techniques. By analyzing rise times and initial bleach amplitudes of the 1S bleach with different excitation wavelength, we found that the hot electron transfer and ultrafast

electron transfer faster than the instrumental response function took place from 1P(e) and 1S(e) state of CdSe QDs, respectively. Furthermore, in our previous studies, electron transfer dynamics in CdSe NR-Au HNs with the different size of Au NPs (~1.5-2.2 nm) were examined.[17] In these studies, the hot electron transfer from CdSe NRs to Au NPs was revealed by analyses of rise times and initial bleach amplitudes. Moreover, the excitation wavelength dependence of the yields of hot electron transfer strongly suggested that hot electron transfer in CdSe NR-Au HNs took place from $2\sigma_e$ state. Mongin et al. reported the sub-20 fs electron transfer from the band-edge state of CdS NRs to Au NPs with the diameter of ~6 nm.[13] Furthermore, Wu et al. synthesized CdSe NPL-Pt HNs and examined their carrier dynamics using femtosecond pump-probe spectroscopy.[15] In CdSe NPL-Pt HNs, ultrafast energy transfer (< 150 fs) and picosecond electron transfer (~9.4 ps) from the band-edge state of CdSe NPLs were reported. However, the hot electron transfer in semiconductor NPL-metal HNs and the carrier dynamics of CdSe NPL-Au HNs have not been examined yet.

In the present study, we synthesized and characterized CdSe NPL-Au HNs. The electron transfer processes from CdSe NPL-Au HNs were examined using the femtosecond pump-probe spectroscopy. Furthermore, we discussed the effect of quantum confinement dimensionality on the electron transfer processes in Au NPs attached CdSe nanocrystals.

7.3   Experimental section

Synthetic methods of CdSe NPLs and CdSe NPL-Au HNs were described in Chapter 2. The structures of CdSe NPLs and CdSe NPL-Au HNs were characterized by scanning transmission electron microscopy (STEM, TECNAI 20, 200 keV, FEI). UV-vis absorption and luminescence spectra of CdSe NPLs and CdSe NPL-Au HNs were recorded using an U-4100 (Hitachi) and a Fluorolog-3 (Jobinyvon-Spex), respectively. The transient absorption spectra were measured using femtosecond pump−probe techniques. CdSe NPLs and CdSe

NPL-Au HNs were excited at 400 nm with an amplified mode-locked Ti:sapphire laser (Spitfire and Tsunami, Spectra-Physics, repetition rate: 1 kHz). A repetition rate of 0.5 kHz was achieved by an optical chopper (Model 3501, New Focus, Inc.). Absorption transients were probed by delayed pulses of a femtosecond white-light continuum generated by focusing a fundamental laser pulse into a D_2O cell and were detected by a polychromator-CCD combination (Spectra Pro-275, Acton Research Co., and Spec-10, Princeton Instruments). The temporal resolution was ~100 fs.

7.4   Results and discussion

STEM images of CdSe NPLs and CdSe NPL-Au HNs were shown in Figure 7.1. The average length of short and long axes of CdSe NPLs were estimated to be ~5.8 nm and ~21.3 nm from STEM images, respectively. From the STEM images of CdSe NPL-Au HNs, the average diameter of Au NPs (bright spherical part in Figure 7.1b) and lateral size of CdSe NPLs were estimated to be 1.1 ± 0.3 nm and 5.8 nm $\times$ 20.8 nm, respectively. Steady-state absorption and luminescence spectra of CdSe NPLs and CdSe NPL-Au HNs were illustrated in Figure 7.2. In the absorption spectrum of CdSe NPLs, two narrow absorption band at 507 nm and 478 nm corresponding to electronic transitions from heavy-hole and light-hole valence band-edge states to the conduction band edge (heavy-hole band and light-hole band), respectively. Absorption peaks of CdSe NPL-Au HNs have similar wavelengths to those of CdSe NPLs, however, an absorption tail in the longer wavelength region ($\geqq$ 510 nm) was slightly observed in CdSe NPL-Au HNs. The absorption tail in CdSe NPL-Au HNs was likely due to the absorption of small Au NPs or the light scattering. In the luminescence spectrum of CdSe NPL-Au HNs, the band-edge luminescence of CdSe NPLs centered at 511 nm was strongly quenched, indicating the carrier transfer from CdSe NPLs to Au NPs (Figure 7.2c).

Transient absorption spectra of CdSe NPLs and CdSe NPL-Au HNs excited at 400 nm were shown in Figure 7.3. Because of the low excitation intensity (0.5 $\mu J/cm^2$), multiexcitons did not contribute in these measurements. Although two bleach bands corresponding to the heavy-hole and light-hole bands were clearly observed in both spectra, the relaxation of transient absorption signal in CdSe NPL-Au HNs was much faster than that in CdSe NPLs. The transient absorption dynamics at the heavy-hole bleach band of CdSe NPLs and CdSe NPL-Au HNs were shown in Figure 7.4, and fitted with the bi-exponential function and the sum of a stretched exponential function and an exponential function, respectively. These fitting results are summarized in Table 7.1. The heavy-hole band dynamics of CdSe NPL-Au HNs could be also fitted by the sum of four exponential functions with the lifetime of 0.86 ps (44.7%), 3.6 ps (30.4%), 41.2 ps (13.6%), and 1.7 ns (11.3%). These lifetimes were slower than the lifetime of electron transfer from 1S(e) state in CdSe QD-Au HNs (Table 6.1 in Chapter 6). However, since the interpretation of fitting with four exponential functions were very complex, we fitted the heavy-hole band dynamics of CdSe NPL-Au HNs by using a sum of a stretched exponential function and an exponential function. The average lifetime of a stretched exponential component, defined as $\tau_{ave} = (\tau_1/\beta)\Gamma(1/\beta)$, was estimated to be ~3.2 ps, which was likely attributed to the average lifetime of electron transfer from the band-edge state of CdSe NPLs to Au NPs. The slower electron transfer from band-edge state in CdSe NPL-Au HNs as compared to that in CdSe QD-Au HNs was likely due to the difference of electronic coupling constant. CdSe NPLs have much larger lateral size as compared to the diameter of CdSe QDs (~4.2 nm), leading to the weak electronic coupling in CdSe NPL-Au HNs.

The growth kinetics at the heavy-hole band of CdSe NPLs and CdSe NPL-Au HNs were shown in Figure 7.5a. Furthermore, the initial bleach amplitude of the heavy-hole band divided by the ground state absorption at the excitation wavelength (ΔOD / $OD_{400\,nm}$) were

plotted against the excitation intensity (Figure 7.5b). As clearly shown, the growth kinetics and initial bleach amplitude of CdSe NPL-Au HNs were very similar to those of CdSe NPLs. In contrast with CdSe QD-Au HNs and NR-Au HNs (Chapter 6), these results indicates that the hot electron transfer from CdSe NPLs to Au NPs and ultrafast electron transfer from band-edge state did not occur. CdSe NPLs have relatively continuous electronic structures resulting from the lateral extension in CdSe NPLs, leading to the hot electron relaxation via phonon emission.[18] Previous studies reported that the hot electron relaxation process in CdSe QDs and CdSe NRs are mainly interpreted in terms of Auger cooling and not due to the phonon emission, respectively.[19-22] Therefore, the suppression of hot electron transfer from CdSe NPLs to Au NPs could originate from the difference of the electronic structures and hot electron relaxation process. Moreover, the average diameter of Au NPs in CdSe NPL-Au HNs (~1.1 nm) were smaller than those in CdSe QD-Au HNs (~1.3-2.0 nm) and NR-Au HNs (~1.5-2.2 nm) in Chapter 6. The size difference of Au NPs likely affects to the difference of rate of hot electron transfer. Therefore, in CdSe NPL-Au HNs with small Au NPs (~1.1 nm), hot electron transfer could not be observed because of the very small rate of hot electron transfer from CdSe NPLs to Au NPs.

In addition, the ultrafast electron transfer process from a conduction band-edge state much faster than the instrumental response function was suppressed in CdSe NPL-Au HNs as well as CdSe NR-Au HNs in Chapter 6. In CdSe NPL-Au HNs, CdSe NPLs have relatively large lateral size (short axis: ~5.8 nm, long axis: ~20.8 nm) and Au NPs attached to the edge of CdSe NPLs. Therefore, as mentioned above, the electronic coupling between CdSe NPLs and Au NPs is likely weaker as compared with CdSe QD-Au HNs and CdSe NR-Au HNs. According to previous studies,[23,24] the strong electronic coupling between donor and acceptor leads to the ultrafast electron transfer in an adiabatic process. Therefore, the ultrafast electron transfer from a band-edge state of CdSe nanocrystals with different quantum confinement

dimensionality probably depended on the difference of electronic coupling constant in each HNs.

7.5 Conclusion

In conclusion, we synthesized and characterized CdSe NPL-Au HNs. The electron transfer dynamics from CdSe NPLs to Au NPs with the diameter of ~1.1 nm were examined using the femtosecond transient absorption spectroscopy. In the transient absorption measurements under 400 nm excitation, the fast relaxation of the band-edge bleach band was clearly observed in CdSe NPL-Au HNs, indicating the electron transfer from the conduction band-edge state of CdSe NPL to Au NPs. The growth kinetics of band-edge bleach band of CdSe NPL-Au HNs was similar to that of CdSe NPLs. In addition, the initial band-edge bleach amplitude were nearly identical with each other. In contrast with CdSe QD-Au HNs and NR-Au HNs, these results indicate that the hot electron transfer from CdSe NPLs to Au NPs did not take place. In CdSe NPLs, the density of states in conduction band were much larger than that in CdSe QDs and NRs because of the large lateral size of CdSe NPLs. Therefore, in contrast with CdSe QDs and NRs, the hot electron in CdSe NPLs relaxed to the band-edge state via a phonon emission process. Consequently, the hot electron transfer did not occur in CdSe NPL-Au HNs because of relatively continuous band structures and hot electron relaxation by a phonon emission. Furthermore, the comparison of initial bleach amplitudes at the band-edge bleach band revealed that the ultrafast electron transfer did not occur in CdSe NPL-Au HNs in contrast with CdSe QD-Au HNs. The suppression of the ultrafast electron transfer much faster than the instrumental response function in CdSe NPL-Au HNs likely resulted from the weak electronic coupling between CdSe NPLs and Au NPs.

References

(1) Murray, C. B.; Norris, D. J.; Bawendi, M. G. Synthesis and characterization of nearly monodisperse CdE (E = sulfur, selenium, tellurium) semiconductor nanocrystallites. *J. Am. Chem. Soc.* **1993**, *115*, 8706–8715.

(2) Peng, X.; Manna, L.; Yang, W.; Wickham, J.; Scher, E.; Kadavanich, A.; Alivisatos, A. P. Shape control of CdSe nanocrystals. *Science*, **2000**, *404*, 59–61.

(3) Manna, L.; Scher, E. C.; Alivisatos, P. A. Synthesis of Soluble and Processable Rod-, Arrow-, Teardrop-, and Tetrapod-Shaped CdSe Nanocrystals. *J. Am. Chem. Soc.* **2000**, *122*, 12700–12706.

(4) Ithurria, S.; Dubertret, B. Quasi 2D Colloidal CdSe Platelets with Thicknesses Controlled at the Atomic Level. *J. Am. Chem. Soc.* **2008**, *130*, 16504−16505.

(5) Ithurria, S.; Tessier, M. D.; Mahler, B.; Lobo, R. P. S. M.; Dubertret, B.; Efros, Al. L. Colloidal Nanoplatelets with Two−dimensional Electronic Structure. *Nat. Mater.* **2011**, *10*, 936−941.

(6) Mahler, B.; Nadal, B.; Bouet, C.; Patriarche, G.; Dubertret, B. Core/Shell Colloidal Semiconductor Nanoplatelets. *J. Am. Chem. Soc.* **2012**, *134*, 18591–18598.

(7) Tessier, M. D.; Spinicelli, P.; dupont, D.; Patriarche, G.; Ithurria, S.; Dubertret B. Efficient Exciton Concentrators Built from Colloidal Core/Crown CdSe/CdS Semiconductor Nanoplatelets. Nano Lett., 2014, 14, 207−213.

215

(8) Pedetti, S.; Ithurria, S.; Heuclin, H.; Patriarche, G.; Dubertret, B. Type−II CdSe/CdTe Core/Crown Semiconductor Nanoplatelets. *J. Am. Chem. Soc.* **2014**, *136*, 16430−16438.

(9) Baghani, E.; O'Leary, S. K.; Fedin, I.; Talapin, D. V.; Pelton, M. Auger–Limited Carrier Recombination and Relaxation in CdSe Colloidal Quantum Wells. *J. Phys. Chem. Lett.* **2015**, *6*, 1032–1036.

(10)   Pelton, M.; Ithurria, S.; Schaller, R. D.; Dolzhnikov, D. S.; Talapin, D. V. Carrier Cooling in Colloidal Quantum Wells. *Nano Lett.* **2012**, *12*, 6158−6163.

(11)   Kunneman, L. T.; Tessier, M. D.; Heuclin, H.; Dubertret, B; Aulin, Y. V.; Grozema, F. C.; Schins, J. M.; Siebbeles, L. D. A. Bimolecular Auger Recombination of Electron−Hole Pairs in Two-Dimensional CdSe and CdSe/CdZnS Core/Shell Nanoplatelets. *J. Phys. Chem. Lett.* **2013**, *4*, 3574–3578.

(12)   Khon, E.; Mereshchenko, A.; Tarnovsky, A. N.; Acharya, K.; Klinkova, A.; Hewa-Kasakarage, N. N.; Nemitz, I.; Zamkov, M. Suppression of the Plasmon Resonance in Au/CdS Colloidal Nanocomposites. *Nano Lett.* **2011**, *11*, 1792−1799.

(13)   Mongin, D.; Shaviv, E.; Maioli, P.; Crut, A. Banin, U.; Fatti, N. D.; Vallée, F. Ultrafast Photoinduced Charge Separation in Metal−Semiconductor Nanohybrids. *ACS Nano* **2012**, *6*, 7034–7043.

(14)   Sagarzazu, G.; Inoue, K.; Saruyama, M.; Sakamoto, M.; Teranishi, T.; Masuo, S.; Tamai, N. Ultrafast Dynamics and Single Particle Spectroscopy of Au–CdSe Nanorods.

Phys. Chem. Chem. Phys. **2013**, *15*, 2141–2152.

(15)   Wu, K.; Li, Q.; Du, Y.; Chen, Z.; Lian, T. Ultrafast Exciton Quenching by Energy and Electron Transfer in Colloidal CdSe Nanosheet−Pt Heterostructures. *Chem. Sci.* **2015**, *6*, 1049−1054.

(16)   Wu, K.; Chen, J.; McBride, J. R.; Lian, T. Efficient Hot−Electron Transfer by a Plasmon−Induced Interfacial Charge−Transfer Transition. *Science* **2015**, *349*, 632−635.

(17)   Sagarzazu, G.; Inoue, K.; Saruyama, M.; Sakamoto, M.; Teranishi, T.; Tamai, N. Hot-electron transfer in Au-CdSe nanorods. *Submitted.*

(18)   Sippel, P.; Albrecht, W.; Bok, J. C.; Dijk-Moes, R. J. A.; Hannappel, T.; Eichberger, R.; Vanmaekelbergh, D. Femtosecond Cooling of Hot Electrons in CdSe Quantum-Well Platelets. *Nano Lett.* **2015**, *15*, 2409–2416.

(19)   Kambhampati, P. Hot Exciton Relaxation Dynamics in Semiconductor Quantum Dots: Radiationless Transitions on the Nanoscale. *J. Phys. Chem. C* **2011**, *115*, 22089−22109.

(20)   Klimov, V. I. Optical Nonlinearities and Ultrafast Carrier Dynamics in Semiconductor Nanocrystals. *J. Phys. Chem. B* **2000**, *104*, 6112−6123.

(21)   Guyot−Sionnest, P.; Wehrenberg, B.; Yu, D. Intraband Relaxation in CdSe Nanocrystals and the Strong Influence of the Surface Ligands. *J. Chem. Phys.* **2005**, *123*, 074709.

(22)   Yu, P.; Nedeljkovic, J. M.; Ahrenkiel, P. A.; Ellingson, R. J.; Nozik, A. J. Size

Dependent Femtosecond Electron Cooling Dynamics in CdSe Quantum Rods. *Nano Lett.*

2004, *4*, 1089–1092.

(23)   Yang, Y.; Rodríguez−Córdoba, W.; Xiang, X.; Lian, T. Strong Electronic Coupling

and Ultrafast Electron Transfer between PbS Quantum Dots and TiO_2 Nanocrystalline

Films. *Nano Lett.* **2012**, *12*, 303−309.

(24)   Tisdale, W. A.; Zhu, X. Y. Artificial Atoms on Semiconductor Surfaces. *Proc. Natl.*

Acad. Sci. U. S. A. **2011**, *108*, 965−970.
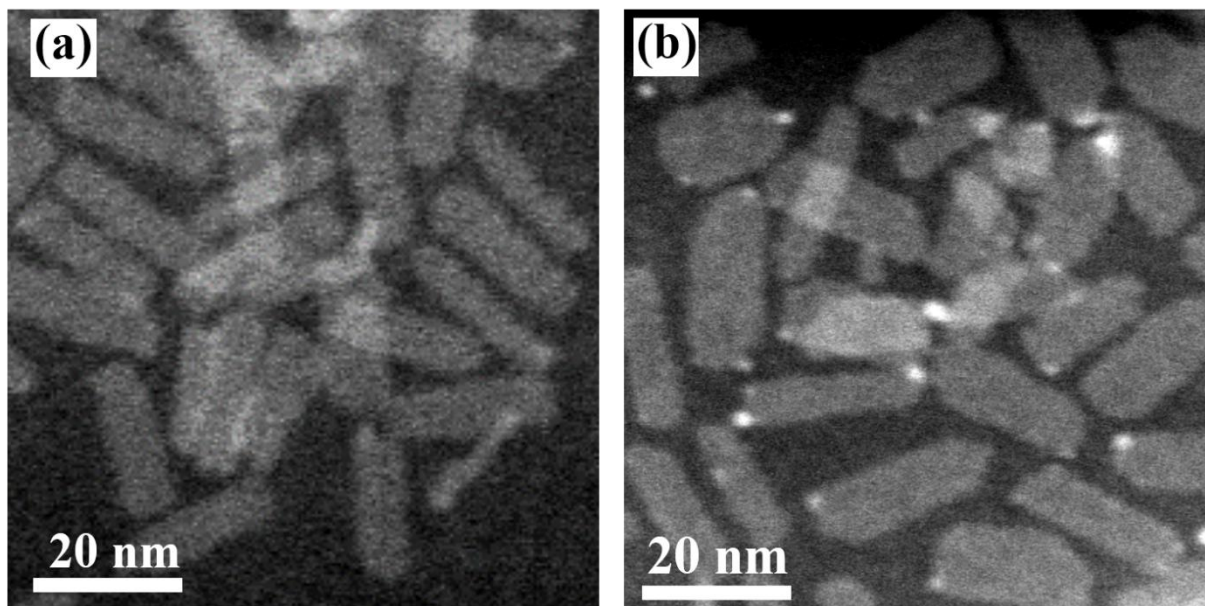
Figure 7.1 STEM images of (a) CdSe NPLs and (b) CdSe NPL-Au HNs with the Au NPs size

of ~1.1 nm.
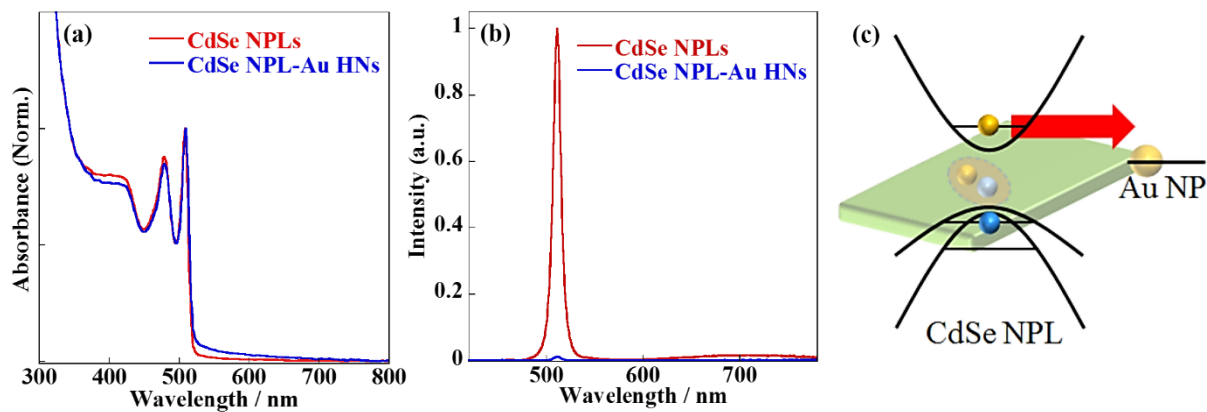
Figure 7.2 Steady-state (a) absorption and (b) luminescence spectra of CdSe NPLs and CdSe NPL-Au HNs. (c) The energy diagram and scheme of carrier transfer from CdSe NPLs to Au NPs.
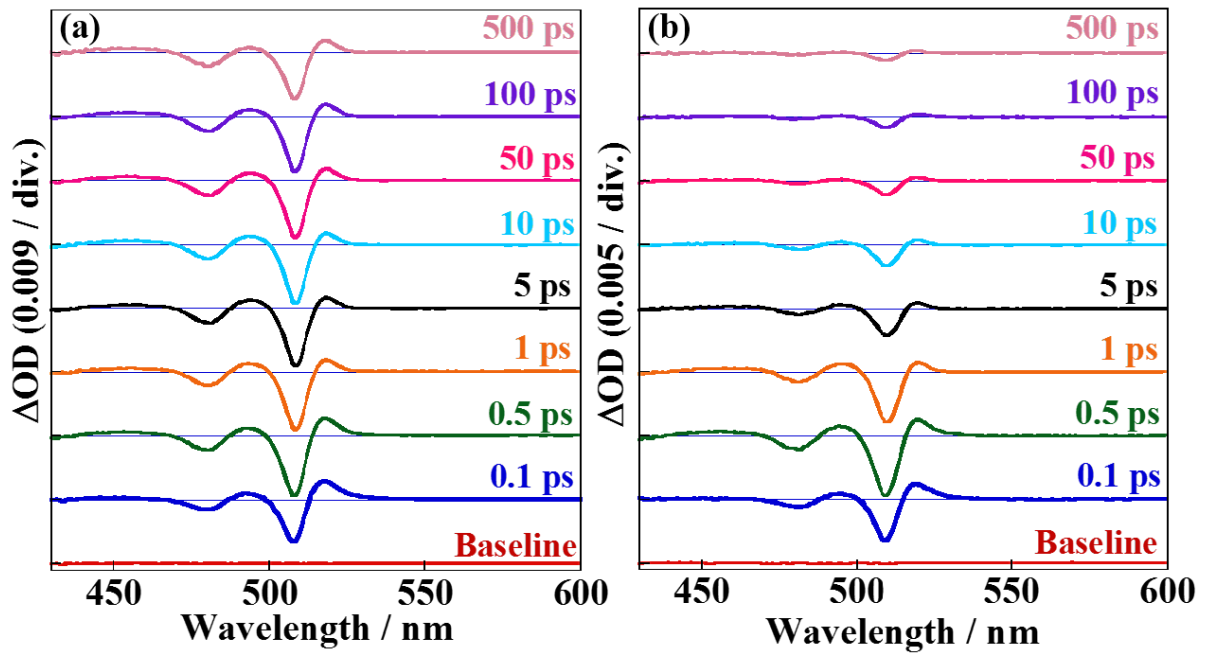
Figure 7.3 Transient absorption spectra of (a) CdSe NPLs and (b) CdSe NPL-Au HNs excited

at 400 nm.
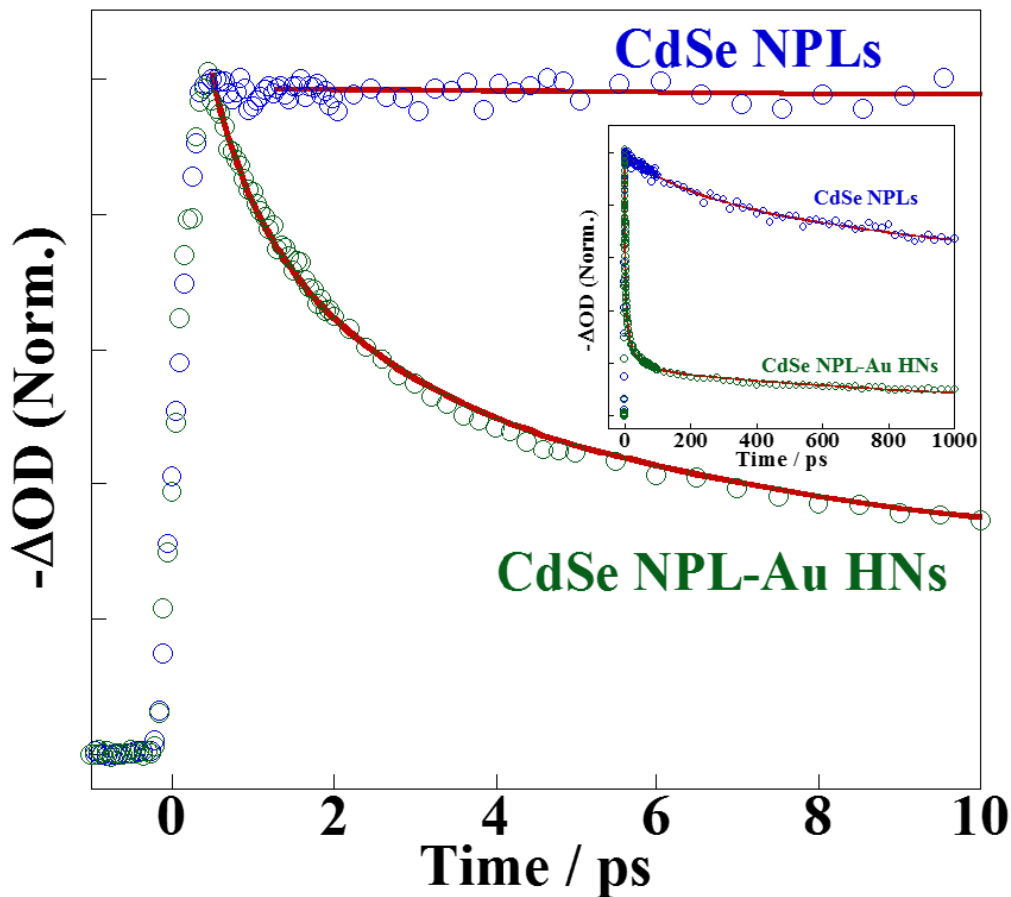
Figure 7.4 Transient absorption dynamics at the heavy-hole band of CdSe NPLs (blue circles)

and CdSe NPL-Au HNs (green circles) and simulation curve (red line). The inset shows the

heavy-hole bleach dynamics of each sample in the long time region.

Table 7.1 Fitting results of heavy-hole band dynamics for each sample with the F(t) =

$A_2exp(-t/\tau_2) + A_3exp(-t/\tau_3)$ for CdSe NPLs, and $G(t) = A_1exp(-(t/\tau_1)^\beta) + A_3exp(-t/\tau_3)$ for CdSe

NPL-Au HNs.

Sample	τ_1 / ps	β	τ_2 / ps	τ_3 / ns
CdSe NPLs			230 (17.3%)	4.8 (82.7%)
CdSe NPL-Au HNs	0.21 (94.0%)	0.27		1.4 (6.0%)
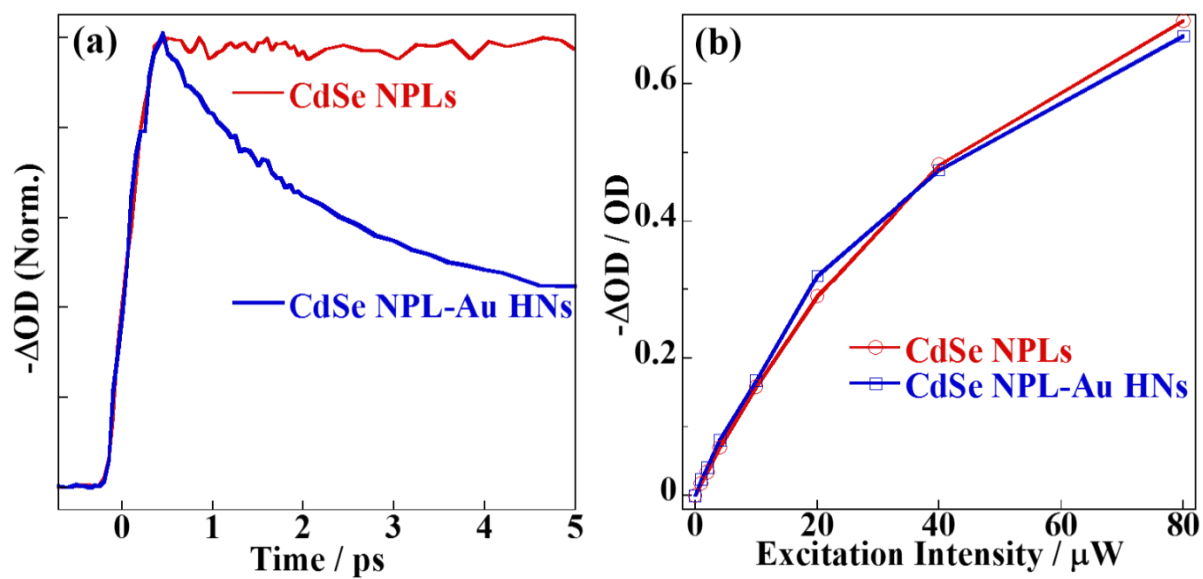
Figure 7.5 (a) Growth kinetics and (b) initial bleach amplitude at heavy-hole band of CdSe

NPLs and CdSe NPL-Au HNs excited at 400 nm.

Summary

In summary, we analyzed the hot electron transfer and ultrafast electron transfer from the band-edge state of colloidal semiconductor nanocrystals to acceptor molecules and metal nanoparticles by femtosecond pump-probe spectroscopy. We examined elementary electron transfer processes from CdSe/CdS core/shell QDs (CSQDs) and CdSe NPLs to methyl viologen (MV^{2+}) in Chapter 3 and 4, respectively. In CdSe/CdS CSQD-MV^{2+} complexes, the hot electron transfer from CdSe/CdS CSQDs to MV^{2+} was clearly observed and the shell thickness dependence of hot electron transfer rate was different from that of electron transfer rate from 1S(e) state. The yield of hot electron transfer from CdSe/CdS CSQDs with thicker shell can be estimated to be ~82%. In CdSe NPL-MV^{2+} complexes, the face-dependent electron transfer from CdSe NPLs to MV^{2+} was revealed. Moreover, in contrast with CdSe/CdS CSQD-MV^{2+} complexes, the hot electron transfer from CdSe NPLs to MV^{2+} was not observed. The hot electron in CdSe NPLs relaxes to the band-edge state by the phonon emission because of the relatively continuous electronic structure of NPLs, although the dominant hot electron relaxation process in discrete electronic states of CdSe QDs is the Auger cooling process. Therefore, the difference of the electronic structure and hot electron relaxation processes result in the suppression of hot electron transfer in CdSe NPL-MV^{2+} complexes.

We examined the carrier transfer dynamics in PbS QD-Au HNs using femtosecond pump-prove spectroscopy with the state-selective excitation technique in Chapter 5. The ps-scale carrier transfer from PbS QDs to Au NPs was detected in 1S bleach dynamics and became faster with increasing the diameter of Au NPs. However, the hot carrier transfer from PbS QDs to Au NPs did not observe from rise time analyses of 1S bleach band. In addition to ps-scale carrier transfer, ultrafast carrier transfer from band-edge states much faster than the instrumental response function were suggested from analyses of initial 1S bleach amplitude excited at 1S transition. The difference between ps-scale and ultrafast carrier transfer from

band-edge states is probably attributed to the hole and electron transfer from PbS QDs to Au NPs, respectively.

In Chapter 6 and 7, we discussed the electron transfer dynamics from the band-edge state and higher excited states of CdSe QDs, NRs, and NPLs to Au NPs. In CdSe QD-Au HNs, rise time analyses of 1S bleach band revealed the hot electron transfer from CdSe QDs to Au NPs, whose lifetime and yields are estimated to be ~300 fs and ~50%. Moreover, the ultrafast electron transfer from 1S(e) state of CdSe QDs to Au NPs was detected from the comparisons of initial 1S bleach amplitudes under 1S excitation. In addition, the excitation wavelength dependence of the initial 1S bleach amplitude suggested that the hot electron transfer occurred from 1P(e) state of CdSe QDs to Au NPs. In our previous studies, the electron transfer dynamics from CdSe NRs to Au NPs was examined. Hot electron transfer from CdSe NRs to Au NPs were clearly observed, and the fastest lifetime and maximum yield of hot electron transfer in CdSe NR-Au HNs were estimated to be ~0.5 ps and ~23%. However, the ultrafast electron transfer from the band-edge state of CdSe NRs to Au NPs did not observed. In addition, we examined the electron transfer dynamics from CdSe NPLs to Au NPs in Chapter 7. Both hot electron transfer and ultrafast electron transfer from band-edge state did not occur in CdSe NPL-Au HNs. The hot electron transfer from CdSe nanocrystals to Au NPs was observed in CdSe QD-Au HNs and NR-Au HNs. As mentioned above, in contrast with CdSe QDs and NRs, CdSe NPLs have the relatively continuous electronic structure, leading the fast hot electron relaxation via phonon emission. Therefore, the suppression of hot electron transfer from CdSe NPLs to Au NPs was probably originated from the difference of the continuous electronic states and hot electron relaxation mechanism. Furthermore, the ultrafast electron transfer from band-edge state faster than the instrumental response function was observed in only CdSe QD-Au HNs. CdSe NRs and NPLs have large long axis (~14.0 nm) and lateral size (~5.8 nm × ~21.3 nm), which induces the weak electronic coupling between

CdSe nanocrystals and Au NPs. Therefore, the difference of ultrafast electron transfer from CdSe nanocrystals with different quantum confinement dimensionality was likely due to difference of electronic coupling strength.

In this study, we found that the yield of hot electron transfer from QDs (three dimensional quantum confinement systems) is higher than those from NRs and NPLs. Furthermore, CdSe/CdS CSQDs-MV^{2+} complexes with the shell thickness of ~0.6 nm shows the highest yield of hot electron transfer (~82%), which is likely due to the modification of electronic structure in core/shell nanostructures. However, the detailed shell thickness dependence of hot electron transfer is not clarified. In the future works, analyses of hot electron transfer from CdSe/CdS CSQDs with various shell thickness is necessary for understanding the shell thickness dependence of the rate and yield of hot electron transfer. Moreover, the selection of core and shell materials modify the electronic structure and carrier relaxation processes in semiconductor nanocrystals. Therefore, the interfacial potential engineering of semiconductor nanocrystals by utilizing the hetero nanointerface probably allows to achieve the higher efficiency of hot carrier extraction and optimization of the structure of semiconductor nanocrystals.

Acknowledgement

Publications lists

(1) Chiang, W.-Y.; <u>Okuhata, T.</u>; Usman, A.; Tamai, N.; Masuhara, H. Efficient Optical Trapping of CdTe Quantum Dots by Femtosecond Laser Pulses. *J. Phys. Chem. B* **2014**, *118*, 14010–14016.

(2) <u>Okuhata, T.</u>; Kobayashi, Y.; Nonoguchi, Y.; Kawai, T.; Tamai, N. Ultrafast Carrier Transfer and Hot Carrier Dynamics in PbS−Au Hybrid Nanostructures. *J. Phys. Chem. C* **2015**, *119*, 2113–2120.

(3) Wang, L.; Tian, Y.; <u>Okuhata, T.</u>; Tamai, N. Charge Transfer Dynamics and Auger Recombination of CdTe/CdS Core/Shell Quantum Dots. *J. Phys. Chem. C* **2015**, *119*, 17971–17978.

(4) <u>Okuhata, T.</u>; Tamai, N. Face–Dependent Electron Transfer in CdSe Nanoplatelet–Methyl Viologen Complexes. *J. Phys. Chem. C* **2016**, *120*, 17052–17059.